Metabolic reprogramming and vulnerabilities of prostate cancer stem cells independent of epithelial-mesenchymal transition

Esther Aguilar Fadó

Metabolic reprogramming and vulnerabilities of prostate cancer stem cells independent of epithelial-mesenchymal transition

Esther Aguilar Fadó

PhD Thesis

2014

The image used in the cover was obtained from the artpistol website (http://www.artpistol.co.uk).

Artist: Nisbet Wylie.

PROGRAMA DE DOCTORADO EN BIOTECNOLOGÍA

Departamento de Bioquímica y Biología Molecular

Facultad de Biología

Metabolic reprogramming and vulnerabilities of prostate cancer stem cells independent of epithelial-mesenchymal transition

Memoria presentada por Esther Aguilar Fadó para optar al grado de Doctora por la Universitat de Barcelona

Josep Centelles Serra

Director y tutor

Marta Cascante Serratosa

Codirectora

Esther Aguilar Fadó

Doctoranda

To Cesc, my family and all the people who have shared my life experience during the last years.

My sincere thanks to Dr. Josep Centelles, Dr. Marta Cascante, Dr. Timothy Thomson and Dr. Silvia Marín for their support to make this PhD Thesis possible.

My sincerest gratitude and appreciation to Dr. Hockenbery, for giving me the opportunity to work in his lab, and to Dr. Fionnuala Morrish, for all the guidance and advice she gave me

“After climbing a great hill, one only finds that there are many more hills to climb”

Nelson Mandela

INDEX

1. ABBREVIATIONS

1. ABBREVIATIONS

α-KG α-ketoglutarate

2-DG 2-deoxyglucose

ACYL ATP citrate lyase

ADP Adenosine diphosphate

ALDH Aldehyde dehydrogenase

ALT Alanine transaminase

AMP Adenosine monophosphate

AMPK AMP-activated protein kinase

ATP Adenosine triphosphate

BAX Bcl-2-associated X protein

BCA Bicinchoninic acid

BCL2 B-cell lymphoma 2

BPTES Bis-2-(5-phenylacetamido-1,2,4-thiadiazol-2-yl)ethyl

CAMs Cell Adhesion Molecules

CPT1 Carnitine palmitoyltransferase 1

CSCs Cancer stem cells

CTCs Circulating tumor cells

CXCL12 C-X-C motif chemokine 12

DCA Dichloroacetate

DHEA Dehydroepiandrosterone

DMK Dimethyl ketone

ECAR Extracellular acidification rate

EDTA Ethylenediaminetetraacetic acid

EMT Epithelial-mesenchymal transition

FACS Fluorescence-activated cell sorter

FASN Fatty acid synthase

FBA Flux balance analysis

FBS Fetal bovine serum

FCCP carbonilcyanide p-trifluoromethoxyphenylhydrazone

FH Fumarate hydratase

G6PDH Glucose-6-phosphate dehydrogenase

GAC Glutaminase C

GAPDH Glyceraldehyde-3-phosphate dehydrogenase

GC/MS Gas chromatography coupled with mass spectrometry

GLDC Glycine decarboxylase

GLDH Glutamate dehydrogenase

GLS Glutaminase

GLS1 Glutaminase 1

GLS2 Glutaminase 2

GLUT1 Glucose transporter 1

GLUT3 Glucose transporter 3

GLUT4 Glucose transporter 4

GSMMs Genome-scale metabolic models

GSSG Oxydized glutathione

GT Glycolytic tax

H_2DCFDA 2',7' dichlorodihydrofluorescein diacetate

HIF-1α Hypoxia-inducible factor 1, alpha subunit

HK Hexokinase

HK1 Hexokinase 1

HK2 Hexokinase 2

IDH Isocitrate dehydrogenase

IDH3 isocitrate dehydrogenase 3

IGF1 Insulin-like growth factor 1

KGA Kidney-type glutaminase

KRAS Kirsten rat sarcoma

Lac Lactate

LC/MS Liquid chromatography coupled with mass spectrometry

LDH Lactate dehydrogenase

LDH-A Lactate dehydrogenase A

LGA Liver-type glutaminase

LKB1 Liver kinase B1

MAPK Mitogen-activated protein kinase

MDCK Madin-Darby canine kidney

ME Malic enzyme

MET Mesenchymal-epithelial transition

MetSCs Metastatic stem cells

MFA Metabolic flux analysis

MIDA Mass isotopomer distribution analysis

miRNAs micro RNAs

mTOR Mammalian target of rapimycin

MTT 3-[4,5-dimethylthiazol-2-yl]-2,5-diphenyltetrazolium bromide

NADPH Nicotinamide adenine dinucleotide phosphate

NMR Nuclear magnetic resonance

NRF2 Nuclear factor erythroid 2-related factor 2

OCR Oxygen consumption rate

OCT1 Octamer-binding transcription factor 1

OS Other sources

OT Oxythiamine

OXPHOS Oxidative phosphorylation

PBS Phosphate buffered saline

Pc Pentose cycle

PC Pyruvate carboxylase

PCR Polymerase chain reaction

PDH Pyruvate dehydrogenase

PDHK1 Pyruvate dehydrogenase kinase 1

PDHKs Pyruvate dehydrogenase kinases

PDP Pyruvate dehydrogenase phosphatase

PDP2 Pyruvate phosphatase 2

PET Positron Emission Tomography

PFK Phosphofructokinase

PFK1 Phosphofructokinase 1

PFK2 Phosphofructokinase 2

PGC-1α Peroxisome proliferator-activated receptor c coactivator 1

PI Propidium iodide

PI3K Phosphoinositide 3-kinase

PK Pyruvate kinase

PKM2 Pyruvate kinase m2 isoform

POX/PRODH Proline oxidase/proline dehydrogenase

PPP Pentose Phosphate Pathway

Pyr Pyruvate

R5P Ribose-5-phosphate

RAS Rat sarcoma

Rb Retinoblastoma

RHO Rhodopsin

RNAi RNA interference

ROS Reactive oxygen species

SDH Succinate dehydrogenase

SDS Sodium dodecyl sulfate

SDS-PAGE Sodium dodecyl sulfate polyacrylamide gel electrophoresis

SHMT1 Serine hydroxymethyltransferase 1

SHMT2 Serine hydroxymethyltransferase 2

siRNA Small interfering RNA

SLC2A1 Solute carrier family 2, member 1

SOG Serine biosynthesis, one-carbon metabolism and the glycine cleavage system

TCA Tricarboxylic acid

TGFβ Transforming growth factor beta

THF Tetrahydrofolate

TICs Tumor-initiating cells

TIGAR TP53-inducible glycolysis and apoptosis regulator

TKT Transketolase

TKTL1 Transketolase-like 1

TRAIL TNF-related apoptosis-inducing ligand

VEGF Vascular endothelial growth factor

VEGFR-2 Vascular endothelial growth factor receptor 2

Wnt Wingless-type

ZEB1 Zinc finger E-box binding homeobox 1

ZEB2 Zinc finger E-box binding homeobox 2

2. INTRODUCTION

2. INTRODUCTION

2.1 CANCER: GENERAL OVERVIEW

Cancer comprises a large number of diseases characterized by the appearance of abnormal cells that divide unrestrained from physiological control. Some cancer cells are able to migrate from their sites of origin and spread to other parts of the body through blood and lymph vessels, a process known as metastasis. Metastases are the major cause of death from cancer. According to the World Health Organization, estimates for 2012 were 14.1 million new cases of cancer and 8.2 million cancer deaths worldwide. The most common cancers by primary site location were lung, prostate and colorectum in men and breast, colorectum and cervix uteri in women (*1*).

The origin of cancer is multifactorial and influenced by exogenous (tobacco, infectious organisms, chemicals and radiation) and endogenous (inherited mutations, hormones, immune conditions and metabolic alterations) factors (www.cancer.org). Cancer development and progression is a complex process that involves the acquisition of functional and genetic abnormalities. Fourteen years ago, Hanahan and Weinberg described the “hallmarks of cancer” that were considered as essential capabilities shared by most cancer cells to drive malignancy. In 2011, due to intensive research in cancer in the last decade, these properties were re-evaluated and expanded with the addition of two new hallmarks: metabolic reprogramming and evasion from immune destruction (*2*) (**Figure 2.1**).

Normal cells tightly regulate the balance between proliferation and death to ensure cell number homeostasis within a given adult tissue. In highly proliferative adult tissues, homeostasis is achieved by balancing proliferation with terminal differentiation, followed, or not, by programmed cell death. However, cancer cells deregulate the production and release of growth promoting signals that control cell proliferation and the entry into and progression through the cell cycle. In most cases, activation of oncogenes (growth promoting) and/or inactivation of tumor suppressor (growth inhibitory) genes lead to uncontrolled cell cycle progression and/or

inactivation of apoptotic mechanisms (*3*). Examples of oncogenes include growth factor signaling molecules (growth factors and receptors, signal transduction molecules like RAS, MAPK, etc.), transcription factors (e.g. MYC) and apoptosis inhibitors (e.g. BCL2). Tumor suppressor genes generally encode four classes of proteins, namely cell cycle regulators (e.g. Rb and p53), receptors or signal transduction molecules for paracrine factors that inhibit cell proliferation (e.g. transforming growth factor β (TGFβ)), proteins that promote apoptosis (e.g. BAX) and proteins that participate in DNA damage repair.

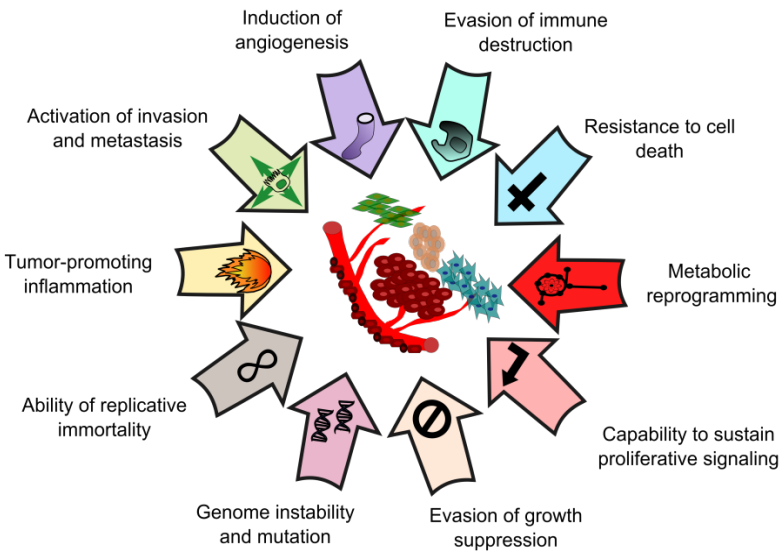

Figure 2.1 The hallmarks of cancer

The Hallmarks of cancer comprise ten capabilities required during a multistep tumor pathogenesis to enable cancer cells to become tumorigenic and ultimately malignant. Metabolic reprogramming, one of the emerging hallmarks, has been identified as a promising target for the treatment of cancer as there is a deregulation of bioenergetic controls that lead to an abnormal use of metabolic pathways to sustain their biosynthetic and energetic needs. Adapted from Hanahan, D. and R.A. Weinberg, Hallmarks of cancer: the next generation. Cell, 2011. 144(5): p. 646-74, Copyright© 2011, with permission from Elsevier.

In order to sustain uncontrolled proliferation, cancer cells reprogram and adjust their metabolism to fulfill the increased demand of energy and macromolecules. Alterations in oncogenes and tumor suppressor genes can drive the dependency of tumors on specific metabolic substrates, such as glucose and glutamine, as well as impose these changes on the wiring of metabolic pathways. However, it is important to note that metabolites themselves have been recognized as oncogenic by virtue of their capacity to alter cell signaling or block cellular differentiation.

During the multistep development of cancer, tumor cells may adapt to suppress the immune system's defense mechanisms and even prime immune cells to promote tumor growth. It is still unclear how tumor cells escape the immune system recognition but some studies propose a direct interference with the cells of the adaptive immune response through alteration of the tumor microenvironment (*4*).

Tumorigenesis occurs as a consequence not only of the deregulation of numerous gene networks and biochemical or signaling pathways, but also of many non-genetic factors, including tumor microenvironment stresses such as hypoxia, lactic acidosis or nutrient deprivation. The integration of these non-genetic factors within the genetic framework of cancer is the next logical step in understanding tumor heterogeneity. Research over the last few years has indeed elucidated that, many of the hallmarks of cancer delineated by Hanahan and Weinberg are provided by cells and components from the stroma, including endothelial cells, pericytes, fibroblasts, leukocytes and extra-cellular matrix (*5*). All these cellular and molecular interactions occurring in the tumor microenvironment are closely linked to the processes of angiogenesis and metastasis.

Angiogenesis has long been known to play a major role in supporting cancer cell growth and development. Once the tumor mass has reached a critical size, formation of a new and more extensive network of blood vessels to supply nutrients and oxygen to cancer cells and remove waste products is an essential step in allowing the tumor to expand and spread. Tumor cells and even cancer-associated fibroblasts (*5*) promote the angiogenic switch by providing angiogenesis inducing factors (mainly vascular endothelial growth factor (VEGF) and fibroblast growth factor (FGF)) and reducing the activity of angiogenesis inhibitory pathways (*6*). As the cancer progresses, the angiogenic process also offers a route for invasive tumor cells to disseminate directly, via the blood circulatory system, or indirectly, via the lymphatic system (*7*) and allow the establishment of metastasis to distant sites. A receptive microenvironment is required for tumor cells to engraft distant tissues and metastasize. Several studies have indicated the formation of a pre-metastatic niche (i.e. a site of future metastasis that is altered in preparation for the arrival of tumor cells) at the secondary sites before the primary tumor metastasizes (*8-10*), suggesting that metastatic cells are able

to adapt to their new metabolic environment, which can differ to a greater or lesser extent from the primary sites with respect to its nutrient and oxygen availability. Metastatic cells must exhibit a remarkable and dynamic flexibility that enables them to rapidly switch between metabolic states (*11*). In addition, the homeostasis of the metastatic sites can be disrupted as consequence of the metabolic activity of metastatic cells. This has been observed in bone metastases, where metastatic prostate cancer cells secrete glutamate to their extracellular environment as a side effect of cellular oxidative stress protection, promoting the development of pathological changes in bone turnover (*12*). Further studies are required to analyze these metabolic interplays between metastatic cells and tumor microenvironment in order to design more specific therapies.

The main focus of this thesis is the characterization of the metabolic reprogramming of two distinct cell subpopulations, which will be described below, endowed with different capabilities to carry out the processes of invasion and metastasis. Recent discoveries linking specific metabolic alterations to cancer development have strengthened the idea that altered metabolism is more than a side effect of malignant transformation, and may in fact be a functional driver of tumor growth, progression and metastasis in some cancers. In the following sections, the processes of invasion and tumor metastasis will be covered in depth and subsequently the importance of specific metabolic alterations associated with cancer development and the relevance of their study will be described.

2.2 INVASION AND METASTASIS

Metastasis represents the most life-threatening aspect of tumorigenesis and is the leading cause of death by cancer. In recent years, intensive research in this field has shed light on some of the molecular strategies employed by metastatic cells to leave the primary tumor, disseminate and grow new colonies in distant organs (*13*). The process initiates when motile tumor cells invade and break through the basement membrane and extracellular matrix and intravasate into the bloodstream or the lymphatic circulation. Then tumor cells are transported along vessels and finally arrive to a new location, where they extravasate, and only those metastatic cells that are

able to survive and proliferate successfully will establish a secondary tumor (metastasis).

The molecular cross-talk between tumor cells and their stroma contributes to the complex multistep process of the metastasis cascade and it starts from the very beginning with the local invasiveness. Before tumor cells breach the basement membrane to initiate invasion, they release angiogenic factors to stimulate endothelial cells of nearby blood vessels (*14*) to establish a vascular network for transport of nutrients to and removal of waste products from the tumor site. Moreover, the blood vessels within the tumor's vicinity can provide a route for detached cells to enter the circulatory system and metastasize to distant sites (*15*). The deregulated expression of cell adhesion molecules (CAMs) that mediate cell-cell and cell-non-cellular interactions results in the dissociation of cells from the primary tumor, changes in cell polarity and a gain of a cell motile phenotype (*16*). Among these CAMs, integrins and selectins have evidenced their key role in the malignant progression of various cancer types, including colon, lung and melanomas (*17*). Moreover, cadherins, immunoglobulin-like-cell-adhesion molecules, the hyaluronan receptor CD44 and integrins can modulate signal-transduction pathways by interacting with molecules such as receptor tyrosine kinases, components of the Wnt signaling pathway and Rho-family GTPases (*18*). Besides changes in cell adhesion molecules, tumor cells and inflammatory cells within the reactive stroma release proteases that degrade components of the extracellular matrix and also contribute to the activation (through proteolytic cleavage) of chemokines and growth factors, present in an inactive form, further contributing to local invasion and phenotypic changes in tumor cells (*19*). Some of the inductive signals released by the reactive stroma activate and promote an epithelial-mesenchymal transition (EMT) in tumor cells. This biological process is physiologically used for wound healing in mature organisms and plays critical roles in early embryonic morphogenesis (*20*). The importance of EMT in the metastatic cascade will be presented below.

2.2.1 Role of the epithelial-mesenchymal transition in the acquisition of motility

Most human solid tumors are carcinomas that originate from epithelial cell types throughout the body. As mentioned earlier, in order for carcinoma cells to break away

from neighboring cells and start invasion, they must lose cell-cell and cell-non-cellular adhesions and acquire a motile phenotype. Tumor cells achieve these changes by shedding many features of their epithelial phenotype and acquiring the morphology and gene expression pattern of mesenchymal cells, with enhanced migratory and invasive capabilities (*21*). The activation of an EMT program is mainly prompted by 1) genetic and epigenetic changes sustained during tumor formation that make tumor cells responsive to EMT-inducing factors and 2) inductive signals released by the reactive stroma that cause tumor cells to enable their EMT program.

EMT is characterized by the combined loss of epithelial cell junction proteins, incuding E-cadherin, α-catenin, claudins, occluding and zonula occludens protein 1, and an increased expression of mesenchymal markers, such as N-cadherin, vimentin and fibronectin (*22-23*). The most salient hallmark of EMT in many invasive carcinomas is functional loss of E-cadherin and/or repression of the gene encoding this protein (*24*), frequently accompanied with an induction of the "cadherin switch", by which the expression of E-cadherin is replaced by the expression of N-cadherin (*25*).

The induction of an EMT program is, in part, initiated by growth factors, including hepatocyte growth factor, epidermal growth factor and TGFβ. These factors induce downstream activation of several EMT-inducing transcription factors including Snail, Slug, Twist1 and zinc finger E-box binding homeobox 1 (Zeb1) and 2 (Zeb2) (*26-28*). Several of these transcription factors directly repress E-cadherin transcription. In addition to the direct effects of EMT transcription factors on gene expression, changes at the RNA level regulate EMT progression. Certain miRNAs regulate the epithelial phenotype and EMT (*29*), including members of the miR-200 family and miR-205 that inhibit the translation of ZEB1 and ZEB2 mRNAs (*30*) (*31*). Also, miR-29b and miR-30a inhibit SNAIL1 expression, reverting the EMT phenotype (*32*) (*33*). On the other hand, EMT is characterized by extensive differences in the splicing of specific RNAs, responsible for the generation of diverse proteins isoforms in mesenchymal cells as compared to epithelial cells. During EMT, many of the changes at the level of splicing result from the rapid downregulation of the expression of the epithelial splicing regulatory proteins 1 and 2, resulting in mesenchymal protein isoforms that help to define alterations in adhesion, motility and signaling pathways (*34*). Additional factors

in the tumor microenvironment facilitate the initiation of EMT, exemplified by hypoxia, which can induce EMT in carcinoma cells via activation of either Snail (*35*) or Twist1 (*36*).

Although EMT represents a process of fundamental importance conducive to tumor dissemination and metastatic spread of cancer cells, there are evidences to suggest that many invasive and metastatic carcinomas do not undergo a complete transition to a mesenchymal phenotype or even lack signs of EMT. Well-differentiated epithelial morphology has been identified in several invasive tumors (*37*) and within secondary metastatic lesions (*38*). Due to differences in cellular responses, not all the cell types within a tumor may promote in the same way signal transduction cascade that initiate EMT, resulting in partial or incomplete EMT (**Figure 2.2**). Furthermore, a reversible EMT model has been proposed to describe the transient activation of the EMT program that carcinoma cells undergo during tumor metastasis (*39*). This suggests that after their initial dissemination, the tumor cells that have acquired a mesenchymal phenotype may need to reverse to an epithelial identity via a mesenchymal-epithelial transition (MET) in order to regain the ability to proliferate and form epithelial growths in distant organ sites. This is in agreement with the observations that E-cadherin is often detected in distant metastases, which may derive from cells that have previously undergone an EMT (*40*). Finally, although malignant cells may disseminate from primary tumors mainly as individual mesenchymal-like cells, multicellular aggregates or clusters are also found (**Figure 2.2**). This process, known as collective migration, is characterized by clusters of epithelial cells that detach from the site of the primary tumor and migrate as independent aggregates through the adjacent extracellular matrix. Interestingly, a recent study that modeled the dynamics of EMT-activated cell migration, found that the induced EMT cell population initially exhibited >95% mesenchymal phenotype, including N-cadherin, fibronectin and vimentin, as well as reduced expression of E-cadherin and occlusion, but only around 16% of mesenchymal cells were observed eventually to migrate individually. This mismatch between initial and final phenotypes for migratory behaviors and biomarker expression was consistent with an intermediate level of phenotypic plasticity. Cells may exhibit dynamic behaviors, permitting reversion to an epithelial phenotype or maintaining a

mesenchymal phenotype (*41*).

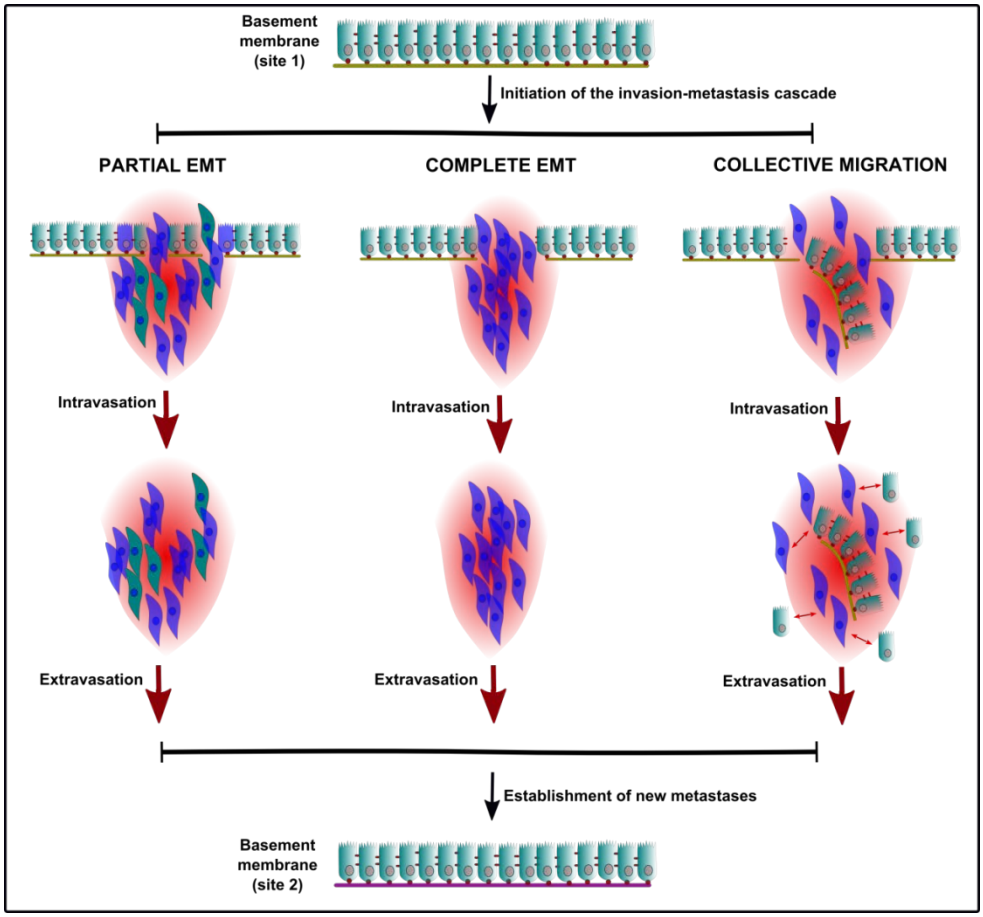

Figure 2.2 Mechanisms driving cell invasion and migration

During the initiation of the invasion-metastasis cascade, epithelial cells can increase their invasiveness by transdifferentiation into a motile mesenchymal phenotype via a complete or partial EMT. Epithelial cells can also adopt increased invasiveness yet retaining well-differentiated morphology and cohesiveness. In this case, cells can invade surrounding tissues and metastasize by collective migration. Invading cells intravasate into blood or lymphatic vessels to enter the circulation. Subsequently, surviving cells extravasate and colonize new metastatic sites, where cells that have undergone progressive steps of EMT can revert to a well-differentiated epithelial phenotype. EMT, epithelial-mesenchymal transition.

2.2.2 Tumor heterogeneity: cancer stem cells (CSCs), circulating tumor cells (CTCs) and metastatic stem cells (MetSCs)

Within the last few years several concepts have evolved that provide possible mechanisms and sources of tumor heterogeneity and how tumors become metastatic and therapy resistant, finally resulting in tumor relapse and a poor patient outcome (*42*). Currently there are two models that explain tumor cell heterogeneity: 1) the hierarchical cancer stem cell (CSC) model, where self-renewing CSCs sustain the entire

tumor population by giving rise both to progenitor cells that are capable of self-renewal and also to differentiating clones with more limited self-renewal potential that contribute to overall tumor heterogeneity, and 2) the stochastic (tumor microenvironment-driven) model in which cancer cells evolve clonally, and virtually every single cell can self-renew and propagate tumors. In this model, the self-renewal capability of each cell is determined by distinct signals from the tumor microenvironment. Recent studies have suggested that tumor heterogeneity may exist in a model that combines both the CSC and the stochastic models (*43*). Although these models may explain tumor cell heterogeneity through epigenetic mechanisms, it should be emphasized that tumor cell heterogeneity is also a result of genetic drift caused by the sequential acquisition of mutations that promote the aggressiveness and metastatic potential of derivative cancer cells. Tumor cells subpopulations generated either by clonal genetic mutations or as a result of epigenetic changes may display features of CSCs, or not, in which case they are generically defined as neoplastic non-CSCs.

CSCs, also known as tumor initiating cells (TICs), are endowed with high tumorigenic capacity, display strong self-renewal and survival properties, and may be the cells that drive tumor formation, maintain tumor homeostasis and mediate tumor metastasis (*44*). Despite studies demonstrating that the EMT can induce non-CSCs to enter a CSC-like state (*45-48*) other cell models show that epithelial CSCs, and not the mesenchymal EMT-derived cells, are able to survive in the circulation and form distant metastasis (*49*). In fact, an alternative “cooperative” model proposes a supporting role for tumor cells that have undergone EMT to aid metastasis. By mixing uniquely labeled epithelial and mesenchymal tumor cells to generate primary tumors, Tsuji et al. (2008) reported that epithelial cells require the cooperation of mesenchymal cells to lead the way for intravasation and CSCs generation. Also Celià-Terrassa et al. (2012) showed that collaboration between TICs displaying an epithelial phenotype and cells having undergone EMT accelerated metastatic colonization by the TICs. These studies suggest that epithelial and mesenchymal tumor cells may cooperate to successfully form metastatic tumors (*50*). Although different degrees of EMT and mechanisms for migration have been proposed (commented in the previous Section) to show the

coexistence of epithelial and mesenchymal cells along the metastatic process, how the EMT and CSC programs overlap remains controversial.

The features of stemness that characterize the CSC phenotype, rather than being a fixed entity, is a plastic quality of tumor cells that can be lost and gained, or expressed to different degrees (*51-52*). It has been shown that CSCs in squamous cell carcinoma switch between preferentially migratory or proliferative phenotypes (*53*), leading to the theory of the existence of stationary and migratory CSCs and to the connection with circulating tumor cells (CTCs). CTCs are those tumor cells that penetrate the blood and lymphatic vessels, enter the circulation (intravasation) and survive. From this entry point, CTCs move away from the primary site and circulate within the vessels, a hostile environment due to the resistance provided by the immune system and the mechanical stresses of blood flow. The identification of these cells is a prognostic factor associated with the evolution of tumors and progression to metastasis (*54-55*). CTCs will eventually extravasate in distant organs and after escaping from the circulation, they will have to survive, proliferate and finally develop a secondary tumor at distant sites. This complex process also requires the integration of multiple factors and events, such as tumor invasion, angiogenesis and the interaction between tumor cells and the local microenvironment at a distant site. However, not all CTCs are endowed with tumor-initiating cell potentials and, indeed, most of them are largely in a nonproliferative quiescent state. This cell trait confers CTCs with resistance to antiproliferative treatments (*56*) and protection against chemotherapy that would kill the primary tumor cells (*57*).

Thus, the concept of metastatic stem cells (MetSCs) refers to those CTCs with the ability to reinitiate macroscopic tumor growth in a distant tissue (*58*). To achieve this, MetSC must promote cell survival and antiapoptotic pathways as well as preserve their self-renewal potential. It has been shown that the PI3K/Akt/mTOR signalling cascade plays key roles in widely divergent physiological processes, including cell survival of disseminated cancer cells in a foreign and hostile environment. Src confers survival advantages to breast cancer cells in the bone microenvironment by amplifying the responsiveness of the PI3K/Akt survival pathway to CXCL12 and insulin-like growth factor 1 and antagonizing TRAIL-induced apoptosis (*59*). Moreover, activation of the

PI3K/Akt/mTOR pathway in prostate cancer radioresistant cell lines is associated with enhanced EMT and CSC markers (*60*). Notch and Wnt molecular pathways promote self-renewal within stem cell niches and are also involved in supporting the metastasis-initiating capacity of MetSCs. Tenascin C and periostin, which are extracellular matrix molecules, were demonstrated to regulate key signaling pathways involved in the maintenance of cancer stem cell features and the activity of Wnt and Notch pathways (*61*). Tenascin C and periostin are involved in the formation of lung metastasis in breast cancer (*61*).

The predilection of MetSC (from the primary CSCs or from CTCs, as their origin is not exactly known) to establish and form metastases preferentially in one or another organ site (organotropism) has long been noted. As described in Stephen Paget's seed and soil hypothesis, a receptive microenvironment ("soil") is required for tumor cells ("seed") to engraft distant tissues and form metastasis. Paget revealed in his analysis a non-random pattern of metastasis in visceral organs and bones and concluded that metastases formed only when the seed finds compatible soil (*62*). For example, breast cancers often spread to the lungs, liver and brain, while prostate cancers usually head for the liver and the bone (*63-64*). As a result of prior communication between the growing tumor and the site of metastasis, there are early changes in secondary organs which occur before tumor cells arrive and create what is known as the pre-metastatic niche. Several studies have shown the crucial role of bone marrow-derived cells in priming distant tissues for tumor metastasis and how cells of hematopoietic lineage populate distant organ tissues prior to the arrival of the tumor cells, preparing the premetastic microenvironment (*8-10*).

2.2.3 Types of metastasis and the need for EMT and MET

As discussed above, the involvement of EMT during metastasis is likely to be dynamic, as CSCs display a cellular plasticity that enables them to transition between epithelial-like and mesenchymal-like states. However, it is a matter of debate how subsequent MET fits into the metastatic process and whether a MET is essential. As proposed in (*65*), two different types of metastasis can be established: 1) metastases with a differentiated phenotype that retain the hierarchical organization of the primary

tumor and 2) metastases with an undifferentiated phenotype and with a permanent EMT and stemness-like state. In type 1 metastasis, the resulting macrometastases are largely epithelial. This raises the question of why tumor cells need to revert to an epithelial state in order to successfully grow. First, the mesenchymal-like state is associated with relative quiescence and high invasive capacity, whereas the epithelial-like state is associated with establishment of cell polarity and extensive proliferation. Second, some studies have shown that induction of EMT by Snail and Zeb2 directly represses cell division by inhibiting cyclin D activity (*66-67*) and that activation of Twist1 is associated with reduced tumor cell proliferation (*68*), indicating that reversion of EMT may be required to provide such growth advantage. Similarly, several miRNAs involved in regulating the EMT also exert control over the CSC state, including those of the miR-200 family (*69*). The absence of EMT-inducing signals or the presence of MET-inducing signals at distant sites are two scenarios that could explain how the reversion of the EMT program takes place. There are evidences that suggest that the metastatic niche could regulate epithelial-mesenchymal plasticity and promote lung colonization by inducing MET (*70*). Also, the importance of the tumor microenvironment in modulating the plasticity of epithelial and mesenchymal CSCs for successful metastatic colonizaton has been observed in breast cancer (*71*).

In type 2 metastases, undifferentiated metastases can be established from 1) an undifferentiated primary tumor (intrinsic subtype) or 2) a differentiated primary tumor (induced subtype). In this case, phenotypic plasticity is not evident and genetic alterations are proposed to be the major driving force. In both subtypes the most prominent examples are found among breast cancers, where highly aggressive tumors (such as the claudin-low and basal-type breast cancer) exhibit a normal mammary stem cell gene profile and thus contain high numbers of intrinsic CSCs, whereas luminal-type breast cancers correlate with a mature mammary luminal cell phenotype and contain low numbers of intrinsic CSCs (*72-74*). In the intrinsic subtype, CSCs are likely to exist in primary tumors from the very early stages of tumorigenesis and may be the oncogenic derivatives of normal-tissue stem or progenitor cells. Interestingly, for the induced subtype, the most likely and relevant cause for the switch from a differentiated to an undifferentiated tumor is treatment with rounds of chemotherapy

and acquired resistance to therapy (*75*). This can result in the selection of genetic alterations that allow cells to maintain stem cell features (e.g. drug resistance and self-renewal) and sustained uncontrolled proliferation, without a need to re-differentiate, and become the sources for primary tumor recurrence and metastasis (*76*).

2.2.4 Targeting EMT and CSC phenotypes in tumor metastasis

Over the last few years, the process of metastasis and the deciphering of its mechanisms have received increasing attention from researchers. Different therapeutic strategies are followed to face metastatic cancer, including systemic therapy (chemotherapy, biological therapy, targeted therapy and hormonal therapy), local therapy (surgery, radiotherapy), or a combination of both. In order to choose the most appropriate treatment, it is not sufficient to simply characterize the primary tumor (size, location and number of metastatic tumors) but it is essential to analyze those cells that have participated in the invasion-metastasis cascade. Our comprehension of the pathways that orchestrate the metastatic process has evolved and increasing knowledge in gene and phenotypic expression, cellular behavior and biological events in the spread paths of cancer cells, allows new prospects of transferring some of these observations to the clinical practice for improved diagnosis, prognosis and treatment of the metastatic disease.

Conventional chemotherapies can often eliminate the rapidly proliferating cells and the differentiated tumor mass, but fail to eradicate the intrinsically resistant CSCs, inadvertently leading to the expansion of the CSC pool, finally causing tumor relapse. For instance, an enrichment of cells with CSC markers ($CD44^{+}CD24^{low}$) was observed after 12 weeks of treatment of breast cancers with neoadjuvant chemotherapy (*77*). Thus, the acquisition of stem cell-like properties confers cells with enhanced survival and increased resistance to drugs (*78*) as well as resistance to inducers of apoptosis and senescence (*79-80*).

Taken together, the findings that link EMT and CSC traits to drug resistance and enhanced metastatic potential suggest that targeting the EMT/CSC phenotype may hold considerable therapeutic promise. For instance, to selectively target CSCs, cell surface marker expression phenotyping could be used for antibody-directed therapy to

target proteins such as CD133, CD44 or epithelial cell adhesion molecule (*81*). Another strategy has emerged from high-throughput compound screening efforts. A study carried out by Gupta and colleagues identified the antibiotic salinomycin to selectively kill CSCs generated by EMT. I*n vitro* pretreatment of CSCs with salinomycin reduced their ability to initiate tumors and lung metastasis in non-obese diabetic/severe combined immunodeficient mice and, in addition, this antibiotic induced the differentiation of mesenchymal-like cancers *in vivo* (*82*). The modulation of biomarkers that control EMT and MET also offers interesting strategies for therapy. In this line, depletion of Zeb1, either chemically or by RNAi, in mesenchymal-like cells results in a partial reversion to an epithelial phenotype and a gain in drug sensitivity (*83-84*).

Combined therapies have been proven to be more effective, enabling the possibility of targeting different cell properties of the tumor bulk, such as self-renewal, survival and drug resistance. *In vitro* and preclinical treatments studies are currently being carried out to find combinations of drugs that selectively target signaling pathways that are active in stem and progenitor cells, such as the Wnt (*85*), Hedgehog (*86*), Akt-mTOR (*87*) and Notch (*88*). Recently, it was shown that the combination of metformin and the DNA-damaging agent doxorubicin reduced tumor mass and prevented relapse more effectively than either drug alone in a xenograft mouse model (*89*). Interestingly, independent studies demonstrated that metformin reduced the expression of the EMT regulators Zeb1, Twist1, Slug and TGFβ, decreased the proportion of $CD44^{+}CD24^{low}$ cells and prevented mammosphere formation in claudin-low MDA-MB-231 breast cancer cells (*90*).

2.3 TUMOR METABOLIC REPROGRAMMING

The overall process through which living systems (cells or organisms) obtain energy and reducing power from its environment and synthesize the building blocks and macromolecules for their structures is carried out by a highly integrated network of chemical reactions collectively known as metabolism. All these chemical reactions are organized into various enzyme-powered pathways. Enzymes are protein catalysts finely regulated by inhibitor and activator molecules in order to supply the cellular needs. Metabolic reactions are in balance between the breaking down of complex

molecules and energy release to make adenosine triphosphate (ATP) (catabolic pathways) and the energy-consuming processes for the synthesis of new macromolecules (anabolic pathways). Metabolism is regulated by signaling pathways closely linked to the control of cell proliferation and differentiation. Catabolic and anabolic demands vary in different cell types. More specifically, to sustain high proliferation rates, cells often take up nutrients in excess of bioenergetic needs and shunt metabolites into biosynthetic pathways to allow a rapid increase in cell number and an efficient synthesis of all the internal structures for the new daughter cells. The uncontrolled and often rapid proliferation that characterize tumor cells can be supported by a broad rewiring of cellular metabolism that constitutively activates the uptake and metabolism of nutrients that promote continuous growth, survival, invasion, metastasis and resistance to cancer treatments. As mentioned above, metabolic reprogramming has been recognized as one of the ten hallmarks of cancer (*2*), modulated by several oncogenes and tumor suppressors (*91*) and yielding metabolites that can act as oncometabolites and alter cell signaling and block cellular differentiation (*92*).

Some of the most striking changes that characterize tumor metabolic reprogramming include elevation of glycolysis, induction of the pentose phosphate pathway (PPP), upregulation of the lipid and amino acid metabolism, enhancement of mitochondrial biogenesis and increase in glutaminolytic flux (*93*). Some of these reactions and other examples of tumor metabolic reprogramming are shown in **Figure 2.3**. The first investigator to provide evidence for the metabolic role of metabolism in cancer was Otto Warburg, who, almost 90 years ago, noted that rapidly proliferating ascites tumor cells consume glucose at a surprisingly high rate compared to normal cells and secrete most of the glucose-derived carbons as lactate rather than oxidizing pyruvate in the mitochondria, even under aerobic conditions, a phenomenon known as the “Warburg effect” (*94*). Warburg originally proposed that mitochondrial malfunction resulted in an increase in aerobic glycolysis to meet the energy and biosynthetic demands of cancer cells. However, it was determined later that cancer cells with intact mitochondria also showed evidence of the Warburg effect, suggesting that the preference for the glycolytic pathway benefits cancer cells at the level of bioenergetics

and biosynthesis as well as protects cells from oxidative stress that can result from mitochondrial oxidative metabolism (*95*).

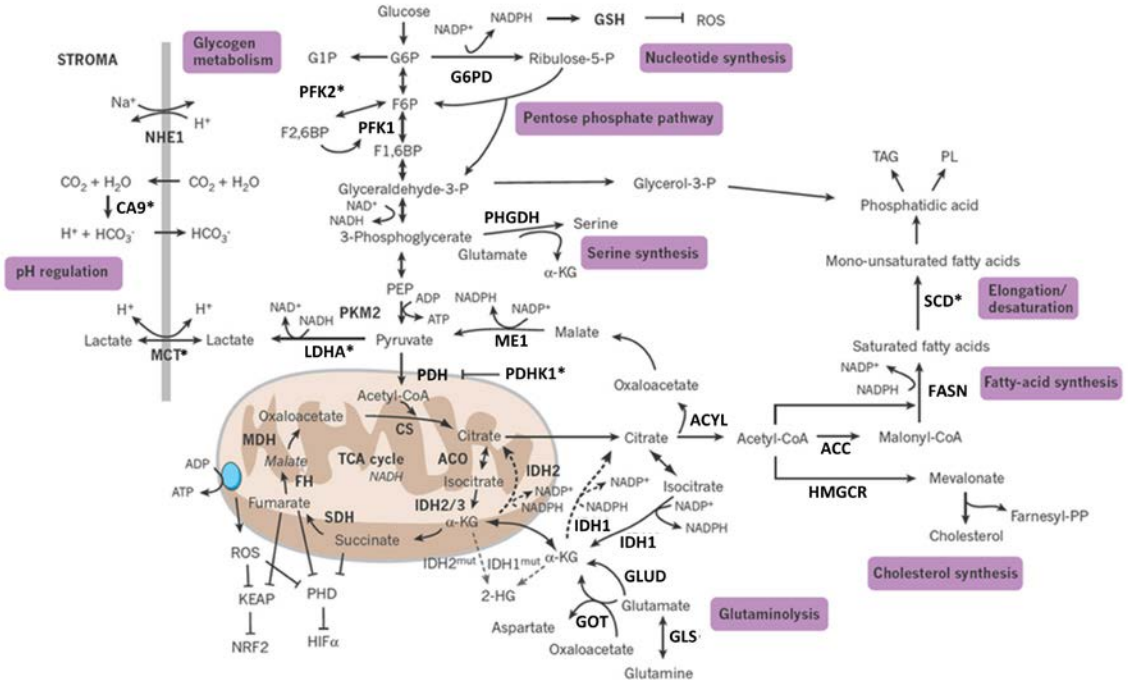

Figure 2.3 Main metabolic pathways involved in tumor metabolic reprogramming

The illustration depicts an overview of the major metabolic pathways involved in the synthesis of macromolecules: nucleotide synthesis, the pentose phosphate pathway, serine synthesis, glutaminolysis, cholesterol synthesis, fatty acid synthesis and elongation/desaturation of fatty acids. The enzymes involved in these pathways are shown in bold and those induced in response to hypoxia are marked with an asterisk. Reductive carboxylation of α-KG by IDH1 and IDH2 produces citrate for lipid synthesis (black dashed arrow). ACC, acetyl-CoA carboxylase; ACYL, ATP citrate lyase; ACO, aconitase; CA9, carbonic anhydrase 9; CoA, coenzyme A; CS, citrate synthase; FASN, fatty acid synthase; F1,6BP, fructose-1,6-bisphosphate; F2,6BP, fructose-2,6-bisphosphate; F6P, fructose-6-phosphate; FH, fumarate hydratase; GLS, glutaminase; GLUD, glutamate dehydrogenase; GOT, glutamic-oxaloacetic transaminase; GSH, glutathione; G1P, glucose-1-phosphate; G6P, glucose-6-phosphate; G6PD, glucose-6-phosphate dehydrogenase; HIF, hypoxia inducible factor; HMGCR, 3-hydroxy-3-methylglutaryl-CoA reductase; KEAP, kelch-like ECH-associated protein 1; LDHA, lactate dehydrogenase A; MCT, monocarboxylate transporters; MDH, malate dehydrogenase; ME1, malic enzyme 1; NHE1, Na^+/H^+ exchange protein 1; NRF2, nuclear factor (erythroid-derived 2)-like 2; PDH, pyruvate dehydrogenase; PDHK1, pyruvate dehydrogenase kinase; PEP, phosphoenolpyruvate; PFK, phosphofructokinase; PHD, prolyl hydroxylases; PHGDH, phosphoglycerate dehydrogenase; PKM2, pyruvate kinase M2; PL, phospholipids; ROS, reactive oxygen species; SCD, stearoyl-CoA desaturase; SDH, succinate dehydrogenase; TAG, triacylglycerides. Adapted by permission from Macmillan Publishers Ltd: Nature. Schulze, A. and A.L. Harris, How cancer metabolism is tuned for proliferation and vulnerable to disruption. Nature, 2012. 491(7424): p.364-73, Copyright ©2012.

Nevertheless, tumor metabolic reprogramming is not limited to glycolytic metabolism enhancement, and should be considered as a dynamic interplay among the different pathways that constitute the metabolic network. In addition, potent oncogenes such as MYC, HIF-1α, Ras and PI3K/Akt are important promoters of cancer metabolic alterations whereas tumor suppressors such as p53 and liver kinase B1/AMP-activated protein kinase (LKB1/AMPK) antagonize those changes and keep cellular metabolism in check (*96-97*). A myriad of metabolic enzymes and pathways are waiting to be explored as targets for cancer therapy (see **Appendix 3**). In the following pages some bioenergetic and biosynthetic metabolic pathways will be described, with special emphasis on their relevance in tumor progression and metastasis.

2.3.1 Glycolysis: bioenergetics and biosynthetic pathways

2.3.1.1 Glycolysis and the Warburg effect

As mentioned in the previous Section, cancer cells predominantly produce energy via enhanced glycolysis regardless of whether they are under normoxic or hypoxic condition (*98*). The metabolism of glucose exclusively through aerobic glycolysis is far less efficient than mitochondrial oxidative phosphorylation (OXPHOS), as the former process generates fewer ATP molecules per unit of glucose (2 molecules *vs*. 36 molecules, respectively). Thus, a high rate of glucose uptake and utilization is required to meet the increased energy needs involved in supporting rapid tumor progression. In fact, the higher glucose uptake observed in cancer cells has been widely exploited in Positron Emission Tomography (PET) imaging using radiolabeled glucose analogs such as ^{18}F-fluorodeoxyglucose as a tracer to visualize tumors (*99*). Additionally, PET allows the tracking of metastatic cells with an accuracy >90%. These findings indicate the close relationship between the Warburg effect and the invasiveness and metastatic potential of tumor cells (*100*).

Many reports have shed light on the benefits and selective advantages of favoring glycolysis over mitochondrial oxidation (*101*). As a consequence of accelerating the glycolytic pathway, ATP production from glycolysis can exceed the amount produced from OXPHOS (*102-103*) and attain levels that are sufficient to meet intracellular

demand and confer a selective advantage to cancer cells. Another important feature of the Warburg effect is the high amount of lactate that is excreted to the extracellular media. Lactate production by the enzyme lactate dehydrogenase (LDH) allows the regeneration of NAD^+, which is essential for glycolysis to continue. Lactate is secreted to the tumor microenvironment via the monocarboxylate transporter 4, and can be uptaken via the monocarboxylate transporter 1 by other cancer cells or by non-neoplastic stromal cells (e.g. if different cancer cell subpopulations with distinct metabolic signatures coexist or when there are well-oxygenated and poorly oxygenated regions within the tumor) and used to feed the tricarboxylic (TCA) cycle for metabolism, a process known as "Reverse Warburg Effect" (*104*), commonly described for the symbiotic relationship between cancer cells and stromal cells (*105*). This symbiosis between lactate-producing and lactate-consuming cancer cells is an effective way for tumors to adapt to the diverse and constantly changing conditions as a result of the leaky and poorly formed tumor blood vessel network (*104, 106*). Furthermore, lactate production creates an acidic extracellular microenvironment that facilitates the activity of metalloproteases for breaking down the extracellular matrix, thus promoting cancer invasion and metastasis (*107*).

Importantly, glycolysis provides cancer cells not only with energy but also metabolic intermediates and precursors that are critical for the biosynthesis of macromolecules and therefore allow cells to increase their biomass and proliferate (*108*). Glycolysis is directly connected to the PPP, which results in the generation of NADPH and ribose-5-phosphate. Both NADPH and ribose-5-phosphate are essential for the biosynthesis of lipids and nucleic acids. In addition, NAPDH contributes to the maintenance of the cellular redox status. Metabolites from glycolysis are also important materials for amino acid production and protein synthesis, molecules required for sustaining active cell division.

Over the last few years, many studies focusing on mitochondrial function in cancer cells have suggested that the Warburg effect is more closely related to alterations in signaling pathways that control the uptake and utilization of glucose than to mitochondrial defects. The resulting high rate of glucose flux must be handled by increased levels or activities of metabolic enzymes, changes that can be accomplished

by oncogenes and tumor suppressor genes as well as regulators of the response to hypoxia. Activation of the PI3K/Akt pathway is probably one of the most important events that drive glycolysis and lactate production, the biosynthesis of biomolecules and the suppression of macromolecular degradation in cancer cells (*109*). Numerous cellular functions are mediated through the activation of Akt/PKB, downstream of PI3K, including metabolism, growth, proliferation, survival, protein synthesis, apoptosis and angiogenesis, the latter being a central event for tumor progression and metastasis (*110*). The mTOR kinase also integrates signals from the PI3K/Akt pathway and senses the energetic and nutrient status to regulate cell growth and proliferation (*111*). PI3K/Akt activation enhances the expression of surface glucose and amino acid transporters, stimulates hexokinase 1 (HK1), hexokinase (HK2) and phosphofructokinase (PFK) activities and is also able to activate the hypoxia inducible factor 1 (HIF-1) transcription factor complex through the upregulation and stabilization of the HIF-1α subunit, even in normoxia. As a result, HIF-1 potentiates even more the enhancement of glycolysis, by upregulating glucose transporters (GLUT1, GLUT3), glycolytic enzymes (HK1, HK2, PFK1, PFK2, aldolase A and C, glyceraldehyde-3-phosphate dehydrogenase (GAPDH), phosphoglycerate kinase 1, enolase 1, pyruvate kinase m2 isoform (PKM2) and LDH-A) and further promoting the conversion of pyruvate to lactate by activating pyruvate dehydrogenase kinase 1 (PDHK1), which in turn inhibits pyruvate dehydrogenase (PDH) activity (*112*). Moreover the oncogene MYC cooperates with HIF-1 and induces most of the glycolytic genes mentioned above (*113*). On the other hand, tumor suppressor genes which code for proteins that normally operate to restrict cellular growth and division or even promote programmed cell death (apoptosis) are usually silenced in cancer cells. For instance, AMPK is activated by LKB1 under stress conditions, such as hypoxia and nutrient deprivation, with a consequent halt in cell growth and attenuation of ATP-consuming processes (*114*). AMPK is also associated with the downregulation of glycolysis through the phosphorylation of PFK2 (*114*). Similarly, p53 represses the transcription of glucose transporters (GLUT1, GLUT4) and, through the upregulation of TIGAR, reduces the activity of fructose 2,6-bisphosphatase (*91*). Thus, loss of signaling pathways governed by tumor suppressor genes leads to the Warburg effect.

Another aspect to be considered is that glycolytic enzymes are not uniquely restricted to carry out glycolysis, as these proteins also contribute to tumor development, survival and, importantly, resistance to cell death (*115*). This is the case of nuclear localized LDH-A and GAPDH, which act as transcriptional coactivators, or for nuclear enolase 1, which acts as a transcriptional repressor. Another interesting example is provided by PKM2, that can translocate to the nucleus and modulate transcription factors, such as Oct4, that play important roles in the control of cell stemness and differentiation (*116*).

2.3.1.2 The pentose phosphate pathway

Cancer cells are highly dependent on the synthesis of nucleotides to maintain sufficient pools to support DNA replication and the production of RNA. Nucleotides consist of a nucleobase, a five-carbon sugar (ribose or deoxyribose), and one or more phosphate groups. The five-carbon sugar (pentose) is mainly synthesized through the PPP. The essentiality of the PPP lies not only in the production of pentose phosphates (ribose-5-phosphate) but also in the synthesis of reducing equivalents such as NADPH (*93*). This cofactor is involved in many essential biosynthetic pathways, acting as an electron source for the reductive synthesis of fatty acids and nucleic acids. Moreover, NAPDH is a key component in cellular antioxidant systems, participating in the reduction of glutathione, a major scavenger of reactive oxygen species (ROS). Classically, cytosolic NADPH is thought to be regenerated mainly via the PPP (*117*), although other potential sources of cytoplasmic NAPDH exist in cells, like those driven by malic enzyme (ME), isocitrate dehydrogenase (IDH), aldehyde dehydrogenase and methylene tetrahydrofolate dehydrogenase (*118-119*).

The PPP is divided into two branches: the oxidative branch and the non-oxidative branch. The oxidative branch consists of three irreversible reactions. In the first reaction, glucose-6-phosphate is transformed into NADPH and 6-phosphogluconolactone by the enzyme glucose-6-phosphate dehydrogenase (G6PDH), and this latter product is subsequently hydrolyzed by 6-phosphogluconolactonase to 6-phosphogluconate. The third reaction, catalyzed by 6-phosphogluconate dehydrogenase, oxidizes 6-phosphogluconate and yields a second NADPH and

ribulose-5-phosphate which is then converted to ribose-5-phosphate, one of the main building blocks of nucleic acids. A key enzyme of the oxidative branch of the PPP, G6PDH, has been found to be overexpressed in multiple cancers (*120-121*). More specifically, G6PDH was suggested as a biomarker for prostatic carcinoma (*122*), supported by recent studies indicating that both G6PDH levels and metabolism through the PPP are increased in prostate cancer (*123-124*). Some studies have demonstrated that silencing of G6PDH in tumor cell lines decreased cell proliferation and enhanced apoptosis (*125*), and that given its recognized importance as a supplier of reducing equivalents, G6PDH is crucial in protection against oxidative stress in mouse embryonic stem cells (*126*). The importance of G6PDH in the survival, proliferation and metastasis of tumor cells makes this enzyme a promising target in cancer therapy, as reviewed recently in (*127*).

The non-oxidative branch of the PPP comprises a series of reversible reactions by which pentose phosphates can be recycled into glycolytic intermediates, or synthesized from glycolytic intermediates to be used for *de novo* generation of ribose-5-phosphate for biosynthesis of nucleotides and nucleic acids. Briefly, a 2-carbon exchange between ribose-5-phosphate and xylulose-5-phosphate catalyzed by transketolase (TKT) produces glyceraldehyde-3-phosphate and sedoheptulose-7-phosphate. These two products generate erytrose-4-phophate and fructose-6-phosphate via a 3-carbon exchange by the action of the enzyme transaldolase. Next, TKT catalyzes again the 2-carbon exchange between a second xylulose-5-phosphate and erytrose-4-phosphate to yield glyceraldehydes-3-phosphate and fructose-6-phosphate, which can be either metabolized in the glycolytic pathway or reintroduced into the PPP. TKT, a key enzyme of the non-oxidative branch of the PPP, belongs to a family of genes that includes genes encoding TKT and two additional TKT isoforms, termed TKT-like 1 (TKTL1) and TKT-like 2. Due to the importance of the non-oxidative pathway in cancer, the contribution of all three TKT isoforms has been examined in cancer cells (*128*) and overexpression of TKTL1 protein has been found in many tumors (*129-133*). Similarly to the upregulation of the PPP generally associated with invasive and metastasizing tumors (*134*), high levels of expression of TKTL1 are correlated with tumor progression and represent an indicator of poor prognosis (*129, 135*). It has also

been demonstrated that silencing of TKTL1 by RNA interference (RNAi) suppressed the growth and proliferation of various tumor cell lines (*136-138*). Finally, it has been also hypothesized that this isoform could generate acetyl-CoA, which would link glycolysis and fatty acid synthesis through the non-oxidative PPP pathway (*128*).

Tumor cells characterized by their high proliferation rates predominantly use the non-oxidative PPP branch to synthesize ribonucleotides *de novo* for the synthesis of RNA and DNA (*139*), as demonstrated in ^{13}C-tracing experiments where a significant proportion of the labeled ribose isolated from nucleic acids in pancreatic adenocarcinoma cells (*140*) and lung cancer cells (*141*) was derived from the non-oxidative branch. In addition, the increased glycolysis and marked Warburg effect observed in many tumor cells can promote the use of the reversible non-oxidative branch (*142*). The PPP can be used by cancer cells for anabolism, to generate building blocks to sustain cell proliferation, or to bolster an antioxidant defense under conditions of oxidative stress (*143*). Given the versatility of the PPP pathway, achieved by the reversible nature of the non-oxidative branch, this pathway can be adapted to the cell demands regarding maintenance of redox homeostasis or need for nucleic acids to generate biomass (*144-145*). As summarized in **Figure 2.4**, in those conditions in which facing oxidative stress is a priority, the PPP is adapted to accelerate the oxidative branch and to direct the non-oxidative branch toward resynthesis of fructose-6-phosphate, which is converted back to glucose-6-phosphate, to be used again as a substrate for the oxidative branch to synthesize NAPDH molecules. However, in rapidly proliferating cells, both the oxidative and the non-oxidative branches can be diverted toward the generation of pentose phosphates. Therefore, depending on which mode is operating, the flux of glucose in glycolysis can be substantially altered. Ramos-Montoya *et al.* reported that the balance between the oxidative and non-oxidative activities was critical for cancer cell survival and vulnerability to anticancer therapies and that targeting specific enzymes from both branches, such as G6PDH and TKT, by using dehydroepiandrosterone (DHEA) and oxythiamine (OT), respectively, was a good strategy to efficiently promote tumor cell death (*146*). Additionally, the inhibition of CDK4 and CDK6 using calcein AM not only inhibits the progression of cell cycle but also exerts an antitumor effect through the

disruption of the balance between the oxidative and non-oxidative branches of the PPP (*147*) (see **Appendix 2**).

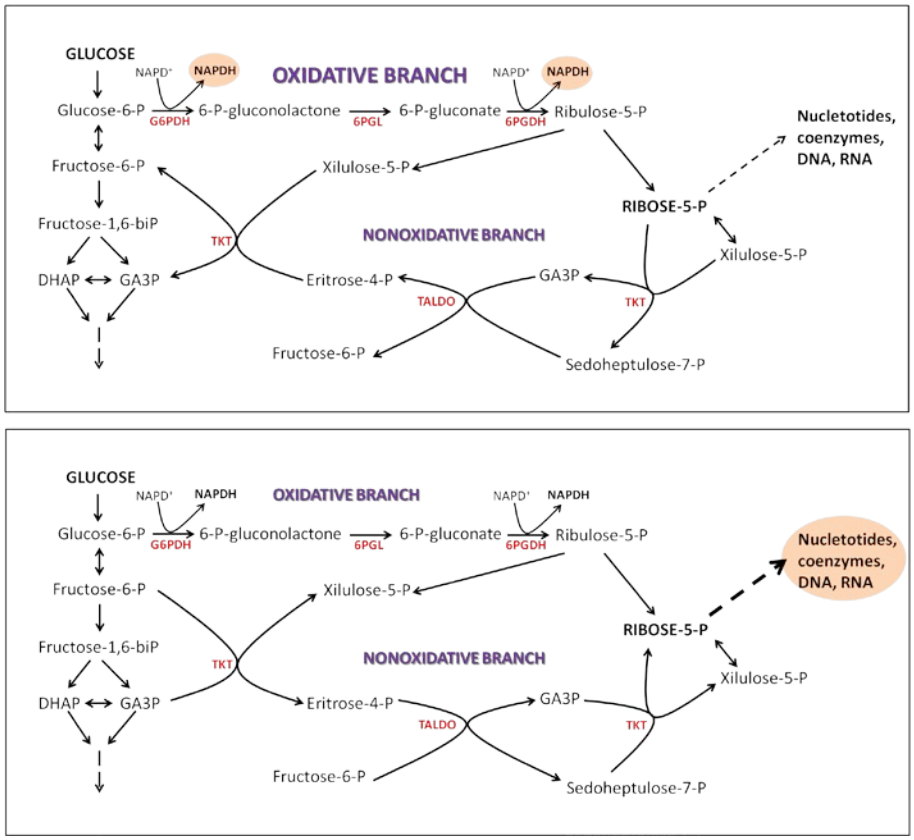

Figure 2.4 Flexibility of the oxidative and non-oxidative branches of the PPP

The PPP can be adapted to satisfy cell needs, such as reduction of the oxidative stress or supply of ribose-5-phosphate for biosynthetic purposes. When reducing equivalents are required to face oxidative stress, the oxidative branch is favored (upper panel) and ribose-5-phosphate is directed back to glycolysis via the reversible non-oxidative branch. The glycolytic intermediates obtained can produce glucose-6-phosphate again, which reenters the oxidative branch of the PPP. When rapidly proliferating cells have a high demand for biosynthetic precursors (lower panel), both the oxidative and the non-oxidative branches favor the synthesis of ribose-5-phosphate. P, phosphate; G6PDH, glucose-6-phosphate dehydrogenase; 6PGL, 6-phosphogluconolactonase; 6PGDH, 6-phosphogluconate dehydrogenase; TKT, transketolase; TALDO, transaldolase; DHAP, dihydroxyacetone phosphate; GA3P, glyceraldehydes-3-phosphate.

The PPP can be modulated allosterically, through its own catalytic products and other metabolites, and by oncogenes and tumor suppressor genes. It has been described that oncogenic transformation by KRAS promotes PPP and glycolytic fluxes because of simultaneous upregulation of G6PDH, pyruvate kinase (PK) and LDH (*148*). In addition, the K-Ras oncogene stimulates glycolysis and drives glycolytic intermediates into the non-oxidative branch in pancreatic ductal adenocarcinoma (*149*). Also, PI3K/Akt

signaling promotes anabolic metabolism through PPP by activating NRF2, involved in the response to cellular stress that activates G6PDH, among other enzymes (*150*). Finally, and to mention an illustrative example of the action of tumor suppressor genes, p53 suppresses the PPP by directly binding to G6PDH and repressing its enzyme activity (*151*).

2.3.1.3 Fatty acid synthesis

In rapidly proliferating cancer cells, there is an increased need for fatty acids to maintain a constant supply of lipids, as these biomolecules play essential biological functions. Fatty acids can be obtained either from dietary sources or intracellular synthesis. While most non-transformed cells rely on dietary-derived fatty acids to meet their biosynthetic and bioenergetic requirements, cancer cells upregulate many of the enzymes involved in *de novo* fatty acid synthesis, functionally related to the glycolytic pathway, in order to synthesize lipids for membrane formation and energy production via β-oxidation and lipid modification of proteins. Notably, the multi-enzyme complex fatty acid synthase (FASN) is highly expressed in many cancers (*152*). This enzyme synthesizes long-chain fatty acids by using acetyl-CoA as a primer, malonyl-CoA (obtained from the carboxylation of another acetyl-CoA, catalyzed by acetyl-CoA carboxylase) as a two-carbon donor, and NAPDH as a reducing equivalent. The predominant product of FASN activity is palmitate, a 16-carbon fatty acid. Further elongation and subsequent desaturation of *de novo* synthesized palmitate generates stearate and oleate, respectively. These reactions are carried out by elongases and desaturases that play an important role in regulating the length and degree of unsaturation of fatty acids and thereby their functions and metabolic fates (*153*).

The high levels of glycolysis observed in cancer cells can lead to an excessive buildup of pyruvate, which can be redirected toward *de novo* fatty acid synthesis. The key enzyme linking glucose metabolism to lipid synthesis is ATP citrate lyase (ACYL), which catalyzes the conversion of mitochondria-derived citrate to cytosolic acetyl-CoA. ACYL expression and activity have been found to be increased in many cancer cells (*154*) and its inhibition by RNAi or the chemical inhibitor SB-204990 decreased cell proliferation and survival of tumor cells displaying aerobic glycolysis (*155*). Hypothetically, as

mentioned in the previous Section, TKTL1 has been also suggested as a potential cytosolic acetyl-CoA source due to the distinct kinetic properties that allow this TKT isoform to catalize the monosubstrate reaction from xylulose-5-phosphate, releasing glyceraldehide-3-phosphate and acetyl-CoA (*128*).

Although the role of lipogenesis in providing proliferative and survival advantages to tumor cells is well known, more recently many studies have focused on the correlation between lipid metabolism and cancer progression to metastatic disease. Synthesis of fatty acids was revealed to be increased in highly invasive and metastatic ovarian cancer spheroid cells enriched for cells with stem cell-like characteristics (*156*) and inhibition of FASN has been demonstrated to decrease the tumorigenic and metastatic potential of colorectal cancer cells *in vitro* and *in vivo* (*157*). Furthermore, mutant p53 in ovarian cancer has been shown to interact with sterol regulatory element-binding proteins and guanidinoacetate N-methyltransferase, among others, leading to increased gene expression of enzymes involved in fatty acid and cholesterol biosynthesis, and favoring metastasis and EMT-like transition (*158*).

2.3.1.4 Amino acids metabolism

Amino acids play central roles both as building blocks of proteins and as intermediates in metabolism as a source of carbon and nitrogen for biosynthesis. Proteins, like DNA, RNA and lipids, are essential cellular components required for the generation of new daughter cells. Humans can synthesize only 11 of the 20 amino acids. The remainder amino acids, which are considered essential amino acids, must be supplied in the food.

Glycolytic intermediates are direct precursors for the biosynthesis of some amino acids. The intermediate 3-phosphoglycerate provides the carbons for cysteine, serine and glycine, whereas pyruvate provides carbons for alanine. On the other hand, oxalacetate and α-ketoglutarate, which are TCA intermediates, also allow the production of non-essential amino acids, such as aspartate, asparagine, glutamate and proline. Importantly, the efflux of these amino acids is only sustainable with the existence of anaplerotic reactions, whose function is to replenish the TCA cycle to maintain the availability of anabolic precursors. Some reports have shown the

involvement of the anaplerotic enzymes pyruvate carboxylase (PC) and glutaminase (GLS) in cancer (*159-160*) but further studies are warranted to assess the relevance of anaplerosis in tumor progression and metastasis.

The profile of tumor-specific glycolytic enzymes can favor amino acid synthesis from glycolysis (*117*). As an example, for the synthesis of serine, glycine and cysteine, the first reaction that comes from glycolysis requires the action of a NAD^+-dependent dehydrogenase that catalyzes the oxidation of 3-phosphoglycerate to 3-phosphopyruvate. Thus, as a consequence of the Warburg effect and the high levels of LDH expression and activity present in many cancer cells, lactate production and efficient regeneration of NAD^+ may benefit those biosynthetic reactions that rely on this cofactor. On the other hand, the enhanced expression of the PKM2 isoform in many cancers (*161*), which has a reduced enzymatic activity compared to the pyruvate kinase m1 isoform (*162*) but enables metabolic flexibility, has been shown to promote amino acid synthesis, among other biomolecules, to supply those cellular components required under nutrient stress. Interestingly, some reports have described a link between PKM2 activity and serine metabolism (*163*). PKM2, beyond its glycolytic role, has been proposed to interact with HIF-1α as a transcriptional coactivator in the nucleus and stimulate the expression of HIF-1 target genes, including GLUT1, LDH-A and PDHK1 (*164*), thus promoting glycolysis (and NAD^+ regeneration by LDH activity) and inhibiting OXPHOS.

Recent reports have shown the contribution of the non-essential amino acids serine and glycine in supporting tumor growth (*165*). Serine and glycine are involved in one-carbon metabolism, where folate and methionine cycles integrate nutritional status from amino acids, glucose and vitamins, generate diverse precursors for the synthesis of lipids, nucleotides and proteins, control the redox cell status and participate in methylation reactions. Serine is converted reversibly to glycine by serine hydroxymethyltransferase (cytosolic SHMT1 or mitochondrial SHMT2), a reaction that produces one-carbon units, which enter the tetrahydrofolate (THF) cycle. Glycine can also be cleaved by the mitochondrial glycine cleavage system to yield one-carbon units that are transferred to the THF cycle (*119*). The metabolic pathways of serine synthesis, one-carbon metabolism and the glycine cleavage system (**Figure 2.5**) have

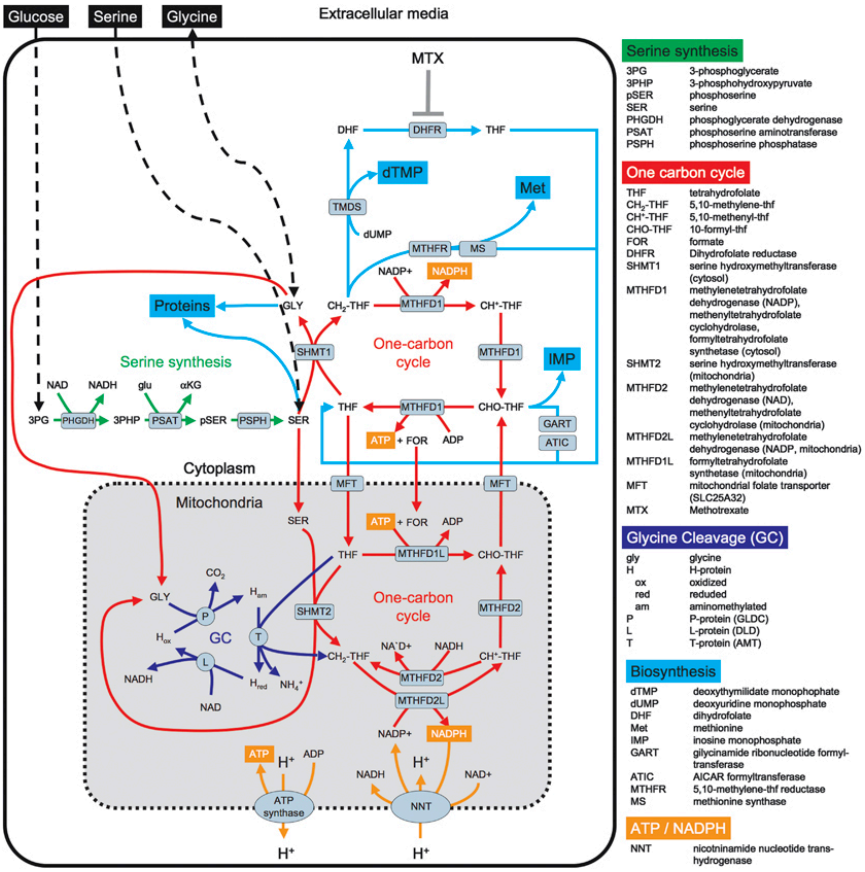

Figure 2.5 Serine synthesis, one-carbon cycle and glycine cleavage (GC) system

Schematic representation of the reactions involved in serine synthesis (green), one-carbon cycle (red) and glycine cleavage (GC) system (blue) and the crosstalk with other metabolic pathways. This is an open-access article distributed under the terms of the Creative Commons Attribution-NonCommercial-ShareAlike 3.0 Unported License. (http://creativecommons.org/licenses/by-nc-sa/3.0/)

been correlated with gene signatures of cell proliferation and MYC target gene activation (*166*). More specifically, Jain and coworkers showed that the mitochondrial, but not the cytosolic, glycine biosynthetic pathway correlates with the rate of proliferation of cancer cells (*167*) and demonstrated that silencing of the mitochondrial isoform SHMT2, but not SHMT1, decreased cell proliferation in highly proliferative cancer cell lines (*167*). Also, high levels of glycine decarboxylase (GLDC), a component of the glycine cleavage system, together with high expression of glycine C-acetyltransferase, SHMT1/2, 3-phosphoserine phosphatase and phosphoserine aminotransferase, were found in TICs in non-small cell lung cancer (*168*), suggesting that this tumor-initiating cell subpopulation relies on serine/glycine metabolism for tumorigenesis.

2.3.2 Mitochondrial metabolism

Mitochondrial metabolism is involved in multiple essential cell functions. Much of the cellular energy is generated within this highly compartmentalized organelle through a process termed oxidative phosphorylation (OXPHOS) and a number of cataplerotic and anaplerotic reactions from the TCA cycle take place there. Altered mitochondrial function has been related to diverse pathological conditions, including cardiovascular disorders, muscular degeneration, neurodegenerative disorders (*169*) and cancer (*170*). Mitochondrial metabolism contributes actively to the production of reactive oxygen species (ROS), essential for oncogenic-induced cell proliferation and tumorigenesis (*171*). In addition to their role in cellular metabolism, mitochondria regulate redox signaling to and from mitochondria (*172*), modulate calcium levels (*173*) and initiate cellular apoptosis (*174*).

2.3.2.1 TCA cycle and OXPHOS

There is a considerable body of evidence that challenges the classical Warburg hypothesis of the almost exclusively role of aerobic glycolysis in tumorigenesis and multiple investigators have demonstrated that mitochondria are indeed functional in most tumor cells (*175-177*) and their involvement in cancer cell metabolism is now well accepted (*178*). As cancer cells are in an altered metabolic state, it is likely that glycolysis and mitochondrial metabolism interchange in a wave pattern during the proliferation and transformation of cancer cells, constantly subjected to changes in their tumor microenvironment, with fluctuating hypoxia, low pH and nutrient deprivation (*179*).

OXPHOS is the mitochondrial metabolic pathway that allows cells to synthesize ATP from the oxidation of nutrients. During OXPHOS, electrons from NADH and $FADH_2$ molecules (electron donors) are transferred to electron acceptors, such as oxygen. These redox reactions are carried out by a series of protein complexes located in the mitochondrial inner membrane, and release energy which is used to form ATP. Different types of cancer displaying different states of differentiation display different reliance on glycolytic and mitochondrial ATP (*180*). The sensitivity of cells to the glycolytic inhibitor 2-deoxyglucose (2-DG) or to the OXPHOS inhibitor oligomycin can

help assess the dependencies of cancer cells on bioenergetic pathways (*181*). It is well known that glycolysis plays an important role in cancer energy metabolism, especially in hypoxic conditions, but many tumor cells use OXPHOS or a mixture of glycolysis and OXPHOS as a pathway for energy production (*182*), highlighting the importance of metabolic flexibility for cell survival. Importantly, the TCA cycle is a central pathway in the metabolism of nucleotides, lipids and amino acids (*183*). The reactions that constitute the TCA cycle are not exclusively mitochondrial as some TCA enzymes and intermediates are located also in the cytosol (*184*). **Figure 2.6** depicts the biosynthetic and bioenergetic reactions that result from the combination of the TCA cycle and OXPHOS metabolism.

The fact that cancer cells may retain TCA cycle and OXPHOS function does not mean that these cells have no defects in mitochondrial metabolism. Dysfunction of the TCA cycle due to mutations in several mitochondrial proteins, including aconitase, isocitrate dehydrogenase (IDH), succinate dehydrogenase (SDH) and fumarate hydratase (FH) is associated with some types of cancer (*185-186*). An abnormal expression and activity of aconitase, which catalyzes the isomerization of citrate to isocitrate in the TCA cycle, have been implicated in prostate tumorigenesis (*187*), resulting in increased mitochondrial activity in metastatic prostate counterparts compared to normal prostate epithelial cells (*188*). IDH converts isocitrate to α-ketoglutarate (α-KG). The nuclear genome encodes three IDH isoforms: IDH1 and IDH2, which are $NADP^+$-dependent isoforms, and IDH3, which is a NAD^+-reliant enzyme. IDH1 and IDH2 mutations have been identified in 70% of grade II-III glioma and secondary glioblastomas (*189-190*) as well as in patients with acute myeloid leukemia (*191*). To date there have been no reports of cancer-associated mutations in any of the IDH3 subunits. Mutated IDHs are unable to efficiently catalyze the oxidative decarboxylation of isocitrate and acquire a new enzymatic function which converts α-KG to the oncometabolite 2-hydroxyglutarate, which can contribute to the EMT phenotype (*192*) and tumor progression (*92*) SDH is a four-subunit enzyme complex that catalyzes the oxidation of succinate to fumarate in the TCA cycle with the simultaneously reduction of ubiquinone to ubiquinol in the electron transport chain. Inherited or somatic mutations in its subunits have been associated with several types

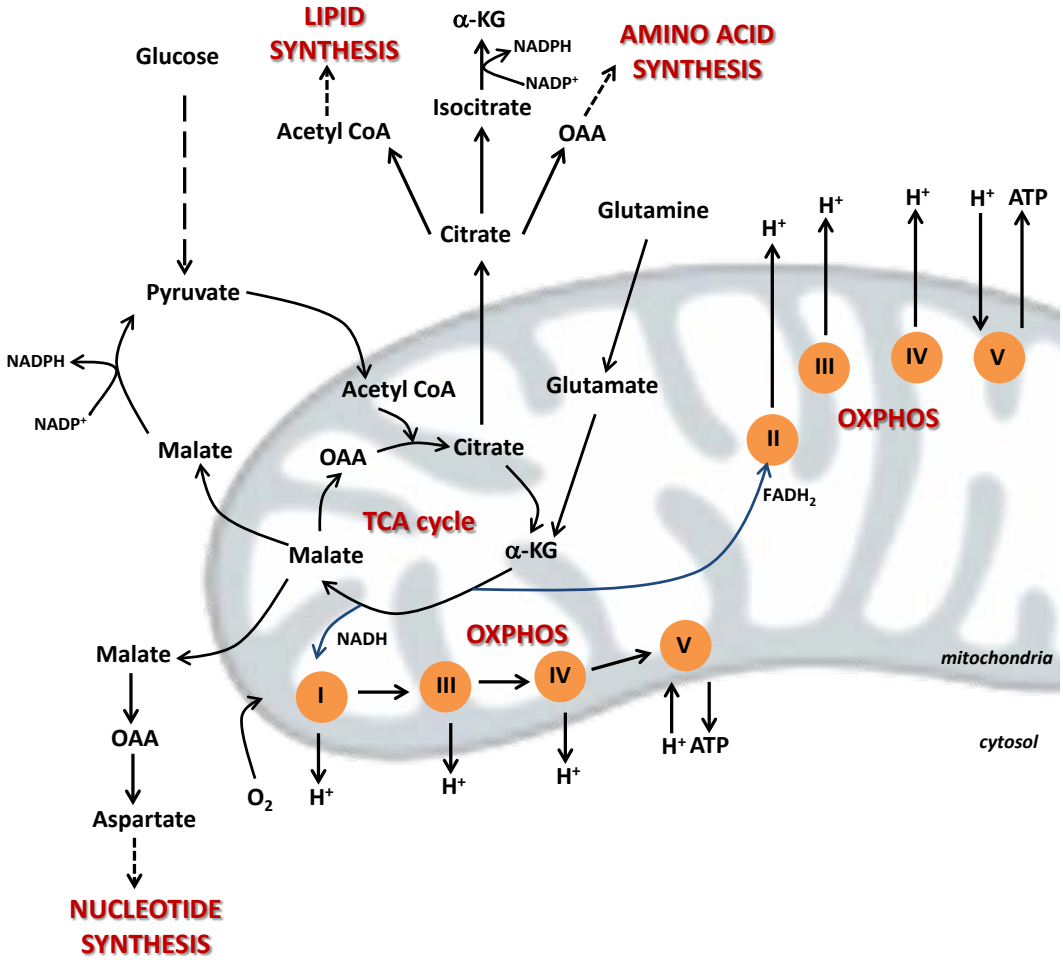

Figure 2.6 Biosynthetic and bioenergetic reactions of the TCA cycle and OXPHOS

Schematic representation of biosynthetic pathways derived from TCA intermediates and the OXPHOS bioenergetic pathway. TCA intermediates, such as citrate and malate, are precursors for nucleotide, amino acid and lipid synthesis. The reducing equivalent (NADPH) produced in some of these reactions also contribute to biosynthetic processes. The OXPHOS consists in the transference of electrons (redox reactions) through several mitochondrial complexes (I, II, III and IV), creating a gradient of protons (H^+). Protons flow back to the mitochondria through the ATPase (complex V) which results in the synthesis of ATP. α-KG, α-ketoglutarate; OAA, oxalacetate; I, complex I (NADH dehydrogenase); II, complex II (succinate dehydrogenase); III, complex III (cytochrome bc_1 complex); IV, complex IV (cytochrome c oxidase); V, complex V (ATP synthase).

of cancer including pheochromocytoma, paranglioma, renal cell carcinoma and papillary thyroid carcinoma (*193-195*). The accumulation of succinate as a result of SDH inhibition inhibits cytosolic HIF-1α prolyl hydroxylases, leading to the stabilization and activation of HIF-1α under normoxic conditions, which in turn promote a glycolytic phenotype, angiogenesis and metastasis, ultimately leading to tumor progression (*196*). FH is a TCA enzyme that catalyzes the reversible hydration/dehydration of

fumarate to malate. FH mutations predispose to multiple cutaneous and uterine leiomyomas as well as to hereditary leiomyomatosis and renal cell cancer (*197-198*). FH-deficient cells accumulate high levels of fumarate that, similarly to succinate, may act as an oncometabolite and contribute to tumorigenesis (*92*).

Another important step located at the crossroad between glycolysis and the TCA cycle is the metabolism of pyruvate. Pyruvate produced by glycolysis can remain in the cytosol and be reduced by LDH, or alternatively can be converted in the mitochondria to acetyl-CoA by the pyruvate dehydrogenase complex (PDH) and afterwards participate in the TCA cycle. This metabolic decision depends on the balance between the PDH status and the overactivation of LDH. PDH activity is modulated by reversible phosphorylation, catalyzed by pyruvate dehydrogenase kinases (PDHKs) and pyruvate dehydrogenase phosphatases (PDPs). The inhibition of PDH by phosphorylation is closely linked to the Warburg effect and may result from HIF-1-mediated expression of PDHK1 (*199*).

Recently, several reports have highlighted the correlation between mitochondrial metabolism and metastasis. Lebleu and coworkers showed that the PGC-1α-mediated mitochondrial biogenesis and respiration in cancer cells was functionally relevant for metastatic dissemination (*200*). In addition, aberrant TCA cycle coupled to an increased mitochondrial superoxide production has been linked to tumor cell migration and metastasis (*201*). On the contrary, undifferentiated and cancer stem cell phenotypes have been associated with preferential glycolytic over mitochondrial metabolism in several tumor types (*180, 202-203*).

2.3.2.2 Glutaminolysis

Glutamine is the most abundant free amino acid in circulation and in intracellular pools. This amino acid is used by cells for both bioenergetic and biosynthetic needs. Glutamine can act as a carbon source or nitrogen donor and consequently is used as a precursor for the synthesis of amino acids, proteins, nucleotides and lipids. Once taken up by the cell, much of the glutamine is primarily converted to glutamate by GLS. There are three isoforms of human glutaminase, encoded by two genes: the kidney-type (KGA/GLS1) and its glutaminase C (GAC) splice variant and the liver-type

(LGA/GLS2), all of them described to be involved in cancer (*204-205*). Because glutamate can yield α-KG, a TCA intermediate, glutamine constitutes an important anaplerotic source (*206*). To a lesser extent, α-KG acts also as a substrate for dioxygenases that modify proteins and DNA and contribute to cell signaling and epigenetic networks (*207*). Glutamate is also a precursor of glutathione, essential for redox homeostasis, and non-essential amino acids like alanine, aspartate, serine and glycine, which are required for protein synthesis. Conversion of glutamate to α-KG takes place either through oxidative deamination by glutamate dehydrogenase (GLDH) or by transamination to produce the non-essential amino acids. Under glucose-deprived conditions or glycolytic impairment, glutamine conversion to glutamate and further to α-KG through GLS and GLDH reactions, respectively, becomes a major bioenergetic pathway to promote survival (*208*). Glutamine oxidation can also supply carbons to ME, with the consequent production of NADPH reducing equivalents that, together with glutathione, maintain oxidative stress under control. These reactions that help to increase the intracellular NADPH/$NADP^+$ ratio have been shown to be particularly essential in KRas-driven pancreatic adenocarcinoma cells (*209*). On the other hand, both glutamine addiction and GLS activity are critical for MYC-mediated oncogenesis (*210-213*).

Additional recently unveiled functional roles for glutaminolysis include the participation of glutamine in reductive carboxylation, especially in rapidly growing tumor cells with defective mitochondria that are unable to efficiently synthesize citrate or other TCA intermediates for biosynthetic purposes (*214*). This reductive metabolism has been also observed in tumor cells exposed to hypoxia (*215-216*). The main enzymes that drive this pathway are mitochondrial and cytosolic isoforms of $NADP^+$/NADPH-dependent IDHs, which transform glutamine to citrate that provides both acetyl-CoA for fatty acid synthesis and four-carbon intermediates that can be used to produce the required TCA intermediates and related precursors. Inhibition of this alternative pathway for biosynthesis of lipids and other biomolecules has important implications not only for cancer cell proliferation and survival, but also in the more complex setting of cancer cell migration, invasion, tumor angiogenesis and metastasis (*217*). On the other hand, some reports have hypothesized that the

ammonia produced from the reaction carried out by the glutaminase enzyme plays a role in pH homeostasis (*218*). As a consequence of the Warburg effect and high lactate accumulation, tumor cells rely on pH-regulating systems to combat the excessive generation of protons (*219*). Ammonia release from glutamine is significantly stimulated under acidic conditions in LLC-PK1 cells (*220*). Intracellular pH control is essential for cell proliferation and survival and the metabolic reprogramming described for cancer cells is feasible in an alkaline intracellular pH context, as the activity of many enzymes is pH-sensitive (e.g. LDH and PFK1) (*221*). Interestingly, an increased intracellular pH is necessary for driving migration in multiple mammalian cell types, and a decreased extracellular pH promotes degradation of the extracellular matrix for cell invasion and metastasis (*222*).

2.4 STUDY AND CHARACTERIZATION OF TUMOR CELL METABOLISM

The past decade has seen a deeper understanding of cancer-associated metabolic rewiring thanks to the characterization of differences in metabolic requirements between normal and malignant cells, allowing the proposal of specific metabolic regulators as therapeutic targets to forestall tumor growth and metastatic progression. In this Section we will present some of the powerful tools for the characterization of cell metabolic metabolism and the kind of information they provide.

2.4.1 Metabolomics: characterization of the metabolome

In the field of cancer research, genomics, epigenomics, transcriptomics and proteomics strategies focused on gene, mRNA and protein profiles, respectively, have led to the identification of new tumor subtypes as well as gene, epigenetic, transcriptional and protein biomarkers for certain types of cancer and targetable mutations (*223-224*). On the other hand, metabolomics approaches have been used to quantify and analyze dynamic changes in metabolites and metabolic pathways, with subsequent inferences of the metabolic reprogramming underlying cancer and tumor progression. The study of metabolism is commonly addressed from an integrated perspective that aims to consider the entire metabolic network. For a long time, metabolomics has not received as much attention in clinical research as the “omic” technologies mentioned above.

Now, the challenge of a truly systems biology approach is the integration of the several layers of molecular information that provide each kind of omics data (*225*).

Metabolomics presents many advantages over the other omic approaches: 1) cell metabolome (the complete set of endogenous metabolites found within a cell) is the final downstream product of gene transcription, therefore, changes in the metabolome are amplified relative to changes in the transcriptome and the proteome (*226*), 2) the metabolome is closer to the phenotype of the biological system studied, 3) profiling of metabolic biomarkers is less costly than profiling mRNAs or proteins, and 4) it is easier to compare data over several conditions and biochemical derangements, as a given metabolite (unlike a transcript or protein) is the same in every cell or organism (*227*). Therefore, since the set of all metabolites is directly linked to the actual state of a cell and thus to the phenotype, portraying metabolomes is optimally suited for the determination of biomarkers that are typical for certain diseases or stages of disease progression.

Metabolomics studies can be classified into global metabolite profiling or targeted metabolomics. Global metabolomic surveys changes in the quantities of a large number of metabolites under certain conditions to identify metabolic profiles and trends, whereas targeted metabolomics analyzes changes in predetermined metabolites that are hypothesized to be altered under certain conditions. Specific methodical steps are required for the characterization of cell metabolism, involving metabolites extraction methods, techniques to quantify the metabolite changes and bioinformatics tools for data analysis and integration (*228*). A number of analytical techniques are currently used for metabolomic studies, depending on the metabolites of interest. Nuclear magnetic resonance (NMR) is one of the most common analytical methods for urine and plasma analysis (*229*). However, NMR suffers from poor sensitivity. Gas chromatography and liquid chromatography coupled with mass spectrometry (GC/MS and LC/MS) are widely accepted techniques for metabolite separation and analysis. Metabolites must be treated to obtain volatile derivatives in order to use the GC/MS technique efficiently. Organic acids, fatty acids and sugars are the best-suited metabolites for GC/MS analysis. Compared to NMR, GC/MS provides higher resolution and sensitivity. In contrast, LC/MS can overcome the limitations of

derivatization chemistry in GC/MS and cover a broad range of metabolites, including both volatile and non-volatile compounds.

Nevertheless, the invaluable data obtained using metabolomics approaches are restricted in that they provide only the metabolic pattern and thus a static metabolic map. Therefore, to complete the metabolic picture, the determination of the dynamics derived from the participation of metabolites in numerous reactions using metabolic pathway-based approaches is required. The analysis of metabolic flux distributions within cells is addressed by the emerging field known as fluxomics (*230-231*) that, together with metabolomics, successfully contributes to progress in the characterization of metabolic reprogramming underlying cancer and tumor progression.

2.4.2 Fluxomics: metabolic flux analysis

2.4.2.1 Determination of metabolic fluxes

To date, two major fluxomics tools have been developed: Flux balance analysis (FBA) and ^{13}C metabolic flux analysis (^{13}C-MFA).

FBA predicts metabolic flux distributions at steady state by making use of *in silico* genome-scale metabolic models (GSMMs) (*232*), assembled and manually-curated from annotated genome, biochemical and cell phenotype data (*233*). The calculation of net fluxes uses mass balancing, which means that, overall, the sum of all molar fluxes entering and leaving a metabolite pool must be zero. The flux map distribution can be constrained by *in vitro* metabolic measurements, such as metabolites consumptions and productions rates, thus limiting upper and lower bounds on fluxes. In addition, an assumed biological objective function is imposed on the computational model, for example, maximizing proliferation rates or ATP production (*234*). However, due to the complexity of these metabolic networks, there is usually a significant level of uncertainty affecting unmeasured exchanges and internal reactions. Physiologically meaningful flux solutions need to be narrowed down from all the possible flux distributions by imposing additional constraints on the system and by optimizing the objective function when performing FBA. Reconstructions of human metabolism such

as RECON1 (*235*), the Edinburg human metabolic network (*236*) or the most recent reconstructions of human metabolism, RECON2 (*237*), are emerging as a potential solution to decipher the mechanism underlying diseases with a strong metabolic component, in the context of systems biology, such as cancer or diabetes (*238*). Genome-scale constraint-based metabolic models have been used for a variety of applications, involving studies on evolution (*239*), metabolic engineering (*240*), genome annotation (*241*) or drug discovery (*242*). This approach can be also useful to predict the metabolic flux distribution changes after *in silico* gene knockout, to unveil the essentiality of a particular gene of interest (*243*). GSMMs have a high relevance in cancer research as they can efficiently capture the complexity of tumor metabolism in a holistic manner and permit the improvement of existing therapies or development of new therapeutic strategies (*241*) (see **Appendix 3**).

In ^{13}C-MFA, the biochemical network model is simplified and a handful of measured extracellular rates can provide sufficient data to estimate all remaining metabolic fluxes in the model. Furthermore, this approach takes into consideration ^{13}C-tracer-based data obtained after culturing cells with ^{13}C-labeled substrates, such as glucose or glutamine, which provides additional constraints for reducing the space of possible flux distributions (*244*). These ^{13}C-assisted metabolomics experiments are addressed in the next Section. Thus, the ^{13}C-MFA approach is a very reliable tool for measuring *in vivo* metabolic fluxes (*245*).

2.4.2.2 ^{13}C-based experiments

The use of substrates containing stable isotopes, such as ^{13}C, is a powerful tool to obtain information about the activity of different metabolic pathways within a cell. These experiments consist of incubating cells with ^{13}C-labeled metabolites (also known as tracers), resulting in metabolites containing ^{13}C atoms downstream of the initial ^{13}C-labeled substrate. Depending on the metabolic pathway followed by the tracer, ^{13}C atoms are incorporated in distinct numbers and at different positions into the newly synthesized metabolites. Thus, different mass isotopomers (or isotopologues) are obtained, which refers to molecules that differ only in the isotopic composition (e.g. lactate containing 2 or 3 ^{13}C atoms, independently of their position, are lactate mass

isotopomers) (*246*). Also positional isotopomers (or isotopomers) can result from the metabolism of the ^{13}C-substrate, resulting in molecules having the same number of ^{13}C atoms but differing in their positions (e.g. lactate containing 1 ^{13}C atom in position 1 or position 2 are lactate isotopomers) (*246*). For a specific metabolite, the number of possible ^{13}C mass isotopomers depends on the number of carbons (n) and is n+1, whereas the number of possible ^{13}C positional isotopomers is 2^n. For example, three-carbon molecules such as lactate can potentially give 3+1=4 mass isotopomers, termed m0, m1, m2 and m3 depending on whether 0, 1, 2 or 3 ^{13}C atoms are present in the molecule. On the other hand, 2^3=8 positional isotopomers are possible, therefore a lactate molecule denoted as m1 can correspond to three possible positional isotopomers ($^{13}C_1$-$^{12}C_2$-$^{12}C_3$, $^{12}C_1$-$^{13}C_2$-$^{12}C_3$ and $^{12}C_1$-$^{12}C_2$-$^{13}C_3$). GC/MS analysis can resolve mass isotopomers whereas NMR is able to define positional isotopomer distribution in product metabolites that derive from a given ^{13}C-labeled precursor molecule (*247*).

Several considerations should be taken into account when designing isotopic labeling experiments. In order to produce well-resolved metabolic fluxes, the selection of the appropriate tracers and the labeled products to be analyzed for a given system is the major challenge (*248*). The selection of optimal tracers depends on the metabolic question that we aim to address. A single optimal tracer cannot give all the information required for determining all metabolic fluxes within a given network model. Thus, prior to the ^{13}C-based experiment, a decision must be made whether an overall picture of metabolism is sought or only certain fluxes are of interest. The issue of tracer choice is more complex in mammalian cell systems, such as tumor cells, which are cultured in complex media containing multiple nutrients that can compete with the tracer (*248-249*).

Currently, the most popular choices are ^{13}C-glucose and ^{13}C-glutamine tracers, as these substrates are readily metabolized by most mammalian cells. Metallo *et al*. evaluated several commercially available ^{13}C-glucose and ^{13}C-glutamine tracers and identified tracers for specific metabolic pathways, highlighting [1,2-$^{13}C_2$]-glucose for analyzing the overall metabolic network, glycolysis and the PPP, while [U-$^{13}C_6$]-glucose and multiply labeled glutamine tracers were most informative for the TCA cycle (*248*),

according to other studies using these tracers (*250-252*). Recently, two studies using new frameworks for optimal ^{13}C-tracer experiment designs have identified novel isotopic tracers that were optimal for determining PPP flux ([3,4,5,6-$^{13}C_4$]-glucose) in plants (*253*), and the oxidative branch of the PPP ([2,3,4,5,6-$^{13}C_5$]-glucose) and PC fluxes ([3,4-$^{13}C_2$]-glucose) in mammalian cells (*249*). However, as some of these novel tracers are commercially unavailable, it is important to decide if the improved flux resolution justifies the additional cost of custom synthesis of specific tracers.

^{13}C-based experiments can be divided into two major categories: 1) single labeling experiments, and 2) parallel labeling experiments. For a single labeling experiment design, only one experiment is conducted, which can involve the use of a single labeled substrate (e.g. [1,2-$^{13}C_2$]-glucose), a mixture of tracers of the same compound (e.g. a mixture of [3-$^{13}C_1$]-glucose and [4,5,6-$^{13}C_3$]-glucose), or multiple labeled substrates (e.g. [U-$^{13}C_6$]-glucose and [U-$^{13}C_5$]-glutamine). For a parallel labeling experiment design, two or more tracer experiments are conducted in parallel. In each experiment, a different tracer is used (e.g. [1,2-$^{13}C_2$]-glucose in one experiment and [U-$^{13}C_5$]-glutamine in the other experiment). Typically, parallel experiments are started from the same seed culture to minimize biological variability (*245, 254-255*). The data obtained in parallel experiments is then integrated for ^{13}C-MFA by concurrently fitting all labeling measurements from multiple experiments to a single flux model (*254*). Many of the advantages provided by parallel experiments compared to single experiments are discussed in (*245*).

2.4.2.3 Mass Isotopomer Distribution Analysis

The mass isotopomer distribution of specific ^{13}C-labeled metabolites downstream the tracer, in combination with measurements of the extracellular fluxes involving the tracer and/or other substrates, can be used to determine either some intracellular fluxes or the ratio between some of them. This is achieved by using simple analytical formulas based on previous knowledge of the reactions within the metabolic network. This comparative analysis of tracer-based metabolomic data is known as mass isotopomer distribution analysis (MIDA) and is a useful tool for the characterization of cell metabolic flux distribution without bioinformatics resources (*230*). For example,

the metabolism from [1,2-$^{13}C_2$]-glucose to ribose can be analyzed to determine the approximate contribution of the oxidative and non-oxidative branches of the PPP (**Figure 2.7**) (*146, 256*). The metabolism of glucose-6-phosphate through the oxidative branch results in the loss of 1 carbon atom, yielding m1 ribose ([1-$^{13}C_1$]-ribose). On the contrary, if ribose comes from the non-oxidative branch, [1,2-$^{13}C_2$]-glucose is converted into [1,2-$^{13}C_2$]-fructose, which in turn yields m2 ribose ([1,2-$^{13}C_2$]-ribose). Likewise, mass isotopomer distribution of lactate combined with lactate concentration measurements can be used to estimate the contribution of glucose to lactate via direct glycolysis and via PPP, as described in Section 4.17.1. In addition, ^{13}C propagation from [1,2-$^{13}C_2$]-glucose to glutamate can be analyzed to estimate the approximate relative contributions of PC and PDH to pyruvate entry into the TCA cycle (*257*). Hence, although the estimated flux values are approximate, MIDA has been used to identify relevant biochemical pathways and reactions and to quantify individual flux partitioning ratios (*258*). In addition, these analytically deduced flux ratios can be also included in metabolic flux analysis as constraints.

Another powerful tool to analyze the cellular flux profiles supplement to MIDA is the software "Isodyn" (from "isotopomer dynamics") that enables the simulation of the dynamics of the ^{13}C redistribution in metabolites from central metabolic pathways of living cells. For such simulations, Isodyn uses a classical kinetic model of metabolic pathways linked to a module that computes the distribution of ^{13}C mass isotopomers in metabolites (*259-261*). Isodyn can be supplemented with algorithms to reveal the compartmentation of intracellular metabolic reactions from ^{13}C mass isotopomers data (*262*).

2.4.3 Cellular bioenergetics studies: the XF24 Extracellular Flux Analyzer

The characterization of cancer cell bioenergetics usually consists of independent measurements of oxygen consumption, glucose uptake, lactate production and mitochondrial function. As different protocols are required for every analysis, these assays can be time consuming and often do not provide real-time data. In contrast to traditional methods, the XF24 Extracellular Flux Analyzer (Seahorse Bioscience) is a novel instrument that allows to perform simultaneous measurements of mitochondrial

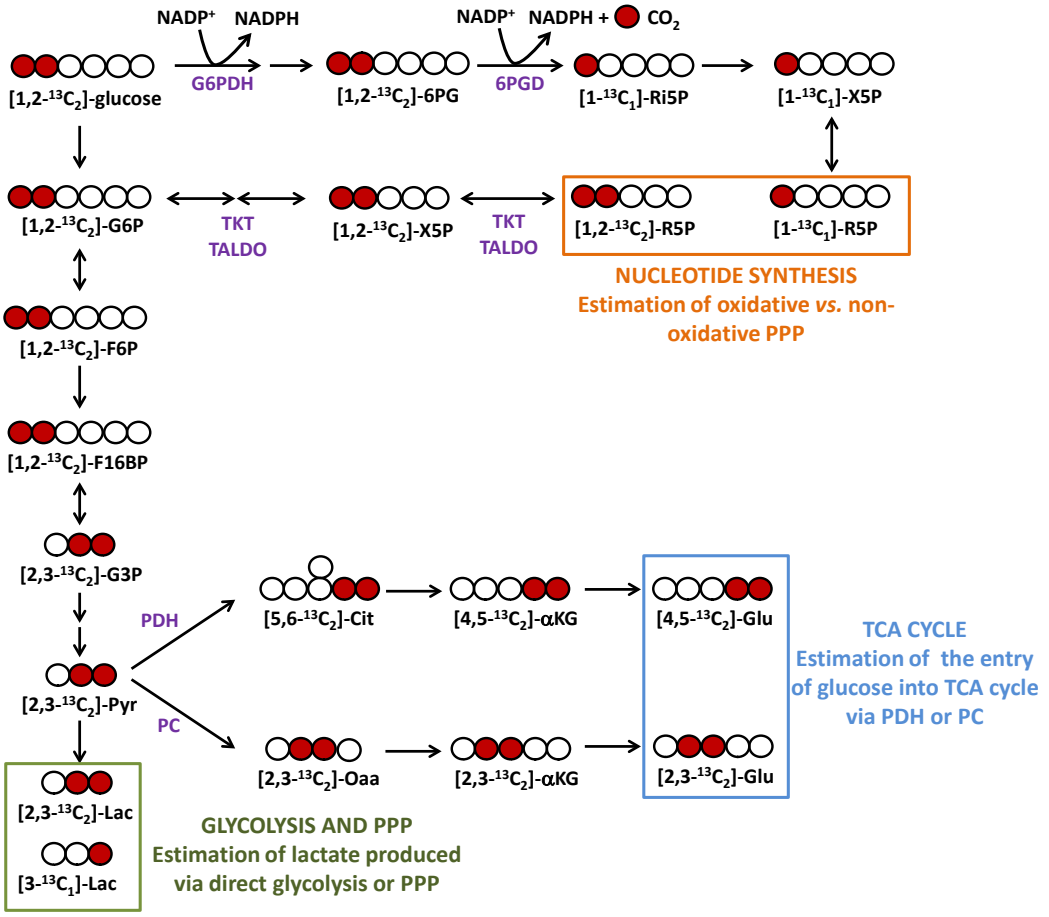

Figure 2.7 ^{13}C-assisted metabolomics experiments using [1,2-$^{13}C_2$]-glucose

The use of [1,2-$^{13}C_2$]-glucose allows estimating the performance of several major metabolic pathways such as pentose phosphate pathway (PPP), glycolysis or tricarboxylic acid (TCA) cycle. The contribution of the oxidative and the non-oxidative PPP branches to ribose-5-phosphate (R5P) production, required for the synthesis of nucleotides, can be estimated by determining the mass isotopomer distribution of RNA ribose through quantifying the percentage of R5P molecules containing one ^{13}C atom (m1 ribose, [1-$^{13}C_1$]-ribose) or two ^{13}C atoms (m2 ribose, [1,2-$^{13}C_2$]-ribose). Also the mass isotopomer distribution of lactate (Lac) gives information about the lactate biosynthetic process, since [2,3-$^{13}C_2$]-Lac (m2 lactate) is produced by direct glycolysis whereas [3-$^{13}C_1$]-Lac (m1 lactate) is produced by a combination of glycolysis and PPP pathways, where [1-$^{13}C_1$]-R5P is reintroduced into glycolysis through the non-oxidative PPP giving m1 labeled glycolytic intermediates (for simplicity, glycolytic intermediates corresponding to this process are not shown in the figure). Pyruvate (from labeled glucose) entry into the mitochondria can also be estimated by analyzing the mass isotopomer distribution of glutamate (Glu). According to the pathway used to shunt pyruvate into the TCA cycle, the positional isotopomer distribution of glutamate will differ. Entry of pyruvate via pyruvate dehydrogenase (PDH) yields [4,5-$^{13}C_2$]-Glu, whereas entry via pyruvate carboxylase (PC) yields [2,3-$^{13}C_2$]-Glu. Details about the procedures used to determine the mass isotopomer distribution of all these metabolites are described in Section 4.16. G6P, glucose-6-phosphate; G6PDH, glucose-6-phosphate dehydrogenase; 6PG, 6-phosphogluconate; 6PGD, 6-phosphogluconate dehydrogenase; Ri5P, ribulose-5-phosphate; X5P, xylulose-5-phosphate; TKT, transketolase; TALDO, transaldolase; F6P, fructose-6-phosphate; F16BP, fructose-1,6-bisphosphate; G3P, glyceraldehyde-3-phosphate; Pyr, pyruvate; Cit, citrate; αKG, α-ketoglutarate.

respiration (oxygen consumption rate, OCR) and glycolysis (extracellular acidification rate, ECAR), allowing analysis of the alterations and interplay of these two dominant energy-yielding pathways in cancer cells.

The XF24 Extracellular Flux Analyzer is a fully integrated instrument that measures in real time the extracellular flux changes of oxygen and protons in the media immediately surrounding adherent cells cultured in a 24-well microplate. The assay requires a disposable sensor cartridge, embedded with 24 pairs of fluorescent biosensors (oxygen and pH) coupled to a fiber-optic waveguide. The waveguide delivers light at various excitation wavelengths (oxygen = 532 nm, pH = 470 nm) and transmits a fluorescent signal, through optical filters (oxygen = 650 nm, pH = 530 nm) to a set of highly sensitive photodetectors. Each fluorophore is uniquely designed to measure a particular analyte. In addition, each sensor cartridge is equipped with four reagent delivery chambers per well for injecting drugs and testing agents into wells which contain the cells under study (**Figure 2.8**). Many studies have described the use of XF assays to define metabolic phenotypes and measure alterations in cancer cell bioenergetics (*263-265*). A recent report demonstrated that the XF24 analyzer was also valid for monitoring mitochondrial respiration and peri-mitochondrial pH changes with relative high throughput on minute quantities of isolated mouse liver and rat heart mitochondria (*266*).

Different kits are available for measuring mitochondrial respiration, glycolysis and fatty acid oxidation in cells. The main advantage compared to other commercial kits is that most of the compounds can be purchased separately (e.g. oligomycin, FCCP, rotenone and antimyin) and therefore the different treatments can be developed according to the specific experiment and cell model. Moreover, the flexibility of the XF assays, in combination with our knowledge of those metabolic pathways closely linked to glycolysis or mitochondrial metabolism, allow the design of custom protocols for addressing specific biological questions. As an example, the Crabtree effect can be easily determined by culturing cells in media containing only glutamine, measure the OCR and ECAR values in this initial condition and then inject glucose, causing a switch from mitochondrial respiration to glycolysis that reflects the preference of cells to use

the glycolytic pathway when glucose becomes available, and this switch can be quantified (*264*).

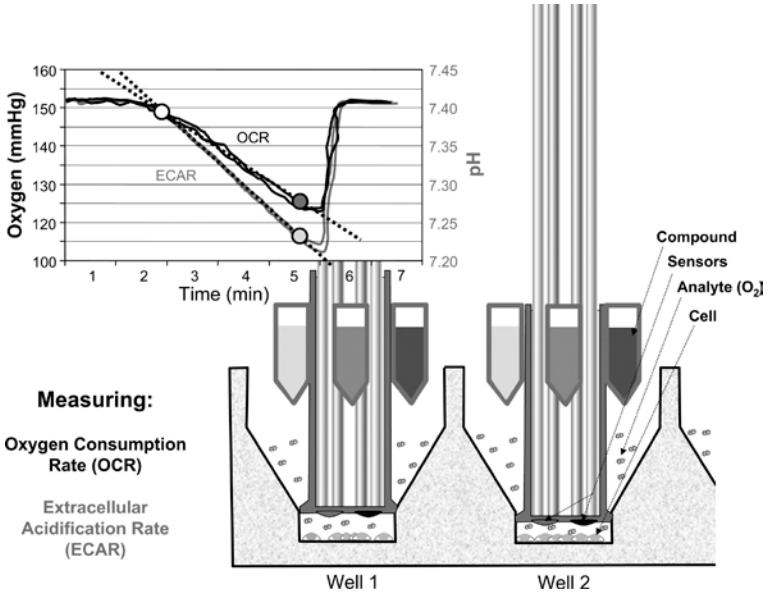

Figure 2.8 How the XF24 Extracellular Flux Analyzer works

The XF24 Extracellular Flux Analyzer measures the rate of change of oxygen (Oxygen Consumption Rate, OCR) and proton concentrations (Extracellular Acidification Rate, ECAR) in the media immediately surrounding living cells, seeded in a 24-well microplate. Here, the representation of 2 wells is shown. Sensors are immersed in the media, near the cells, and are able to detect changes in the analytes (O_2 or H^+). Treatments can be performed by injecting compounds through one of the four delivery chambers per well incorporated in the cartridge. Republished with permission of AMERICAN PHYSIOLOGICAL SOCIETY, from Wu, M., et al., Multiparameter metabolic analysis reveals a close link between attenuated mitochondrial bioenergetic function and enhanced glycolysis dependency in human tumor cells. Am J Physiol Cell Physiol, 2007. 292(1): p. C125-36, Copyright © 2007; permission conveyed through Copyright Clearance Center, Inc.

Here, in Section 2.4, we have introduced several techniques and methodologies that, combined, offer very valuable information to elucidate how the metabolism of cancer cells works and identify differential metabolic signatures that characterize different types of cancer and cancer cell subpopulations that participate in the multiple stages of tumor progression. To accomplish the objectives of this thesis, these techniques will be used to perform the metabolic characterization of a prostate cancer cell model comprising cell subpopulations endowed with uncoupled CSC and EMT phenotypes, which will be presented below.

2.5 METABOLIC CHARACTERIZATION OF TWO CLONAL SUBPOPULATIONS DISPLAYING UNCOUPLED CSC AND EMT PROGRAMS

This thesis is focused on the metabolic characterization of two clonal subpopulations isolated from an established prostate cancer cell line (PC-3), one expressing an epithelial-CSC gene program (**PC-3M)** and a second population displaying a strong mesenchymal-EMT gene program (**PC-3S**). The epithelial tumor subpopulation displays strong self-renewal, tumorigenic and metastatic phenotypes, while the mesenchymal subpopulation, although invasive, is unable to establish metastatic growth (*49*). These cell subpopulations cooperate among each other as shown in **Figure 2.9**, where the mesenchymal tumor cells facilitate the escape of the epithelial tumor cells from the local implantation sites, thus favouring metastatic spread of the latter. Importantly, despite the fact the mesenchymal tumour subpopulation facilitated the spread of tumour cells from local sites, only the epithelial tumour subpopulation was capable of growing metastases at distant organs.

Apart from PC-3M and PC-3S cells, two PC-3M cell variants were produced and their metabolism was also characterized. These cell variants were obtained by induction of a constitutive EMT by transduction of the PC-3M cells with the EMT factor SNAI1 (**PC-3M SNAI1**). SNAI1 belongs to the Snail family proteins that are regulatory factors of EMT, a process that plays essential roles in embryogenesis and development and has been associated with metastasis in carcinomas (*28, 267*). SNAIL, together with other EMT transcription factors such as TWIST or ZEB, promotes the EMT program by repressing the epithelial phenotype, enhancing mesenchymal traits including motility, and inducing the ability to degrade the basement membrane and the extracellular matrix. In cancer cells, the induction of the EMT program, in addition to invasion and motility, involves intravasation of invasive cells into blood and lymphatic vessels and their subsequent extravasation (*268*), as explained previously in Section 2.2. The induction of the EMT program in PC-3M cells shuts down their self-renewal gene program and abolishes their anchorage-independent growth *in vitro* and tumor formation and establishment of metastasis *in vivo* (*49*). Conversely, the inhibition of the characteristics of pluripotency was achieved by knock down of SOX2, KLF4 and MYC in

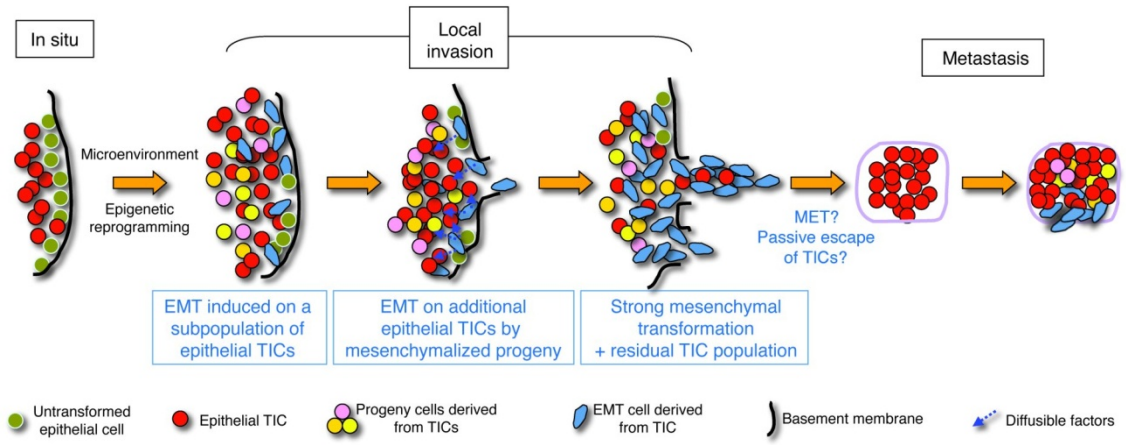

Figure 2.9 Cooperation between tumor cell subpopulations expressing either epithelial/CSC or mesenchymal/EMT programs

In this model TICs, with properties of CSCs, undergo the EMT under the influence of environmental factors. This results in epigenetic reprogramming, including a repression in those cells of pluripotency programs that sustain cell self renewal. These "mesenchymalized" cells, in turn, either through direct cell-cell interaction or through diffusible factors, drive the mesenchymal conversion of additional populations of TIC/CSCs that have not yet undergone EMT, resulting in a reinforcement of the mesenchymalization of the tumor. The predominantly mesenchymalized populations of tumor cells complete the breach of local barriers and thus the tumor becomes fully invasive. The tumor cells escaping from the local site would thus be a combination of stably mesenchymalized tumor cells, cells retaining TIC/CSC properties that leave the tumor following paths open by actively invading cells (passive escape), or TIC/CSCs that have undergone transient EMT (active escape). After hematogenous or lymphogenous spread, TIC/CSCs that have not undergone EMT or that have reverted to an epithelial program and phenotype from their transient EMT (MET) can establish distant metastases. This cycle may be repeated at the metastatic site. Tumor cells with stable mesenchymal-like phenotypes that have escaped from the local tumor site but that do not revert to an epithelial gene program and phenotype would not have the capacity to establish distant metastases. EMT, epithelial-mesenchymal transition; TIC, tumor-initiating cell; MET, mesenchymal-epithelial transition. Republished with permission of AMERICAN SOCIETY FOR CLINICAL INVESTIGATION, from Celia-Terrassa, T., et al., Epithelial-mesenchymal transition can suppress major attributes of human epithelial tumor-initiating cells. J Clin Invest, 2012. 122(5): p. 1849-68, Copyright © 2012; permission conveyed through Copyright Clearance Center, Inc.

PC-3M cells (**PC-3M SKM triple-KD**). The expression of these transcription factors, together with the expression of other pluripotency-related genes such as Nanog or Lin28, is closely linked to tumor progression and metastasis as they provide tumor cells with metastatic and tumor initiating capacities, resulting in a gain of CSC or TIC properties (*49, 269*). Thus, the triple knock down of these factors in PC-3M cells resulted in a suppression of their self-renewal properties and metastatic program (*49*).

Our dual-cell prostate cancer model of invasion and metastasis, with its unique clearcut distinction between CSC *vs*. EMT programs/phenotypes, presents a superb

opportunity to define the metabolic wirings that characterize these programs and to identify therapeutic targets and tumor progression biomarkers. Recently, the interest in elucidating the metabolic properties of CSCs has notably increased as a strategy for the identification of metabolic vulnerabilities that could offer new possibilities for targeting these cells (*270*). Also some reports have shown that EMT transcription factors affect tumor metabolism, like the Snail-G9a-Dnmt1 complex which silence the expression of the enzyme fructose-1,6-biphosphatase in basal-like breast cancer, inducing a metabolic reprogramming that synergizes with the loss of E-cadherin to sustain CSC-like properties during dissemination and metastasis (*271*). However, many of these studies have been carried out using cell models with the coexistence of several tumor subpopulations or even with cells displaying coupled EMT and CSC phenotypes, thus preventing the study whether each of these two gene programs can contribute separately to tumor metabolic reprogramming. Therefore, a major advantage of our model is the virtual absence of overlap that each cell subpopulation presents between the expression of either CSC or EMT programs, thus facilitating the identification of regulators, effectors, markers and targets specific to one or the other. In addition, our dual-cell model is amenable to reciprocal switching between the two programs by introducing or silencing EMT or pluripotency factors, as described before.

3. OBJECTIVES

3. OBJECTIVES

Continuous advances in molecular biology have paved the way for new discoveries in cancer research that have led to the design of more selective and efficient therapies. However, once cancer culminates in invasive and metastatic disease, the survival rates plummet because the current treatments are largely ineffective against metastases. So far, and in comparison with the many cancer-driving genes that have been discovered, only a handful of metastasis-inducing genes and proteins have been validated and the mechanisms underpinning their metastatic potentials are still being elucidated. Furthermore, the need for identification, isolation and molecular characterization of CSCs is required to unveil the complex molecular events mediating invasion, metastasis, therapeutic resistance and relapse. Over the last few years, several molecular profiling strategies have been applied for the study of the metastatic disease, among which metabolomics and fluxomics have emerged as powerful tools that, in combination, allow the elucidation of the metabolic reprogramming accompanying specific cancer cell phenotypes. Here, the combined use of these promising strategies has shed light on those metabolic properties and vulnerabilities that differ between neoplastic cells that display very distinct metastatic and invasive capacities. The main objective of this thesis is focused on the characterization of the metabolic reprogramming and vulnerabilities of uncoupled CSC and EMT phenotypes present in our dual cell model and represented by the highly related cell subpopulations PC-3M and PC-3S cells, respectively. Additionally, two cell variants obtained by modulation of EMT (PC-3M SNAI1) or pluripotency (PC-3M SKM triple-KD) factors and displaying intermediate features between the extreme CSC and EMT phenotypes will be also characterized to specifically associate the link of cell metabolism with the self-renewal/pluripotency and EMT programs.

In order to accomplish this main objective, namely the identification of the metabolic reprogramming and the potential metabolic vulnerabilities in PC-3M and PC-3S cells, and their dependence on the CSC and EMT programs, it will be assessed specifically by:

1. Characterization of the glycolytic profile and contribution of glucose metabolism to bioenergetics and synthesis of cell building blocks (nucleotides, fatty acids and amino acids) in PC-3M and PC-3S cells (**Chapter I**).

2. Characterization of the glycolytic profile of PC-3M SNAI1 and PC-3M SKM triple-KD to analyze the dependence of glycolysis on the epithelial gene program and the pluripotency gene network (**Chapter I**).

3. Characterization of the mitochondrial function, the dynamics of the TCA cycle and glutaminolysis in PC-3M and PC-3S cells (**Chapter II**).

4. Characterization of the mitochondrial function and glutaminolysis in PC-3M SNAI1 and PC-3M SKM triple-KD to analyze the dependence of mitochondrial respiration and glutamine metabolism on the epithelial gene program and the pluripotency gene network (**Chapter II**).

The metabolic information provided by each approach will be gradually integrated to better understand the importance of the distinct metabolic pathways to the CSC (PC-3M) and non-CSC (PC-3S) phenotypes.

4. MATERIALS AND METHODS

4. MATERIALS AND METHODS

4.1 Cell culture

PC-3M and PC-3S were clonally derived from the human cell line PC-3, isolated from the bone metastasis of a prostate adenocarcinoma (*272*). As described in (*49*), both sublines carry the integrated firefly luciferase gene coding region cloned in the Superluc pRC/CMV vector (Invitrogen). The PC-3M clone was selected by limiting dilution from PC-3 cells isolated from liver metastases produced in nude mice subsequent to intrasplenic injection of PC-3 cells (*273*). PC-3S cells were selected by limiting dilution from parental PC-3 cells. Both cell subpopulations were cultured at 37°C in a 5% CO_2 atmosphere in RPMI 1640 media (Sigma-Aldrich or Biowest) with 10 mM glucose and 2 mM glutamine supplemented with 10% Fetal Bovine Serum (FBS) (PAA Laboratories), 1% pyruvate (1 mM) (Biological Industries), 1% streptomycin (100 μg/mL) / penicillin (100 units/mL) (Gibco), 1% nonessential amino acids (Biological Industries) and 200 μg/mL geneticin (Gibco) to maintain the chromosomal integration of the luciferase gene.

The two PC-3M cell variants used in several experiments were obtained as follows (a more detailed description of the generation of these cells can be found in (*49*)). The EMT factor SNAI1 was retrovirally transduced and overexpressed in PC-3M cells (PC-3M SNAI1) causing a strong EMT with downregulation of E-cadherin, upregulation of fibronectin and enhanced invasiveness in *in vitro* assays. Of interest, this was accompanied with an inhibition of features of CSC, including spheroid growth under anchorage-independent growth conditions (*49*). In the case of the cell variant PC-3M SKM triple-KD cells, PC-3M cells were subjected to triple knock down by means of lentiviral transduction of shRNAs specific for the pluripotency factors SOX2, KLF4 and MYC. The consequence of this triple knock down was a loss of self-renewal properties, as determined by the inhibition of spheroid growth (*49*).

4.2 Cell proliferation and viability assay

To evaluate cell proliferation, cells were counted using a Scepter™ Handheld Automated Cell Counter (Merck Millipore, Billerica, MA, USA). PC-3M and PC-3S cells were seeded ($1.5 \cdot 10^5$ and $5 \cdot 10^5$, respectively, in 100-mm culture dishes) and next day medium was replaced with fresh media (t = 0 h) and then proceed with cell counting every 24 h until 72 h. For cells transfected with siRNAs, cell proliferation was assessed as follows. PC-3M and PC-3S cells were plated in 6-well plates at a concentration of $0.5 \cdot 10^5$ and $1 \cdot 10^5$ cells per well, respectively. Cells were transfected after 24 h (conditions are detailed in Section 4.13), medium was replaced after 6 h (t = 0h). At 24, 48, 72, 96 and 120 h post t = 0 h, cells were counted as described previously.

Proliferation and viability was also assessed by Hoechst staining (HO33342; Sigma-Aldrich). HO33342 (2'-[4-ethoxyphenyl]-5-[4-methyl-1-piperazinyl]-2,5'-bi-1H-benzimidazole trihydrochloride trihydrate) is a cell-permeable DNA stain that is excited by ultraviolet light and emits blue fluorescence at 460-490 nm. It binds preferentially to adenine-thymine (A-T) regions of DNA and is used for specifically staining the nuclei of living or fixed cells and tissues. Briefly, cells were seeded in 96-well plates and media was replaced after 24 h with complete fresh media containing the drug under study or nutrient-deprived media. At the end of the experiment, media was removed, cells were washed with PBS, the supernatant was aspirated and 100 μL of 0.01% SDS was added to each well. Plates were then frozen at -20°C until analyzed. To analyze the samples, plates were thawed at 37°C until fully liquid and 100 μL of HO33342 stain solution were added to each well, minimizing light exposure. HO33342 stain solution was prepared by diluting HO33342 stock solution (10 mg/mL in H_2O) with Assay Buffer containing 1 M NaCl, 0.1 M EDTA, 1 M Tris, pH 7.4. Plates, covered with tinfoil, were placed on a shaker and incubated at 37°C for 1 h in the dark. Finally, fluorescence was measured in a fluorescence plate reader at 355 nm excitation and 460 nm emmission.

4.3 *In vitro* invasiveness assay

Transwell chambers (Costar) with 8 μm diameter pore membranes were coated with growth factor-reduced Matrigel (BD Biosciences) at 410 μg/mL and human umbilical

cord hyaluronic acid (Sigma-Aldrich) at 100 μg/cm^2. Cells ($6.45 \cdot 10^4$/well in 96-well plates) were serum deprived overnight, detached, resuspended in media supplemented with 0.5% FBS and then seeded onto the precoated Transwell inserts, with the lower chamber containing media supplemented with 0.5% FBS. After 24 h, cells migrating to the lower chamber were collected by detachment with trypsin-EDTA, washed with PBS, stained with propidium iodide (PI) (0.01 mg/mL) and counted by flow cytometry using a known quantity of flow cytometry calibration beads (~10^6 beads/mL). Each experiment was done in quadruplicate.

4.4 Spheroid formation assay

Cells (10^3/well) were seeded on 24-well Ultra Low Attachment culture plates (Corning) in complete culture media containing 0.6% methyl cellulose (Sigma-Aldrich) and allowed to grow for 15 days. At the end of the experiment, spheroids were stained, incubating cells with 0.5 mg/mL MTT (3-[4,5-dimethylthiazol-2-yl]-2,5-diphenyltetrazolium bromide) for 2-4 h and then each well was scanned for posterior spheroid quantification, using ImageJ software (free software that can be downloaded from http://imagej.nih.gov/ij/download.html).

4.5 Cell cycle analysis

Cell cycle analysis was assessed by flow cytometry using a fluorescence-activated cell sorter (FACS). $1 \cdot 10^5$ PC-3M and $2 \cdot 10^5$ PC-3S cells were seeded on 6-well plates and after 24 h media was replaced with complete fresh media containing the drug under study or nutrient-deprived media. Cells were collected 48 h later, fixed with 70% cold ethanol and stored in the ethanol fixative at -20 °C. To prepare the samples for cell cycle analysis, cells were centrifuged, washed with PBS and resuspended in buffer consisted of PBS and 0.2 mg/mL RNAse A (REAL Laboratories) and incubated for 1 h at 37°C. Prior to analysis, 0.05 μg/mL PI was added. For cell cycle phase distribution analysis the FlowJo®software (Tree Star, Inc.) was used, and the percentages of cells in G1, S and G2 were obtained.

4.6 Apoptosis assay

Apoptosis was assessed by evaluating the binding of annexin-V to phosphatidylserine, which is externalized early in the apoptotic process. $1 \cdot 10^5$ PC-3M and $2 \cdot 10^5$ PC-3S cells were seeded on 6-well plates and treated as described above for the cell cycle analysis assay. After cell collection and centrifugation, cells were resuspended in 95 μL binding buffer containing 10 mM HEPES/NaOH (pH 7.4), 140 mM NaCl and 2.5 mM $CaCl_2$. Then, 3 μL of Annexin V-FITC conjugate (1 μg/mL) were added and the suspension was incubated in darkness for 30 min, at room temperature. After the incubation, 500 μL of binding buffer were added to the cell suspension and just before FACS analysis (1 min) cells were stained with 20 μL PI (1 mg/mL). Data from $1 \cdot 10^4$ cells were collected and analyzed.

4.7 Measurement of media metabolites

Glucose, lactate, glutamate and glutamine were determined by spectrophotometry (COBAS Mira Plus, Horiba ABX) from cell culture media by monitoring the production of NAD(P)H in specific reactions for each metabolites at 340 nm wavelength (*148*). Glucose concentration was measured using hexokinase (HK) and glucose-6-phosphate dehydrogenase (G6PDH) coupled enzymatic reactions (commercial enzymatic kit). Lactate concentration was determined by lactate dehydrogenase (LDH) reaction, which was carried out at 37°C by adding media sample to a cuvette containing 1.55 mg/mL NAD^+ and 87.7 U/mL LDH in 0.2 M hydrazine, 12 mM EDTA buffer, pH 9. Determination of glutamate concentration was done by its conversion to α-ketoglutarate (α-KG) through glutamate dehydrogenase (GLDH) reaction in the presence of ADP. This reaction was performed at 37°C by adding media sample to a cuvette containing 2.41 mM ADP, 3.9 mM NAD^+ and 39 U/mL GLDH in 0.5 M glycine, 0.5 M hydrazine, pH 9.0. Glutamine was determined by its conversion first to glutamate through glutaminase (GLS) reaction and subsequently quantification of glutamate concentration as described above. GLS reaction was performed by adding media sample to a cuvette containing a mixture consisted of 125 mU/mL GLS in 125 mM acetate, pH 5.0. Reaction was carried out for 30 min at 37°C in agitation.

Alanine, serine, glycine and branched-chain aminoacids (BCAA) (leucine, valine, isoleucine) concentrations in cell media were determined by ion-exchange chromatography with a Biochrom 30 amino acid analyzer (Pharmacia Biochrom Ltd, Cambridge, UK). 70 μL of 150 μM norleucine was used as internal standard and added to 500 μL of media. Solvent was evaporated to complete dryness using a SpeedVac. The samples were resuspended in 500 μL of lithium citrate, pH 2.2 buffer and filtrated with 0.22 μm filter. 30 μL of sample were injected onto the Biochrom 30 lithium system according to the manufacturer's protocol. A set of lithium citrate buffers were used as mobile phase for separation during 115 minutes and post column derivatization with ninhydrin allowed amino acid detection at 570 and 440 nm. The retention time of the peak on the chart allowed the identification of the amino acid and the area under the peak indicated the quantity of amino acid present.

The metabolite consumption/production normalized rates are derived from the measured metabolites concentrations and corrected according to the measured cell proliferation (under exponential growth conditions). From the same plates where sample media were obtained, cell numbers were determined as described in Section 4.2. All the values are expressed in micromol or nanomol of metabolite consumed or produced per hour and 10^6 cells (μmol/h·10^6 cells or nmol/h·10^6cells)

4.8 Enzyme activities

Fresh cell culture plates were rinsed with phosphate buffered saline (PBS) and scrapped with lysis buffer (20 mM Tris-HCl pH 7.5, 1 mM dithiothreitol, 1 mM EDTA, 0.2% Triton X-100, 0.02% sodium deoxycholate) supplemented with protease inhibitor cocktail (Sigma-Aldrich). Cell lysates were disrupted by sonication using a titanium probe (VibraCell, Sonics & Materials Inc., Tune: 50, Output: 30) and immediately centrifuged at 12000 xg for 20 min at 4°C. The supernatant was separated and used for the determination of specific enzyme activities determined by spectrophotometry (COBAS Mira Plus, Horiba ABX) by monitoring NAD(P)H production or disappearance at 340 nm wavelength. All enzymatic activities were normalized by protein content in the supernatant, determined by the bicinchoninic acid (BCA) assay.

4.8.1 Lactate dehydrogenase (LDH, EC 1.1.1.27)

LDH specific activity was measured by adding diluted sample to a cuvette containing 0.2 mM NADH in 100 mM KH_2PO_4/K_2HPO_4, pH 7.4, at 37°C. Reaction was initiated by the addition of pyruvate at a final concentration of 0.2 mM.

4.8.2 Transketolase (TKT, EC 2.2.1.1)

TKT specific activity was determined by adding samples to a cuvette containing 5 mM $MgCl_2$, 0.2 U/mL triose phosphate isomerase, 0.2 mM NADH, 0.1 mM thiamine pyrophosphate in 50 mM Tris-HCl, pH 7.6, at 37°C. The reaction was initiated by the addition of a substrate mixture containing ribose-5-phosphate (R5P) and xylulose-5-phosphate. This substrate mixture was prepared by dissolving 50 mM R5P in 50 mM Tris-HCl, pH 7.6, in the presence of 0.1 U/mL ribulose-5-phosphate-3-epimerase and 1.7 mU/mL phosphoriboisomerase and incubated with agitation at 37°C for 1 h and then stored at -20°C until use.

4.8.3 Glucose-6-phosphate dehydrogenase (G6PDH, EC 1.1.1.49)

G6PDH specific activity was measured by adding samples to a cuvette containing 0.5 mM $NADP^+$ in 50 mM Tris-HCl, pH 7.6, at 37°C. Reaction was initiated by the addition of glucose-6-phosphate at a final concentration of 2 mM.

4.8.4 Alanine transaminase (ALT, EC 2.6.1.2)

ALT specific activity was measured using a two-reagent commercial kit (ABX Pentra). Reagent 1 consisted of 140 mM Tris pH 7.5, 709 mM L-alanine, ≥ 1700 U/L LDH and reagent 2 consisted of 85 mM α-KG and 1.09 mM NADH. Reaction was initiated by the addition of samples to a cuvette containing reagents 1 and 2 mixed in a 4:1 proportion.

4.9 Western Blotting

Cell extracts were obtained from either fresh cells or frozen plates using RIPA buffer (50 mM Tris pH 8.0, 150 mM NaCl, 0.1% SDS, 1% Triton X-100 and 0.5% sodium deoxycholate) supplemented with protease inhibitor cocktail (Sigma-Aldrich). The

same procedure described in Section 4.8 was followed to obtain cell protein extracts. Protein concentration from the supernatant was determined by the BCA assay. 30-40 μg of protein were loaded and separated by 10% SDS-PAGE and proteins were transferred to a polyvinylidene fluoride membrane. Membranes were blocked by incubation with PBS-Tween (0.1% (v/v)) containing 5% non-fat dried milk for 1-2 h at room temperature. Then, membranes were incubated with primary antibodies according to the conditions indicated below. In order to remove the excess of primary antibody, membranes were rinsed with PBS-Tween (0.1% (v/v)) and incubated with the appropriate horseradish peroxidase-conjugated secondary antibody for 1 h at room temperature. Afterwards, membranes were washed again with PBS-Tween (0.1% (v/v)) before protein detection. All blots were treated with the Immobilon ECL Western Blotting Detection Kit Reagent (Millipore) and developed after exposure to Fujifilm X-ray film in the darkroom. The following primary antibodies were used: ATP-Citrate lyase (ref. 4332, Cell Signaling, 1/1000, incubation o/n at 4°C), CPT1 (ref. SAB1410234, Sigma, 1/200 incubation o/n at 4°C), PDH (ref. ab110330, Abcam, 1/1000, incubation o/n at 4°C), PDH-P (ref. ABS204, Millipore, 1/10000, incubation o/n at 4°C), PDHK1 (ref. 3820S, Cell Signaling, 1/1000, o/n at 4°C), GLS1 (ref. ab93434, Abcam, 1/1000, incubation o/n at 4°C), GAC (ref. 19958-1-AP, Proteintech, 1/200, incubation o/n at 4°C), KGA (ref. 20170-1-AP, Proteintech, 1/1000, incubation o/n at 4°C), and actin (ref. 69100, MP Biomedicals, 1/120000, 30 min at room temperature). The following secondary antibodies were used: anti-mouse (ref. PO260, Dako, 1/3000, 1 h at room temperature) and anti-rabbit (ref. NA934V, Amersham Biosciences, 1/3000, 1 h at room temperature).

4.10 ATP measurement

The quantity of ATP present in cells was measured by CellTiter-Glo® Luminescent Cell Viability Assay (Promega, Madison, WI). The ATP assay was performed according to the manufacturer's instructions. Luminescent intensity from each well was measured with a FLUOstar Optima plate reader (BMG Labtech, Offenberg, Germany). The ATP values obtained were normalized to the number of cells determined by the Hoechst staining (Section 4.2).

4.11 RNA isolation, reverse transcription and gene expression analysis

RNA isolation was performed from fresh or frozen pellets or cultured plates using Trizol® reagent (Invitrogen) following the manufacturer's instructions. Importantly, all pipette tips, tubes and eppendorfs used along the isolation process were RNAse-free. Briefly, Trizol® was added to samples and cell homogenates were mixed with chloroform and centrifuged, resulting in an upper aqueous phase, an interphase and a lower organic phase. RNA was precipitated from the aqueous phase by adding cold isopropanol and leaving the samples in the cold room overnight. Next, samples were centrifuged at 12000 xg for 15 min at 4°C and supernatant was removed and the pellet was washed three times with cold 75% ethanol. After ethanol evaporation at room temperature, RNA was resuspended in RNAse-free water for subsequent spectrophotometric quantification with a Nanodrop instrument (Thermo, Wilmington, DE). Next, cDNA was obtained from 1 μg of RNA using random hexamers (Roche) and M-MLV reverse transcriptase (Invitrogen) according to the manufacturer's indications. Gene expression analysis was performed by quantitative real-time RT-PCR (ABI Prism 7700 Sequence Detector System, Applied Biosystems), using either gene-specific TaqMan® assays (Applied Biosystems) or the Universal Probe Library system (UPL; Roche), following the specific running conditions recommended in each case. For the TaqMan® assays, the resulting cDNA was mixed with PCR Master Mix™ containing the specific TaqMan® probes for each gene (TKT: Hs00169074_m1; G6PD: Hs00166169_m1; TKTL1: Hs00202061_m1; SOX2: Hs01053049_s1; PPIA: Hs99999904_m1). Subsequently, ΔΔCt method was used for calculating the fold changes in gene expression using PPIA as reference (housekeeping) gene. In the case of the transcripts quantified with the UPL system, RT-PCR assays were performed on a LightCycler 480 instrument (Roche) and analyzed with the LightCycler 480 Software release 1.5.0. The amplification levels of RN18S1 and HMBSE were used as an internal reference to estimate the relative levels of specific transcripts, and relative quantification was determined by the ΔΔCt method. Probes and sequences from the UPL system were:

GENE	UPL PROBE		OLIGONUCLEOTIDES 5'→3'
PDHK1	#21	FW	aaatgccacgtaaccaaagc
		REV	agagcggagaccctgtcttga
PDP2	#49	FW	agctgggtcctgactaggg
		REV	tccgtccggtcagttcag
SNAI1	#11	FW	gctgcaggactctaatccaga
		REV	atctccggaggtgggatg
KLF4	#82	FW	gccgctccattaccaaga
		REV	tcttcccctctttggcttg
ESRP1-HA	#18	FW	attcggatccatgacggcctctccggatac
		REV	gaatctcgacttaggcgtagtcaggcacgtcgtaaggataaatacaaacccattctttgggtag
ESRP2-HA	#34	FW	attcggatccatgactccgccgccgccgccg
		REV	gaatgtcgacttaggcgtagtcaggcacgtcgtaaggatacaaacacaccattggttgggggc
GAC	#85	FW	ctgcagagggtcatgttgaa
		REV	atccatgggagtgttattcca
KGA	#11	FW	gcaaaataatgaaccccaaatta
		REV	tggcataaatgtaaacacaagctaa
RN18S1	#40	FW	ggagagggagcctgagaaac
		REV	tcgggagtgggtaatttgc
HMBS	#26	FW	tgtggtgggaaccagctc
		REV	tgttgaggtttccccgaat

4.12 Transcriptomic analysis

Cells were grown to 70-80% confluence, lysed and RNA isolated with the RNeasy Kit (Qiagen, Hilden, Germany), including a DNase digestion step. For microarray analysis, RNAs were amplified, labeled and hybridized to Affymetrix U133 2.0 Plus arrays (Affymetrix, Santa Clara, CA). Microarray data were normalized using the robust multi-array (RMA) algorithm (2). Next, we employed a conservative probe-filtering step, eliminating those probes with a maximum expression value lower than 5. To identify differentially expressed genes, we applied Significance Analysis of Microarrays (SAM-R) (3), selecting those genes with a False Discovery Rate below 10% (Q < 10). Comparative transcriptomic analysis between PC-3M and PC-3S was performed on independent triplicate samples.

4.13 siRNA transfection

PC-3M and PC-3S cells were transfected using the transfection reagent Metafectene (Bioentex, Munich, Germany) according to the manufacturer's instructions. Briefly, $0.5 \cdot 10^5$ PC-3M and $1 \cdot 10^5$ PC-3S cells were seeded in 6-well plates and after 24 h, 30 nM of either control siRNA (siNEG) or siRNA against TKTL1 (siTKTL1) were transfected.

RNAi sequences employed were purchased from Dharmacon (Lafayette, CO, USA). The highest efficiency in TKTL1 gene silencing was accomplished with 5'-GGAGUUGCAUGUGGAAUGG-3' (catalog no. J-004736-06). and the siNEG was a non-targeting siRNA, sequence not provided by the manufacturer (catalog no. D-001810-03).

4.14 Mitochondrial staining

10^5 cells were seeded onto sterile glass coverslips in 24-well plates 16-24 h before treatment. For immunofluorescence analysis, PC-3M and PC-3S cells seeded on coverslips were incubated with 300 nM MitoTracker® CMXRos (Invitrogen, CA, USA) 30 min at 37˚C. After incubation, cells were washed in PBS, fixed in 4% formaldehyde and mounted in ProLong® Gold Antifade Mountant with DAPI. Optical sections were acquired using a Leica TCS SP5 confocal system (Leica Microsystems, Manheim).

4.15 ^{13}C-tracer-based metabolomics

To carry out these ^{13}C-tracer-based experiments, at the beginning (t = 0 h) culture media was replaced by fresh media containing either 10 mM 100% or 10 mM 50% [1,2-$^{13}C_2$]-glucose (Sigma-Aldrich), 10 mM 100% [U-$^{13}C_6$]-glucose (Sigma-Aldrich) or 2 mM 100% [U-$^{13}C_5$]-glutamine (Sigma-Aldrich) and after the incubation period indicated in each case, media, pellets and cell cultured plates were collected. Media samples were frozen at -20°C for ulterior determination of glucose, lactate, glutamate and glutamine concentrations as described in Section 4.7. These media samples were also used for determination of the mass isotopomer distributions in glucose, lactate, alanine, glutamate, serine and glycine. Pellets were obtained by trypsinization and kept at -20°C until the analysis of mass isotopomer distribution of ribose and fatty acids. Cultured plates were frozen in liquid nitrogen and stored at -80°C for the analysis of mass isotopomer distribution of tricarboxylic acid (TCA) cycle intermediates.

Analysis of ^{13}C-labeled extracellular and intracellular metabolites for mass isotopomer distribution was done by gas chromatography coupled to mass spectrometry (GC/MS). GC/MS was performed using an Agilent 7890A GC equipped with a HP5 capillary

column connected to an Agilent 5975C MS. Fatty acids GC/MS analysis was performed employing a GCMS-QP 2012 Shimadzu equipped with a bpx70 (SGE) column. In all cases, 1 μL of sample was injected at 250°C using helium as a carrier gas at a flow rate of 1 mL/min.

Supplementary data for mass isotopomer distribution of the analyzed metabolites and the conditions of each ^{13}C-tracer experiment are shown in **Appendix 1**.

Different procedures for metabolite isolation, derivatization and detection were used for each metabolite as described below.

4.15.1 Glucose from culture media

Glucose was isolated from cell culture media using a tandem set of Dowex-1X8/Dowex-50WX8 ion-exchange columns, through which glucose was eluted with water. After that, water was evaporated to dryness under airflow and isolated glucose was heat to 100°C first with 2% (v/v) hydroxylamine hydrochloride in pyridine for 30 min and then acetic anhydride for 60 min more for derivatization. Excess of reagent and solvent was removed by evaporation with N_2 flow, and glucose derivative was dissolved in ethyl acetate for GC/MS analysis under chemical ionization mode.

4.15.2 Lactate from culture media

Culture media was acidified by addition of hydrochloric acid (HCl) and the lactic acid produced was extracted with ethyl acetate and evaporated to dryness under N_2 flow. Dried lactate was incubated at 75°C for 1 h in presence of 2,2-dimethoxypropane and methanolic HCl. Next, n-propilamine was added to the reaction mixture, kept at 100°C for 1 h and evaporated to dryness under N_2 flow. To remove the n-propylamine-HCl salt, the precipitate obtained was resuspended in ethyl acetate and filtrated through a glass wool packed Pasteur pipette. After drying the filtered solution under N_2 flow, dichloromethane and heptafluorobutyric anhydride were added and incubated at room temperature for 10 min. After that, sample was evaporated to dryness under N_2 and resuspended in dichloromethane for GC/MS analysis under chemical ionization mode.

4.15.3 Glutamate from culture media

Sample media was passed through a Dowex-50WX8 (H^+) column. Amino acids were eluted with 2 N NH_4OH and the solution was evaporated to dryness under airflow. To further separate glutamate from glutamine, the amino acid mixture was passed through a Dowex-1X8 ($C_2H_3O_2^-$) column. Glutamine was removed with water, and glutamate was collected by elution with 0.5 N acetic acid. The acid-fraction containing glutamate was evaporated to dryness. Dried glutamate was therefore incubated in butanolic HCl at 100°C for 1 h. The excess of reagents was removed under N_2 and the precipitate was dissolved in dichloromethane and trifluoroacetic anhydride, and left at room temperature for 20 min. Then, samples were dried under N_2, and the derivative was dissolved in dichloromethane for injection into GC/MS equipment. GC/MS analysis was performed under electron impact mode, which yields C2-C4 and C2-C5 glutamate fragments.

4.15.4 Alanine, serine and glycine from culture media

Sample media was passed through a Dowex-50WX8 (H^+) column. Amino acids, including alanine, serine and glycine, were eluted with 2 N NH_4OH and the solution was evaporated to dryness under airflow. Dried samples were then kept at 100°C for 1 h in butanolic HCl. The excess of reagents was removed under N_2 flow and the precipitate was dissolved in dichloromethane. The derivatization reaction was completed with the addition of trifluoroacetic anhydride, and left at room temperature for 20 min. Then, samples were dried under N_2, and the amino acids derivatives were dissolved in dichloromethane for injection into GC/MS equipment, where they were analyzed under chemical ionization mode.

4.15.5 Ribose from cell extracts

Ribose from RNA was isolated from the aqueous phase after addition of Trizol® (Invitrogen) to the cell pellets, as described in Section 4.11. Purified RNA was hydrolyzed in 2 N HCl at 100°C for 2 h and the solvent was evaporated to dryness under airflow. RNA ribose was derivatized as previously described for glucose (Section 4.12.1) and GC/MS analysis was performed under chemical ionization mode.

4.15.6 Palmitate and estereate from cell extracts

Fatty acids from cultured cells were hydrolized from the interphase and lower phase after addition of Trizol® to the cell pellets, as described in Section 4.11, by adding 100% ethanol and 30% potassium hydroxide. Samples were then incubated at 70°C overnight, and afterwards free fatty acids were extracted with petroleum ether, which was subsequently evaporated to dryness under N_2 flow. Fatty acids were then derivatized adding methanolic HCl and incubated at 70°C for 1 h and after that the solution was evaporated under N_2. Fatty acids derivatives were dissolved in hexane and GC/MS analysis was performed under chemical ionization mode.

4.15.7 TCA intermediates from cell extracts

TCA cycle intermediates from cultured cells were extracted from liquid nitrogen frozen cultured plates with addition of 100% methanol:H_2O (1:1) mixture and scrapping on ice. Then, cell extracts were sonicated using a titanium probe (VibraCell, Sonics & Materials Inc., Tune: 50, Output: 30). Chloroform was added to the cell lysate and tubes were placed in a shaker for vigorous agitation at 4°C for 30 min. After that, samples were centrifuged and the upper aqueous phase was separated and evaporated to dryness under airflow at room temperature. TCA cycle intermediates were derivatized by adding 2% (v/v) methoxyamine hidrochloride in pyriridine and shaked vigorously at 37 °C for 90 min. Next, N-methyl-N-(tert-butyldimethylsilyl)trifluoroacetamide (MBTSTFA) + 1% tert-butyldimetheylchlorosilane (TBDMCS) was added and samples were incubated for 1 h at 55°C and finally transferred to GC/MS vials. GC/MS analysis was performed under electron impact ionization mode.

4.16 GC-MS data reduction

Spectral data obtained from a mass spectrometer simply represent the distribution of ions of a certain compound (or its fragments) with different molecular weights. The value for each observed m/z is given by the experimental isotope incorporation, the presence of natural abundance of ^{13}C in the background and, when corresponds, the ^{12}C isotope impurity in the ^{13}C-labeled precursor used as a tracer (e.g. glucose or

glutamine). Furthermore, the derivatizing reagents often contain isotopes (e.g. Si isotopes) which contribute to the mass isotopomer distribution of the derivatized compound as well. Therefore, correction for all such contributions is necessary before the amount of isotope incorporation and its distribution in the compound of interest can be determined. This correction was performed by using regression analysis employing in-house developed software. The algorithm used corrects all the previous detailed contributions over the observed spectral intensities of each ion cluster, and provides the mass isotopomer distribution in the analyzed metabolite due to incorporation of ^{13}C atoms from the tracer used as precursor. Results of the mass isotopomers in any of the ion clusters were reported as fractional enrichments of molecule isotopomers, defined as the fraction of molecules having a certain number of isotope substitutions. Thus, they are designated as m0, m1, m2, etc. where the number indicates the number of labeled carbons (^{13}C) in the molecule corrected as described above. Note that the sum of all mass isotopomers of the ion clusters is equal to 1 (or 100%).

4.17 Mass isotopomer distribution analysis

Apart from the mass isotopomers results (m0, m1, m2, etc.), some ratios and calculations can be made in order to elucidate the contribution of specific metabolic pathways to the synthesis of a certain compound. Some of these ratios are explained along the results presented in Section 5. However, the estimation of the glucose-derived lactate from specific metabolic pathways is detailed here, due to the numerous equations that must be taken into account.

4.17.1 Contribution of glycolysis, PPP and other pathways to the synthesis of lactate

The amount of lactate produced from glucose via glycolysis, PPP or other substrates can be estimated by combining lactate concentrations and the mass isotopomer distribution of lactate in cell culture media, using 10 mM 50% [1,2-$^{13}C_2$]-glucose as a tracer. These calculations are made assuming that PC-3M and PC-3S cells only produce lactate (without lactate consumption). Thus, the amount of unlabeled lactate present in the media at the beginning of the incubation with the glucose tracer will contribute

to the m0 lactate pool at the end of the experiment. Mass isotopomer distribution of the produced lactate ($Lac_{Total}(m0,m1,m2,m3)t_f$) was multiplied by final lactate concentration to obtain the absolute mass isotopomer distribution of total lactate in mM ($[Lac_{Total}(m0,m1,m2,m3)t_f)]$ (mM)). Next, initial lactate concentration was subtracted from the concentration of total lactate m0 (mM) to obtain the produced lactate, in mM, without including the initial unlabeled lactate. Next, relative mass isotopomer distribution of produced lactate ($Lac_{Prod}(m0,m1,m2,m3)t_f$) was recalculated by dividing ($[Lac_{Total}(m0,m1,m2,m3)t_f)]$ (mM)) values by total produced lactate ($[Lac_{Prod}]$), obtained by subtracting initial lactate concentration from final lactate concentration.

From the recalculated mass isotopomer distribution of produced lactate, the percentage of lactate that comes from glucose through direct glycolysis (glycolytic tax, GT) was calculated as follows:

$GT = Lact_{Prod}(m2) * 2/ Glc(m2)t_i$ (%)

where $Glc(m2)t_i$ is the percentage of [1,2-$^{13}C_2$]-glucose in the cell culture media at the beginning of the experiment. Next, maximum feasible amount of lactate coming from glycolysis ($[Lac_{ProdGlyc}]$) was obtained by multiplying GT by produced lactate:

$[Lac_{ProdGlyc}]$ = GT * $[Lac_{Prod}]$ (mM)

In order to calculate the amount of lactate from glucose coming through the pentose phosphate pathway (PPP), that is, the Pentose Cycle (Pc) parameter, we used the next expression, which includes values of mass isotopomer distribution of total lactate:

$$Pc = \{Lac_{Tot}(m1)_{tf}/Lac_{Tot}(m2)_{tf}\}/\{3+Lac_{Tot}(m1)_{tf}/Lac_{Tot}(m2)_{tf}\}$$

The Pc parameter is defined as the relative amount of glucose metabolized through glycolysis related to the glucose metabolized through PPP. A detailed description of this parameter and the deduction of the equation can be found in *Lee et al*., 1998 (*274*).

Lactate from glucose coming through PPP [$Lac_{ProdPPP}$] was obtained by multiplying Pc value per the maximum feasible amount of lactate coming from glycolysis, determined before:

$[Lac_{ProdPPP}] = Pc * [Lac_{ProdGlyc}]$(mM)

In order to calculate the amount of lactate produced from other sources different from glucose [Lac_{ProdOS}], the maximum lactate produced from glycolysis and lactate coming from glucose through PPP was subtracted to produced lactate:

$[Lac_{ProdOS}] = [Lac_{Prod}] – [Lac_{ProdGlyc}] – [Lac_{ProdPPP}]$ (mM)

4.18 Reactive oxygen species (ROS) levels measurement

Total intracellular ROS levels were determined by means of flow citometry using the H_2DCFDA probe (Invitrogen). Cells were incubated with incubation buffer (5.5 mM glucose in PBS containing 5 μM H_2DCFDA for 30 min at 37 ˚C and 5% CO_2. This first incubation allows cells to incorporate the probe. After that, this solution was replaced by warm culture media (including 10 μM BPTES in the experiment described in **Chapter II**) and cells were incubated for 45 min at 37˚C and 5% CO_2. This second incubation allows the activation of the probe by the action of intracellular esterases. Next, cells were trypsinized and resuspended in a PBS solution consisted of 50 μM H_2DCFDA and 20 μg/mL PI. Internalized and activated probe reacts with ROS and emits fluorescence when excited at 492 nm. Emitted fluorescence was recorded by flow citometry at 520 nm wavelength. For ROS analysis, only negative PI cells were considered.

4.19 Intracellular glutathione content

Total glutathione content was determined by glutathione reductase enzymatic method. Fresh cells were lysed with 5% 5-sulfosalicylic acid (Sigma-Aldrich) solution, vortexed and disrupted by two freezing/thawing cycles in liquid N_2 and 37˚C water bath. 50 μL of this solution was separated for subsequent protein quantification. Cell extracts were kept at 4˚C for 10 min and centrifuged at 10000 xg for 10 min. For glutathione quantification, a working solution consisted of 15 U/mL of glutathione

reductase and 40 μg/mL of 5,5'-Dithiobis(2-nitrobenzoic acid) (Sigma-Aldrich) dissolved in assay buffer (100 mM K_2HPO_4/KH_2PO_4, 1 mM EDTA, pH 7.0) was prepared. Glutathione standards were prepared from a 50 mM oxidized glutathione (GSSG) stock solution. Reaction was initiated by mixing 150 μL of working solution with 10 μL of cell extract (diluted 1:5 or 1:10) or 10 μL of GSSG standard (final concentrations from 0 to 12.5 μM). Next, 50 μL of 0.16 mg/mL NADPH solution was added and the increase in absorbance was recorded at 340 nm wavelength. Total glutathione concentration was normalized by protein content determined by the BCA method.

4.20 Oxygen consumption rate (OCR) and extracellular acidification rate (ECAR)

A XF24 Extracellular Flux Analyzer (Seahorse Bioscience) was used to measure the rate change of dissolved oxygen and protons in media immediately surrounding adherent cells cultured in a XF24-well microplate (Seahorse Bioscience). PC-3M and PC-3S cells were seeded in XF24-well microplates at $4.5 \cdot 10^4$ cells/well and $9.0 \cdot 10^4$ cells/well, respectively, in 100 μL of growth medium, adding 100 μL more after 3-5 h, and then incubated at 37 °C with 5% CO_2 overnight. After overnight incubation and 1 h before the Seahorse assay, growth media was replaced by basal media (unbuffered DMEM; Sigma-Aldrich) with or without supplements, depending on the experiment). The sensor cartridge with the four reagent delivery chambers (A, B, C and D) per well was loaded with the injecting testing agents and calibrated prior to the start of the Seahorse experiment. The different experimental tests performed and the composition of the initial basal media as well as the final concentrations of the injected compounds are indicated below. For OCR and ECAR baseline values, OCR and ECAR results were further normalized to the number of cells present in each well, quantified by the Hoechst staining (Section 4.2). Responses to the different treatments are expressed as LOG2 to indicate the fold change comparing the measured point immediately after and before the corresponding injection. All the drugs used for these experiments were purchased from Sigma-Aldrich.

4.20.1 Glucose test

Analysis of the OCR decrease after glucose addition (Crabtree effect). Basal media contained 2 mM glutamine.

PORT	COMPOUND	FINAL CONCENTRATION
A	Glucose	18.75 mM

4.20.2 Etomoxir test

Analysis of the contribution of fatty acid β-oxidation to OCR by injecting etomoxir, a carnitine palmitoyltransferase 1 (CPT1) inhibitor, which impairs the transport of fatty acids into the mitochondria. Basal media contained 3 mM glucose and 5 mM carnitine.

PORT	COMPOUND	FINAL CONCENTRATION
A	Etomoxir	30 μM

Both glucose and etomoxir tests, showed the following OCR profile after injection of the compounds:

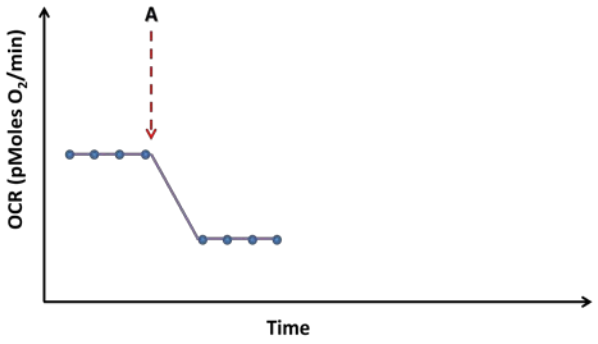

4.20.3 Mito Stress test

Analysis of the mitochondrial function and potential by injection of oligomycin (ATP synthase inhibitor), carbonilcyanide p-trifluoromethoxyphenylhydrazone (FCCP) (mitochondrial uncoupler) and rotenone + antimycin (mitochondrial complex I and III inhibitors, respectively). FCCP response was further enchanced by pyruvate. For the different experiments using this test, four types of basal media were used: minimal

media (without glucose and glutamine), glucose media (with 17 mM glucose), glutamine media (with 2 mM glutamine) and full media (2 mM glutamine and 17 mM glucose).

PORT	COMPOUND	FINAL CONCENTRATION
A	Oligomycin	5 μM
B	FCCP + Pyr	600 nM + 2 mM
C	Rotenone + Antimycin	2 μM + 2 μM

The simplified OCR profile for the Mito Stress test is depicted here:

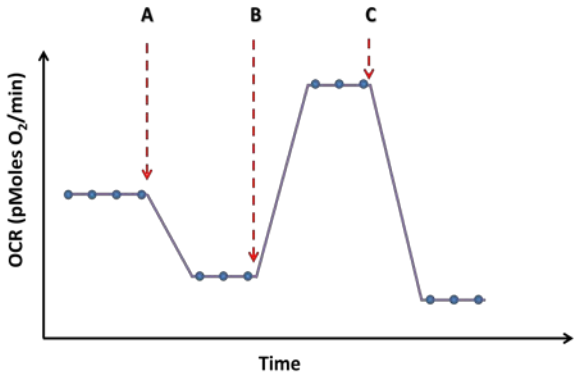

4.20.4 Oxamate and DCA titrations

Oxamate is a LDH inhibitor whereas dichloroacetate (DCA) inhibits pyruvate dehydrogenase kinases (PDHKs) and consequently allows the activation of the pyruvate dehydrogenase (PDH) complex. This experiment was performed to analyze the effect of promoting the entry of pyruvate into the mitochondria and elucidate the degree of PDH activity in PC-3M and PC-3S cells. Basal media contained 2 mM glutamine and 10 mM glucose. Accumulated oxamate and DCA concentrations were reached after each injection.

PORT	COMPOUND	FINAL CONCENTRATION
A	Oxamate	10 mM
B	Oxamate	30 mM
C	Oxamate	50 mM
D	Oxamate	70 mM

PORT	COMPOUND	FINAL CONCENTRATION
A	DCA	10 mM
B	DCA	20 mM
C	DCA	30 mM
D	DCA	40 mM

The OCR profile for oxamate and DCA titrations follows a similar trend, being the highest OCR fold change achieved after the first injection (port A):

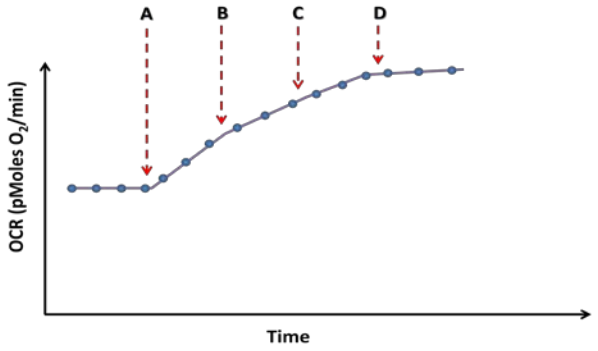

Another assay was performed, where the effect of the coinjection of oxamate and DCA was analyzed. These two experiments, performed in parallel, were compared:

PORT	COMPOUND	FINAL CONCENTRATION
A	Basal media	(indicated above)
B	Oxamate	30 mM

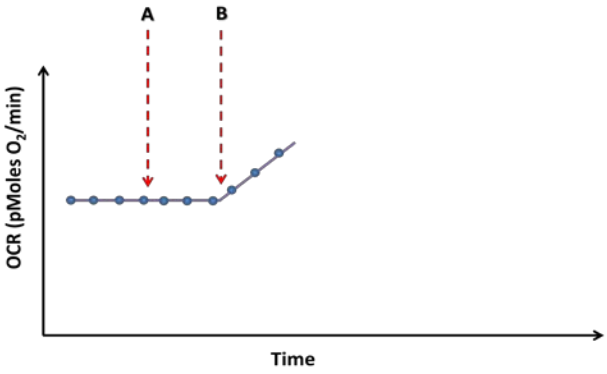

and

PORT	COMPOUND	FINAL CONCENTRATION
A	DCA	10 mM
B	Oxamate	30 mM

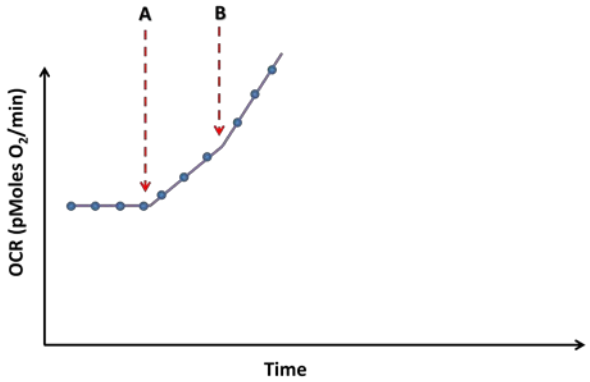

4.21 Statistical analysis

For statistical analysis, the two-tailed Student's t-test for independent samples was applied. In figures, bars represent mean ± standard deviation (SD) and number of replicates (n) is indicated in each case. Single asterisk indicates a significant difference at p-value < 0.05, double asterisks indicate a significant difference at p-value < 0.01 and triple asterisk indicate a significant difference at p-value < 0.001. Non-significant differences (p-value > 0.05) are indicated in some cases as NS.

5. RESULTS AND DISCUSSION

Identification of glucose metabolism through glycolysis and biosynthetic pathways in a dual prostate cancer cell model displaying uncoupled CSC and EMT phenotypes

5.1.1 Introduction

It is widely accepted that cancer cells have high rates of aerobic glycolysis, a process known as the "Warburg effect", and that most tumor cells are more dependent on this metabolic pathway for ATP synthesis and to match the increased anabolic needs for precursor metabolites (*275*). Nevertheless, more recently the tricarboxilic acid (TCA) cycle and oxidative phosphorylation (OXPHOS), which will be addressed more specifically in **Chapter II**, have been shown to play a significant role in cancer cells (*276-278*). Global metabolic analysis has elucidated major metabolic differences between cancer *vs*. non-cancer cells or advanced *vs*. primary tumors, but little is known about the metabolic properties associated with different cancer cell phenotypes that result from the intrinsic tumor cell heterogeneity.

Chapter I focuses on the characterization of the glycolytic profiles of our dual prostate cancer cell model comprising PC-3M and PC-3S cell subpopulations (described in Section 2.5) with regards to bioenergetics and biosynthetic pathways closely linked to glycolysis. As described in the Introduction, CSC and EMT phenotypes constitute two important driving forces for the metastatic cascade. A search for phenotype-specific metabolic requirements, in this case at the level of the glycolytic metabolism, represents an interesting approach to better understand the metabolic vulnerabilities of heterogeneous tumor cell populations with distinct phenotypes and propose metabolic targets that could be used for therapeutic purposes.

We have addressed the study of metabolic reprogramming linked to the glycolytic pathway mainly through biochemical assays, ^{13}C-assisted metabolomics and Seahorse

Bioscience technology, and the following interconnected pathways have been explored: i) aerobic glycolysis (the Warburg effect), ii) pentose phosphate pathway (PPP), iii) fatty acid metabolism and iv) amino acid synthesis from glucose.

In addition to the comparison between PC-3M and PC-3S cells, we have also performed the characterization of cell proliferation and glycolytic profile of two additional PC-3M cell variants (PC-3M SNAI1 and PC-3M SKM triple-KD) that display an intermediate CSC-EMT phenotype. The goal here is to test the importance of EMT (represented by SNAI1 transduction) and the Yamanaka pluripotency factors (as explored by knockdown of SOX2, KLF4 and MYC) in the maintenance of the metabolic characteristics displayed by the highly metastatic PC-3M subpopulation. The procedures for obtaining these cell variants are described in Section 4.1.

5.1.2 Results and discussion

5.1.2.1 Metastatic prostate CSCs display an enhanced glycolytic metabolism and are more sensitive to glucose deprivation and 2-DG treatment.

In order to characterize the metabolism associated with CSC and EMT cell phenotypes displaying clear-cut differences in local invasiveness and metastatic potential, we worked with two clonal cell subpopulations (PC-3M and PC-3S) derived from the PC-3 prostate cancer cell line. These cells were previously obtained from the parental PC-3 cell line and several genomics and functional studies were carried out, as described in (*49*), to define their main differential transcriptomic and functional characteristics. Thus, in this unique dual-cell model, the PC-3M subpopulation is enriched in CSC features, is highly metastatic and expresses an epithelial phenotype, whereas the PC-3S subpopulation lacks CSC properties but displays an EMT program (mesenchymal-like phenotype) and it is highly locally invasive but poorly metastatic. **Figure 5.1.1.A** illustrates the remarkable differences between these two subpopulations in terms of *in vitro* cell proliferation. Under conditions of exponential growth, doubling times were 20-24 h for PC-3M and 50-65 h for PC-3S cells. **Figures 5.1.1.B** and **5.1.1.C** also illustrate the invasive potential and clonogenic capacity of these cells (i.e. ability to grow in suspension culture), confirming that PC-3M cells grow faster than PC-3S cells and are more clonogenic, whereas PC-3S cells show a higher invasive capacity.

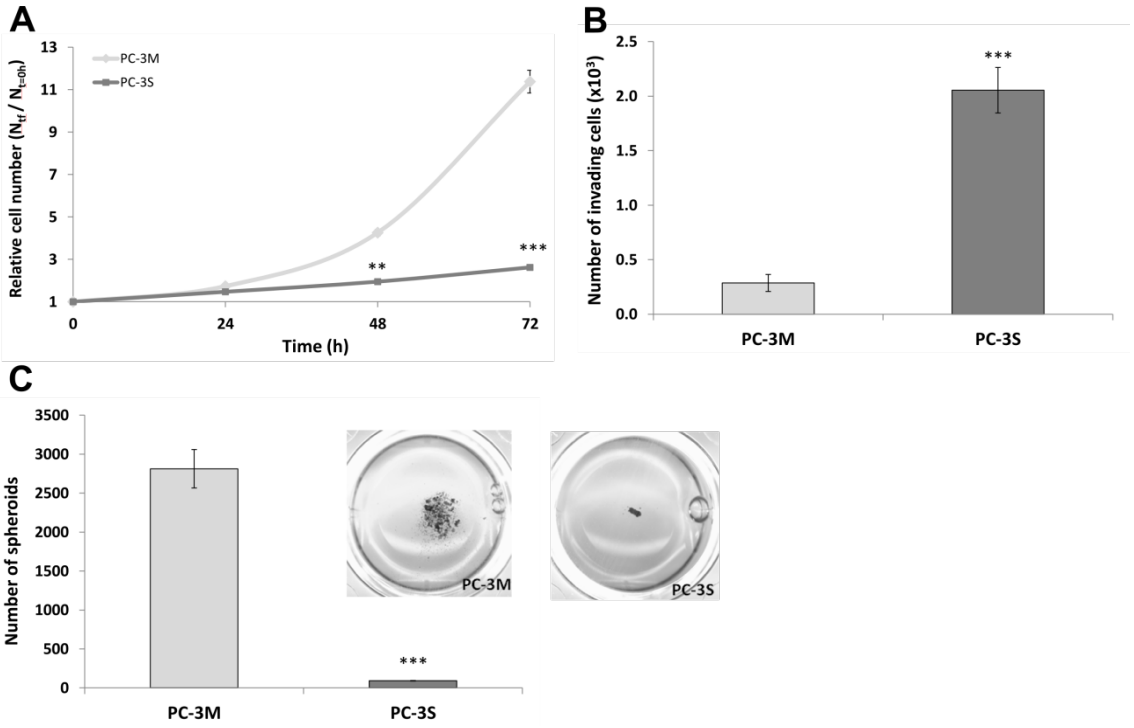

Figure 5.1.1 Comparative cell proliferation, invasive potential and clonogenic assays (PC-3M *vs*. PC-3S)

(**A**) Proliferation rate of PC-3M and PC-3S cell subpopulations grown in full RPMI 1640 media, expressed as relative cell number ($N_{tf}/N_{t=0h}$), where N_{tf} and $N_{t=0h}$ corresponds to the final and initial number of cells, respectively. (**B**) Invasive potential was evaluated in 8 μm-pore Transwell chambers coated with Matrigel and hyaluronic acid. $6.45 \cdot 10^4$ cells seeded on the upper chamber were scored for invading cells after 24 h, as described in Section 4.3. (**C**) Spheroid formation capacity was assessed using low-attachment plates. 10^3 cells seeded in the presence of 0.6% methyl cellulose were scored for spheroids after 15 days, as described in Section 4.4. Data are the mean ± SD from at least n=3. Significant differences were assessed compared to PC-3M cells by Student's t-test: *p < 0.05, **p < 0.01 and ***p < 0.001.

This isogenic cell model is unique and distinct from most other known cellular models of differential cancer cell "aggressiveness" in that, in our model, the subpopulation displaying CSC features of (PC-3M) expresses a strong epithelial gene program and is poorly autonomously invasive in *in vitro* assays but are highly metastatic *in vivo*, whereas the subpopulation with non-CSC features (PC-3S) expresses a mesenchymal gene program suggestive of a stable EMT, and is highly invasive *in vitro* yet poorly metastatic *in vivo* (*49*). Other laboratories have found that the induction of EMT and consequent expression of a mesenchymal gene program confers CSC properties, including the instauration of a Warburg effect (*271*). Unlike these mixed-cell tumor

models, our PC-3M and PC-3S cell model provides us with the unique opportunity to test hypotheses on the metabolic wiring underlying a CSC phenotype that is fully uncoupled from EMT.

As an initial approach to our analysis, we considered the hypothesis that our epithelial CSC subpopulation (PC-3M) and the mesenchymal EMT subpopulation (PC-3S) might display a different degree of the Warburg effect. In order to characterize the glycolytic profile of our dual cell model, we assessed the extracellular acidification rate (ECAR), which predominantly reflects the production of lactic acid derived from glycolysis, with little contribution from CO_2 produced in the TCA cycle. This analysis was performed in full media conditions (10 mM glucose + 2 mM glutamine) (**Figure 5.1.2.A**). The results obtained clearly showed that ECAR was significantly higher in PC-3M than in PC-3S cells. Consistent with these results, PC-3M cells consumed more glucose and produced more lactate than PC-3S cells (**Figure 5.1.2.B**), in agreement with a significantly higher lactate dehydrogenase (LDH) activity (**Figure 5.1.2.C**). In addition, to characterize if the contribution of glycolysis and PPP to the production of lactate is different in PC-3M and PC-3S cells, we incubated cells with 10 mM 100% [1,2-$^{13}C_2$]-glucose and analyzed the mass isotopomer distribution of extracellular lactate. The metabolism of [1,2-$^{13}C_2$]-glucose through direct glycolysis yields m2 lactate, whereas its metabolism through the PPP yields m1 lactate. Results indicated that m2 was the most abundant isotopologue of lactate, and this value was higher in PC-3M cells (**Figure 5.1.2.D**). In order to estimate the contribution of direct glycolysis, the PPP and carbon sources other than glucose (OS) to the production of lactate, we considered the mass isotopomer distribution of lactate and the initial and final lactate concentrations from a parallel experiment where 10 mM 50% [1,2-$^{13}C_2$]-glucose was used as tracer. From these data and using the equations described in Section 4.17.1, we estimated the pathway-specific production of lactate. As shown in **Figure 5.1.2.E**, direct glycolysis is the main source of lactate in both cell subpopulations. PC-3M cells exhibited a predominant increase in the production of lactate through glycolysis and the PPP. Interestingly, PC-3M cells were able to use OS to produce lactate, whereas PC-3S cells derived lactate almost exclusively from glucose through direct glycolysis and the PPP.

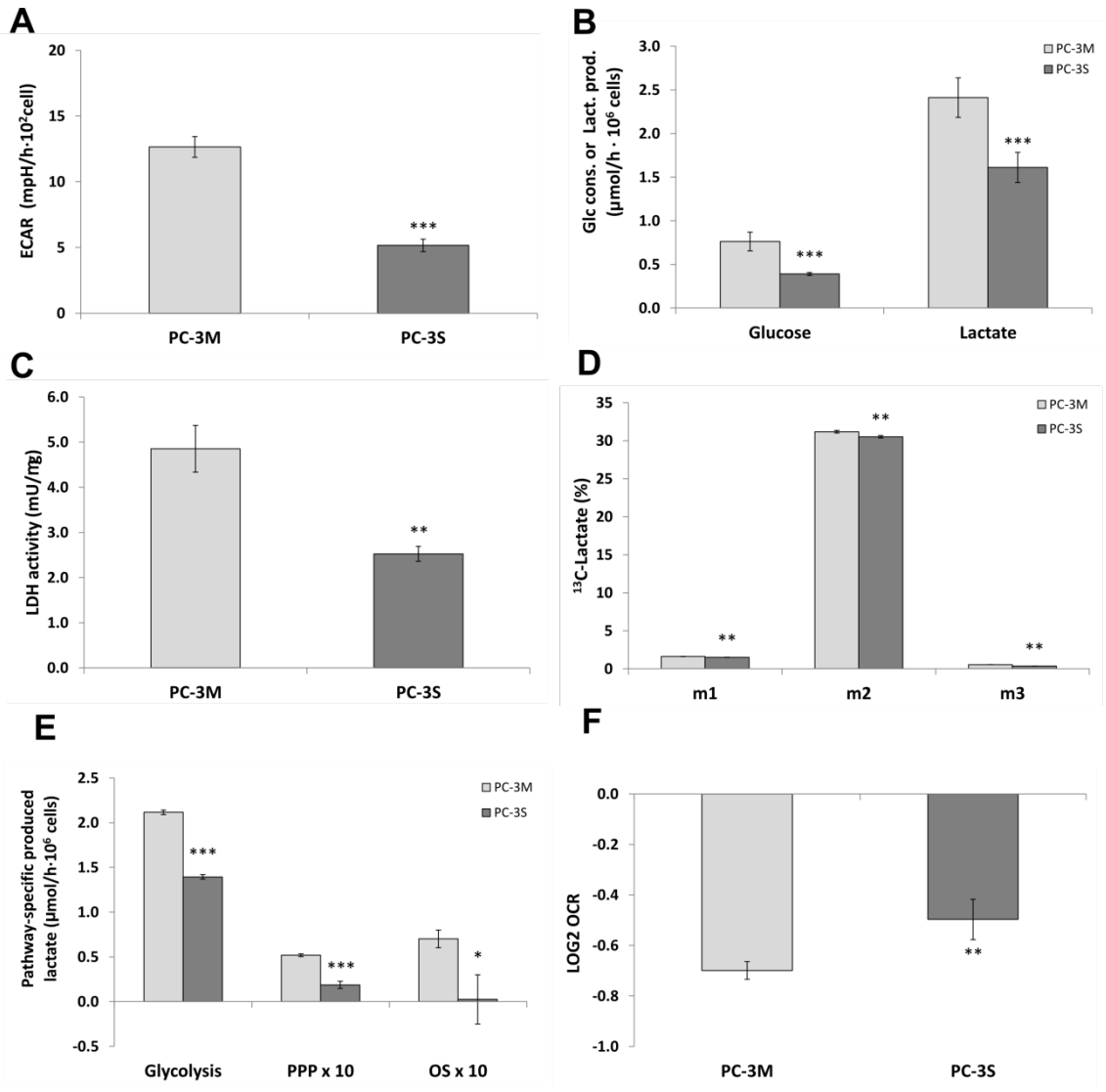

Figure 5.1.2 Comparative glycolytic profile characterization (PC-3M *vs*. PC-3S)

(**A**) The Basal ECAR levels of PC-3M and PC-3S cells, shown as absolute values normalized to cell number. (**B**) Glucose (Glc) consumption and lactate (Lact.) production rates normalized to PC-3M and PC-3S cell numbers. (**C**) Lactate dehydrogenase (LDH) activity normalized to intracellular protein content. (**D**) Mass isotopomer distribution of lactate after 24 h of incubation with 10 mM 100% [1,2-$^{13}C_2$]-glucose. (**E**) Pathway-specific lactate fluxes determined by combining mass isotopomer distribution data from an experiment with 10 mM 50% [1,2-$^{13}C_2$]-glucose and lactate concentrations, as described in Section 4.17.1. (**F**) The Crabtree effect was evaluated by adding glucose to glucose-deprived media and analyzing the fold change (LOG2) in OCR. Data are the mean ± SD from n=3 (B, C, D and E) or from n=5 (A and F). Significant differences were assessed compared to PC-3M cells by Student's t-test: *$p < 0.05$, **$p < 0.01$ and ***$p < 0.001$.

To further analyze the importance of glycolysis in these cells, the Crabtree effect was analyzed, which involves the inhibition of mitochondrial cell respiration in the presence of high levels of glucose. The amplitude of this reversible short-term effect is

an indicator of the degree of cellular preference for glycolysis as a pathway to obtain energy and metabolic precursors. After cells were incubated in basal media containing glutamine as the only carbon source, glucose was injected and the oxygen consumption rate (OCR) determined. The results showed a significantly stronger reduction in respiration in PC-3M cells as compared to PC-3S cells (**Figure 5.1.2.E**), an indicator that the CSC subpopulation expresses a marked Crabtree effect and thus it displays a stronger preference than non-CSCs for the metabolism of glucose through the glycolytic pathway when this substrate is available.

To further explore the differences in glycolytic dependence between the two subpopulations, we next analyzed the effects of glucose deprivation and 2-deoxyglucose (2-DG) treatment (i.e. blocking the upper part of the glycolytic pathway) and LDH inhibition by oxamate treatment (i.e. inhibition of the lower part of glycolysis). Glucose deprivation and 2-DG treatment reduced more significantly the proliferation of PC-3M cells as compared to PC-3S cells (**Figure 5.1.3.A**). However this decrease in cell proliferation was achieved by distinct mechanisms, as both cell subpopulations showed some contribution from cell death (**Figure 5.1.3.B**) but only PC-3M cells displayed a significant cell cycle arrest at the G1 phase (**Figure 5.1.3.C**). Moreover, glucose deprivation and 2-DG treatment also significantly enhanced glutamine consumption in PC-3M cells (**Figure 5.1.3.D**), indicating that CSCs are more sensitive than non-CSCs to changes in glucose availability and glycolytic impairment and consequently, PC-3M cells compensate for the inhibition of glycolysis by boosting alternative metabolic pathways such as glutaminolysis. On the other hand, oxamate treatment also reduced cell proliferation, more significantly in PC-3M cells (**Figure 5.1.3.E**) probably because of the disruption of the cytosolic NADH/NAD^+ balance as a result of LDH activity inhibition, which is essential for glycolysis to continue.

For tumor cells, glycolysis is an important supplier of ATP. Given the involvement of this metabolic pathway in bioenergetics, we next examined ATP levels after treating cells with 2-DG and oxamate. 2-DG decreased cellular ATP levels in both cell subpopulations but more significantly in PC-3M cells (**Figure 5.1.4.A**), whereas

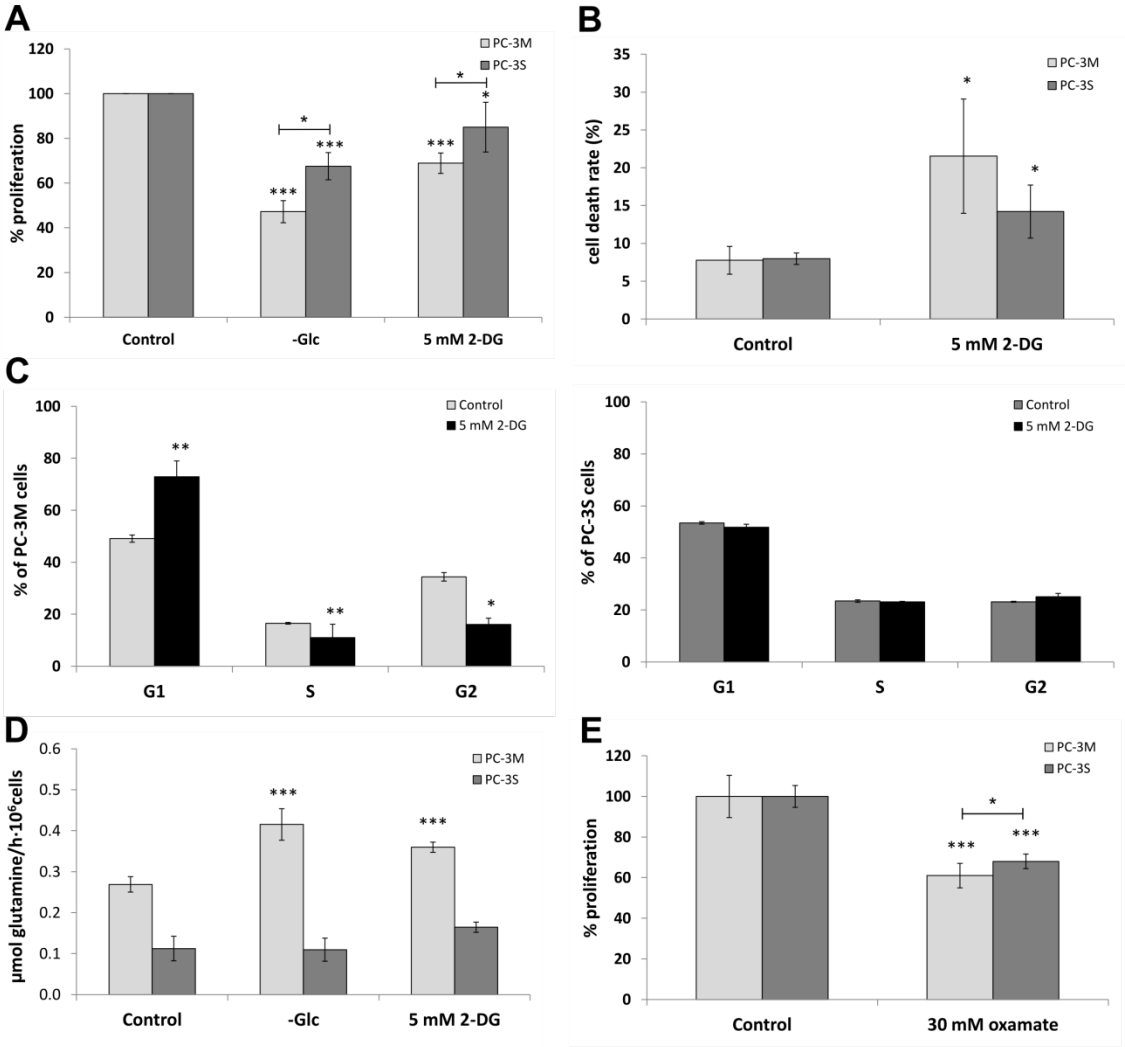

Figure 5.1.3 Differential effects on the proliferation, viability and metabolic adaptation of the disruption of the glycolytic metabolism in PC-3M vs. PC-3S cells

(**A**) Effect of glucose deprivation (-Glc) and 5 mM 2-DG treatment on cell proliferation, determined with HO33342 staining after 48 h of incubation. Results are shown as percentage of proliferation relative to cells cultured in full media and without 2-DG (Control). (**B**) Quantification of cell death in PC-3M and PC-3S cells untreated (Control) or treated with 5 mM 2-DG for 48 h. Plots depict the variations in the percentage of dead cells (apoptotic + necrotic). (**C**) Cell cycle analysis of PC-3M (left panel) and PC-3S (right panel) cells untreated (Control) or treated with 5 mM 2-DG for 48 h. The harvested cells were stained with PI and their DNA content analyzed by flow cytometry. Plots depict the variations in the percentage of cells in each phase of the cell cycle. (**D**) Glutamine consumption rate was determined after 48 h incubation without glucose or with 5 mM 2-DG. (**E**) Effect of 30 mM oxamate treatment on cell proliferation, determined with HO33342 staining after 48 h of incubation. Results are shown as a percentage of proliferation relative to untreated cells. Significant differences are compared to the corresponding PC-3M or PC-3S control condition. Data are provided as the means ± SD for n=3 (n=6 in the case of (A)). After a Student's t-test, differences were considered significant when $p < 0.05$(*), $p < 0.01$(**) and $p < 0.001$(***).

oxamate treatment increased ATP production in both cell subpopulations (**Figure 5.1.4.B**). These results suggest, on the one hand, that CSCs are more sensitive to the ATP drop after inhibition of glycolysis by 2-DG and, on the other hand, that the decrease in cell proliferation observed under oxamate treatment is not related to a reduction in ATP levels. The slight increase in ATP levels after oxamate treatment suggests that LDH inhibition could direct pyruvate towards other energetic pathways such as mitochondrial respiration, which is characterized by a high ATP yield. Indeed, we observed a synergistic effect when cells were co-treated with oxamate and dichloroacetate (DCA), an inhibitor of pyruvate dehydrogenase kinases (PDHKs) that promotes pyruvate dehydrogenase (PDH) activity (**Figure 5.1.4.B**), as the ATP levels increased by 10-20%.

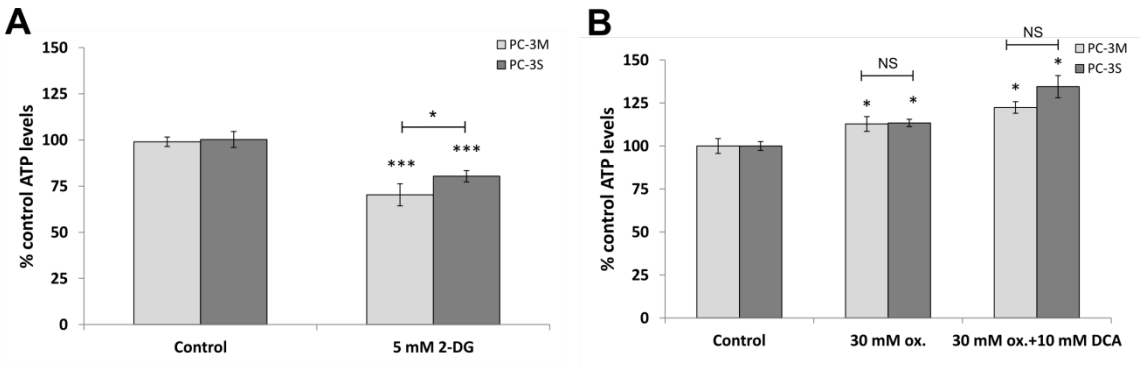

Figure 5.1.4 Differential effects of 2-DG, oxamate and DCA on the ATP content of PC-3M *vs*. PC-3S cells

Intracellular ATP levels were analyzed after 24 h of incubation with (**A**) 5 mM 2-DG, (**B**) 30 mM oxamate or 30 mM oxamate + 10 mM DCA, and values were normalized to DNA content (HO33342 staining). Data are shown as means ± SD from n=3. After using the Student's t-test, differences between treatments *vs*. were considered significant when *$p < 0.05$, **$p < 0.01$ and ***$p < 0.001$, and non-significant (NS) when $p > 0.05$.

We have shown above that our prostate epithelial CSC subpopulation (PC-3M cells) displays a more prominent glycolytic-Warburg profile than the non-CSC subpopulaton (PC-3S cells), consuming more glucose and producing considerable amounts of lactate. In addition, PC-3M cells showed a preference for metabolizing glucose through glycolysis instead of oxidation in the TCA cycle, as reflected by their increased Crabtree effect. Disruption of this metabolic pathway by means of glucose deprivation or 2-DG treatment has a more profound impact on PC-3M cell proliferation and bioenergetics than on PC-3S cells. PC-3M cells also displayed a higher metabolic flexibility that allows

them to compensate the impairment in glycolysis by increasing other energetic and biosynthetic pathways, such as glutaminolysis. This metabolic adaptation observed *in vitro* suggests that, under poor nutrient conditions *in vivo*, CSCs may have the capacity to switch metabolic pathways in order to use alternative energy sources. High glycolytic rates likely benefit cells with elevated proliferation rates through the production of glycolytic intermediates, which are shunted into metabolic pathways to fuel reactions that generate *de novo* nucleotides, NADPH, lipids and amino acids (*279*). Aerobic glycolysis is an inefficient way to generate ATP, as compared to mitochondrial metabolism, but this inefficiency can be compensated by increased glucose flux. Previous studies have suggested that a display of high glycolytic metabolism may be a broadly conserved stem cell property (*270*) and associated with undifferentiated states (*280-281*). Importantly, we note that our CSC subpopulation differs from normal stem cells regarding their quiescent state (*282*) and so more reasonably will depend more on very active metabolic pathways to obtain the energy and intermediates required to sustain their high proliferative state.

We next interrogated whether the glycolytic profile of PC-3M cells was dependent on their epithelial and self-renewal properties and PC-3S cells on their mesenchymal features. We addressed this question by analyzing cell proliferation, glucose consumption, lactate production and sensitivity to 2-DG treatment in PC-3M cell variants (PC-3M SNAI1 and PC-3M SKM triple-KD) displaying intermediate CSC-EMT phenotypes.

Briefly, for obtaining PC-3M SNAI1, the EMT factor SNAI1 was retrovirally transduced and overexpressed in PC-3M cells, causing the induction of a strong EMT with downregulation of E-cadherin, upregulation of fibronectin and enhanced invasiveness in *in vitro* assays. Of interest, this was accompanied with an inhibition of features of CSC, including spheroid formation under anchorage-independent growth conditions (*49*).

To start with the metabolic characterization of the PC-3M SNAI1 cell variant, we confirmed the overexpression of SNAI1 (**Figure 5.1.5.A**) which leads to a significantly decrease in proliferation compared to Control PC-3M cells (**Figure 5.1.5.B**). Next, we

evaluated glucose consumption and lactate production, finding that PC-3M SNAI1 cells reduced their glycolytic phenotype (**Figure 5.1.5.C**), displaying a metabolic behavior closer to that of PC-3S cells. Moreover, PC-3M SNAI1 cells were less affected by 2-DG treatment than Control PC-3M cells (**Figure 5.1.5.D**), which could be a reflection of a switch in their metabolic preferences.

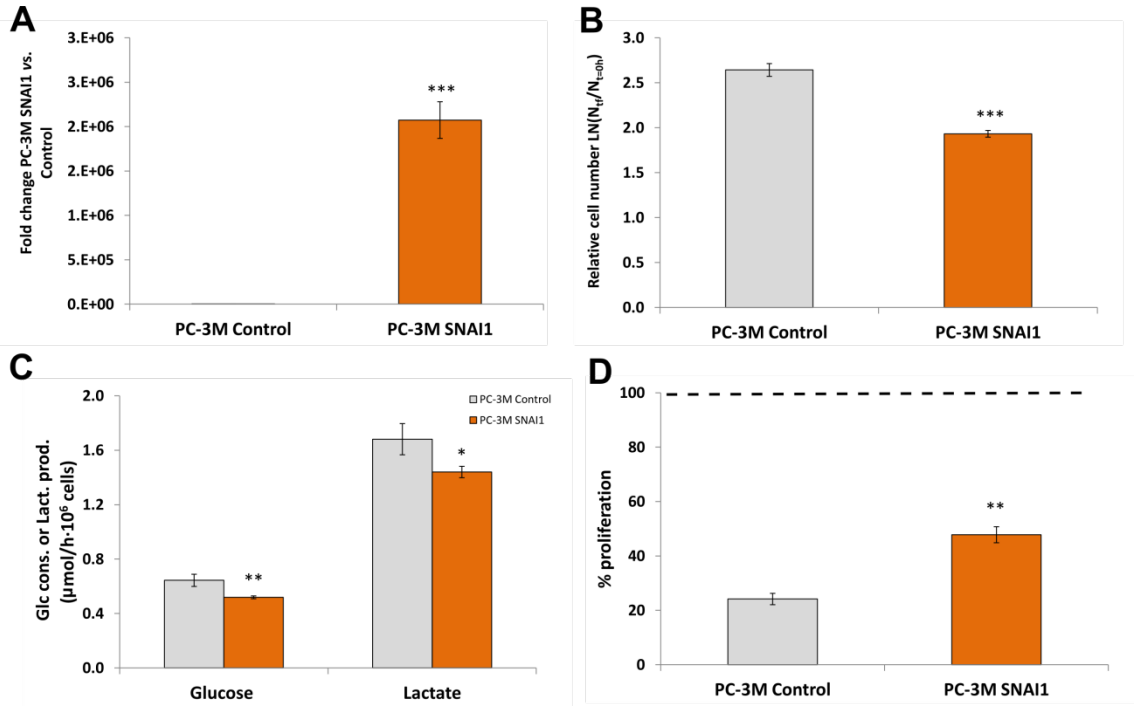

Figure 5.1.5 Overexpression of SNAI in PC-3M cells, proliferation rate and glycolytic profile

(**A**) SNAI1 gene expression relative to PC-3M Control. (**B**) Relative cell number after 96 h of growth in full RPMI 1640 media, considering initial cell number ($N_{t=0h}$) and final cell number (N_{tf}). (**C**) Normalized rates of glucose (Glc) consumption and lactate (Lact.) production. (**D**) Effect of 5 mM 2-DG treatment on cell proliferation, determined with HO33342 staining after 48 h of incubation. Results are shown as percentage of proliferation relative to untreated Control PC-3M or PC-3M SNAI1 cells (100% proliferation). Significant differences are compared to Control PC-3M cells. Data are given as the mean ± SD for n=3 (n=6 in the case of (D)). After a Student's t-test, differences were considered significant when $p < 0.05$(*), $p < 0.01$(**) and $p < 0.001$(***).

Importantly, overexpression of SNAI1 in PC-3M cells slowed down cell proliferation and decreased glycolysis. In our cell model, it correlates with the acquisition of an EMT-non-CSC phenotype. This stands in contrast to other studies supporting that the factor SNAI1 induces glycolysis (*271*). It should be noticed that in that particular study, the cell model used (basal-like breast cancer cells) contained abundant EMT markers and CSC-like characteristics, which prevented the distinction of metabolic features

specific to any particular cell subpopulation. As described above, our model is unique because PC-3M and PC-3S subpopulations express alternative and non-overlapping CSC and EMT gene programs. Therefore, we conclude that the maintenance of a high glycolytic metabolism is associated with the maintenance of a strong CSC phenotype, independent of whether this phenotype is associated with an epithelial (our model) or a mesenchymal (other models) gene program (*283*).

In the case of PC-3M SKM triple-KD cells, PC-3M cells were subjected to triple knock down by means of lentiviral transduction of shRNAs specific for the pluripotency factors SOX2, KLF4 and MYC. The consequence of this triple knock down was a loss of self-renewal properties, determined as an inhibition of spheroid growth (*49*). Since CSCs have the capacity for self-renewal, differentiation into multiple cancer cell lineages, extensive proliferation and are responsible for tumor recurrence and chemotherapeutic resistance (*269, 284*), it is necessary to figure out potential targets that could contribute to eradicate these cells from tumors. Here, our aim is to address the issue whether the glycolytic metabolism of PC-3M cells depends, in addition to its epithelial gene program (shown above), on a pluripotency and self-renewal program sustained by the pluripotency factors SOX2, KLF4 and MYC.

In preliminary determinations, we confirmed the knock downs of SOX2, KLF4 and MYC in this PC-3M cell variant (**Figure 5.1.6.A**). PC-3M SKM triple-KD cells slowed down their proliferation (**Figure 5.1.6.B**) and reduced significantly their glucose consumption and lactate production (**Figure 5.1.6.C**) as compared to control PC-3M cells. In addition, sensitivity to 2-DG was decreased in PC-3M SKM triple-KD cells (**Figure 5.1.6.D**). Therefore, the glycolytic phenotype displayed by PC-3M cells depends on the pluripotency genes SOX2, KFL4 and MYC.

In conclusion, the glycolytic phenotypes displayed by PC-3M cells require the maintenance of a strong epithelial gene program and the expression of the pluripotency gene network represented by SOX2, KLF4 and MYC. Analogous to our CSC subpopulation, it has been shown by many laboratories that aerobic glycolysis is the main bioenergetic and anabolic pathway in pluripotent stem cells, whereas mitochondrial oxidation is attenuated (*285-286*). In addition, promotion of a glycolytic-

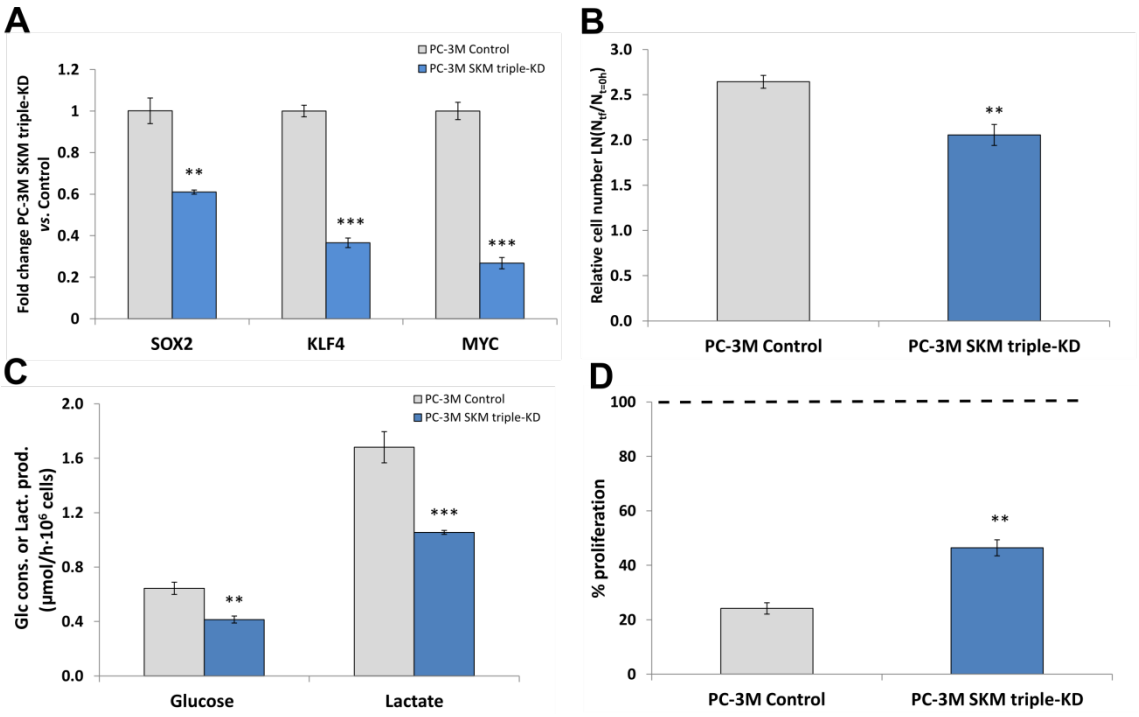

Figure 5.1.6 Knock down of SOX2, KLF4 and MYC in PC-3M cells, cell proliferation and glycolytic profile

(**A**) SOX2, KLF4 and MYC gene expression relative to Control PC-3M cells. (**B**) Relative cell number after 96 h of growth in full RPMI 1640 media, considering initial cell number ($N_{t=0h}$) and final cell number (N_{tf}). (**C**) Normalized rates of glucose consumption and lactate production. (**D**) Effect of 5 mM 2-DG treatment on cell proliferation, determined with HO33342 staining after 48 h incubation. Results are shown as percentage proliferation relative to untreated Control PC-3M or PC-3M SKM triple-KD cells (100% proliferation). Significant differences are compared to Control PC-3M cells. Data are given as the mean ± SD for n=3 (n=6 in the case of (D)). After a Student's t-test, differences were considered significant when $p < 0.01$(**) and $p < 0.001$(***).

dependent and mitochondria-independent phenotype fosters nuclear reprogramming underlying dedifferentiation (*287*).

5.1.2.2 Differential profiles in key enzymes of the pentose phosphate pathway and essentiality of TKTL1 for the invasive non-CSC subpopulation

The pentose phosphate pathway (PPP), as presented in Section 2.3.1.2, is a very important biosynthetic pathway closely linked to glycolysis that produces ribose-5-phosphate required for the synthesis of nucleotides. The PPP comprises two branches. The oxidative branch uses glucose-6-phosphate as a substrate to generate NADPH, thus providing reducing power for other biosynthetic pathways (e.g. fatty acid synthesis) and for controlling oxidative stress. The non-oxidative branch recycles

pentose phosphates to glycolytic intermediates and generates *de novo* ribose-5-phosphate for nucleotide synthesis. Two key enzymes in the PPP are glucose-6-phosphate dehydrogenase (G6PDH) in the oxidative branch and transketolase (TKT) in the non-oxidative branch. A TKT isoform, transketolase-like 1 (TKTL1), also plays a central role in the non-oxidative branch and has been found to be overexpressed in different human cancers (*136*) in association with tumor aggressiveness (*129*). Furthermore, TKTL1 has been proposed by Coy and coworkers as a possible link between PPP and fatty acid synthesis through a monosubstrate reaction (*128*). This hypothesis is represented schematically in **Figure 5.1.7**.

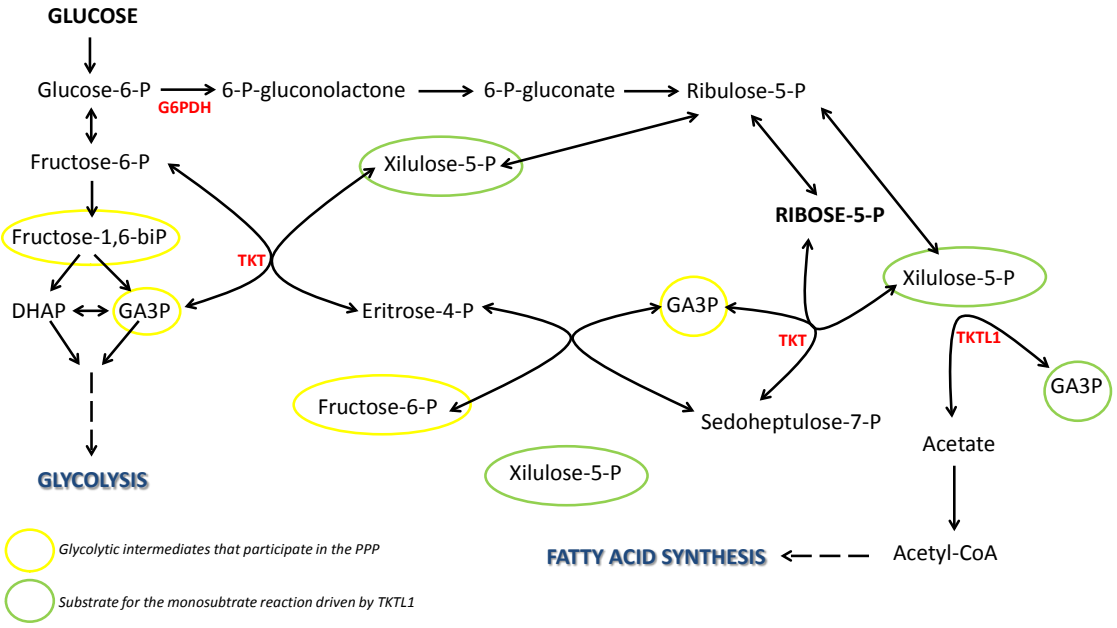

Figure 5.1.7 The PPP and its possible link to fatty acid synthesis through the TKTL1 reaction

TKTL1 catalyzes the monosubstrate reaction from xylulose-5-P, releasing GA3P and acetate, which can yield acetyl-CoA for fatty acid synthesis. G6PDH, glucose-6-phosphate dehydrogenase; TKT, transketolase; TKTL1, transketolase-like 1; P, phosphate; DHAP, dihydroxiacetone-phosphate; GA3P, glyceraldehyde-3-phosphate.

The study of differential PPP fluxes in PC-3M and PC-S cells was approached through mass isotopomer distribution analysis of ribose, the main carbon end product of this pathway. The metabolism of [1,2-$^{13}C_2$]-glucose through the oxidative and the non-oxidative branches of the PPP results mainly in m1 and m2 labeled ribose, respectively. First, we observed that label incorporation to ribose after 24 h of incubation was significantly more efficient in PC-3M cells than in PC-3S cells (**Figure 5.1.8.A**), suggestive of a higher demand for nucleotide biosynthesis to sustain their significantly

higher proliferation rate. Analysis of mass isotopomer distribution of ribose isolated from RNA revealed an increase in m1 and m2 labeled glucose in PC-3M cells (**Figure 5.1.8.B**). However, by comparing the relationship between the oxidative and the non-oxidative branches by calculating the m1/m2 ratio from labeled ribose, we observed a differential contribution of the two PPP branches (**Figure 5.1.8.C**). These results, together with those illustrated in **Figure 5.1.2.E**, suggest the relevance for the highly glycolytic PC-3M cells to redirect back part of glucose-based PPP intermediates to glycolysis using the reversible non-oxidative branch. Moreover, these data were supported by significant differences between G6PDH and total TKT enzyme activities between both cell subpopulations (**Figures 5.1.8.D and 5.1.8.E**). Furthermore, PC-3M cells expressed higher levels of TKT mRNA, whereas PC-3S cells expressed higher levels of G6PDH. Interestingly, TKTL1 was expressed at significantly higher levels (2.5-fold) in PC-3S cells relative to PC-3M cells (**Figure 5.1.8.F**). Importantly, the TKTL1 gene was expressed at much lower levels than TKT. We calculated the fold change of TKTL1 *vs*.TKT gene expression in order to establish a relationship between both TKT isoforms and estimate the contribution of TKTL1 to the total TKT activity, and we found that the TKTL1/TKT gene expression ratio was much higher in PC-3S cells than in PC-3M cells (**Figure 5.1.8.G**).

Previous studies have suggested a role for TKTL1 in late stages of tumor progression (invasion and metastasis). As our dual-cell model represents phenotypically dissociated invasive (PC-3S) and metastatic (PC-3M) cell properties, we next tested the dependence of PC-3M and PC-3S cells on TKTL1 for proliferation, through gene silencing by means of small interfering RNA (siRNA). **Figure 5.1.9.A** shows the highly efficient TKTL1 transcript knock down achieved after 72 h of transfection with TKTL1-specific siRNAs (siTKTL1) compared to cells transfected with a non-targeting siRNA (siNEG). We next analyzed the effect of TKTL1 silencing on global TKT enzyme activity (**Figure 5.1.9.B**) and found that whereas knock down of TKTL1 did not significantly affect the total TKT activity in PC-3M cells, it caused a 40% reduction in total TKT activity in PC-3S cells. This observation is in agreement with **Figure 5.1.8.G** and further demonstrates that TKTL1 contributes more significantly to the total TKT activity in PC-3S than in PC-3M cells. Next, we compared cell proliferation in PC-3M and PC-3S cells

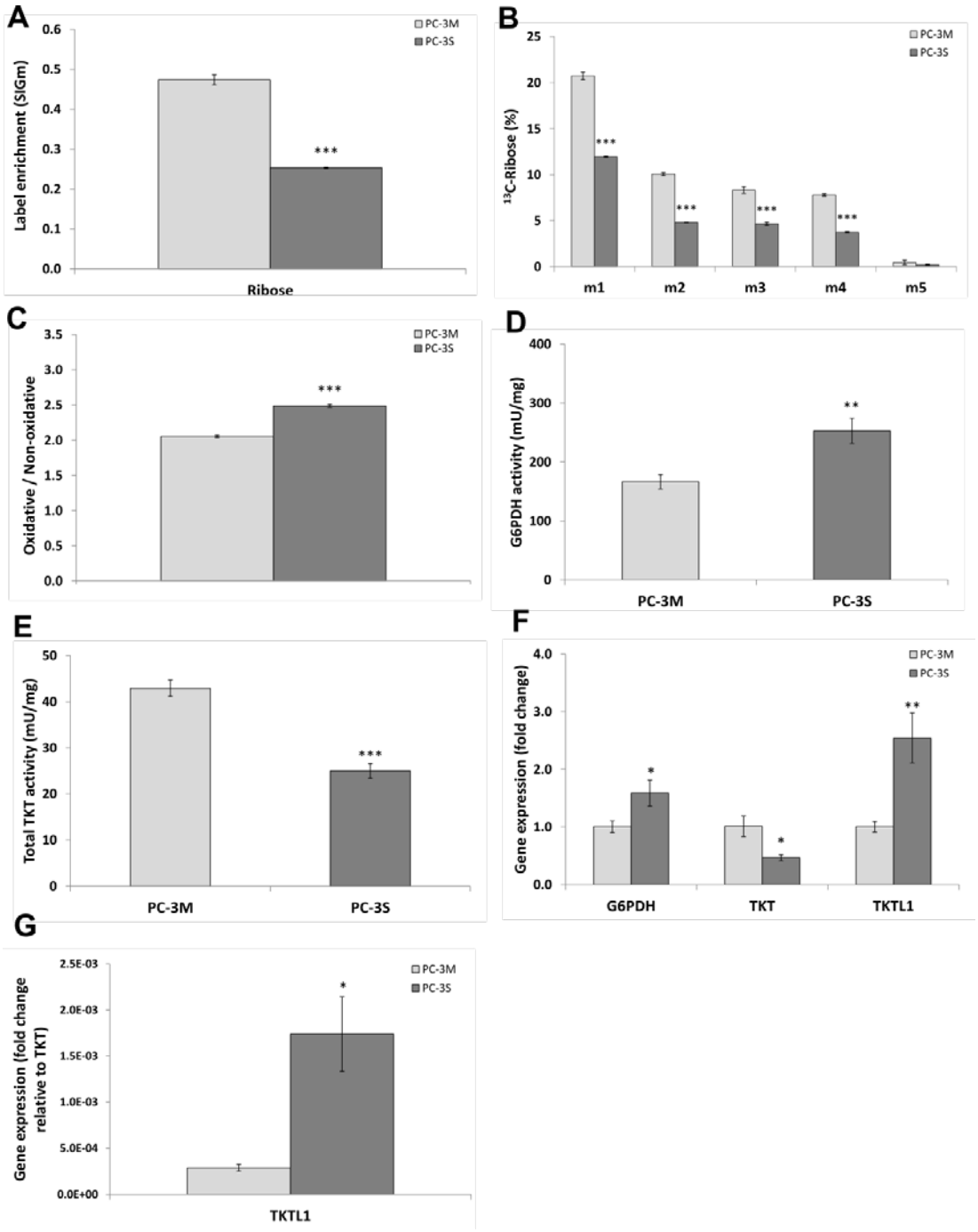

Figure 5.1.8 PPP utilization in PC-3M and PC-3S cells

PC-3M and PC-3S cells were incubated in the presence of 10 mM 100% [1,2-$^{13}C_2$]-glucose for 24 h. Cell pellets were obtained at this time and ribose was isolated from RNA for mass isotopomer distribution analysis. (**A**) Total ^{13}C-Ribose, represented as the sum of m1+m2+m3+m4+m5 labeled ribose. (**B**) Ribose mass isotopomer distribution. (**C**) Oxidative vs. non-oxidative branch of the PPP calculated as m1/m2 ribose. (**D**) G6PDH and (**E**) total TKT enzyme activities normalized to intracellular protein content. (**F**) G6PDH, TKT and TKTL1 gene expression levels determined by RT-PCR using gene-specific TaqMan®, as described in Section 4.11. Fold changes in gene expression are depicted relative to PC-3M cells (**G**) Relationship between TKTL1 *vs*. TKT gene expression, represented as fold change of TKTL1 relative to TKT. In all cases, significance differences compared to PC-3M cells were assessed by Student's t-test (n=3). $p < 0.05$(*), $p < 0.01$(**) and $p < 0.001$(***).

after TKTL1 knock down (**Figure 5.1.9.C**). Cells were transfected with siTKTL1 and siNEG and 72 h post-transfection media was replaced (t = 0 h) and cells were counted at 0, 24, 48 and 72 h for PC-3M cells, and 0, 48, 96 and 120 h for PC-3S cells. Cells still showed a robust TKTL1 knockdown by the end of this experiment (**Figure 5.1.9.D**). It can be seen in **Figure 5.1.9.C** that while cell proliferation was significantly but moderately reduced in PC-3M cells, viability was strongly compromised in the case of PC-3S cells.

As the results obtained so far suggested a key role for TKTL1 in the survival of the invasive non-CSC subpopulation, we next explored if the observed effects could be explained by a disruption of the PPP due to a greater inhibition of global TKT activity in PC-3S cells upon TKTL1 knock down. We incubated cells in the absence (control) or presence of 500 μM oxythiamine (OT), a known TKT inhibitor. After 48 h of incubation, 80% and 66% reduction in total TKT activity was observed in PC-3M and PC-3S cells, respectively (**Figure 5.1.10.A**). Cell proliferation was analyzed in OT-treated cells relative to controls, finding that PC-3M cells were not affected whereas PC-3S cells did decrease their proliferation, although to a much lesser degree as compared to the growth inhibition caused by TKTL1 knock down (**Figure 5.1.10.B**). These results suggest that TKT activity does not explain the reduction in proliferation and viability observed in PC-3M and PC-3S cells in response to TKTL1 silencing.

Our results indicated a differential use of the oxidative and non-oxidative branches of the PPP, supported by a distinct expression of G6PDH and TKT enzymes in the two tumor cell subpopulations under study. Global ^{13}C-label incorporation from glucose to ribose was enhanced in PC-3M cells, which enables rapid nucleotide synthesis for cell proliferation. Upregulation of the PPP has been associated with invasive and metastasizing tumors (*134*). PC-3S cells showed a preference for the oxidative branch, which provides NAPDH moieties to support metabolic processes such as fatty acid synthesis and contribute to the maintenance of redox homeostasis to counter intracellular ROS levels. The enhanced activity of the non-oxidative branch of the PPP in PC-3M cells may represent a mechanism to reinforce their high glycolytic phenotype, allowing a reversible and dynamic connection between glycolysis and the PPP.

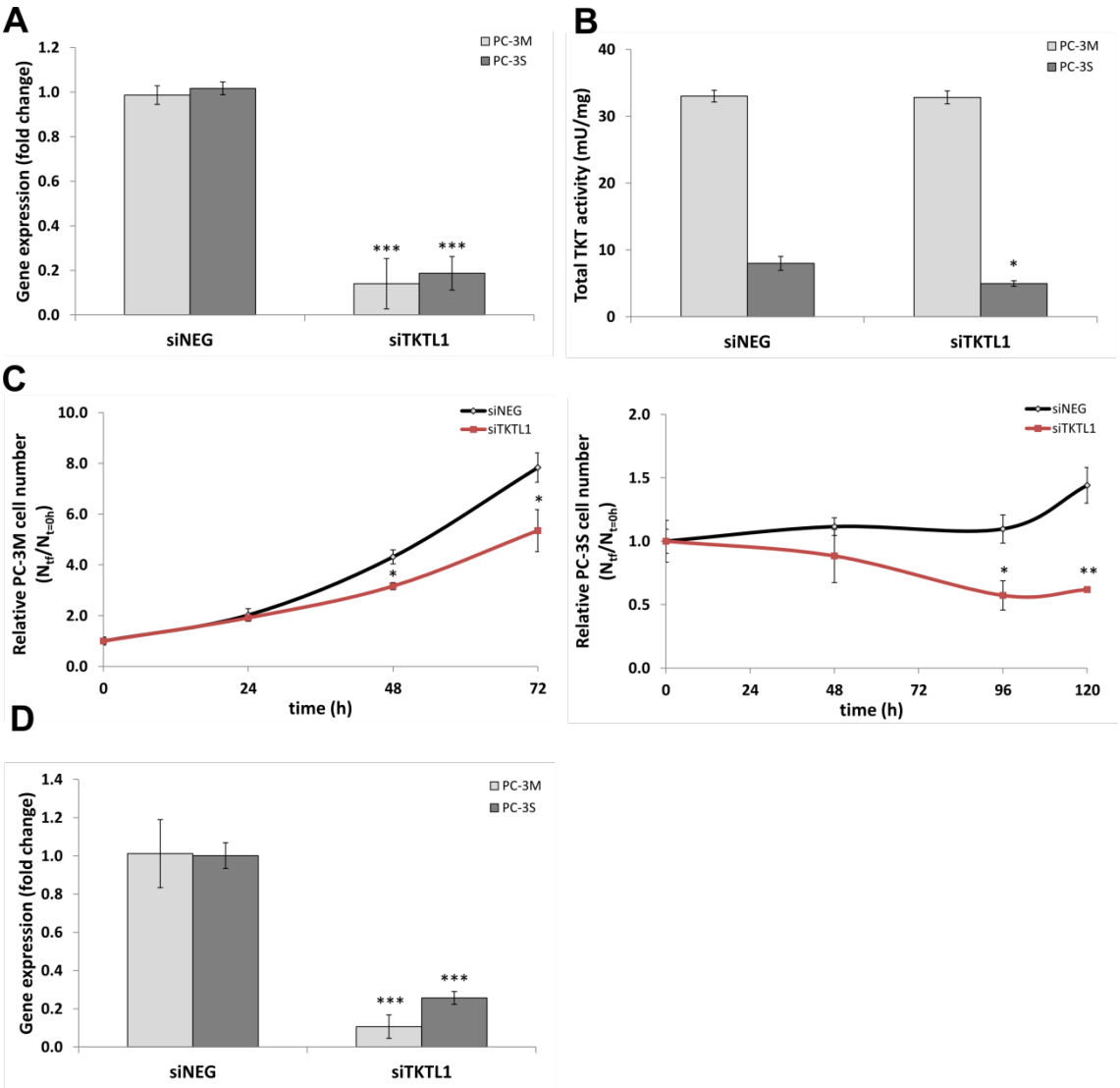

Figure 5.1.9 Effect of TKTL1 inhibition on PC-3M and PC-3S cell proliferation

(**A**) TKTL1 gene expression levels 72 h after transfection with non-targeting siRNA (siNEG) or TKTL1-specific siRNA (siTKTL1) determined by RT-PCR using a TKTL1-specific TaqMan®, as described in Section 4.11. Fold change is relative to siNEG. (**B**) Total TKT enzyme activity determined 96 h after transfection with siNEG or siTKTL1. Results were normalized to intracellular protein content. (**C**) Effect of TKTL1 knock down on PC-3M and PC-3S cell proliferation. Cells were counted at 0, 24, 48 and 72 h for PC-3M cells, and 0, 48, 96 and 120 h for PC-3S cells using a ScepterTM Handheld Automated Cell Counter, as indicated in Section 4.2. (**D**) TKTL1 gene expression level at the end of the cell proliferation analysis shown in (C) (i.e. 144 h post-transfection for PC-3M cells and 192 h post-transfection for PC-3S cells). Data are the mean ± SD from n=3. Significant differences compared to the corresponding PC-3M or PC-3S siNEG condition were assessed using the Student's t-test. *$p < 0.05$, **$p < 0.01$ and ***$p < 0.001$.

Our observations also demonstrate that the TKT isoform TKTL1 is essential for cell proliferation and viability, especially for PC-3S cells. Overexpression of TKTL1 has been reported in different cancer types (*130, 132, 288*), and this enzyme has been shown to

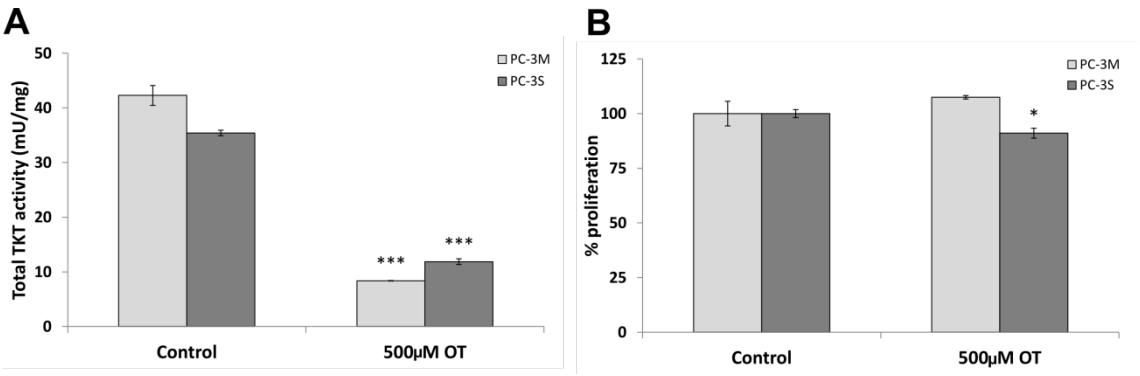

Figure 5.1.10 Role of total TKT activity on cell proliferation

(**A**) Total TKT enzyme activity in the absence (Control) or presence of 500 µM OT after 48 h of incubation. Results were normalized to intracellular protein concentration. (**B**) Effect of TKT activity inhibition on PC-3M and PC-3S cell proliferation after incubation with 500 µM OT for 48 h. Data are the mean ± SD from n=3. Significant differences compared to PC-3M or PC-3S untreated cells (Control) were assessed by Student's t-test. *p < 0.05 and ***p < 0.001.

play an important role in the non-oxidative branch of the PPP of human hepatoma and colon-cancer cells (*138, 289*). Interestingly, some studies have observed a strong TKTL1 activity in invasive tumors, whereas weak or no TKTL1 activity was detected in non-invasive colon carcinomas (*129, 288*). In our dual cell model, the reduction of PC-3M cell proliferation and PC-3S viability caused by TKTL1 knock down was beyond its mere contribution to total TKT activity in the PPP. These observations suggest that TKTL1 plays an additional role in these cells, distinct from their direct function in the PPP but linked to the maintenance of the proliferation and survival of PC-3S cells.

5.1.2.3 PC-3M and PC-3S cells differ in the balance of fatty acid synthesis *vs*. fatty acid oxidation

As fatty acid metabolism is essential for cell growth, we explored differences regarding fatty acid synthesis and oxidation in our dual prostate cancer cell model. In order to examine the status of fatty acid synthesis, we analyzed the mass isotopomer distribution of palmitate in PC-3M and PC-3S cells cultured for 24 h in the presence of 10 mM 50% [1,2-$^{13}C_2$]-glucose (**Figure 5.1.11.A**). A notable increase in m2 and m4 labeled palmitate was found in PC-3S cells, suggesting that a greater amount of glucose-derived carbons is routed into fatty acid synthesis in PC-3S cells compared to PC-3M cells. We also found higher protein expression levels in PC-3S cells of ATP

citrate lyase (ACYL), the primary enzyme responsible for cytosolic fatty acid biosynthesis (**Figure 5.1.11.B**). In addition, in the same experimental conditions described above, analysis of mass isotopomer distribution of stearate, a fatty acid derived from palmitate chain elongation, unveiled higher levels of m2 and m4 labeled stearate (**Figure 5.1.11.C**), reinforcing the hypothesis that fatty acid synthesis could be favored in PC-3S cells.

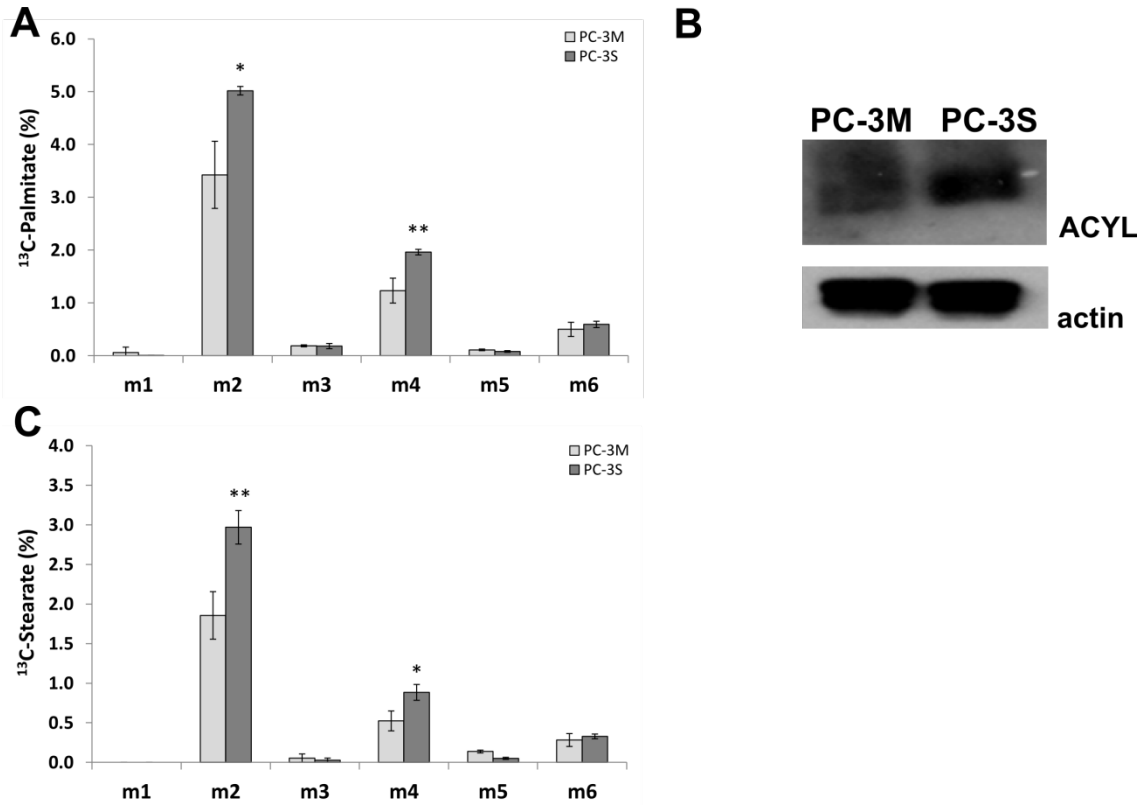

Figure 5.1.11 Fatty acid synthesis in PC-3M and PC-3S cells

(**A**) Mass isotopomer distribution of palmitate after 24 h of incubation with 10 mM 50% [1,2-$^{13}C_2$]-glucose. (**B**) Protein levels of ATP citrate lyase (ACYL) assessed by Western Blotting. Actin was used as loading control. (**C**) Mass isotopomer distribution of stearate after 24 h of incubation with 10 mM 50% [1,2-$^{13}C_2$]-glucose. Bars represent means ± SD (n=3). Significant differences compared to PC-3M cells were assessed by two-tailed Student's t-test. *p < 0.05 and **p < 0.01.

In order to complete the characterization of fatty acid metabolism in these cells, we next studied fatty acid β-oxidation. By designing an experiment using the XF24 Extracellular Flux Analyzer (Seahorse Bioscience) (described in Section 4.20.2), we analyzed the contribution of fatty acid oxidation to OCR. For this experiment, we

exposed cells to etomoxir (a carnitine palmitoyltransferase 1 (CPT1) inhibitor), which impairs fatty acid oxidation and causes a reduction in OCR. This determination showed that respiration was more significantly affected after treatment with etomoxir in PC-3M cells than in PC-3S cells (**Figure 5.1.12.A**). Consistently, higher protein levels of the fatty acid transporter CPT1 were found in PC-3M cells than in PC-3S cells (**Figure 5.1.12.B**).

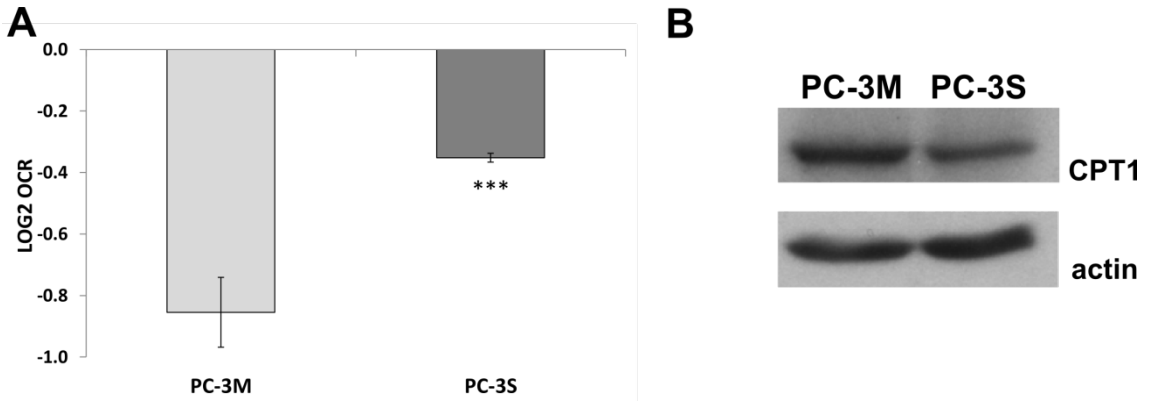

Figure 5.1.12 Fatty acid oxidation in PC-3M and PC-3S cells

(**A**) The contribution of fatty acid metabolism to mitochondrial respiration was measured as the fold change (LOG2) in OCR after 30 μM etomoxir injection, using a XF24 Extracellular Flux Analyzer, as described in Section 4.20.2. (**B**) Protein levels of carnitine palmitoyltransferase 1 (CPT1) determined by Western Blotting. Actin was used as loading control. Data are the mean ± SD from n=5. Significance levels were assessed compared to PC-3M cells by Student's t-test . $p < 0.001$(***).

Together, these observations suggest that PC-3M and PC-3S cells differ in the balance between fatty acid synthesis and degradation. Thus, the enhanced fatty acid synthesis observed in PC-3S cells relative to PC-3M cells suggests that PC-3S cells are more dependent on this activity and therefore more sensitive to perturbations in lipogenesis. This result is further supported by the finding that the oxidative branch of the PPP is more prominent in PC-3S cells, a pathway that yields the cytosolic NADPH units required for fatty acid synthesis. On the other hand, β-oxidation of fatty acids was preferred by PC-3M cells. Fatty acid degradation through β-oxidation can provide a key alternative pathway that supports cancer cell survival when glucose metabolism becomes limiting (*290*). Recent studies have evidenced that fatty acid metabolism and the promyelocytic leukemia (PML) protein play a crucial role in the self-renewal capacity of hematopoietic stem cells and the maintenance of leukemia-initiating cells

(i.e. tumor-initiating cells) (*291*). In contrast to these evidences, other authors who have characterized the metabolic profile of tumor-initiating cells in an ovarian cancer cell model have concluded that fatty acid oxidation was lower in cancer cells compared to a benign counterpart (*292*), although they highlighted the metabolic flexibility of tumor-initiating cells (TICs) to survive under minimal nutrient conditions and utilize those available substrates to satisfy their energy requirements (*293*).

5.1.2.4 Synthesis of amino acids from glucose: distinct metabolic routes characterize alanine, glutamate, serine and glycine metabolism in PC-3M *vs*. PC-3S cells

Nucleotides, lipids and proteins are required for the construction of new cellular components, and thus cancer cells need to accumulate building blocks, including pentoses phosphate, fatty acids and amino acids. Changes in the amino acid demands and preferences result from the metabolic reprogramming associated with tumor progression and are closely linked to the Warburg effect. Alanine, glutamate, serine and glycine may be produced *de novo* by tumor cells themselves. Thus, with the aim to explore in more detail possible differences between our two cell subpopulations in terms of pathways followed by amino acid synthesis from glucose, we determined the profile of consumption and production of these amino acids and incubated cells with 10 mM 100% [1,2-$^{13}C_2$]-glucose for 24 h or 10 mM 100% [U-$^{13}C_6$]-glucose for 48 h (to better highlight some differences, when required), followed by alanine, glutamate, serine and glycine mass isotopomer distribution analysis.

Our results indicated that PC-3M cells accumulated more alanine in the cell media than PC-3S cells (**Figure 5.1.13.A**) and that, after 24 h of incubation with 10 mM 100% [1,2-$^{13}C_2$]-glucose, m2 alanine was the most abundant isotopologue (**Figure 5.1.13.B**). Consistent with these results, PC-3M cells showed higher alanine transaminase (ALT) enzyme activity than PC-3S cells (**Figure 5.1.13.C**). Glutamate showed a behavior that was opposite to that of alanine. Thus, PC-3S cells accumulated significantly more glutamate in the extracellular media than PC-3M cells (**Figure 5.1.14.A**), which was not associated with a higher glutamine consumption (**Figure 5.1.14.A**) After incubation with 10 mM 100% [U-$^{13}C_6$]-glucose for 48 h, we found that both m2 glutamate, coming from glycolysis + 1st turn of the TCA cycle, and m3 glutamate (glycolysis + 2nd turn of

TCA cycle) contributed more significantly to secreted glutamate in PC-3S cells than in PC-3M cells (**Figure 5.1.14.B**). Moreover, m1 glutamate was produced as a result of the entry of unlabeled acetyl-CoA (m0), coming from metabolites other than glucose, into the TCA cycle. We calculated the m1/m3 glutamate ratio to unveil the contribution of these sources other than glucose for the synthesis of acetyl-CoA, and, interestingly, we found that PC-3M cells were able to produce acetyl-CoA using alternative unlabeled substrates (**Figure 5.1.14.C**). As shown above (Section 5.1.2.3), PC-3M cells showed

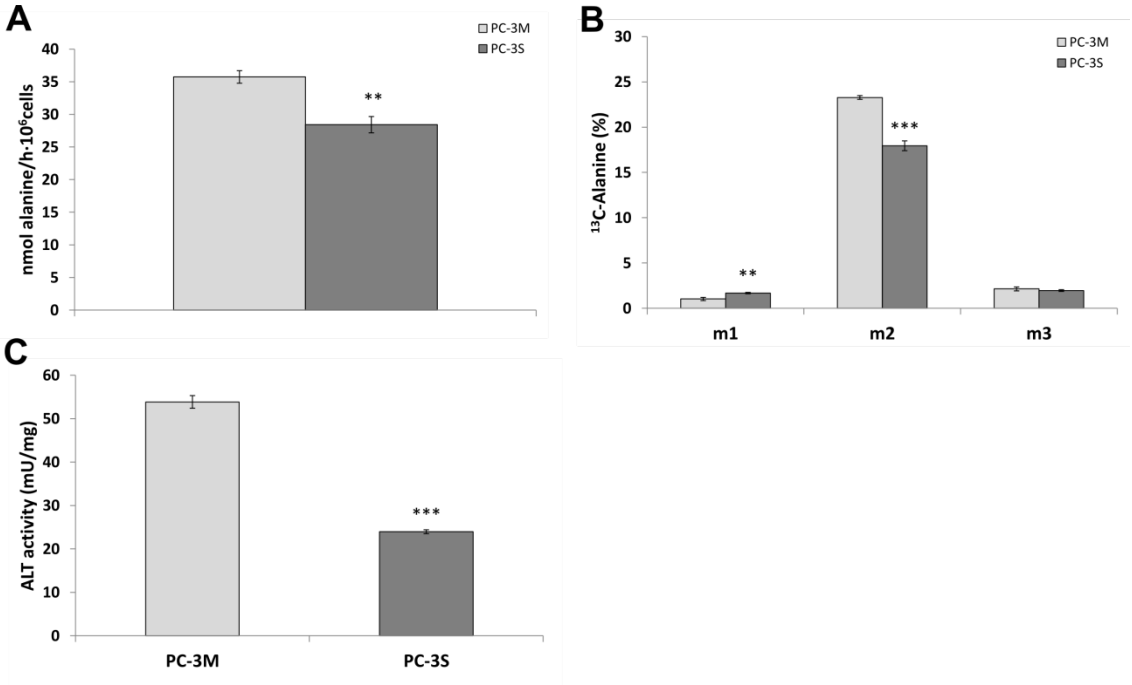

Figure 5.1.13 Alanine metabolism in PC-3M and PC-3S cells

(**A**) Alanine consumption rate. (**B**) Mass isotopomer distribution of alanine after 24 h of incubation with 10 mM 100% [1,2-$^{13}C_2$]-glucose. (**C**) Alanine transaminase (ALT) enzyme activity normalized to intracellular protein concentration. Data are the mean ± SD from n=3. Significance levels were determined relative to PC-3M cells using the Student's t-test: $p < 0.01$(**) and $p < 0.001$(***).

higher fatty acids β-oxidation levels, a metabolic process that yields mitochondrial acetyl-CoA. In addition, we checked the profile of consumption and production of other amino acids present in the cell media to analyze if there were differences at the level of ketogenic amino acids, which are amino acids that can be degraded into acetyl-CoA. PC-3M cells showed higher consumption rates than PC-3S cells of the known ketogenic amino acids isoleucine and leucine, which belong to the branched-chain amino acid (BCAA) family, as well as of threonine, tyrosine, lysine and tryptofan (**Figure**

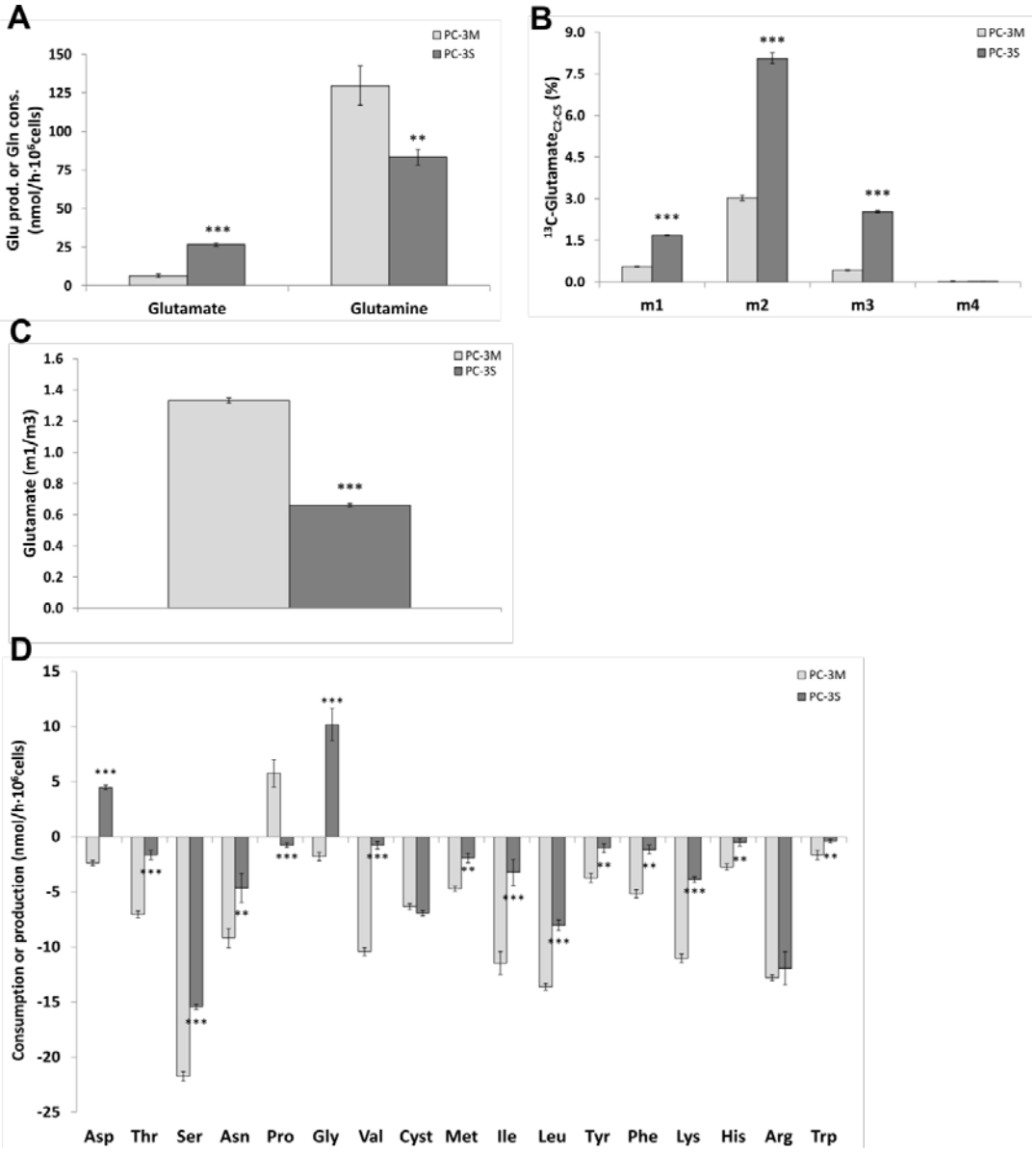

Figure 5.1.14 Glutamate metabolism and global amino acid consumption/production profile in PC-3M and PC-3S cells

(**A**) Glutamate (Glu) production and glutamine (Gln) consumption rates. (**B**) Mass isotopomer distribution of glutamate after 48 h of incubation with 100% [U-$^{13}C_6$]-glucose. (**C**) m1/m3 glutamate ratio (**D**) Amino acids consumption (negative values) and production (positive values) profile. Asp, aspartate; Thr, threonine; Ser, serine; Asn, asparagine; Pro, proline; Gly, glycine; Val, valine; Cyst, cysteine; Met, methionine; Ile, isoleucine; Leu, leucine; Tyr, tyrosine; Phe, phenylalanine; Lys, lysine; His, histidine; Arg, arginine; Trp, tryptofan. Data are the mean ± SD from n=3. Significance levels were determined relative to PC-3M cells using the Student's t-test: $p < 0.01$(**) and $p < 0.001$(***).

5.1.14.D), supporting the notion that the CSC subpopulation is able to metabolize alternative substrates to synthesize acetyl-CoA for the TCA cycle metabolism. Apart from these ketogenic amino acids, PC-3M cells showed higher consumption rates than

PC-3S cells of most of the other amino acids analyzed (**Figure 5.1.14.D**) except for proline, which was effluxed to the extracellular media. PC-3S cells did not excrete proline. This specific case will be addressed in **Chapter II**. **Figure 5.1.15.A** schematically shows the label distributions (m1, m2 and m3) incorporated in glutamate from [U-$^{13}C_6$]-glucose, and the possible contributions of other unlabeled sources to the synthesis of glutamate.

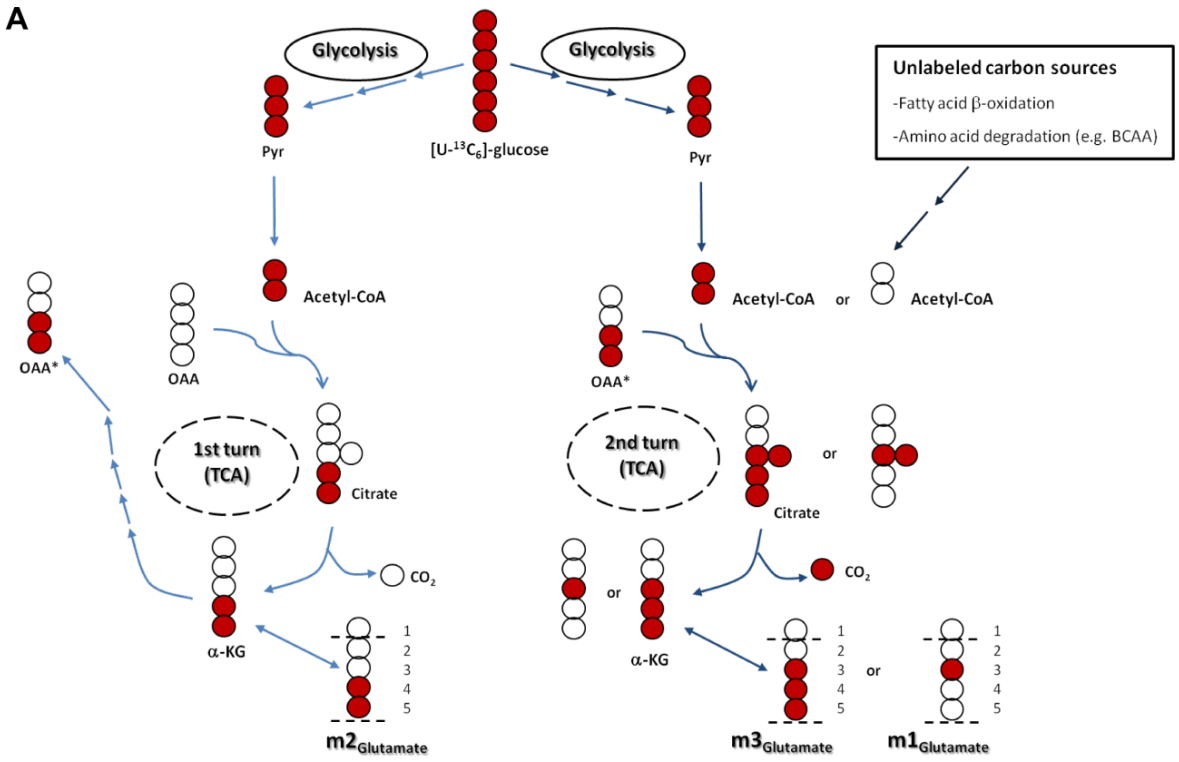

Figure 5.1.15 Glutamate metabolism in PC-3M and PC-3S cells

(**A**) Schematic representation of label distribution from [U-$^{13}C_6$]-glucose to glutamate, after metabolization through glycolysis and 1st or 2nd turn of TCA cycle. The entry of unlabeled Acetyl-CoA coming from sources other than glucose is also considered. Pyr, pyruvate; OAA, oxalacetate; α-KG, α-ketoglutarate; BCAA, branched-chain amino acids; TCA, tricarboxylic acid cycle.

Our data show that PC-3M and PC-3S cells differ in the extent to which glucose contributes to alanine and glutamate synthesis. High levels of production of ^{13}C-alanine from labeled glucose in PC-3M cells can be considered a logical consequence of i) a higher glycolytic-Warburg profile, by which part of the pyruvate is diverted to alanine synthesis instead of lactate, and ii) a higher ALT activity. This is consistent with the known fact that obtaining energy from alanine and alanine-containing peptides is a metabolic property of some CSC-like cells (*294*). On the other hand, PC-3S cells show

more significant ^{13}C-label incorporation into glutamate, suggesting a clear metabolic divergence in our two cell subpopulations between the end of glycolysis and the TCA cycle metabolism. This change in the labeling profile could be related to differences in the ability of pyruvate to enter the TCA cycle metabolism or the contribution of glutamine *vs*. glucose metabolism. This issue will be analyzed and discussed in depth in **Chapter II**.

The glycolytic flux can also be diverted from the glycolytic intermediate 3-phosphoglycerate towards serine synthesis, which in turn may be converted to glycine. Both amino acids provide essential precursors for the synthesis of proteins, nucleic acids and lipids. Taking into account that the media used to culture cells also contains serine and glycine, we found that PC-3M cells consume more extracellular serine than PC-3S cells, and glycine was consumed by PC-3M cells while it was excreted by PC-3S cells (**Figure 5.1.16.A**). Although cell media contained unlabeled serine, we were able to detect labeling in this amino acid after cells were cultured with 10 mM 100% [U-$^{13}C_6$]-glucose for 48 h (**Figure 5.1.16.B**), suggesting the existence of a dynamic flow of serine between the intracellular and extracellular compartments.

Our dual cell model showed a very interesting differential label pattern, in which m3 serine was predominant in PC-3M cells, whereas more evenly distributed representations of m1, m2 and m3 serine were found in PC-3S cells (**Figure 5.1.16.B**). The largely homogeneous m3 labeling of serine in PC-3M cells, together with a paucity of m1 and m2 labeled species, suggests that serine does not accumulate and is efficiently used as a building block for protein synthesis and/or funneled to catabolic reactions which rapidly transform serine to glycine. In line with this, the failure to excrete glycine (**Figure 5.1.16.A**) and the relatively low levels of m2 glycine in PC-3M cells (**Figure 5.1.16.C**) suggests that glycine derived from serine is also rapidly used in these cells for biosynthetic purposes or cleaved to further contribute to one-carbon metabolic reactions that feed into the biosynthesis of nucleotides and lipids and contribute to the generation of NADPH (*295*). In fact, we have found that PC-3M cells expressed much higher levels of glycine decarboxylase (GLDC), the key enzyme catalyzing glycine cleavage, than PC-3S cells (**Figure 5.1.16.D**). Moreover, in addition to GLDC, PC-3M cells also expressed higher levels than PC-3S cells of many of the other

enzymes involved in serine and one-carbon metabolism (**Figure 5.1.16.E**) (*165-166, 296*). Some studies have shown that glycine consumption is a specific feature of rapidly proliferating transformed cells (*167*), and thus glycine metabolism probably contributes to sustain the high proliferation rate of PC-3M cells. Furthermore, and in line with all these observations, as illustrated in the profile of consumptions and productions of amino acids (**Figure 5.1.14.D**), PC-3M cells consumed more methionine than PC-3S cells. Methionine in cells, apart from being used for protein synthesis, participates in the methionine cycle which is intimately coupled to the folate cycle, and both constitute the one-carbon metabolism (*165*).

In contrast, the diversity of serine isotopologues (m1, m2 and m3) observed in PC-3S cells (**Figure 5.1.16.B**) suggests that serine accumulates in these cells as a consequence of a more limited use of this amino acid in comparison to PC-3M cells. Indeed, PC-3S cells also showed more pronounced accumulation of m2 glycine derived from labeled serine (**Figure 5.1.16.C**), suggestive of interconvertions of serine and glycine in reverse reactions through an active tetrahydrofolate (THF) metabolism as well as a limited activity of glycine cleavage systems in these cells (**Figure 5.1.16.D**). Alternatively, due to the slow growth rate of PC-3S cells, compared to PC-3M cells, glycine may not be so avidly used to sustain cell proliferation. Importantly, some reports have demonstrated that higher concentrations of glycine inhibit cell proliferation (*297*). As PC-3S cells accumulate more glycine, as observed in **Figures 5.1.16.B** and **5.1.15.C**, these cells may promote conversion back of glycine to serine, a reaction that depletes the one-carbon pool but prevent the antiproliferative effects of glycine.

From these observations, a possible hypothesis, as represented schematically in **Figure 5.1.17**, would be that PC-3M cells avidly metabolize serine for biosynthesis or to obtain glycine, which is further used or cleaved by the glycine cleavage system, resulting in non-accumulation of glycine. In contrast, PC-3S cells show a pronounced excretion of glycine to the extracellular media probably due to low glycine usage (e.g. for protein synthesis) or low cleavage capacity, as inferred from the gene expression profiles of enzymes in the glycine cleavage system (**Figure 5.1.16.D**) serine, glycine and one-carbon metabolism pathway. Therefore, PC-3S cells avoid intracellular glycine accumulation by excreting this amino acid to the extracellular media and by glycine-

serine recycling through THF-mediated reactions, as suggest the presence of m1 and m2 serine.

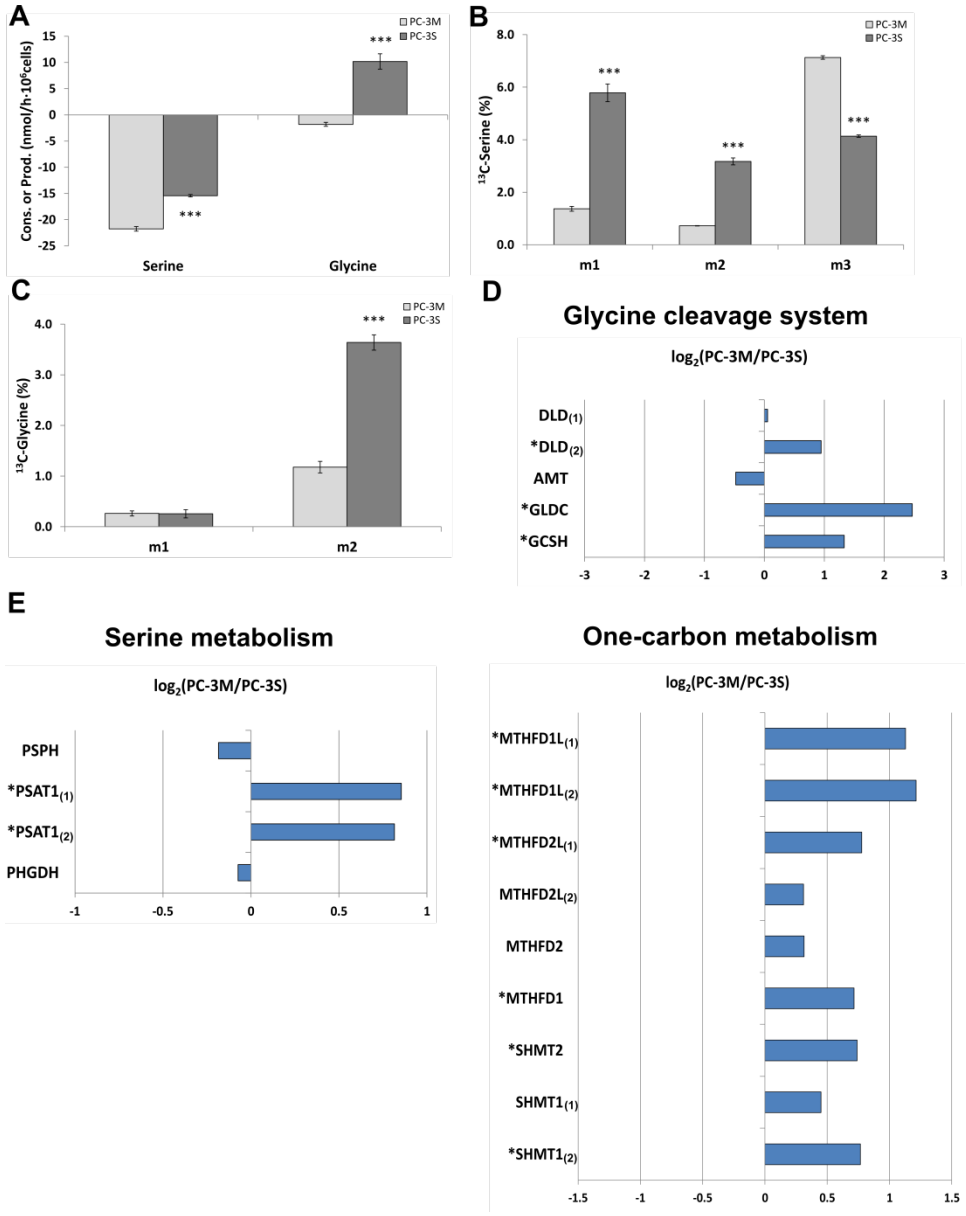

Figure 5.1.16 Serine, glycine and one-carbon metabolism in PC-3M and PC-3S cells (I)

(**A**) Serine and glycine consumption/production profiles after 96 h of culture. Negative values indicate consumption, whereas positive values refer to production. (**B**) Extracellular serine mass isotopomer distribution after 48 h of incubation with 10 mM 100% [U-$^{13}C_6$]-glucose. (**C**) Extracellular glycine mass isotopomer distribution after 48 h of incubation with 10 mM 100% [U-$^{13}C_6$]-glucose. (**D**) Analysis of genes involved in the glycine cleavage system and (**E**) associated with the serine and one carbon metabolism, determined by transcriptomic analysis, as described in Section 4.12. Relative transcript levels are represented as the $\log_2$ of gene expression ratios between PC-3M and PC-3S cells. Asterisk (*) indicates those genes that are differentially expressed at $p < 0.01$ and $\log_2$ fold-change >0.5 or <-0.5. In (A), (B) and (C), bars represent the mean ± SD of n=3 and significant differences compared to PC-3M cells were assessed by Student's t-test. : $p < 0.001$(***). For gene isoforms, the specific Affymetrix probes are: $DLD_{(1)}$, 230426_at; $DLD_{(2)}$, 209095_at; $PSAT_{(1)}$, 220892_s_at; $PSAT_{(2)}$, 223062_s_at; $MTHFD1L_{(1)}$, 225520_at; $MTHFD1L_{(2)}$, 231094_s_at; $MTHFD2L_{(1)}$, 220346_at; $MTHFD2L_{(2)}$, 1554841_at; $SHMT1_{(1)}$, 209980_s_at; $SHMT1_{(2)}$, 224954_at.

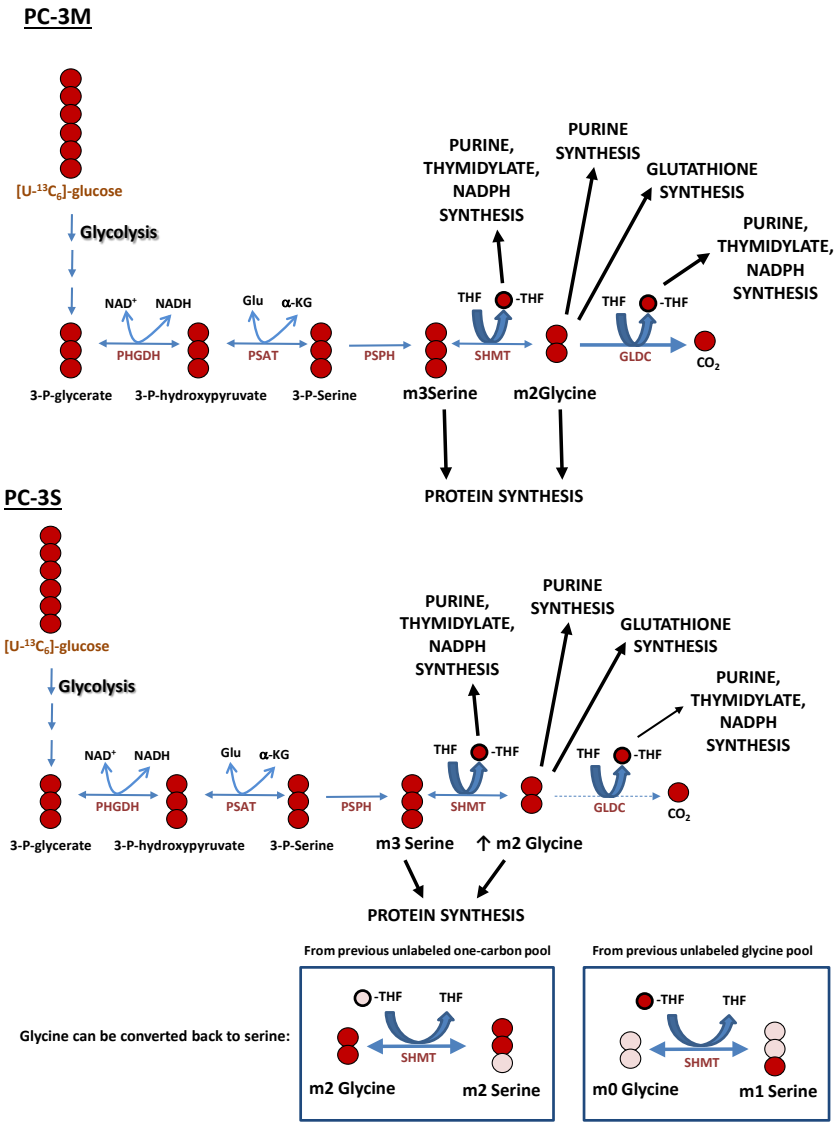

Figure 5.1.17 Serine, glycine and one-carbon metabolism in PC-3M and PC-3S cells (II)

Schematic representation of the reactions involved in the synthesis of m1, m2 and m3 serine from [U-$^{13}C_6$]-glucose in PC-3M cells (upper panel) and PC-3S cells (lower panel). PC-3M cells rapidly metabolize serine and glycine for biosynthetic pathways and additionally, glycine can be cleaved by their more active glycine cleavage system. As a result, glycine is not accumulated in these cells. On the other hand, PC-3S cells accumulate not only m3 serine, but also m1 and m2 serine. This m1 and m2 serine mass isotopomers can result from the conversion back of glycine to serine and considering the participation of labeled and unlabeled substrates, as indicated in the figure. A limited activity of the glycine cleavage system can contribute to the accumulation of glycine in PC-3S cells. Here there is no distinction of the cellular compartments where reactions take place. GLDC is show as a representative enzyme of the glycine cleavage system. PHGDH, phosphoglycerate dehydrogenase; PSAT, phosphoserine aminotransferase; PSPH, phosphoserine phosphatase; SHMT, serine hydroxymethyltransferase; GLDC, glycine decarboxylase.

Recently, serine biosynthesis, one-carbon metabolism and the glycine cleavage system (SOG pathway) have been reported as a candidate pathway for ATP production (*296*), therefore contributing to the energy requirements for biosynthesis. These ATP

molecules result from the recycling of tetrahydrofolate carrying one-carbon units on free tetrahydrofolate, either in the cytosol or in the mitochondria. More interestingly, the SOG pathway contributes also to the generation of NADPH molecules, either in the cytosol or in the mitochondria, required for the synthesis of fatty acid and purines (*166*). (*298*). We have shown evidences of the more active glycine cleavage system in the CSC subpopulation, which takes place in the mitochondrial compartment as depicted in **Figure 2.5** (Introduction). This glycine cleavage pathway also transfers one-carbon units to tetrahydrofolate molecules, therefore contributing to the supply of NADPH and ATP. Alternatively, these mitochondrial NADPH molecules could also contribute to the mitochondrial proton gradient that drives synthesis of ATP by ATP synthase. In the case of PC-3S cells, we hypothesize that they are also able to synthesize ATP and NADPH but these processes are more restricted and conditioned mainly to the directionality of serine/glycine reversible reactions.

We also considered whether the fact that PC-3S cells showed higher levels of glutamate and glycine excretion to the extracellular media could be somehow related to the synthesis of the glutathione tripeptide (glutamate-cysteine-glycine). Cells synthesize glutathione in two ATP-dependent steps. First, the enzyme γ-glutamylcysteine synthetase catalyzes the rate-limiting step in glutathione synthesis where γ-glutamylcysteine is obtained from glutamate and cysteine. Second, glycine is added to the C-terminus of γ-glutamylcysteine via the enzyme glutathione synthetase. Glutathione plays important roles in antioxidant defense, nutrient metabolism, and regulation of cellular processes, including cell differentiation, proliferation and apoptosis (*299*). Higher intracellular levels of this ROS-scavenging enzyme protects cells from oxidative stress and confers resistance to many chemotherapeutics agents and radiation (*299*). PC-3S cells contained more total intracellular glutathione than PC-3M cells (**Figure 5.1.18.A**), suggesting that part of the glutamate and glycine produced could be diverted to the synthesis of glutathione. ROS levels were also higher in PC-3S cells than in PC-3M cells (**Figure 5.1.18.B**), reinforcing the notion that our non-CSC subpopulation requires more reducing units to cope with higher levels of oxidative stress, in the form of glutathione molecules as well as the NADPH moieties generated by the oxidative branch of the PPP. At the same time, the marked pro-glycolytic

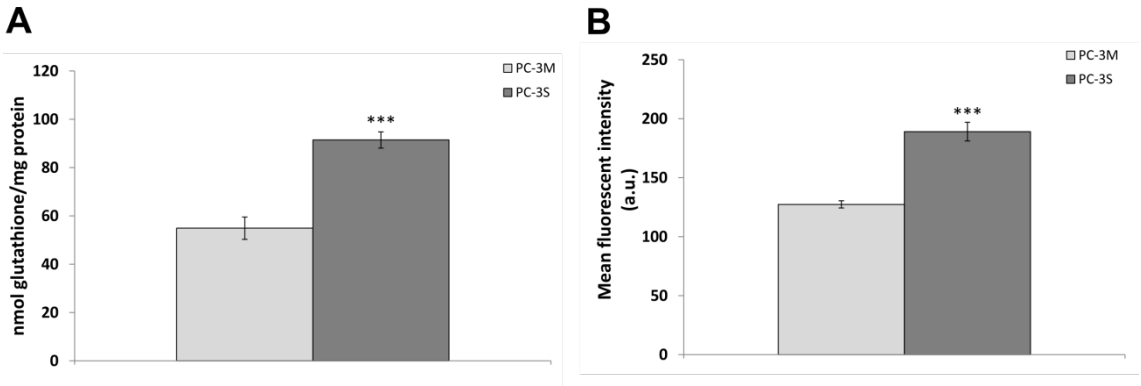

Figure 5.1.18 Intracellular glutathione and ROS levels in PC-3M *vs*. PC-S cells

(**A**) Total intracellular glutathione content. Values are normalized to the protein concentration of the cell extract used for the analysis of glutathione. (**B**) Intracellular ROS levels determined by flow citometry. Results are expressed as the mean fluorescent intensity (MnX). Bars represent the mean ± SD of n=3. Significant differences compared to PC-3M cells were assessed by Student's t-test. $p < 0.001$(***).

phenotype observed in PC-3M cells (e.g. higher preference than PC-3S cells for metabolize glucose through glycolysis instead of mitochondrial oxidation) probably helps this CSC subpopulation to maintain low ROS levels, which is essential to avoid cellular damage and ensure self-renewal capacity (*291*).

Prostate epithelial-CSC and EMT-non-CSC cell subpopulations exhibit a distinct coupling between glycolysis and mitochondrial oxidative phosphorylation and a differential dependence on glutamine metabolism

5.2.1 Introduction

In **Chapter I** we have described the characterization of the glycolytic reprogramming of epithelial PC-3M and mesenchymal PC-3S cells, unveiling a differential dependence on aerobic glycolysis and related biosynthetic pathways. It is generally well established that cancer cells meet their metabolic requirements through the process of aerobic glycolysis characterized in **Chapter I**. The energy provided by glycolysis is thought to be sufficient to satisfy the energy demands associated with high proliferation rates, while simultaneously allowing accumulation of biosynthetic anabolic precursors, such as nucleotides, lipids and amino acids (*275*). Despite high glycolytic rates, cancer cells are also are to resort to mitochondrial respiration to derive a significant fraction of their requirements for ATP molecules (*93*). Nevertheless, there are many controversies regarding the role of mitochondrial metabolism in the processes of invasion and metastasis. Some reports have pointed out that the mitochondrial metabolism does not favor the process of metastasis (*300*) whereas others have placed emphasis on the essentiality of oxidative phosphorylation (OXPHOS) for motility and metastasis of cancer cells (*200*). In order to complete the characterization of the metabolic reprogramming underlying the distinctive prostate CSC and EMT phenotypes of our dual cell model, we have aimed in this **Chapter II** at performing a comparative analysis of the mitochondrial function and glutamine metabolism of these cells.

Similarly to **Chapter I**, here we also analyze the mitochondrial function and glutamine metabolism of the cell variants PC-3M SNAI1 and PC-3M SKM triple-KD, which display an intermediate PC-3M-PC-3S phenotype, to elucidate if the EMT factor SNAI1 and the

pluripotency genes SOX2, KLF4 and MYC also modulate mitochondrial metabolism in our cell model.

5.2.2 Results

5.2.2.1 Prostate mesenchymal non-CSCs have higher mitochondrial respiration activity than epithelial CSCs

In order to start exploring the mitochondrial metabolism underlying the uncoupled CSC and EMT phenotypes that constitute our dual-cell model, we decided to perform a comparative analysis of the mitochondrial potential and function using a pharmacological profiling approach by combining the use of four mitochondrial respiratory chain inhibitors (oligomycin, FCCP, rotenone and antimycin). The design of these experiments is described in Section 4.20.3. **Figure 5.2.1.A** illustrates the oxygen consumption rate (OCR) profiles expected after injection of the different inhibitors, as well as the type of calculations that have been made. Oligomycin is an ATP synthase inhibitor that blocks oxygen consumption for ATP synthesis in the mitochondria. After injection of oligomycin, OCR was reduced in both cell types. The mitochondrial respiration of PC-3S cells was more sensitive to oligomycin inhibition than PC-3M cells (**Figure 5.2.1.B**), suggesting that the non-CSC subpopulation relies more on mitochondrial ATP synthesis than the CSC subpopulation. We also investigated whether cell proliferation was affected by oligomycin treatment and we found that this drug dose-dependently inhibited the proliferation of PC-3S cells significantly more than PC-3M cells (**Figure 5.2.1.C**). We determined the ATP cell content at 2 μM oligomycin and found that ATP levels increased in PC-3S cells but not in PC-3M cells (**Figure 5.2.1.D**), suggesting that the greater reliance of PC-3S cells on mitochondrial ATP synthesis rapidly activated compensatory pathways, like glycolysis. Indeed, a shift from mitochondrial respiration to glycolysis can be detected in both cell subpopulations as an increased extracellular acidification rate (ECAR) after oligomycin injection (**Figure 5.2.1.E**), although ATP levels in PC-3M cells did not show a substantial change.

Next, we tested the OCR response to FCCP, a mitochondrial uncoupling agent that dissipates the proton gradient and uncouples electron transport and mitochondrial

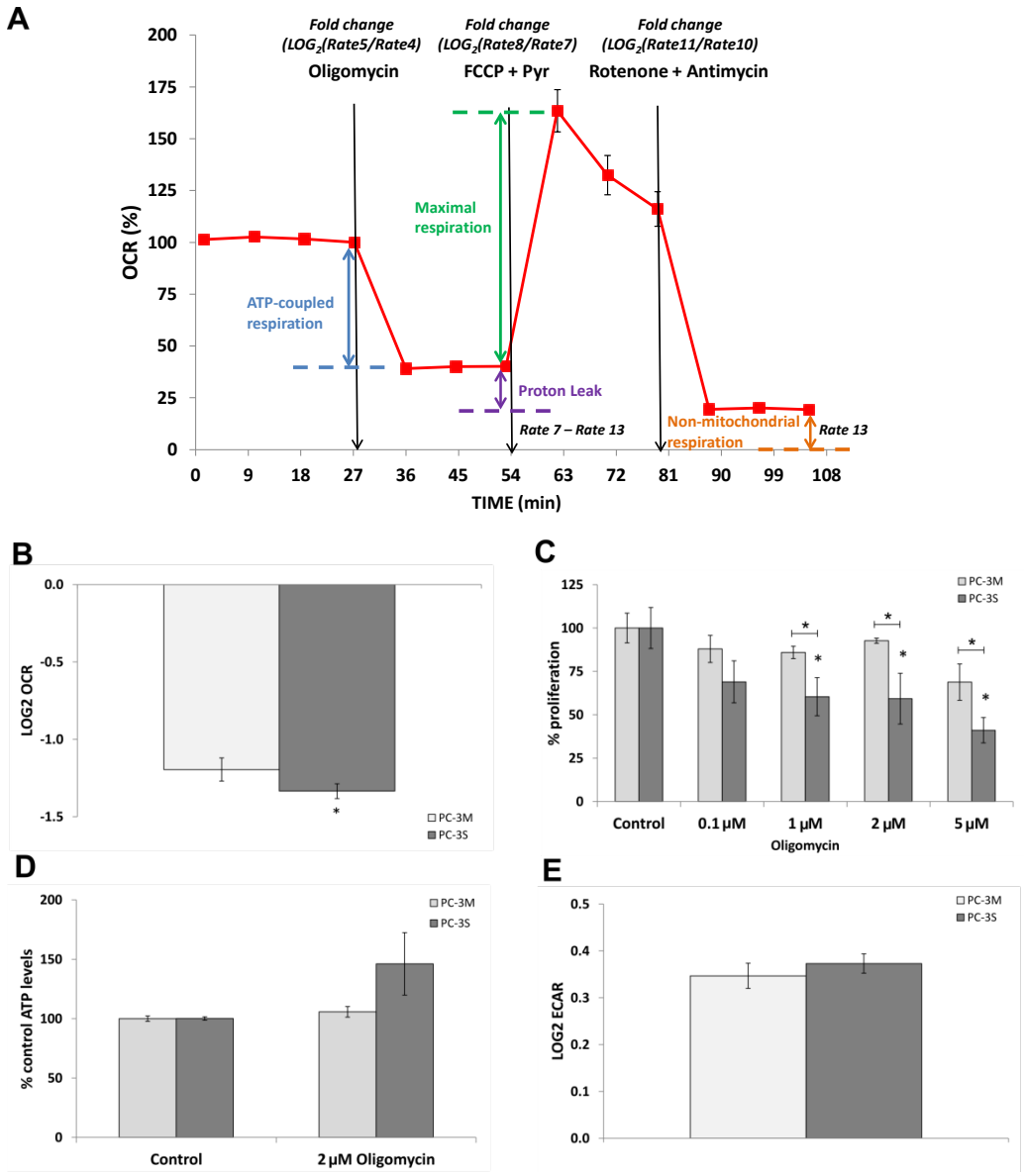

Figure 5.2.1 Characterization of the mitochondrial function in PC-3M *vs*. PC-3S cells (I)

Oxygen consumption rate (OCR) and extracellular acidification rate (ECAR) were determined with the XF24 Extracellular Flux Analyzer instrument. (**A**) Schematic representation of OCR profiles expected following injection of oligomycin, FCCP + Pyr and rotenone + antimycin. Some of the subsequent calculations are shown. Rate 1, rate 2, etc. refers to the 1st, 2nd, etc. time points were OCR and ECAR measurements were made. Concentrations of the different compounds are specified in Section 4.20.3. (**B**) Fold change (LOG2) in OCR after oligomycin injection (mean ± SD of n=5). (**C**) Cells were incubated with the indicated oligomycin concentrations for 24 h and cell proliferation assessed. Results are shown as percentage of proliferation relative to cells cultured in the absence of oligomycin (Control) (mean ± SD of n=3). (**D**) Intracellular ATP levels were analyzed after cells were incubated with 2 µM oligomycin for 24 h (mean ± SD of n=3). (**F**) Fold change (LOG2) in ECAR following oligomycin injection (mean ± SD of n=5). After a Student's t-test, differences compared to PC-3M (Figures B and E) or to Control PC-3M or PC-3S conditions (Figures C and D) were considered significant when $p < 0.05$ (*).

respiration from ATP synthesis, therefore allowing the estimation of the maximal mitochondrial respiratory capacity. To better assess the OCR response, we injected 2 mM pyruvate (Pyr) together with FCCP. Interestingly, the OCR levels in PC-3M cells did not exceed OCR baseline levels (**Figure 5.2.2.A**), suggesting that PC-3S cells are endowed with a significantly higher mitochondrial respiratory capacity than PC-3M cells (**Figure 5.2.2.B**). Finally, we co-injected the mitochondrial complex I and III inhibitors rotenone and antimycin. These inhibitors decreased OCR in both cell subpopulations, although with a significantly more pronounced effect in PC-3S cells (**Figure 5.2.2.C**). Together, these observations indicate that the non-CSC PC-3S subpopulation displays a more prominent mitochondrial function and respiration, and is more dependent on the latter, than the CSC-enriched PC-3M subpopulation.

The respiration rate in the presence of oligomycin is a direct measure of the proton leak rate across the mitochondrial membrane, i.e. the levels of non-ATP linked oxygen consumption or uncoupled respiration. PC-3S cells showed higher rates of proton leak (**Figure 5.2.2.D**). Naturally, all mitochondria possess and endogenous proton leak that, at the same time, can be induced by cellular reactive oxygen species (ROS) production (*301*). In the absence of ATP synthesis, the proton leak completes the proton circuit and restricts leakage of single electrons from the electron transport chain, behaving as an antioxidant and reducing ROS production, which probably may benefit PC-3S cells allowing them to counter their higher intracellular ROS levels (**Chapter I**). Non-mitochondrial respiration, for instance oxygen consumption due to the activity of cytosolic oxidase enzymes, can be determined after sequential additions of oligomycin, FCCP and rotenone + antimycin. No significant differences were found between PC-3M and PC-3S cells (**Figure 5.2.2.E**), confirming that the main differences between the two cell types are due to mitochondrial respiration.

Thus, mitochondrial metabolism is clearly more active in PC-3S than PC-3M cells, as demonstrated by their greater sensitivity to oligomycin, FCCP, rotenone and antimycin treatments, evaluated as fold changes in their respiration rate. In addition, proliferation and ATP levels were more severely affected in PC-3S cells treated with oligomycin, suggesting that mitochondrial complex V is the main ATP supplier for these

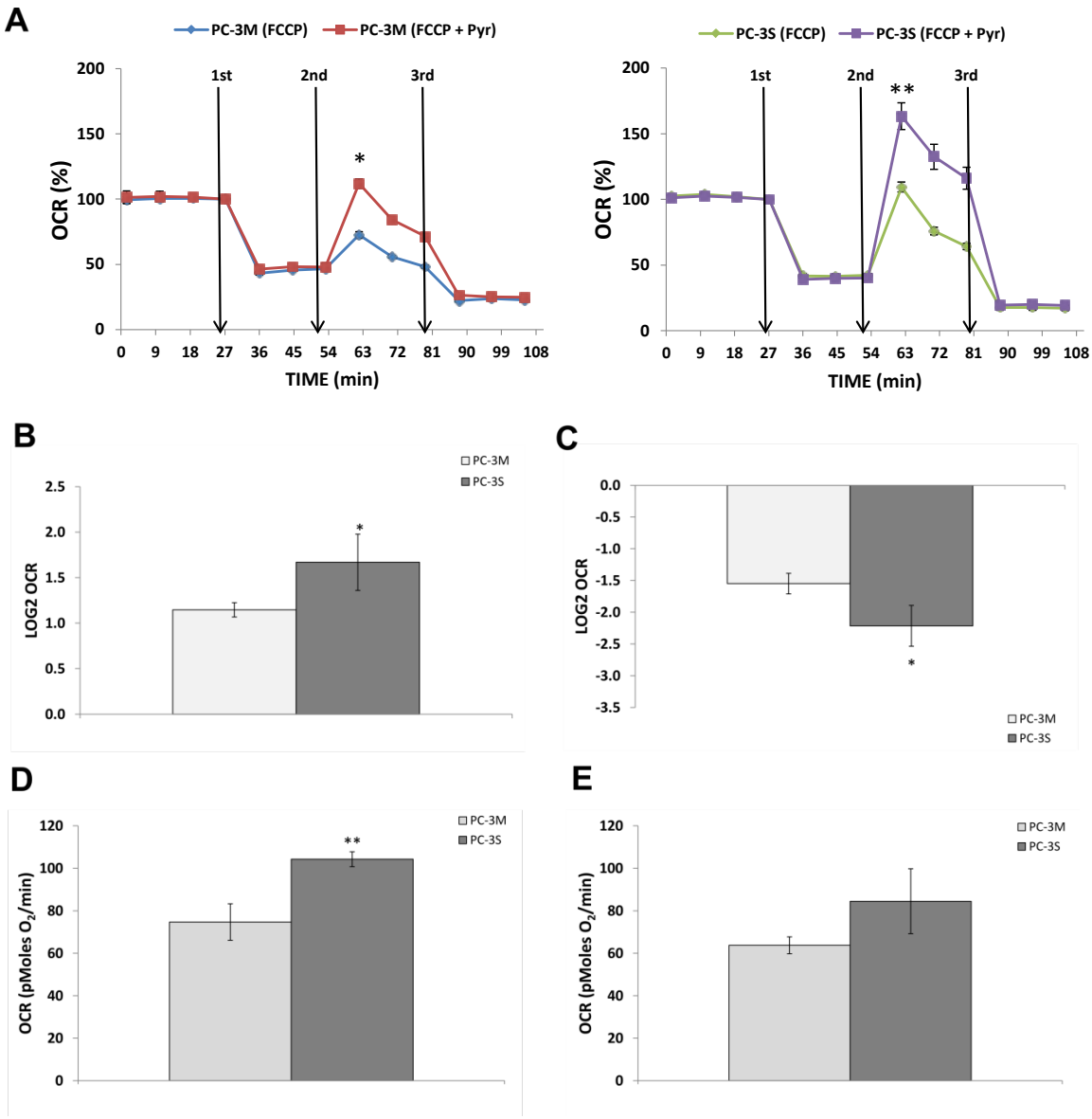

Figure 5.2.2 Characterization of the mitochondrial function in PC-3M *vs*. PC-3S cells (II)

(**A**) Comparison of the effect in PC-3M (left panel) or PC-3S (righ panel) cells on OCR after injection of FCCP alone or with 2 mM pyruvate (Pyr). For significant differences, the response to FCCP and FCCP + Pyr is compared for each cell subpopulation. Injections refer to 1st (oligomycin), 2nd (FCCP or FCCP + Pyr) and 3rd (rotenone + antimycin) treatments. (**B**) Fold change (LOG2) in OCR after FCCP + Pyr or (**C**) rotenone + antimycin injections. (**D**) Proton leak rate, estimated as the difference in OCR after oligomycin treatment and before complete OCR inhibition by rotenone + antimycin treatment. (**E**) Non-mitochondrial respiration was the residual OCR after all mitochondrial inhibitors were injected. Data are the mean ± SD from n=5. After a Student's t-test, differences between PC-3M and PC-3S cells were considered significant when *p < 0.05 and **p < 0.01.

cells. In order to complete the characterization of the mitochondrial potential, we specifically stained the mitochondrial structures of PC-3M and PC-3S cells using the

dye MitoTracker® CMXRos (Invitrogen). Interestingly, these cell subpopulations showed a distinct mitochondrial morphology and organization (**Figure 5.2.3**) very likely related to differences at the level of their mitochondrial dynamics involving fusion and fission processes. PC-3M showed extensive fragmentation/disruption of mitochondria which has been reported to be related with OXPHOS defects and a higher reliance on the use of anaerobic glycolysis to generate energy (*302*). The morphology of the mitochondria in PC-3S cells was more compact, which positively correlates with mitochondria about to undergo a fusion event (*303*), a process that is actively coupled to a proper mitochondrial function and bioenergetics (*304*). Altogether, these results indicate that the non-CSC subpopulation display a mitochondrial organization which potentiates their OXPHOS activity to generate ATP.

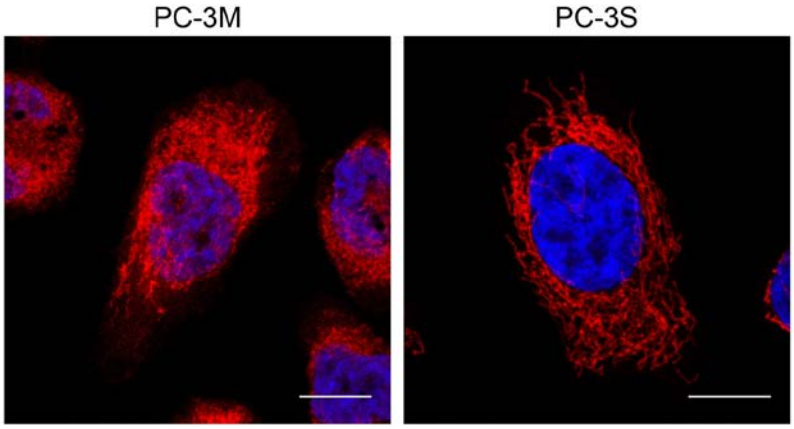

Figure 5.2.3 Mitochondrial morphology in PC-3M and PC-3S cells

Fluorescence emission from PC-3M and PC-3S cells after staining with MitoTracker (red) and DAPI (blue), which target the intracellular mitochondrial network and nucleus, respectively. These staining were carried out as described in Section 4.14.

5.2.2.2 Prostate CSCs use alternative substrates to feed their mitochondrial metabolism

OCR and ECAR profiles were analyzed and compared in full media (glucose + glutamine) as well as in restricted media conditions, including minimal medium (glucose- and glutamine-free), glucose-deprived and glutamine-deprived media (conditions described in Section 4.20.3). Although significant differences were not detected in baseline OCR profiles corresponding to full media condition, PC-3M showed higher OCR values than PC-3S cells in all three restricted media conditions

(**Figure 5.2.4.A**), suggesting that their mitochondrial metabolism is more flexible and able to use other metabolites in these impoverished nutrient conditions. This observation also demonstrates that, although prostate CSCs have more glycolytic potential, their mitochondrial respiration can be also functional and enhanced when required. On the other hand, ECAR (and thus glycolysis) was strongly dependent on glucose availability (**Figure 5.2.4.B**), supporting the importance of this metabolic switch to mitochondrial metabolism under glucose deprivation conditions. We previously demonstrated in **Chapter I** the higher capability of PC-3M cells to use alternative substrates that could contribute to their mitochondrial OCR levels, such as fatty acids (**Figure 5.1.12**), glutamine and other amino acids (**Figure 5.1.14)**.

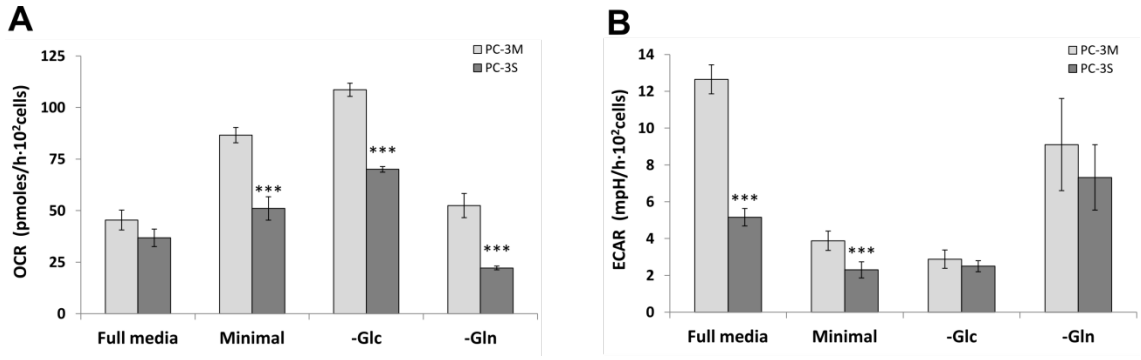

Figure 5.2.4 OCR and ECAR profiles in full and restricted media conditions

(**A**) Oxygen consumption rate (OCR) and (**B**) extracellular acidification rate (ECAR) basal levels in full and restricted media conditions. Media without glucose or without glutamine are named –Glc or –Gln, respectively. Values are normalized to cell number. Bars represent mean ± SD of n=5. Significant differences compared to PC-3M cells were assessed by two-tailed Student's t-test: **p < 0.01 and ***p < 0.001.

To better understand the mitochondrial dynamics, we analyzed the OCR responses to oligomycin, FCCP + Pyr and rotenone + antimycin when only glucose or glutamine were available as carbon sources. Consistent with the observed OCR profiles, the sensitivity to these mitochondrial inhibitors changed as a function of carbon source. With glucose as the only carbon source, exposure to oligomycin showed an opposite behavior to that observed in full media conditions (**Figure 5.2.5.A**) whereas these cell subpopulations did not show significant differences in their responses to FCCP + Pyr (**Figure 5.2.5.B**) and rotenone + antimycin treatments (**Figure 5.2.5.C**). All these observations could be explained by a metabolic readaptation of CSCs to use alternative

substrates in order to fuel mitochondrial respiration, while non-CSCs are highly dependent on glucose and glutamine to maintain a proper mitochondrial function.

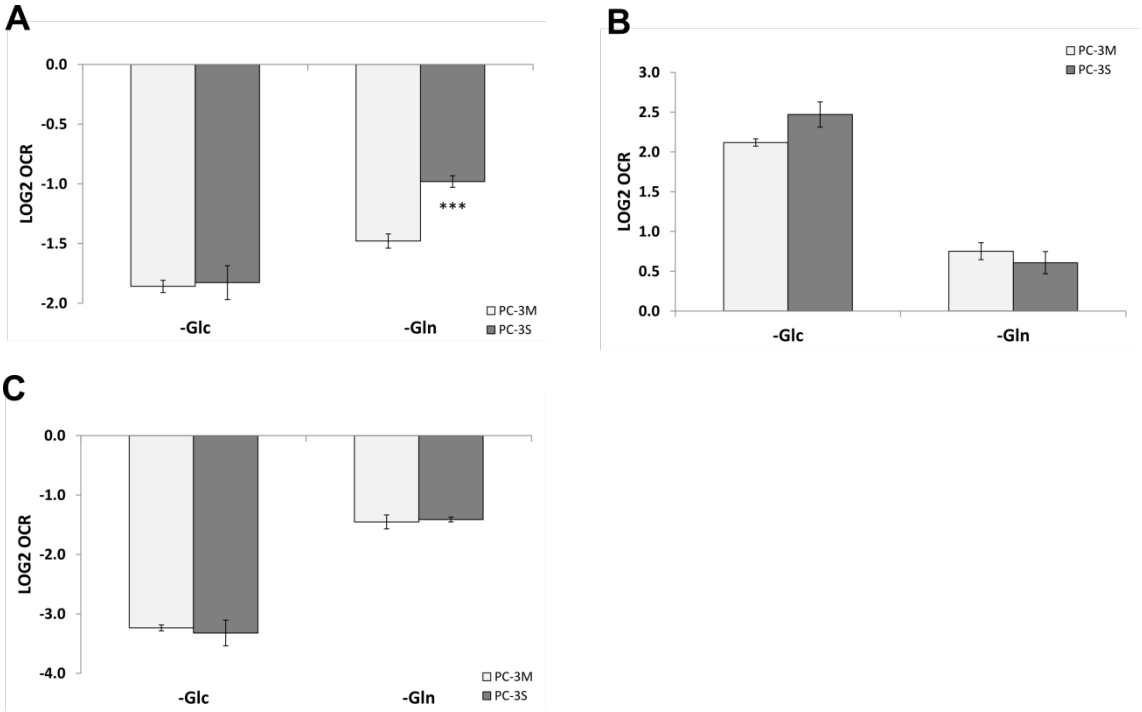

Figure 5.2.5 Response to mitochondrial inhibitors under restricted media conditions

(**A**) Fold change (LOG2) in OCR following oligomycin, (**B**) FCCP + Pyr and (**C**) rotenone + antimycin injections. Before experimental determinations were made using the XF24 Extracellular Flux Analyzer, cells were cultured for 1 h in glucose- or glutamine-deprived media (-Glc or -Gln, respectively), and these conditions were maintained throughout the experiment. Bars represent mean ± SD of n=5. Significant differences compared to PC-3M cells were determined by Student's t-test: ***$p < 0.001$.

The observation that mitochondrial metabolism is more relevant in PC-3S cells proved to be true in full media conditions, where glucose and glutamine were present. The mitochondrial metabolic profile was strongly dependent on the metabolic conditions (nutrient microenvironment). In nutrient-deprived media, mitochondrial metabolism in PC-3S cells was compromised whereas PC-3M cells, due to their higher metabolic flexibility and better ability to use alternative mitochondrial substrates, such as fatty acids, glutamine and other amino acids that feed the mitochondrial metabolism, showed higher respiration rates than PC-3S cells.

5.2.2.3 Glucose and glutamine contribute differentially to the synthesis of TCA intermediates in prostate CSCs and non-CSCs

As the results obtained in Sections 5.2.2.1 and 5.2.2.2 clearly suggest a differential mitochondrial potential between the two subpopulations under study, we sought to better explore the tricarboxylic acid (TCA) cycle metabolism using a ^{13}C-tracer based approach. PC-3M and PC-3S cells were cultured for 24 h in complete media containing 10 mM 100% [1,2-$^{13}C_2$]-glucose and the mass isotopomer distribution of the intracellular TCA intermediates citrate, glutamate, fumarate, malate and aspartate was analyzed by GC/MS. We focused on m2 TCA intermediates, the most abundant labeled isotopologue from [1,2-$^{13}C_2$]-glucose. Of note, although PC-3M cells incorporated more label from glucose to several final products of glycolysis (e.g. lactate and alanine) than PC-3S cells, as described in **Chapter I**, a converse profile was observed in the TCA intermediates analyzed (**Figure 5.2.6.A**). These results point to a significant metabolic divergence between these cell subpopulations, such that the CSC subpopulation, but not the non-CSC subpopulation, may divert most of the pyruvate derived from glycolysis away from mitochondria, consistent with a marked Warburg effect. In this experiment, we also determined mass isotopomer distribution in intracellular pyruvate and calculated the ratio of m2 labeling of TCA intermediates to m2 pyruvate as an indication of the relative amount of pyruvate that was further oxidized in the TCA cycle. Here, we do not distinguish which enzyme (e.g. pyruvate dehydrogenase (PDH), pyruvate carboxylase (PC) or malic enzyme (ME)) is responsible for the incorporation of pyruvate to the TCA cycle (**Figure 5.2.6.B, left panel**). The results show lower ratios of m2 citrate, glutamate, fumarate, malate and aspartate to m2 pyruvate in PC-3M cells (**Figure 5.2.6.B, right panel**), indicative of a decreased fraction of pyruvate entering the TCA cycle in these cells. Furthermore, entry of a second m2 acetyl-CoA from m2 pyruvate into the TCA cycle, specifically by the action of PDH, results in m4 citrate, glutamate and m3 fumarate, malate and aspartate (**Figure 5.2.6.C, left panel**). As with the m2/m2 pyruvate ratio, m4 (citrate and glutamate) and m3 (fumarate, malate and aspartate) to m2 pyruvate ratios were also decreased in PC-3M cells relative to PC-3S cells (**Figure 5.2.6.C, right panel**). Together, these results demonstrate that flux through the oxidative TCA cycle from glucose is higher in PC-3S

cells, reinforcing the importance of mitochondrial metabolism and TCA reactions for this non-CSC subpopulation.

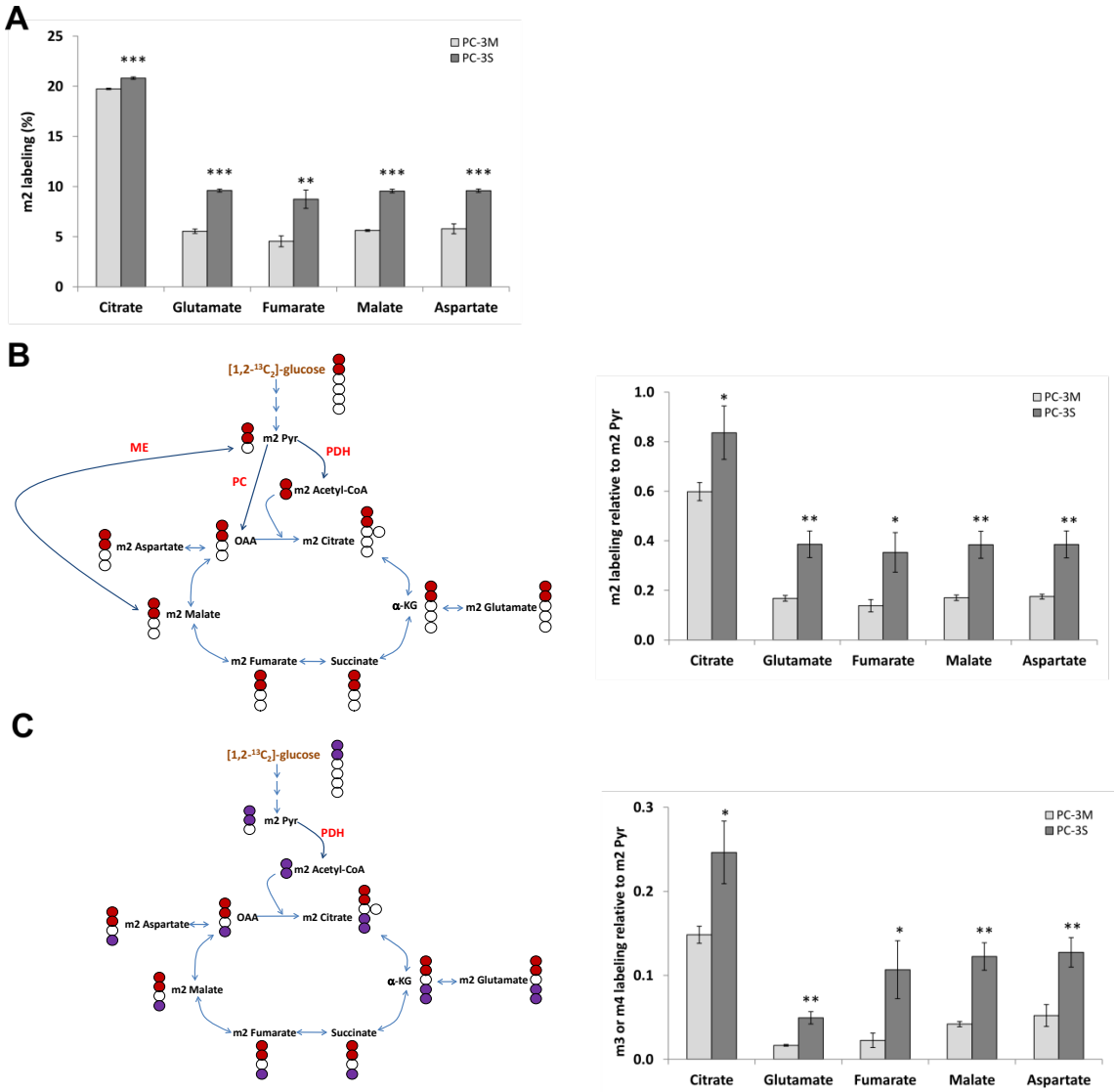

Figure 5.2.6 Glucose contribution to the TCA cycle in PC-3M *vs*. PC-3S cells

(**A**) m2 labeling of TCA intermediates after 24 h of incubation with 10 mM 100% [1,2-$^{13}C_2$]-glucose and GC/MS analysis. (**B, left panel**) Representation of the labeling distribution in TCA intermediates from [1,2-$^{13}C_2$]-glucose in the first turn of the TCA cycle. Here, pyruvate dehydrogenase (PDH), pyruvate carboxylase (PC) and malic enzyme (ME) are considered to contribute to the incorporation of ^{13}C-labeling to the TCA intermediates. (**B, right panel**) Ratio of m2 citrate, glutamate, fumarate, malate and aspartate normalized to m2 pyruvate (Pyr) labeling. (**C, left panel**) Representation of the labeling distribution in TCA intermediates from [1,2-$^{13}C_2$]-glucose with the entry of a second m2 acetyl-CoA into the TCA cycle, considering the PDH reaction as the main contributor. (**C, right panel**) Ratio of m4 citrate, glutamate and m3 fumarate, malate and aspartate normalized to m2 pyruvate (Pyr) labeling. In all cases, bars represent the mean ± SD (n=3). Significant differences compared to PC-3M cells were assessed by Student's t-test: *p < 0.05, **p < 0.01 and ***p < 0.001. Pyr, pyruvate; OAA, oxalacetate; α-KG, α-ketoglutarate.

Additionally, glutamine may contribute to a greater extent to the labeling of the TCA intermediates in CSCs, thus diluting the labeling from glucose. To test the latter hypothesis, we analyzed the labeling profile of TCA intermediates when cells were incubated with 2 mM 100% [U-$^{13}C_5$]-glutamine, comparing m4 mass isotopomers (m5 in the case of glutamate) and considering the oxidative TCA cycle (**Figure 5.2.7.A, left panel**). We found a more significant contribution of this substrate to the synthesis of TCA intermediates in PC-3M cells than in PC-3S cells (**Figure 5.2.7.A, right panel**). We also considered whether glutamine was metabolized through the reductive carboxylation reactions (**Figure 5.2.7.B, left panel**). Analysis of the levels of m5 citrate and m3 aspartate, malate and fumarate indicated that this metabolic pathway was more active in PC-3M cells (**Figure 5.2.7.B, right panel**) than in PC-3S cells. These alternative reactions to the classical oxidative TCA cycle have been described to be present especially in rapidly growing tumor cells with disruption of mitochondrial function that are unable to efficiently synthesize citrate or other TCA intermediates for biosynthetic purposes and enhance additional metabolic pathways (*214, 305*). These results and the ones described in the previous Sections support the notion that the CSCs of our cell model compensate their reduced mitochondrial function by increasing many alternative metabolic pathways to sustain their needs and rapidly adapt to changes in nutrient availability.

As the cellular metabolism of glutamine and proline are closely interrelated, we decided to analyze whether accumulation of proline observed in PC-3M cells (**Chapter I**, **Figure 5.1.14.D**) was related with a higher diversion of glutamine carbons to proline. After incubation of PC-3M and PC-3S cells with 2 mM 100% [U-$^{13}C_5$]-glutamine for 48 h, we observed higher levels of extracellular m5 proline in PC-3M than PC-3S cells (**Figure 5.2.8.A**), therefore proline biosynthesis was favored in the CSC subpopulation. Indeed, the catabolism of proline by the action of the enzyme proline oxidase/proline dehydrogenase (POX/PRODH) results in inhibition of proliferation and induction of apoptosis by means of ROS production (*306*). Cells overexpressing the oncogene MYC, as in the case of PC-3M cells, downregulate POX/PRODH expression and markedly increase the enzymes converting glutamate to proline, such as Δ1-pyrroline-5-carboxylate synthase and Δ1-pyrroline-5-carboxylate reductase 1 (*307*). Therefore, the

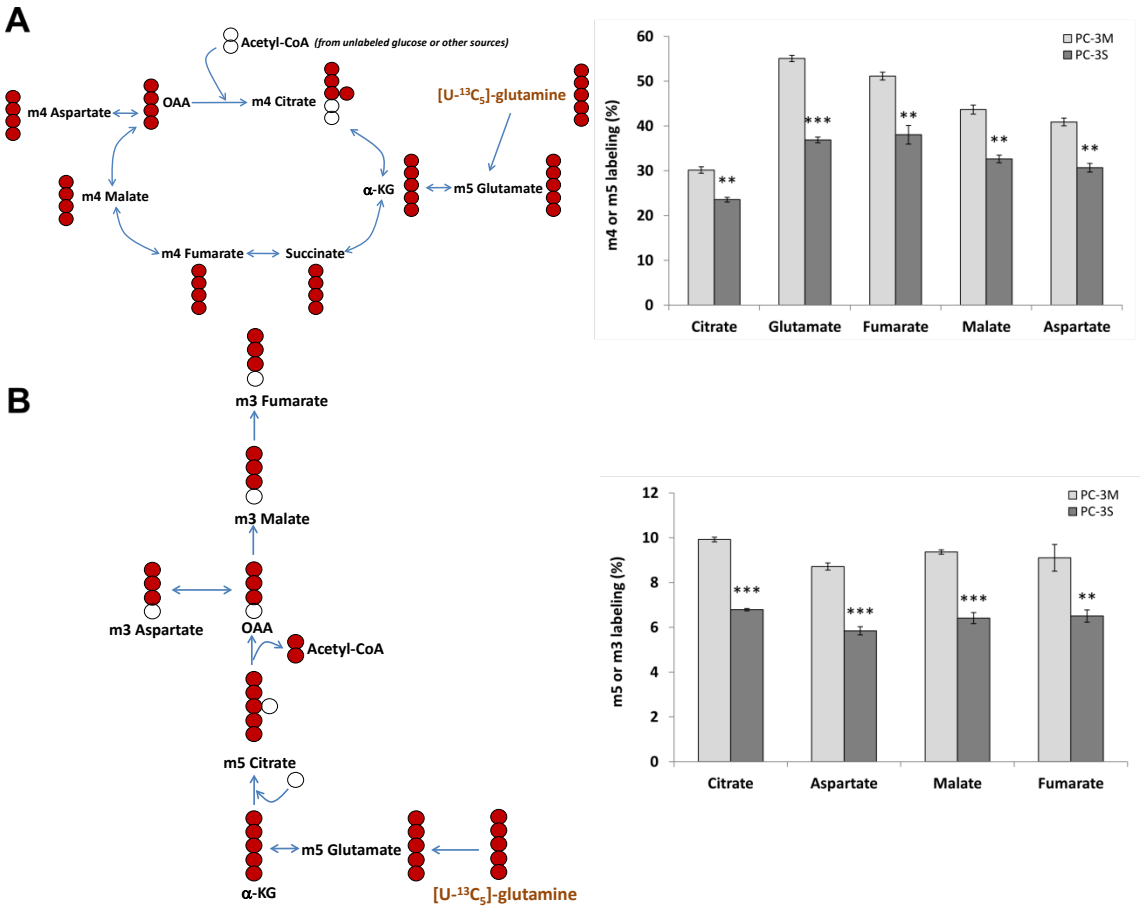

Figure 5.2.7 Glutamine contribution to the TCA cycle in PC-3M *vs*. PC-3S cells

(**A, left panel**) Representation of the labeling distribution in TCA intermediates from [U-$^{13}C_5$]-glutamine, considering the oxidative pathway. (**A, right panel**) m4 (m5 in the case of glutamate) labeling of TCA intermediates after 24 h of incubation with 2 mM 100% [U-$^{13}C_5$]-glutamine and GC/MS analysis. (**B, left panel**) Representation of the labeling distribution in TCA intermediates from [U-$^{13}C_5$]-glutamine, considering the reductive carboxylation reactions. (**B, right panel**) m5 labeling of citrate and m3 labeling of aspartate, malate and fumarate after 24 h of incubation with 2 mM 100% [U-$^{13}C_5$]-glutamine and GC/MS analysis. Bars represent the mean ± SD (n=3). Significant differences compared to PC-3M cells were assessed by Student's t-test: **p < 0.01 and ***p < 0.001. OAA, oxalacetate; α-KG, α-ketoglutarate.

higher expression of MYC in PC-3M, as compared to PC-3S cells, could explain not only the marked conversion of glutamine to glutamate, but also the enhancement in the conversion of glutamate to proline.

5.2.2.4 Pyruvate is diverted away from mitochondria in prostate CSCs due to low PDH activity

Because pyruvate dehydrogenase (PDH) is a key enzyme mediating the entry of pyruvate into mitochondria and thus linking glycolysis to the TCA cycle, we analyzed its

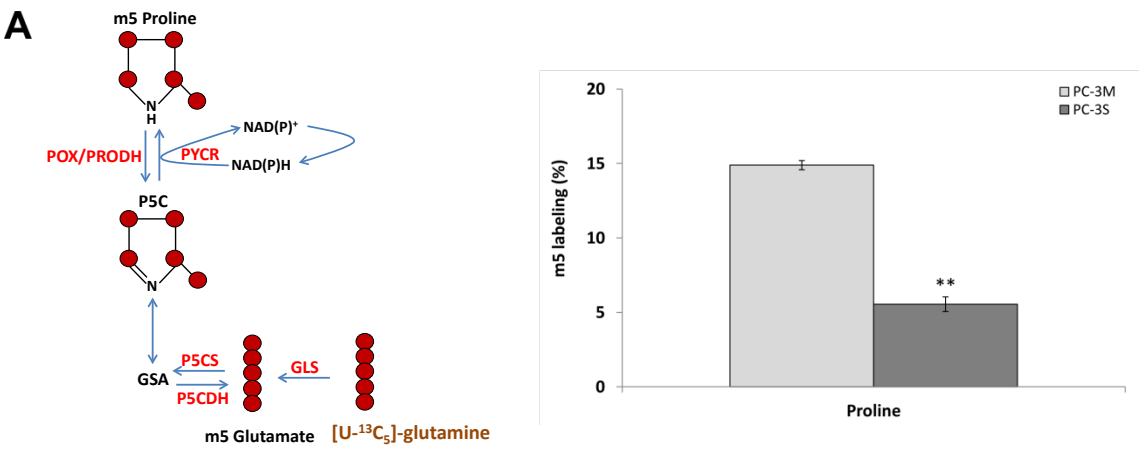

Figure 5.2.8 Glutamine contribution to proline synthesis in PC-3M vs. PC-3S cells

(**A, left panel**) Schematic representation of the reactions involved in [U-$^{13}C_5$]-glutamine conversion to proline. (**A, right panel**) m5 labeling of extracellular proline after 48 h of incubation with 2 mM 100% [U-$^{13}C_5$]-glutamine and GC/MS analysis. Bars represent the mean ± SD (n=3). Significant differences compared to PC-3M cells were assessed by Student's t-test: **p < 0.01. POX/PRODH, proline oxidase/proline dehydrogenase; PYCR, Δ1-pyrroline-5-carboxylate reductase; P5C, Δ1-pyrroline-5-carboxylic acid; GSA, glutamate-γ-semialdehyde; P5CS, Δ1-pyrroline-5-carboxylate synthase; P5CDH, Δ1-pyrroline-5-carboxylate dehydrogenase; GLS, glutaminase.

activity in our dual cell model. For this, we followed two different approaches. Firstly, oxamate titrations were performed to determine its effects on OCR and OCR/ECAR ratio. Oxamate is an inhibitor of lactate dehydrogenase (LDH), which catalyzes the conversion of pyruvate to lactic acid during the last step of glycolysis. Due to the higher LDH activity observed in PC-3M cells, this strategy is expected to increase the availability of pyruvate for the PDH reaction in these cells. Secondly, we performed dichloroacetate (DCA) titrations. DCA inhibits pyruvate dehydrogenase kinases (PDHKs) and therefore counteracts the inactivation of PDH by phosphorylation, leading to increased levels of active PDH. In both tests, we expect an increased entry of pyruvate into the mitochondria, followed by an increase in mitochondrial respiration accompanied with a decrease in ECAR due to diminished lactate production. Treatment of these cells with oxamate and DCA resulted in a more pronounced increase in mitochondrial respiration in the case of PC-3M cells, especially with the DCA treatment (**Figure 5.2.9.A**), indicating that activation of PDH (through PHDKs inhibition) is more effective than only increasing available pyruvate levels (following LDH inhibition) to stimulate the mitochondrial entry of pyruvate. The OCR/ECAR ratios

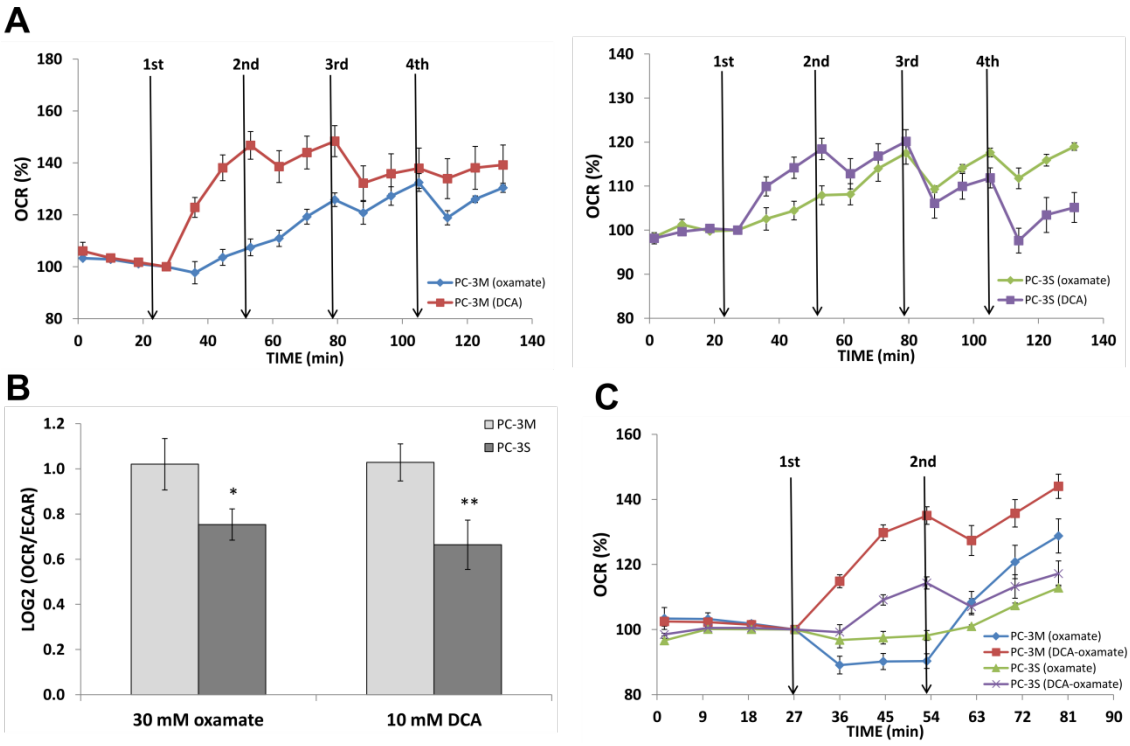

Figure 5.2.9 Effect of oxamate and DCA on the mitochondrial respiration of PC-3M and PC-3S cells

(**A**) Effect of oxamate and DCA titrations on oxygen consumption rate (OCR) of PC-3M (left panel) and PC-3S cells (right panel). Sequential injections of oxamate or DCA (1st, 2nd, 3rd and 4th) were performed to reach final concentrations of 10, 30, 50 and 70 mM for oxamate, and 10, 20, 30 and 40 mM for DCA. (**B**) Fold change (LOG2) in OCR/ECAR ratio after injection of 30 mM oxamate or 10 mM DCA. (**C**) Analysis of the synergistic effect of oxamate and DCA. Oxamate alone or sequential DCA and oxamate were injected and changes in OCR levels evaluated. Data are the mean ± SD from n=5. After a Student's t-test, differences compared to PC-3M cells were considered significant when *p < 0.05, **p < 0.01 and ***p < 0.001.

calculated for 30 mM oxamate and 10 mM DCA injections were also significantly higher in PC-3M cells (**Figure 5.2.9.B**). This was further supported by means of sequential exposure to DCA and oxamate which showed that the oxamate-induced enhancement of OCR in PC-3M cells was additionally boosted after sequential exposure to DCA and oxamate (**Figure 5.2.9.C**). By comparison, these treatments boosted the respiration of PC-3S cells to a significantly lesser degree than that of PC-3M cells, suggesting a higher PDH baseline activity in PC-3S cells that funnels pyruvate from glycolysis towards the TCA cycle under basal conditions, thus limiting the margins for further increments along this pathway. We confirmed our hypothesis by determining the phosphorylation status of PDH, being markedly more phosphorylated (and thus more inactive) in the case of PC-3M cells (**Figure 5.2.10.A**). We also checked

the gene expression levels of two of the major regulators of PDH activity, PDHK1 and PDP2, responsible for phosphorylation and dephosphorylation of the PDH protein, respectively. PDHK1 levels were higher in PC-3M cells, whereas the expression levels of the phosphatase PDP2 were higher in PC-3S cells (**Figure 5.2.10.B**). In addition, we analyzed if enhancement of the PDH activity in PC-3M cells had some effect on cell proliferation, finding that after 48 h of treatment with 10 mM DCA, the proliferation of PC-3M cells was inhibited significantly more than that of PC-3S cells (**Figure 5.2.10.C**). Thus, shifting metabolism from glycolysis to OXPHOS does not benefit the proliferation of PC-3M cells. We hypothesize that promoting the mitochondrial metabolism of cells displaying a preferentially glycolytic phenotype may cause an increased production of reactive oxygen species (ROS) that may compromise cell viability (*95*) as well as induce cell death by activating pro-apoptotic proteins (*308-309*).

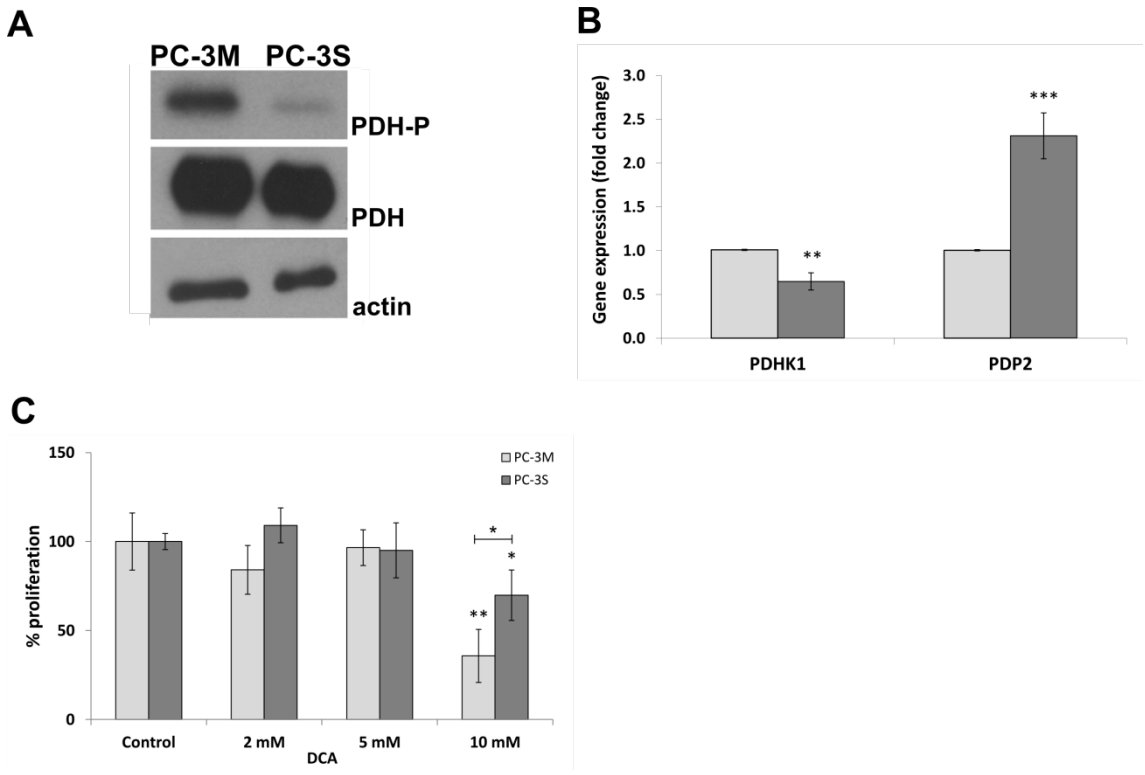

Figure 5.2.10 PDH status in PC-3M and PC-3S cells and effect of DCA on cell proliferation

(**A**) PDH and PDH-P protein levels were determined by Western Blotting. Actin was used as a protein loading and transfer control. (**B**) Gene expression analysis of PDHK1 and PDP2 determined by RT-PCR using gene-specific UPL probes (mean ± SD of n=3). (**C**) Effect of different DCA concentrations on PC-3M and PC-3S cell proliferation, after 48 h of incubation. Cell proliferation was assessed using HO33342 staining (mean ± SD of n=6). Significant differences compared to PC-3M cells (B) or control condition (C) were assessed by two-tailed Student's t-test: *p<0.05, **p<0.01 and ***p<0.001.

Our results also point out the differential contribution of glucose and glutamine to the synthesis of TCA intermediates, highlighting a key role of glutaminolysis, especially in PC-3M cells. The labeling pattern observed after cells were incubated with [1,2-$^{13}C_2$]-glucose or [U-$^{13}C_5$]-glutamine could be explained, in simple terms, by the low PDH activity and the higher glutamine consumption rate in PC-3M cells (**Chapter I**, **Figure 5.1.14**), compared to PC-3S cells. The regulation through phosphorylation of the activity of the mitochondrial gatekeeper PDH is mediated by PDHKs and PDPs. More specifically, in our model we have found higher levels of PDHK1 gene expression in the CSC subpopulation and, conversely, higher levels of PDP2 gene expression in the non-CSC counterpart. Inactivation of PDH by phosphorylation confers cells with a proliferative advantage (*310-311*). Indeed, the metabolic shift from glycolysis to mitochondrial glucose oxidation induced after DCA treatment compromised cell proliferation mostly in PC-3M cells.

In order to further validate the correlation between the mitochondrial metabolism and the CSC and EMT phenotypes in our cell model, we next analyzed the mitochondrial function and PDH status of the cell variants PC-3M SNAI1 and PC-3M SKM triple-KD, introduced in **Chapter I** and displaying an intermediate phenotype between PC-3M and PC-3S cells.

To determine the importance of mitochondrial metabolism in PC-3M SNAI1 cells, we analyzed the response to oligomycin, FCCP + Pyr and rotenone + antimycin by performing an experiment using the XF24 Extracellular Flux Analyzer. These determinations were carried out in the presence of both glucose and glutamine (full media condition), as described previously. We compared OCR baselines and found that PC-3M SNAI1 cells increased their respiration rate relative to control PC-3M cells (**Figure 5.2.11.A**) and, interestingly, this cell variant was more responsive to the three mitochondrial treatments (**Figure 5.2.11.B**). These results were consistent with the acquisition of a more mesenchymal, and thus PC-3S-like, metabolic phenotype. Because of our previous studies that the difference in PDH activity between PC-3M and PC-3S cells correlated with differential mitochondrial capacitites, we interrogated if the increase in mitochondrial function observed in PC-3M SNAI1 cells could be associated with differences in PDH status by analyzing the phoshorylation status of the PDH

enzyme and the gene expression levels of its activity modulators, PDHK1 and PDP2. Contrary to our expectations, we did not find significant differences regarding the phosphorylation levels of PDH (**Figure 5.2.11.C**) or in PDHK1 and PDP2 gene expression levels of PC-3M SNAI1 compared to control PC-3M cells (**Figure 5.2.11.D**). A possible explanation could be that although PDH activity does not increase in this cell variant, the reduction in lactate production (and thus the decrease in the Warburg effect) could favor the availability of pyruvate for mitochondrial metabolism.

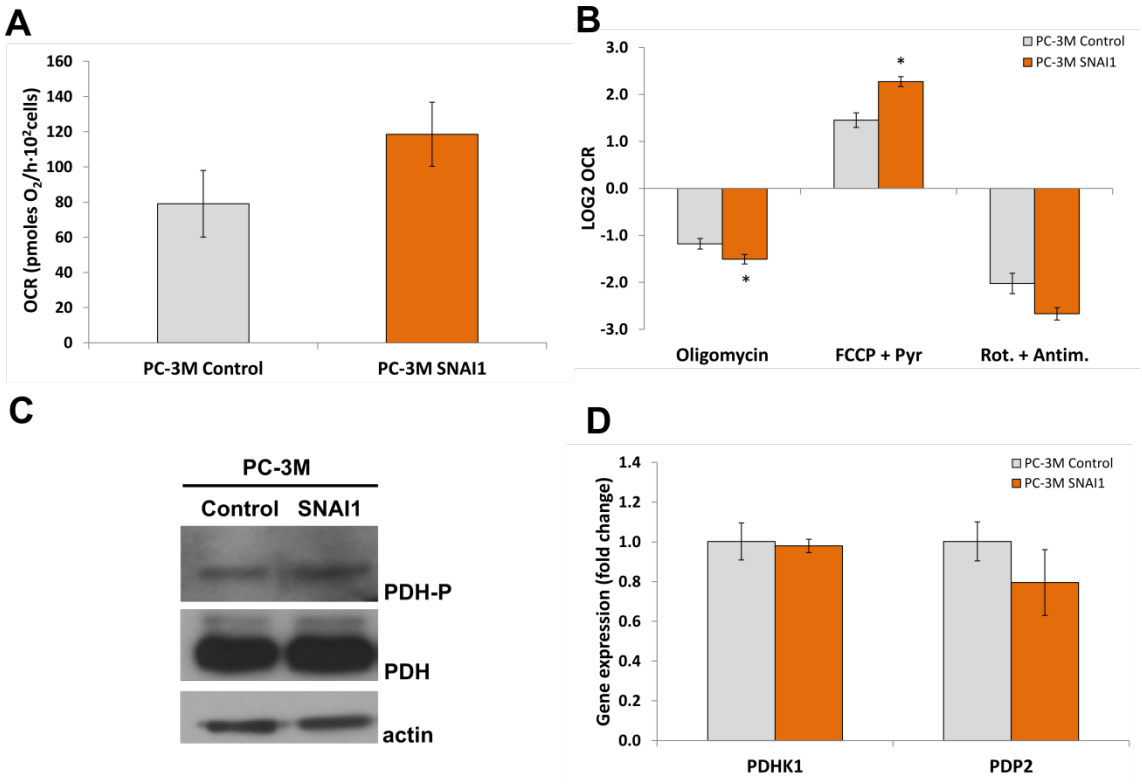

Figure 5.2.11 Mitochondrial function and PDH status in PC-3M SNAI1 cells

Oxygen consumption rate (OCR) was determined by a XF24 Extracellular Flux Analyzer instrument (Seahorse Bioscience). (**A**) Basal OCR in full media conditions, normalized to cell number. (**B**) Fold change (LOG2) in OCR after oligomycin, FCCP + Pyr and rotenone + antimycin (Rot. + Antim.) injections. (**C**) PDH-P and PDH protein levels determined by Western Blotting and using actin as a protein loading and transfer control. (**D**) Analysis of PDHK1 and PDP2 gene expression levels, expressed as fold change relative to control PC-3M cells. Gene expression levels were evaluated by RT-PCR, using transcript-specific UPL probes. Bars represent mean ± SD of n=5 (A and B) or n=3 (D). Significant differences compared to Control PC-3M cells were assessed by two-tailed Student's t-test. $p < 0.05$(*).

Next, we determined the mitochondrial potential of PC-3M SKM triple-KD cells. The OCR baseline was analyzed as well as the OCR response to oligomycin, FCCP + Pyr and rotenone + antimycin treatments. PC-3M SKM triple-KD cells showed higher OCR

baseline levels (**Figure 5.2.12.A**) but only the response to FCCP + Pyr was significantly increased relative to control PC-3M cells (**Figure 5.2.12.B**). No remarkable differences were found between PC-3M SKM triple-KD and Control PC-3M cells regarding PDH phosphorylation status (**Figure 5.2.12.C**) and PDHK1 and PDP2 gene expression levels (**Figure 5.2.12.D**). These results point out that, in our cell model, expression of the pluripotency genes SOX2, KLF4 and MYC may be more associated with glycolytic metabolic reprogramming (**Figure 5.1.6**, **Chapter I**). Cellular baseline respiration and maximal respiration capacity (FCCP + Pyr) are increased in PC-3M SKM triple-KD cells but the responses to the inhibition of complex V (oligomycin) and complexes I and III (rotenone + antimycin) do not significantly change OCR response relative to control PC-3M cells.

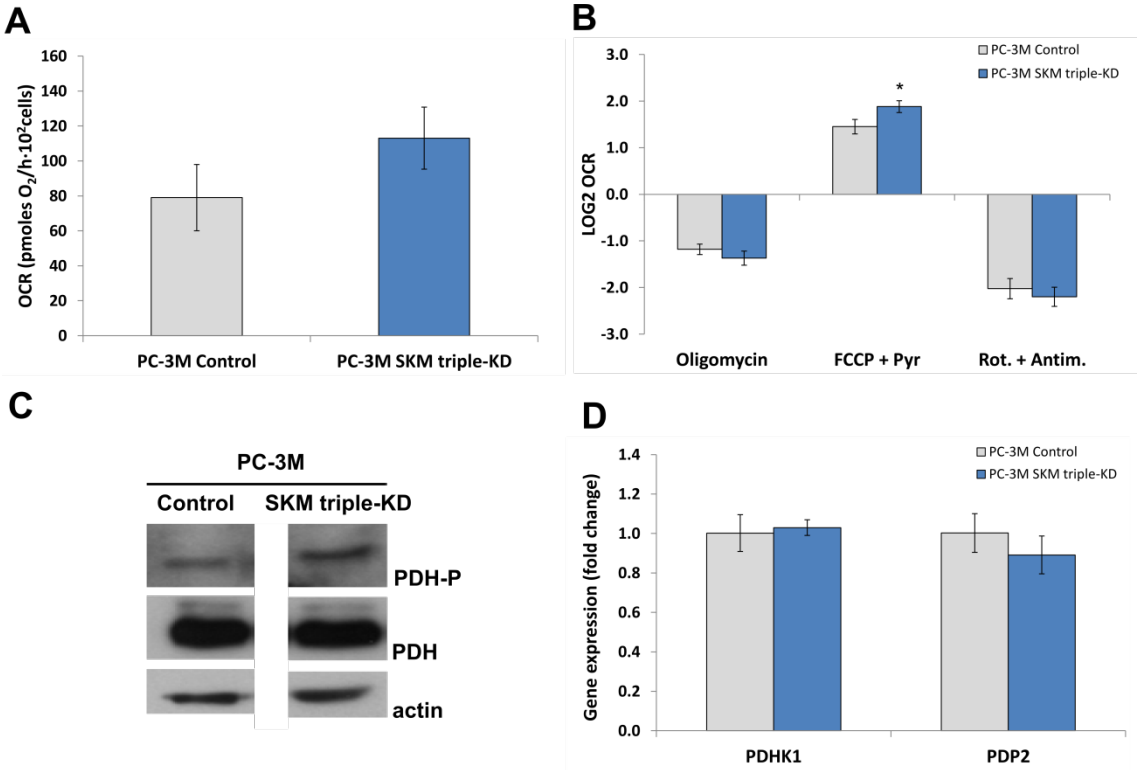

Figure 5.2.12 Mitochondrial function and PDH status in PC-3M SKM triple-KD cells

Oxygen consumption rate (OCR) was determined by a XF24 Extracellular Flux Analyzer instrument (Seahorse, Bioscience). (**A**) Basal OCR in full media conditions, normalized to cell number. (**B**) Fold change (LOG2) in OCR after oligomycin, FCCP + Pyr and rotenone + antimycin injections. (**C**) PDH-P and PDH protein levels determined by Western Blotting, using actin as a protein loading control. (**D**) Analysis of PDHK1 and PDP2 gene expression levels, expressed as fold change relative to control PC-3M cells. Gene expression levels were evaluated by RT-PCR, using gene-specific UPL probes. Bars represent mean ± SD of n=5 (A and B) or n=3 (D). Significant differences compared to Control PC-3M cells were assessed by two-tailed Student's t-test. $p < 0.05$(*).

Therefore, in this Section we have demonstrated that, under full media conditions, there is a correlation between the expression of an epithelial CSC phenotype with a more marked Warburg effect and a mesenchymal non-CSC phenotype with a preference for OXPHOS. The simultaneous loss of epithelial and CSC features and gain of mesenchymal and non-CSC traits by overexpression of the EMT factor SNAI1 or downregulation of the pluripotency factors SOX2, KLF4 and MYC is accompanied with a shift from a marked glycolytic phenotype to an increased use of the mitochondrial metabolism.

5.2.2.5 Prostate CSCs and non-CSCs differ in their dependence on glutaminase reaction and show a differential expression of the GAC and KGA glutaminase isoenzymes

In light of the contribution of glutamine to the TCA cycle metabolism in PC-3M cells, we further explored the effect of inhibiting glutaminolysis on cell proliferation and viability in our dual cell model and the ability of cells to shift their metabolism when required. Glutamine-dependent metabolism can contribute to cellular biosynthetic and energetic demands, and the importance of this metabolic pathway is particularly relevant in cells overexpressing the oncogene MYC (*312-313*), which is the case of PC-3M cells (*49*). We therefore investigated the essential role of the glutaminase reaction in the survival and proliferation of PC-3M and PC-3S cells using the glutaminase inhibitor bis-2-(5-phenylacetamido-1,2,4-thiadiazol-2-yl)ethyl (BPTES). Both cell types reduced significantly their proliferation rate when exposed to BPTES, particularly marked in the case of PC-3M cells (**Figure 5.2.13.A**). Treatment with BPTES caused a decline of cells in the S phase in PC-3M cells and a modest accumulation of PC-3S cells in the G1 phase of the cell cycle (**Figure 5.2.13.B**). We found that PC-3M and PC-3S cells adapted their metabolism after BPTES treatment, by slightly stimulating glucose consumption and, more significantly, lactate production (**Figure 5.2.13.C**). BPTES treatment has been associated with an elevated glycolytic flux as a compensatory mechanism to produce products derived from glutamine, like α-ketoglutarate (α-KG) (*314*). We next compared the effects on cell death of exposure to 2-DG (inhibitor of glycolysis) and BPTES, separately or in combination. Interestingly, the additive effect

on cell death by combined incubation with both drugs was more prominent for PC-3M cells (**Figure 5.2.13.D**), indicating that the compensatory mechanisms that PC-3M cells show after metabolic inhibitions (e.g. glycolytic or glutaminolysis inhibition) are more essential for their survival and viability.

The above results pointed to a strong dependence of PC-3M cells on glutamine metabolism. Glutamine is involved in numerous metabolic pathways, including anaplerotic reactions, biosynthesis of nucleotides, proteins and glutathione, NAPDH production (via malic enzyme) and maintenance of the pH. Because glutamine is anaplerotically used to fill the TCA cycle, we tested if the inhibition of cell proliferation by BPTES could be rescued after culturing cells for 48 h with the cell permeable α-KG analog dimethyl ketone (DMK). As shown in **Figure 5.2.14.A**, a non-significant rescue in PC-3M proliferation was observed after incubation with DMK of cells pretreated with BPTES. In the case of PC-3S cells, the treatment with BPTES + DMK increased slightly cell proliferation as compared to BPTES treatment, although it did not reach statistical significance. This suggested that glutamine exerts in these cells a crucial activity that is independent of its anaplerotic function, especially in PC-3M cells, and necessary for optimal cell proliferation. Apart from their known anaplerotic role, glutamine oxidation also supports redox homeostasis by supplying carbons to malic enzyme and yielding reducing equivalents (NADPH) and by glutamine-derived glutamate that can participate in the synthesis of glutathione, one of the most important cellular antioxidants (*209*). Recently, it has been shown that cells with defective mitochondria or transient mitochondrial impairment under hypoxia metabolize glutamine via reductive carboxylation mediated by NADPH-dependent isoforms of isocitrate dehydrogenase to provide carbons for biosynthetic purposes (e.g. TCA intermediates and fatty acids) (*214-215, 315*). A less explored function of the glutaminase reaction that cannot be substituted by α-KG analogs is its capacity to counteract acidic conditions by the release of ammonia after glutamine is metabolized to glutamate (*218*).

In order to investigate non-anaplerotic activities associated with glutamine metabolism, we first studied the effect of BPTES on intracellular glutathione content and ROS levels of our cell model. Because glutamine metabolism yields glutamate

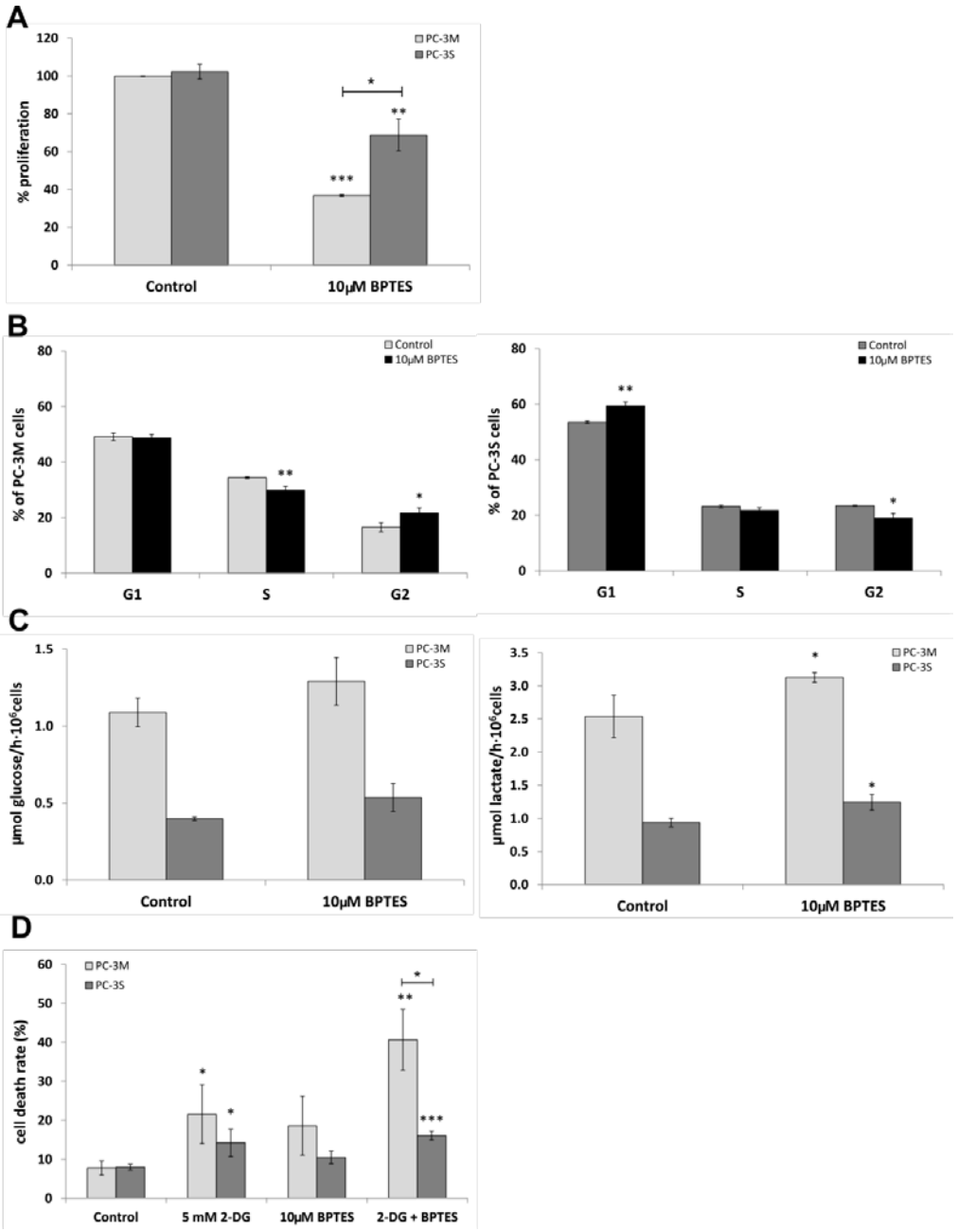

Figure 5.2.13 Effects of glutaminase inhibition on cell proliferation, metabolic adaptation and viability

(**A**) Cells were incubated with 10 μM BPTES for 48 h and the effect on cell proliferation determined by HO33342 staining. Results are shown as percentage of proliferation relative to cells cultured without BPTES (Control). (**B**) Cell cycle analysis of PC-3M (left panel) and PC-3S (right panel) cells untreated or treated with 10 μM BPTES for 48 h. The harvested cells were stained with propidium iodide and their DNA content analyzed by flow cytometry. Plots depict the variation of the percentage of cells in each phase (G1, S or G2) of the cell cycle. (**C**) Glucose consumption (left panel) and lactate production (right panel) were determined after 48 h of incubation without (Control) or with 10 μM BPTES. (**D**) Analysis of cell death in PC-3M and PC-3S cells cultured in control media or media containing 5 mM 2-DG, 10 μM BPTES or 5 mM 2-DG + 10 μM BPTES for 48 h. Plots depict the variation of the percentage of death cells (apoptotic + necrotic cells). Data are the mean ± SD of n=3, except in Figure A, where n=6. Significant differences between BPTES treatment and the corresponding control (PC-3M or PC-3S cells) were assessed by Student's t-test and are indicated as $p < 0.05$(*), $p < 0.01$(**) and $p < 0.001$(***).

molecules, we expected to observe glutathione synthesis to be affected after BPTES treatment. Surprisingly, although ROS production increased in PC-3M and PC-3S cells after inhibition of glutaminase by BPTES (**Figure 5.2.14.B)**, the intracellular glutathione content of PC-3M cells was not altered (**Figure 5.2.14.C**). In the case of PC-3S cells, the glutathione content decreased upon BPTES treatment, showing that glutamine metabolism is indeed important for the synthesis of glutathione molecules in this cell subpopulation. Thus, these results fail to provide a mechanistic explanation for the essentiality of the glutaminase reaction for optimal cell proliferation, in particular for the PC-3M metastatic CSC subpopulation.

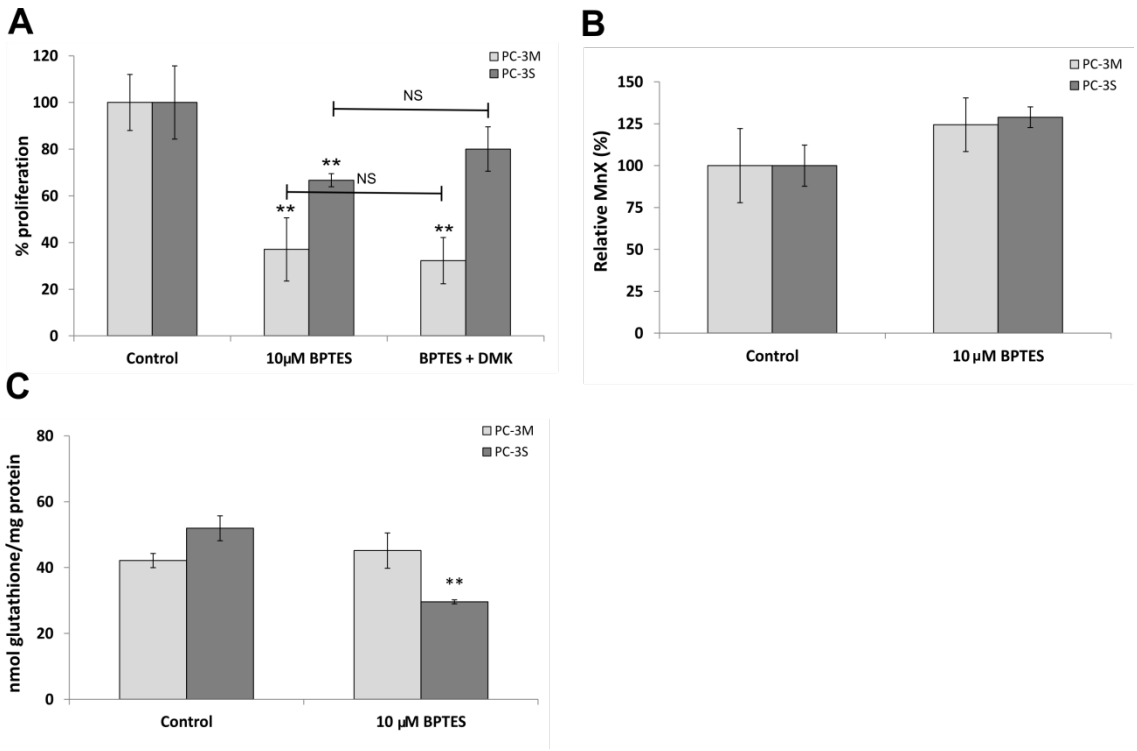

Figure 5.2.14 Rescue with DMK and effect on ROS and glutathione levels after inhibition of glutaminase

(**A**) Cells were incubated with 10 μM BPTES in the presence or absence of 2 mM DMK for 48 h and the rescue in cell proliferation assessed. Cell proliferation was determined by HO33342 staining (mean ± SD of n=6). Here, treatment with BPTES is also compared with BPTES + DMK treatment for each cell subpopulation. (**B**) Intracellular ROS levels after 48 h of incubation without (Control) and with 10 μM BPTES. Values are shown as percentage of mean fluorescent intensity (MnX) relative to the corresponding control PC-3M or PC-3S. The fluorescent signal was measured by flow citometry (mean ± SD of n=3). (**C**) Intracellular glutathione levels present in cells untreated or treated with 10 μM BPTES for 48 h. Values are normalized to protein concentration (mean ± SD of n=3). Significant differences between treatments and the corresponding control (PC-3M or PC-3S cells) were assessed by Student's t-test. $p < 0.01$(**). For non-significant differences: $p > 0.05$(NS).

Recent findings have shown that glutamine provides cellular resistance to acidic conditions through the release of ammonia (*218*). To investigate this, we first tested the effect of a relatively acidic pH environment on cell proliferation. After 48 h of incubation in pH 7.1 media, PC-3M cells decreased more significantly their proliferation than PC-3S cells as compared to cells grown in standard media (pH 7.9) (**Figure 5.2.15.A**). Next, to determine the contribution of the glutaminase reaction as an acid buffer, we analyzed if the incubation of cells with BPTES in relatively acidic conditions accentuated the decline in cell proliferation observed in the absence of this drug. We compared these results with an analogous experiment, where cells were incubated in relatively acidic conditions with or without the buffering system included in RPMI cell media, sodium bicarbonate ($NaHCO_3$), thus mimicking the hypothetical role that we are assigning to glutaminase reaction. As shown in **Figure 5.2.15.B**, there was a synergic growth inhibitory effect between relatively low pH and BPTES, more pronounced in the case of PC-3M cells. The absence of $NaHCO_3$ also negatively impacted cell proliferation under acidic conditions (**Figure 5.2.15.B**).

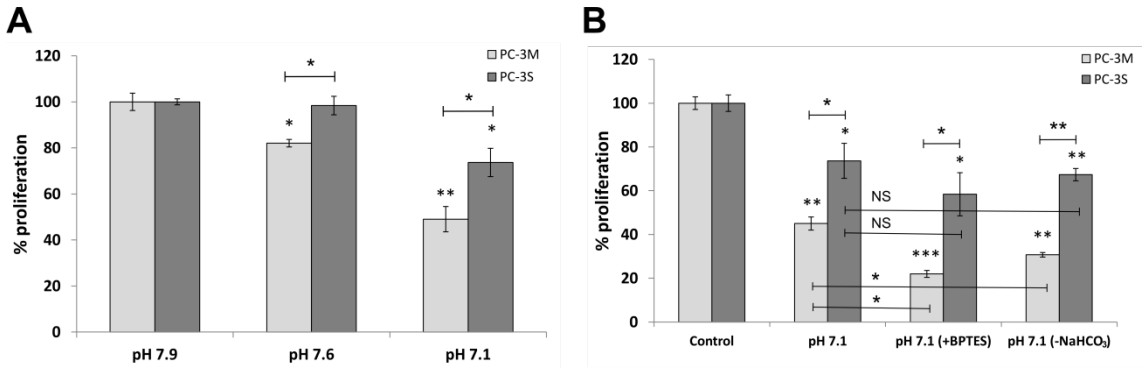

Figure 5.2.15 Contribution of glutaminase to the buffering of relatively acidic cell media

(**A**) Effect of acidic pH (pH lower than 7.9) on PC-3M and PC-3S cell proliferation, assessed with HO33342 staining, after 48 h of incubation in control media (pH 7.9) or acidic media (pH 7.6 and pH 7.1). These pH values correspond to the final pH obtained after equilibrium with the CO_2 inside the cell incubator. (**B**) Effect on cell proliferation of acidic media, and the combination of low pH with BPTES (pH 7.1 (+BPTES)) or without bicarbonate buffering (pH 7.1 (-$NaHCO_3$)). Cells were cultured for 48 h under the indicated conditions. Results are shown as percentage of proliferation relative to the corresponding PC-3M or PC-3S control (pH 7.9). Data are the mean ± SD of n=3. After a Student's t-test, differences between controls and conditions (as well as other comparisons indicated in the graph) were considered significant when *$p < 0.05$, **$p < 0.01$ and ***$p < 0.001$. For non-significant differences: $p > 0.05$(NS).

These observations suggest that the glutaminase reaction contributes to the buffering of protons, and provide a mechanistic explanation of the augmented compromise in cell proliferation caused by the inhibition of glutaminase under relatively acidic conditions, particularly evident in PC-3M cells**.**

Taken together, these data suggest that a significant role for glutaminase in our cells could be the buffering of extracellular pH, in addition to simply provide nutrition. As PC-3M cells express a marked Warburg effect, with consequent high lactate production and accumulation, they could require such an additional mechanism to survive this acidic stress. The above described mechanisms reveal previously unexplored vulnerabilities of CSCs that may be worth exploiting therapeutically.

The human glutaminase 1 (GLS1) gene codes for two alternatively spliced isoforms, the high activity kidney-type glutaminase (KGA) and the low K_M glutaminase C (GAC) variant. mRNA and protein levels of both isoforms, KGA and GAC, have been found to be elevated in various tumor types (*204, 316*) but, more recently, GAC has been proposed as the better adapted isoenzyme to provide for the increased metabolic needs of tumor cells (*205*) and its importance for cancer cell growth under acidic pH has been highlighted (*218*). We have found that levels of total GLS1 protein were higher in PC-3M than PC-3S cells (**Figure 5.2.16.A**), consistent with their higher glutamine consumption rate (**Chapter I**, **Figure 5.1.14**). Importantly, gene expression analysis and Western Blotting using isoform-specific probes against GAC and KGA revealed much higher levels of the GAC isoform in PC-3M cells than in PC-3S cells (**Figures 5.2.16.B and 5.2.16.C**), whereas no remarkable differences were found for the KGA isoform (**Figures 5.2.16.B** and **5.2.16.D**). These results point out an interesting correlation between the GAC isoform expression and the prostate epithelial CSCs and mesenchymal non-CSCs phenotypes, that could explain the differential dependence on the glutaminase activity observed in PC-3M and PC-3S cells. The glutaminase reaction is necessary for both cancer cell types, but the most remarkable need for the buffering of protons observed in PC-3M cells, probably as a consequence of their higher Warburg effect, make us to propose that an increased expression of GAC may result

advantageous as this glutaminase isoform has been previously described to be more active than KGA in low pH conditions (*218*).

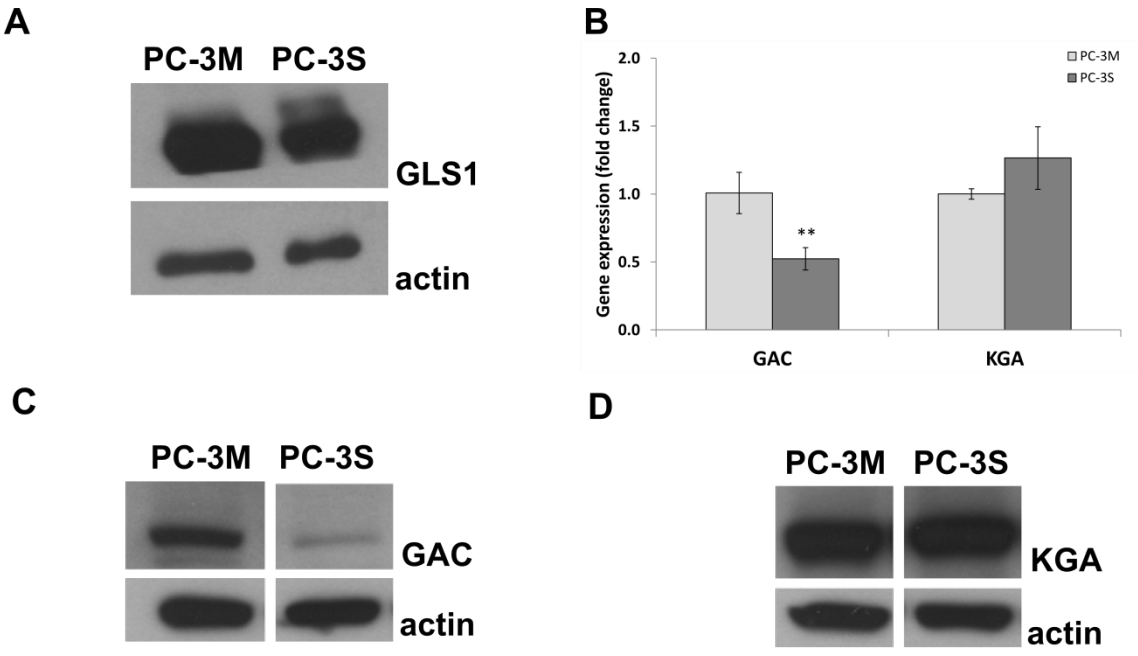

Figure 5.2.16 Expression of glutaminase and glutaminase isoforms in PC-3M and PC-3S cells

(**A**) Total glutaminase 1 (GLS1) protein levels determined by Western Blotting. Actin was used as a protein loading control. (**B**) Expression levels of glutaminase C (GAC) and kidney-type glutaminase (KGA) isoforms, expressed as fold change relative to PC-3M cells. Gene expression was determined by RT-PCR using isoform-specific UPL probes. (**C**) Protein levels of GAC and (**D**) KGA isoforms determined by Western Blotting. Bars represent the mean ± SD of n=3. Significant differences compared to PC-3M cells were assessed by Student's t-test. $p < 0.01$(**).

Next, we explored glutamine metabolism in the PC-3M SNAI1 and PC-3M SKM triple-KD cell variants. As these PC-3M cell variants acquire some phenotypic characteristics of PC-3S cells due to SNAI1 overexpression (PC-3M SNAI1), which induces EMT, or SOX2, KLF4 and MYC triple knock down (PC-3M SKM triple-KD), with loss of self-renewal and pluripotency traits, we sought to analyze the importance of the maintenance of epithelial and self-renewal properties on the glutamine metabolism of PC-3M cells.

Assessment of glutamine uptake showed a reduction in glutamine consumption in PC-3M SNAI1 cells (**Figure 5.2.17.A**), as well as a reduced sensitivity to BPTES treatment (**Figure 5.2.17.B**). In our studies, glutaminase activity was relevant for cell proliferation

in low pH conditions especially for the PC-3M subpopulation. We tested cell growth of PC-3M and PC-3M SNAI1 cells at pH 7.0 (control pH was 7.8) in the absence and presence of 10 μM BPTES. We found that the proliferation of PC-3M SNAI1 cells was

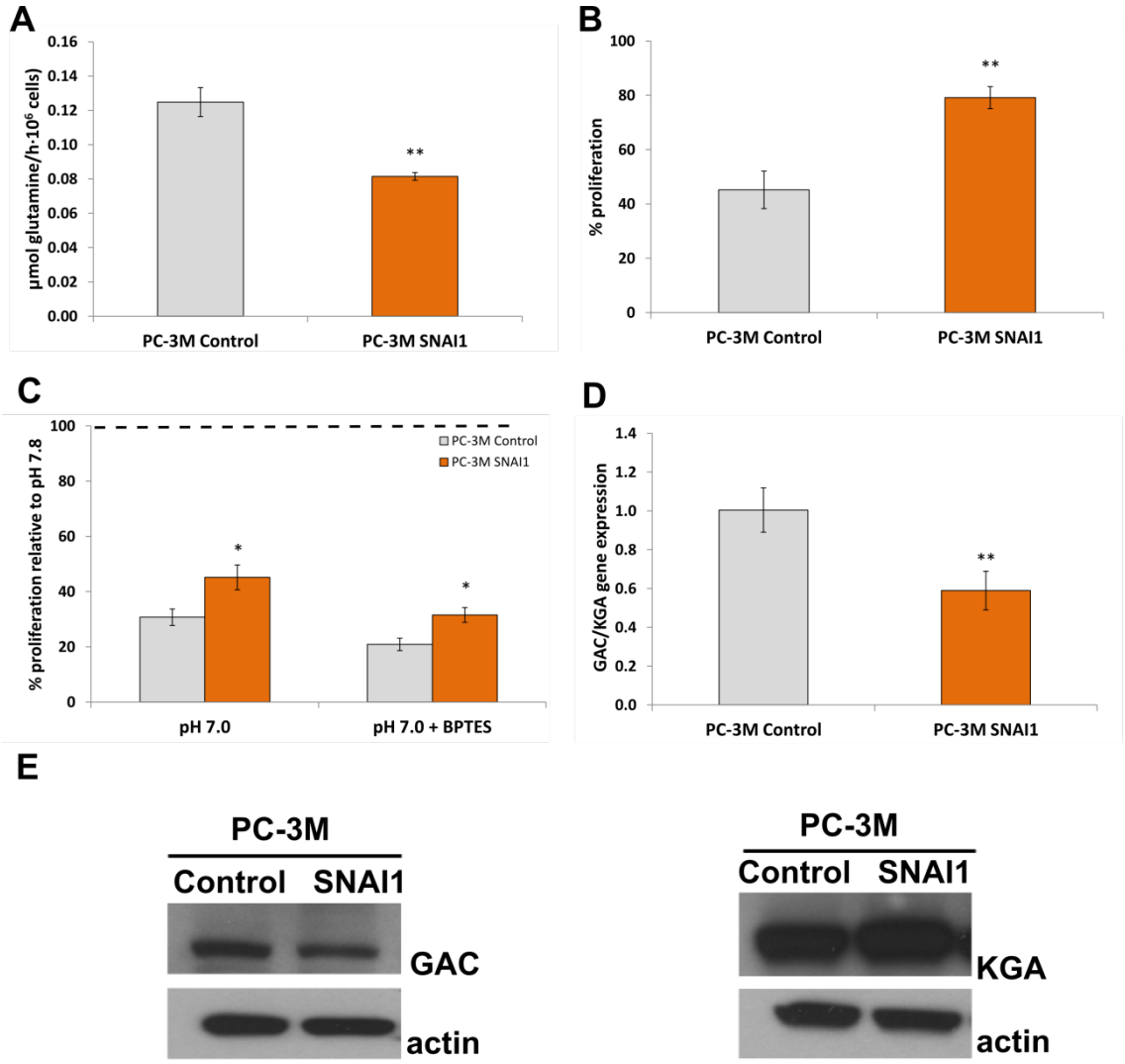

Figure 5.2.17 Glutamine metabolism, dependence on glutaminase reaction and glutaminase isoforms profile in PC-3M SNAI1 cells

(**A**) Glutamine consumption rate of Control PC-3M cells vs. PC-3M SNAI1. (**B**) Cells were incubated with 10 μM BPTES for 48 h and cell proliferation was assessed with HO33342 staining. Results are shown as percentage of proliferation relative to control PC-3M or PC-3M SNAI1 cells cultured without BPTES (100% proliferation). (**C**) Effect of acidic media (pH 7.0) and acidic media + 10 μM BPTES (pH 7.0 + BPTES) on cell proliferation. Cells were cultured for 48 h under the indicated conditions and cell proliferation was assessed with HO33342 staining. Results are shown as the percentage of proliferation relative to control PC-3M or PC-3M SNAI1 cells growth in standard pH conditions (pH 7.8) (100% proliferation). (**D**) Isoform-specific transcript level ratios of the glutaminase C (GAC) and kidney-type glutaminase (KGA) isoforms. (**E**) Protein levels of GAC and KGA isoforms, determined by Western Blotting with isoform-specific antibodies. Actin was used as protein loading control. Data are the mean ± SD of n=3. After a Student's t-test, differences between Control PC-3M and PC-3M SNAI1 cells were considered significant when $p < 0.05$(*) and $p < 0.01$(**).

less sensitive to low pH and that glutaminase inhibition did not decrease cell proliferation to the same extent as control PC-3M cells (**Figure 5.2.17.C**). The reduced sensitivity of PC-3M SNAI1 cell proliferation to low pH can be hypothetically explained by their reduced glycolytic rate that results in disminished production of lactate relative to control PC-3M cells and thus less dependence on the buffering capacity of glutaminase. We next checked the levels of the GLS1 isoforms GAC and KGA, and interestingly found that the GAC/KGA ratio both at transcript (**Figure 5.2.17.D**) and protein expression (**Figure 5.2.17.E**) levels decreased in PC-3M SNAI1 cells. This shows that induction of EMT by overexpression of SNAI1 in PC-3M cells causes a shift in the profile of GLS1 isoforms.

Next, we assessed how knock down of pluripotency genes in PC-3M cells affected glutamine metabolism. We found that glutamine consumption was reduced in PC-3M SKM triple-KD cells (**Figure 5.2.18.A**) and that their proliferation rate was less affected than control PC-3M cells by glutaminase inhibition, although without reaching statistical significance (**Figure 5.2.18.B**). The oncogene MYC regulates genes involved in cell cycle and glycolysis but also engages glutaminolysis (*211*), thus its knock down is expected to alter and reduce glutamine dependency in PC-3M cells. Next, we compared the effect of low pH and BPTES on proliferation. The proliferation of PC-3M SKM triple-KD cells was less affected by low pH and glutaminase inhibition than control PC-3M cells (**Figure 5.2.18.C**). Similarly to PC-3M SNAI1, the reduced production of lactate (thus, less accumulation of protons to the extracellular media) may allow PC-3M SKM triple-KD cells to proliferate under relatively low pH conditions without an imperative need to remove an excess of protons, thus explaining their reduced dependence on glutaminase reaction as compared to PC-3M cells. Finally, we determined the levels of GAC and KGA isoforms and found that the GAC/KGA ratio of transcript isoform expression levels in the PC-3M SKM triple-KD cells (**Figure 5.2.16.D**) did not show a significant decline when compared to control PC-3M cells. However, we observed a decrease in the expression levels of the GAC isoform protein (**Figure 5.2.16.E**). These results, together with those described for PC-3M SNAI1 cells, are supportive of the importance of the GAC isoform to confer acid resistance to CSCs with high proliferative rates and marked Warburg effect. They also show that a switch in

the relative expression ratios of the GAC and KGA isoforms of glutaminase is achieved *via* expression of the EMT factor SNAI1, and also, although

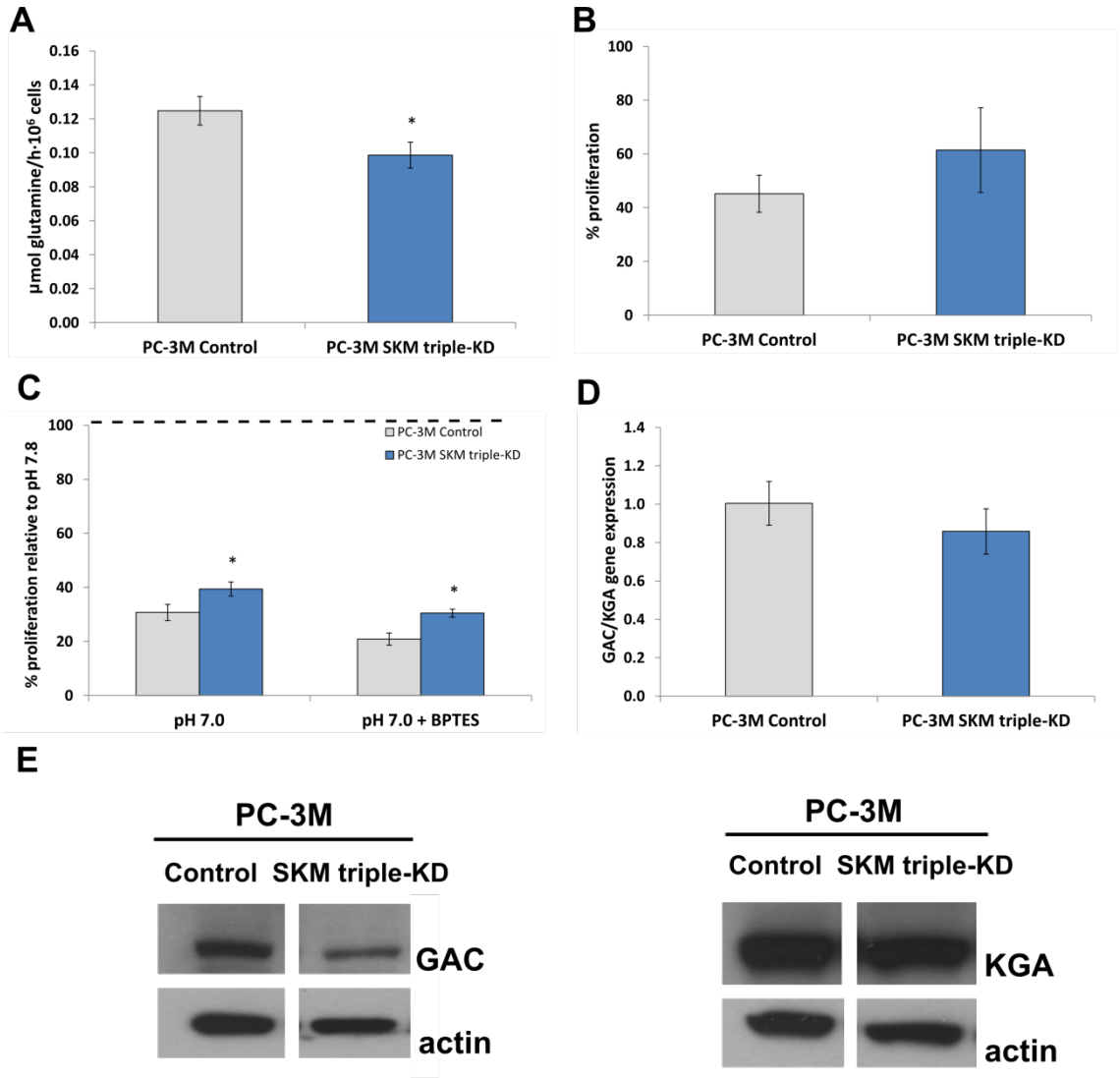

Figure 5.2.18 Glutamine metabolism, dependence on glutaminase reaction and glutaminase isoforms profile in PC-3M SKM triple-KD cells

(**A**) Glutamine consumption rate of Control PC-3M cells vs. PC-3M SKM triple-KD. (**B**) Cells were incubated with 10 µM BPTES for 48 h and cell proliferation determined by HO33342 staining. Results are shown as percentage proliferation relative to PC-3M Control or PC-3M SKM triple-KD cells cultured without BPTES (100% proliferation). (**C**) Effect of acidic media (pH 7.0) and acidic media + 10 µM BPTES on cell proliferation. Cells were cultured for 48 h under the indicated conditions and cell proliferation assessed with HO33342 staining. Results are shown as the percentage of proliferation relative to control PC-3M or PC-3M SKM triple-KD cells growth in standard pH conditions (pH 7.8) (100% proliferation). (**D**) Isoform-specific transcript level ratios of the glutaminase C (GAC) and kidney-type glutaminase (KGA) isoforms. (**E**) Protein levels of GAC and KGA isoforms, determined by Western Blotting using isoform-specific antibodies. Actin was used as a protein loading control. Data are the mean ± SD of n=3. After using Student's t-test, differences between Control PC-3M and PC-3M SKM triple-KD cells were considered significant when $p < 0.05$(*).

less prominently so, by the pluripotency gene network represented by SOX2, KLF4 and, probably more importantly, MYC. Therefore, our results emphasize the importance for CSC proliferation and survival of non-anaplerotic functions of glutamine and the glutaminase reaction, including buffering effects to counteract the high levels lactate production associated with a strong Warburg effect.

6. GENERAL DISCUSSION

6. GENERAL DISCUSSION

Cellular heterogeneity in cancer is well recognized and results in the coexistence within a tumor of different subpopulations endowed with distinct tumorigenic capacities. Genetic, epigenetic, transcriptional and post-translational changes drive tumor cell heterogeneity, by which tumor cells express different programs that contribute to the acquisition of the phenotypic characteristics required for successfully contribute to tumor progression through selection, cooperation or additional ecological processes. The phenotypic heterogeneity of tumors also translates as metabolic heterogeneity, by which neoplastic and non-neoplastic cells (including cells from tumor microenvironment) can display distinct prevalent metabolic states in order to sustain their specific needs. Metabolic rewiring of cancer cells favors their adaptation, survival and growth in adverse conditions, including oncogenic, environmental and drug-induced stress. It is becoming increasingly important to characterize such differential metabolic states and their inferred vulnerabilities because of the mounting evidences that metabolic heterogeneity lies at the heart of the phenotypic heterogeneity of neoplastic cells that define cellular states relevant for tumor biology and progression, including cancer stem cells (CSC) and cells expressing the epithelial-mesenchymal transition (EMT) program. Here, we have performed comprehensive comparative analyses of the bioenergetic and biosynthetic metabolic pathways derived from glucose and other nutrients sources, by using a dual-cell prostate cancer cell model as a tool to unveil key metabolic nodes and vulnerabilities specific to distinct cancer cell subpopulations. In this cell model, the PC-3M subpopulation displays CSC properties, high metastatic potential and an epithelial gene program, while the PC-3S subpopulation expresses EMT markers and displays low metastatic capacity but high invasive potential. Our study has unveiled different contributions of metabolic pathways in these two clonal neoplastic subpopulations, and the integration of the comprehensive metabolic information that we have generated provides a clear scenario of the differential metabolic networks that characterize the CSC and non-CSC subpopulations of our cell model.

A marked Warburg effect characterizes the CSC phenotype whereas oxidative phosphorylation prevails in non-CSCs

Glycolysis and oxidative phosphorylation (OXPHOS) constitute two major pathways for energy generation and the synthesis of biosynthetic precursors. The results described in **Chapter I** (5.1.2.1) and **Chapter II** (5.2.2.1) reveal that PC-3M cells, characterized by an epithelial CSC phenotype, present a more glycolytic profile whereas the PC-3S cells, which display a mesenchymal non-CSC phenotype, rely more on OXPHOS. These differential metabolic preferences result in different sensitivities to glycolytic (e.g. 2-DG) or mitochondrial (e.g. oligomycin) inhibitors of these essential metabolic pathways in PC-3M and PC-3S cell subpopulations, respectively. Similar to our results, recent evidences by other laboratories suggest that the preference for aerobic glycolysis and the parallel decrease or silencing of mitochondrial activity found in many tumors is specifically associated with CSCs, which results in a selective growth advantage, reduction of mitochondrial-derived ROS and resistance to apoptosis (*317*). Aerobic glycolysis provides to the highly proliferative PC-3M cells with a rapid source of energy (ATP) as well as glycolytic intermediates that participate in the biosynthesis of numerous macromolecules, such as nucleotides, lipids and proteins. Mechanistically, a higher activity of LDH and the inactivation of the PDH complex, as observed in PC-3M cells, can favor the Warburg effect and, at the same time, reduce the levels of pyruvate that are diverted to the mitochondria.

On the other hand, our results also suggest that the association found by others between the EMT gene program and cell metabolism might have been misinterpreted because of the use of cell models in which CSC phenotypes are coupled to an EMT program within the same cell subpopulation. As a result, the metabolic characteristics associated with self-renewal and tumor-initiating ability (CSCs) are generally not discriminated from the metabolic states associated with invasive and migratory capacities, more related to EMT (*318*). In this regard, our cell model is unique in that it permits to characterize metabolic states associated with fully dissociated CSC or EMT programs. A relevant general conclusion that reconciles our work with that of other laboratories is that all CSCs display common metabolic states consistent with high glycolysis, regardless of whether their prevalent gene programs are epithelial or

mesenchymal. Conversely, non-CSCs tend to exhibit more active OXPHOS. In fact, recent studies in line with our own experimental observations have demonstrated that, compared to metastatic cancer cells, circulating cancer cells expressing mesenchymal and EMT traits activate a bioenergetic program that uses mitochondrial biogenesis and OXPHOS through a marked upregulation of PGC-1α (*200*). In addition, we have observed that PC-3S cells show higher levels of ROS than PC-3M cells (**Chapter I**, 5.2.1.4), which may be a consequence of their higher mitochondrial OXPHOS metabolism. As promotion of the EMT depends on the intracellular redox status (*319*), ROS has been recognized as an inducer of the EMT program by induction of the transcription factor SNAI1 (*320-321*). However, high levels of oxidative stress require efficient defense mechanisms to avoid the production of excessive ROS that could compromise cell viability, instead of acting as a signal inducer. Therefore, the higher glutathione content in PC-3S cells probably contribute to the maintenance of optimal amounts of ROS. Indeed, glutathione synthesis may be favored in PC-3S as these cells accumulate an excess of glutamate and glycine, two of the amino acids required for the synthesis of the glutathione tripeptid.

Our cell model also affords the study of the dependence of the observed phenotypes on epithelial or mesenchymal gene programs, by modulating the expression of EMT factors, or on pluripotency gene networks, by modulating the expression of pluripotency factors. Our analyses have revealed that overexpression of the EMT factor SNAI1 or knock down of the pluripotency factors SOX2, KLF4 and MYC in the PC-3M cell subpopulation, which causes the loss of epithelial and CSC properties and promote the acquisition of a mesenchymal-EMT program, is linked to the reduction of the glycolytic potential with a gain in mitochondrial function (**Chapter I**, 5.1.2.1 **Chapter II**, 5.2.2.4). More specifically, overexpression of SNAI1 significantly enhanced the mitochondrial potential of PC-3M cells, whereas knock down of SOX2, KLF4 and MYC was more strongly associated with a decrease in glucose consumption and lactate production, thus reducing the glycolytic flux. These findings provide interesting insights into possible mechanistic links between high glycolytic metabolism and pluripotency, on the one hand, and high mitochondrial metabolism and EMT, on the other.

CSCs display higher metabolic flexibility and capacity to switch carbon source usage

Our results also showed that the above mentioned metabolic profiles are flexible and very dependent on the metabolic conditions (nutrient microenvironment) to which PC-3M and PC-3S are subjected. Specifically, PC-3M cells showed a greater capacity than PC-3S cells to metabolize carbon substrates other than glucose (e.g. fatty acids and different amino acids (**Chapter I**, 5.1.2.1 and 5.1.2.4, respectively)) and adapt their metabolism depending on the available nutrients (e.g. increase glutamine consumption as a response to glucose-deprived media (**Chapter I**, 5.1.2.1). This flexibility enables metastatic PC-3M cells to rapidly switch between metabolic states according to their changing environment. This trait has been correlated with self-renewing cell subpopulations and their ability to seed and grow in multiple microenvironments (*322*). Celià-Terrassa *et al*. showed that PC-3M cells, but not PC-3S cells, readily produced large tumors in NOD-SCID mice after intramuscular injection (*49*). Therefore, the metabolic flexibility observed *in vitro* in PC-3M cells may benefit their survival *in vivo* in foreign microenvironments and consequently the establishment of metastasis.

Glutaminolysis: a key metabolic feature and vulnerability of CSCs

The importance of glutaminolysis has been explored in depth in **Chapter II**, 5.2.2.5. Our results indicate that glutamine metabolism is enhanced in the PC-3M cell subpopulation. Taking into account that, unlike PC-3S cells, most of the pyruvate derived from glycolysis in PC-3M cells is diverted to the synthesis of lactate, glutamine is able to supply carbons to replenish the TCA cycle and obtain those TCA intermediates required for biosynthetic or energetic purposes. Apart from its contribution to the oxidative TCA cycle, glutamine also contributes substantially to the synthesis of TCA intermediates via reductive carboxylation in PC-3M cells. The relevance in these cells of the glutaminase reaction was explored using the glutaminase inhibitor BPTES, which differentially affected the viability and proliferation of PC-3M cells over PC-3S cells. Glutaminolysis has been described to be particularly relevant in cells expressing the oncogene MYC (*313*) as is the case for PC-3M cells (*49*). Consistently, we have found that knock down of MYC, together with SOX2 and KLF4, in

PC-3M cells reduced glutamine consumption. On the other hand, the acquisition of an EMT program by overexpression of SNAI1 led to a reduction in glutamine metabolism in our cell model. Contrary to our results, other studies have found that the overexpression of SNAI1 in MDCK cells decreased the expression of glutaminase 2 as well as the mitochondrial potential (*323*). However, in that study, all the metabolic characterization associated with the overexpression of SNAI1 was carried out using a very heterogeneous cell model, displaying different tumorigenic potentials depending on the cell lot (*324*). This underlines the importance of studying distinct cell subpopulations with uncoupled CSC and EMT programs to better associate the effects of modulating pluripotency or EMT genes on cell metabolic reprogramming.

As glutamine participates in numerous reactions, we aimed at elucidating the mechanisms underlying the important role played by glutaminase in our dual-cell model, especially in the case of the CSC subpopulation. We thus explored the importance of glutaminolysis in anaplerosis and non-anaplerotic activities in our cells (**Chapter II**, 5.2.2.5). Our data showed that the proliferation of PC-3M cells was not significantly rescued when a cell-permeable α-KG analog was introduced to compensate for a reduced glutamine anaplerosis after BPTES treatment. This unexpected result suggests that glutaminolysis contributes to functions other than TCA anaplerosis to maintain an optimal proliferative state, particularly in PC-3M cells.

Non-anaplerotic functions of glutamine metabolism include its participation as a nitrogen donor in the *de novo* synthesis of purines and pyrimidines nucleotides (*325*), its derivation to reductive carboxylation reactions under conditions of dysfunction of mitochondrial respiration (*206, 214*) and its contribution to redox maintenance by synthesis of glutathione and by the aspartate-oxaloacetate-malate pathway which results in the generation of pyruvate and NADPH (*209*). Regarding oxidative stress and glutathione synthesis, inhibition of glutaminase with BPTES caused an increase in the levels of ROS in both cell subpopulations but, intriguingly, it reduced glutathione content only in PC-3S but not PC-3M cells. Thus, these observations rule out the participation of glutamine in glutathione synthesis as a mechanistic explanation for the observed compromise in PC-3M cell proliferation caused by inhibition of glutaminase. Another non-anaplerotic function of glutamine that is also independent of α-KG is the

buffering capacity provided by ammonia moieties that result from the conversion of glutamine to glutamate catalyzed by glutaminase (*206*). This deamidation reaction is predicted to protect cells from acidic conditions. As described in **Chapter I**, PC-3M cells produce high levels of lactic acid as a result of their strong glycolytic activity coupled to a high LDH enzymatic activity. The consequent acidic environment may be highly deleterious to the cells unless a compensatory buffering system is engaged to facilitate cell survival. Indeed, we have found that PC-3M cell proliferation was clearly more affected than PC-3S cells when cultured in lower pH (e.g. 7.0) compared to standard pH (e.g. 7.8). Furthermore, there was a synergistic growth inhibitory effect between inhibition of glutaminase by BPTES and culture of the cells in relatively acid conditions. Based on these observations, we conclude that protection from acid conditions is a critical survival factor for PC-3M cells, whose growth is compromised, in part, by a marked Warburg effect that leads to the production of high levels of lactate. The creation of this acidic environment has been shown to promote local invasion and metastasis (*326*), but as numerous biological reactions are strictly pH dependent, low pH values may be detrimental to cancer cell growth. Thus, cancer cells must be able to counteract the excessive levels of lactic acid to ensure normal cell proliferation.

Relevant to the observed differential role for glutaminase in our dual cell model, our analysis of glutaminase 1 (GLS1) isoforms has unveiled that the glutaminase C (GAC) isoform is expressed at considerably higher levels in PC-3M than PC-3S cells. Some studies have reported that under acidic pH, GAC activity is higher than that of kidney-type glutaminase (KGA) (*218*) and that GAC mRNA, but not KGA mRNA, has pH-response elements in the 3'-untranslated region (3'-UTR) that can stabilize this transcript under acidic conditions (*327*). Interestingly, the EMT factor SNAI1 conferred to PC-3M cells with less sensitivity to low pH (pH 7.0 *vs*. standard pH 7.8) for proliferation and also transcriptionally regulated the relative expression levels of the GAC and KGA isoforms of glutaminase, which was also reflected at the protein level. Knock down of the pluripotency factors SOX2, KLF4 and MYC also diminished the sensitivity of PC-3M cells to low pH. Both observations support the notion that the reduction in glycolysis and thus lactic acid production, either by a gain in the EMT program or partial loss of pluripotency properties, reduces the need for acid buffering

and therefore the dependence on the glutaminase reaction. Overall, our results suggest that, in addition to its role in anaplerosis, anabolic pathways, bioenergetics and maintenance of the oxidative stress, a major role for glutaminase to maintain the survival and proliferation of CSCs in our dual-cell model is closely linked to its contribution to resistance to acidic environments through its active participation in the buffering of the excess of protons present both in the extracellular cell media and the intracellular space, generated by metabolic states employed by these cells to display their "aggressive" features.

Amino acids metabolism provides biosynthetic precursors and protection towards acidity in CSCs

As shown in **Chapter I**, 5.1.2.4, PC-3M and PC-3S cells display a distinct pattern of amino acids consumption and production. We have further characterized the metabolism of several amino acids derived from glucose, in which PC-3M and PC-3S cells showed different metabolic profiles, as in the case of serine and glycine biosynthesis. Highly proliferating cells have a higher demand for both amino acids as they are closely related to the synthesis of metabolic precursors, such as nucleotides, proteins and lipids (*167*). More specifically, differential serine and glycine consumption/production profiles together with a distinct mass isotopomer distribution in serine unveiled that PC-3M cells avidly metabolize serine for biosynthesis or to obtain glycine, which is further used or cleaved by the glycine cleavage system, resulting in a depletion of glycine. In contrast, PC-3S cells show a net excretion of glycine to the extracellular media as well as the presence of the serine mass isotopomers m1 and m2 which likely result from glycine-serine recycling through THF-mediated one-carbon metabolism. Combining these results and the metabolism of other amino acids (described in **Chapter I**, 5.1.2.4) together with the need for CSCs to protect themselves from excessive exposure to acid conditions, we propose a metabolic network in which the participation of amino acids could also contribute to the buffering system for pH regulation, especially in PC-3M cells, as depicted schematically in **Figure 6.1**. On the one hand, serine can be converted to glycine in the cytosol or the mitochondria, yielding cytosolic or mitochondrial NADPH, respectively. Mitochondrial NADPH can contribute to the synthesis of ATP when energy is required.

Interestingly, the mitochondrial glycine cleavage system, which seems to be overexpressed in PC-3M cells, can release an ammonia molecule after cleavage of glycine, thus contributing to the neutralization of protons coming from lactic acid. On the other hand, PC-3M cells do not accumulate glutamate, unlike PC-3S cells that accumulate high amounts of this amino acid (**Chapter I**, 5.1.2.4). Therefore, glutamate in PC-3M cells may be rapidly metabolized to favor the glutaminase reaction and the release of ammonia, as in the case of the phosphoserine aminotransferasa (PSAT) reaction step in the serine biosynthetic pathway or in the alanine production from pyruvate by the action of alanine transaminase (ALT), where glutamate is converted to α-KG. Another important issue is the elimination or recycling of α-KG to avoid its accumulation. This can be achieved by converting α-KG to TCA intermediates (via oxidative or reductive carboxylation reactions) required for energetic or biosynthetic purposes. Considering the amino acid consumption and production profiles shown in **Chapter I**, 5.1.2.4, another possibility would be the contribution of α-KG (as an amino group acceptor) to the uptake of amino acids such as branched-chain amino acids (BCAA) (leucine, isoleucine and valine), aspartate or lysine, whose consumption is enhanced in PC-3M cells, thus yielding glutamate that could participate again in the synthesis of serine or in other metabolic pathways. In addition, the BCAA leucine is able to directly bind and activate glutamate dehydrogenase (GLDH) (*328*) to stimulate the deamidation of glutamate and thereby the release of an ammonia molecule that can further protect cells from acidic conditions. Moreover, glutamate can be a substrate for the synthesis of proline, a metabolic reaction that is favored in PC-3M cells, as evidenced by the net excretion of proline (**Chapter I**, 5.1.2.4) and higher label incorporation from glutamine (**Chapter II**, **5.2.2.3**) in these cells. Similarly to glutamine, proline metabolism has been associated with the oncogene MYC (*307*). The biosynthesis of proline may be preferable to its catabolism in order to avoid the step catalyzed by the tumor suppressor proline oxidase/proline dehydrogenase (POX/PRODH), which results in ROS production and antiproliferative and proapoptotic effects (*306*). However, the role of proline in tumor metabolic reprogramming has not yet been clearly elucidated. The reduced cofactors NADH or NADPH are used for biosynthesis of proline, and although this metabolic process involves the consumption of ATP, it allows the recycling of the reduced cofactors NADH or NADPH to NAD^+ or

$NADP^+$. Thus, indirectly, proline synthesis can favor the redox status for glycolysis to continue and limit the need to produce lactate for NAD^+ recycling. Moreover, by oxidizing NADPH to $NADP^+$, the synthesis of proline may form a metabolic interlock with the oxidative branch of the PPP, thereby linking proline to glucose metabolism.

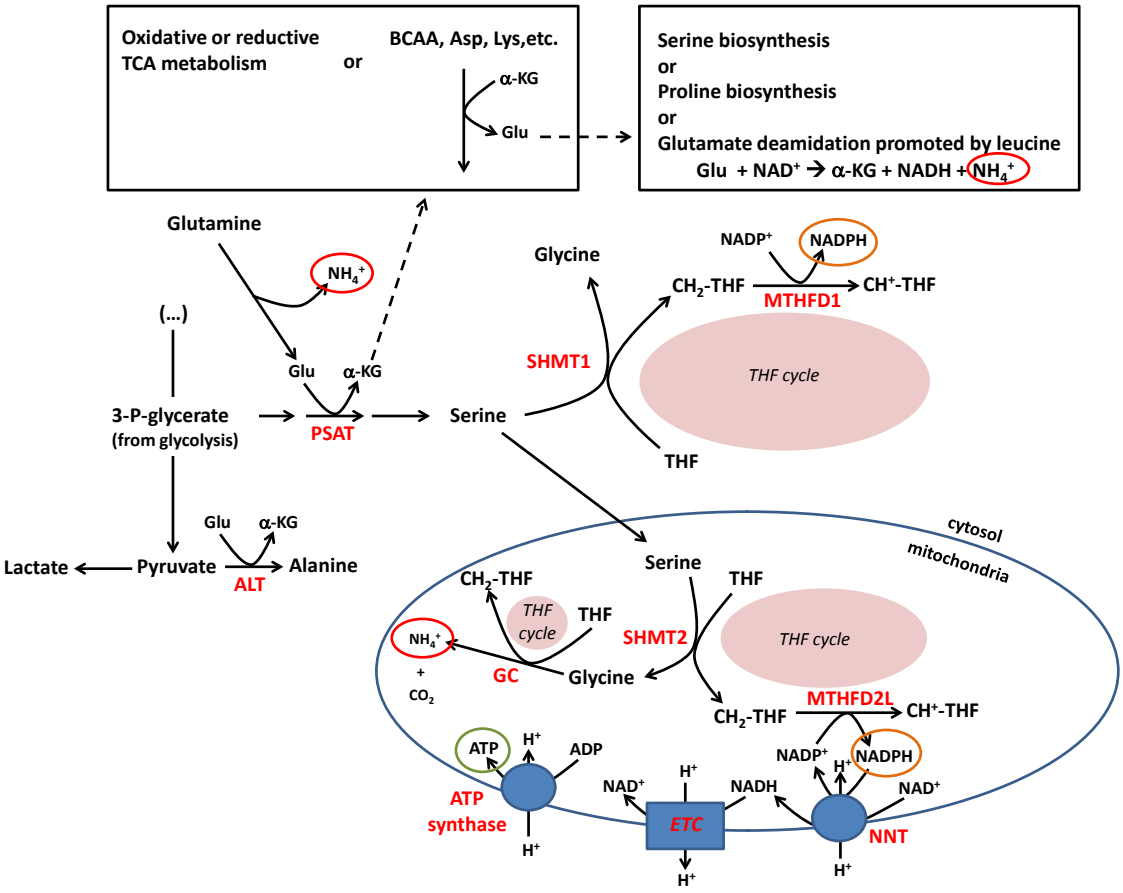

Figure 6.1 Schematic representation of the amino acid metabolism and its link with the production of NADPH, ATP and NH_4^+.

The biosynthesis of serine from 3-P-glycerate and the conversion of pyruvate to alanine can favor glutaminolysis and the release of ammonia. The serine, glycine and one-carbon metabolism contribute to the synthesis of reducing equivalents (NADPH) and energy (ATP) in addition to ammonia moieties resulting from the activity of the GC system. Different amino acids as well as the TCA reactions can participate to the recycling of α-KG to Glu, as indicated. PSAT, phosphoserine aminotransferase; SHMT1, serine hydroxymethyltransferase (cytosol); SHMT2, serine hydroxymethyltransferase (mitochondria); MTHFD1, methylenetetrahydrofolate dehydrogenase (NADP), methenyltetrahydrofolate cyclohydrolase, formyltetrahydrofolate synthetase (cytosol); MTHFD2L, methylenetetrahydrofolate dehydrogenase (NADP, mitochondria); GC, glycine cleavage; NNT, nicotinamide nucleotide transhydrogenase; ETC, electron transport chain; ALT, alanine transaminase; ATP, adenosine triphosphate; Asp, aspartate; Lys, lysine; Glu, glutamate; α-KG, α-ketoglutarate; THF, tetrahidrofolate; BCAA, branched-chain amino acids.

The importance of the regulation of redox balance and regeneration in cancer metabolism has been emphasized previously by several reports (*329-330*). Altogether, we propose that the metabolism of amino acids that have been characterized in these cells confers substantial benefits to sustain cell proliferation by supplying energy and metabolic precursors as well as by protection from acidic environments, especially in the CSC cell subpopulation.

Differential reliance of CSCs and non-CSCs on the oxidative and non-oxidative branches of the PPP

As shown in **Chapter I**, PC-3M and PC-3S cells display a differential profile regarding the use of the oxidative and the non-oxidative branches of the PPP (5.1.2.2). PC-3S cells showed higher levels of glucose-6-phosphate dehydrogenase (G6PDH) expression and less accumulation of ^{13}C labeling from [1,2-$^{13}C_2$]-glucose in ribose than PC-3M cells. The oxidative branch of the PPP, which yields two NADPH molecules, is probably promoted in PC-3S cells to face their increased levels of ROS (5.1.2.4) and to sustain their higher synthesis of fatty acids (5.1.2.3). The key enzyme responsible for the synthesis of fatty acids, fatty acid synthase, has been linked to the EMT program through regulation of VEGF/VEGFR-2 and fatty acid-binding protein 1 (*331*). The lipid composition of the cell membrane is very important for those cells, like PC-3S cells, that display an invasive phenotype, as it determines membrane fluidity, remodeling of the extracellular matrix and the ability to form invasive structures such as invadopodia (*332*). On the other hand, PC-3M cells clearly have a higher demand for nucleotides in order to sustain their higher proliferation rate, and they supply their need using preferentially the non-oxidative branch of the PPP, which is more flexible and directly connected to glycolytic intermediates. Contrary to PC-3S cells, β-oxidation of fatty acids is preferred by PC-3M cells over fatty acid synthesis, which provides them not only with energy but also with mitochondrial acetyl-CoA moieties that can feed the mitochondrial metabolism or allow the synthesis of TCA intermediates

Additionally, through the characterization of the PPP in our dual-cell model, we have found a differential expression of transketolase-like 1 (TKTL1) and we have shown that TKTL1 knock down affects PC-3M cell proliferation and compromises PC-3S viability.

Our analysis indicates that TKTL1 plays an essential role in PC-3S cells beyond its mere transketolase activity in the PPP. Some studies have observed a strong TKTL1 activity in invasive tumors, whereas weak or no TKTL1 activity was detected in non-invasive colon carcinomas (*129, 288*), which is in accordance with our cell model which comprises a cell subpopulation endowed with high invasive/low metastatic capacity (PC-3S cells) and another with high metastatic/low invasive potential (PC-3M cells). TKTL1 has been proposed by Coy and coworkers as a possible link between the PPP and fatty acid synthesis by means of a monosubstrate reaction that yields cytosolic acetyl-CoA (*128*). In order to unveil the relevance of TKTL1, especially in the invasive PC-3S cells, a more thorough metabolic characterization would be required to elucidate whether fatty acid synthesis or other metabolic pathways are impaired after inhibition of the TKTL1 isoenzyme.

<u>General lessons regarding the metabolic rewiring and vulnerabilities of CSC vs. non-CSC tumor cell subpopulations that can be drawn from our dual-cell prostate cancer model</u>

In this thesis we have provided a comprehensive body of evidence of the metabolic reprogramming and vulnerabilities associated with non-overlapping CSC and EMT phenotypes expressed in a dual-cell model of prostate cancer, consisting of epithelial PC-3M and mesenchymal PC-3S subpopulations. A schematic metabolic map of the most relevant pathways and vulnerabilities in PC-3M or PC-3S cells that have been revealed in this thesis is illustrated in **Figures 6.2** and **6.3**, respectively, and considering full media conditions.

The following description briefly summarizes our main observation regarding the metabolic rewiring and vulnerabilities displayed by our CSC *vs*. non-CSC model, based on which we suggest some additional treatments that could be tested to differentially target heterogeneous tumor cell subpopulations. In PC-3M cells, glycolysis appears to be largely uncoupled from TCA cycle and OXPHOS, deriving most of the pyruvate to lactate production or, alternatively, to alanine, indicative of a marked Warburg effect. Therefore, a good strategy to target the CSC subpopulation would be either to block glycolysis (e.g. 2-DG) or promote OXPHOS, via PDH activation using DCA or a combination of DCA + oxamate (LDH inhibitor) to further force the entry of pyruvate

into the mitochondrial metabolism. Forcing PC-3M cells to switch from glycolysis to OXPHOS dramatically affects not only their bioenergetic and biosynthetic resources

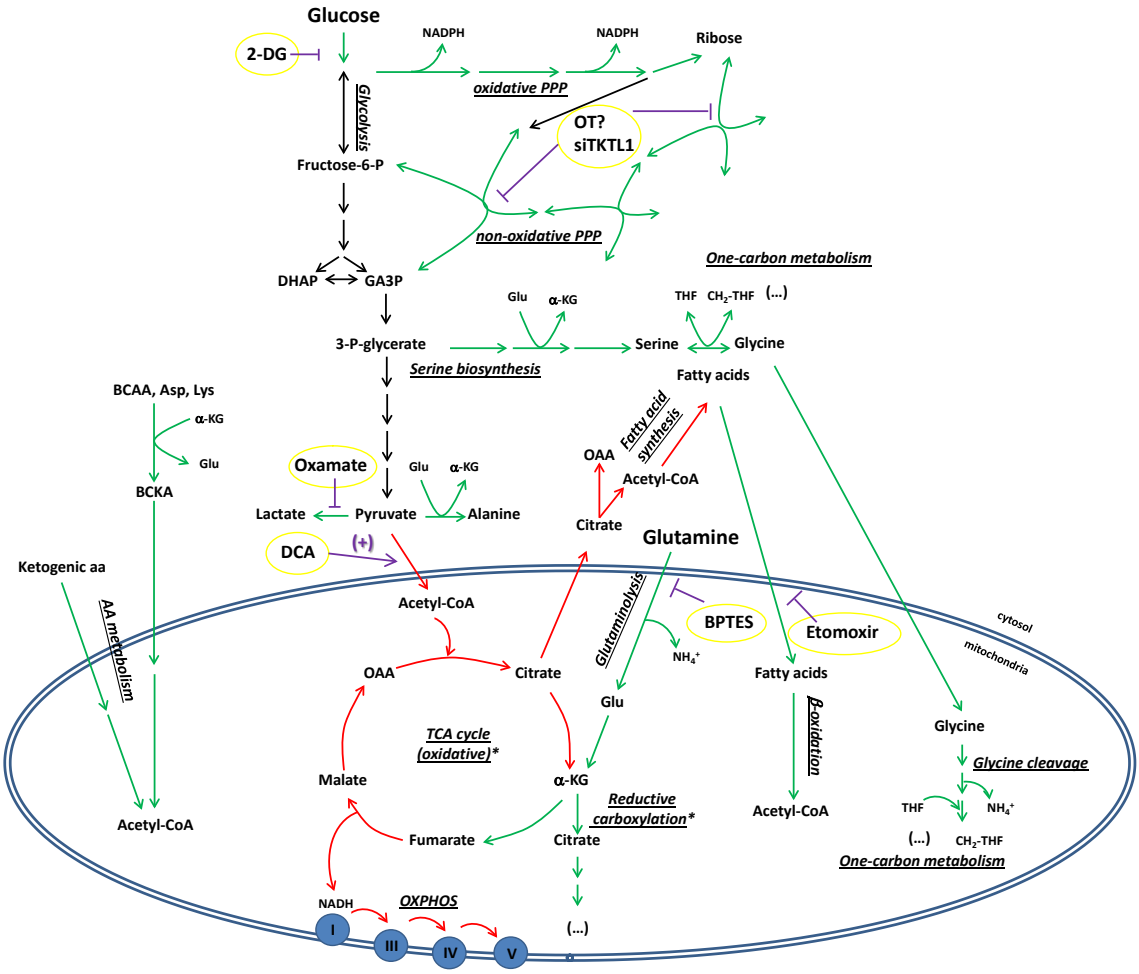

Figure 6.2 Metabolic reprogramming and vulnerabilities in PC-3M (CSC phenotype)

PC-3M cells display a high metabolic flexibility and capacity of using different metabolic pathways. This illustration depicts the most relevant metabolic pathways for PC-3M cells (as compared with PC-3S cells) in **green**, and the less relevant in **red**. Drugs are highlighted in yellow and purple indicates the reactions that are affected by the drugs. PPP, pentose phosphate pathway; OXPHOS, oxidative phosphorylation; DHAP, dihydroxyacetone-P; GA3P, glyceraldehyde-3-P; Glu, glutamate; α-KG, α-ketoglutarate; THF, tetrahidrofolate; OAA, oxalacetate; BCAA, branched-chain amino acids; BCKA, branched-chain keto acids; 2-DG, 2-deoxyglucose; OT, oxythiamine; siTKTL1, siRNA targeting transketolase-like 1; DCA, dichloroacetate; BPTES**,** Bis-2-(5-phenylacetamido-1,3,4-thiadiazol-2-yl)ethyl sulfide. *These reactions can take place either in the cytosol or the mitochondria.

but also the redox balance (ROS) and subsequently their self-renewal and pluripotency traits (*291*). Due to the metabolic flexibility displayed by PC-3M cells, blocking glycolysis enhances compensatory mechanisms, such as glutaminolysis, that could be considered as potential targets for combination therapies (*333*). We propose that the simultaneous inhibition of glycolysis and those alternative carbon sources that feed

the metabolism of PC-3M cells (e.g. glutamine, fatty acids and amino acids) may be deleterious for CSCs and thus substantially reduce their potential to proliferate and survive *in vitro* and limit their metastatic potential *in vivo (322)*. Moreover, PC-3M cells show an efficient

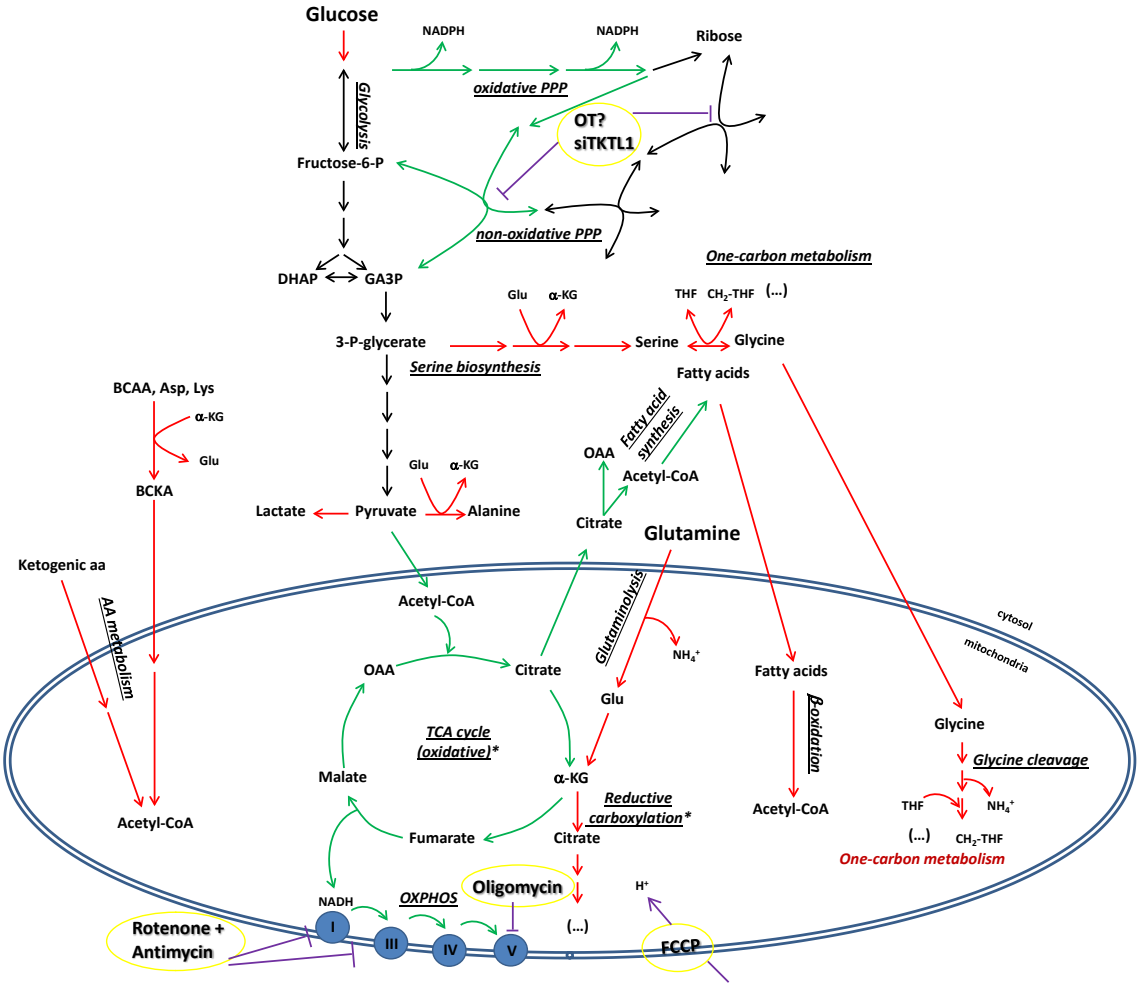

Figure 6.3 Metabolic reprogramming and vulnerabilities in PC-3S (EMT phenotype)

PC-3S cells display a significant coupling between glycolysis and OXPHOS and a limited metabolic flexibility. This illustration depicts the most relevant metabolic pathways for PC-3S cells (as compared with PC-3M cells) in green, and the less relevant in **red**. Drugs are highlighted in yellow and purple indicates the reactions that are affected by the drugs. PPP, pentose phosphate pathway; OXPHOS, oxidative phosphorylation; DHAP, dihydroxyacetone-P; GA3P, glyceraldehyde-3-P; Glu, glutamate; α-KG, α-ketoglutarate; THF, tetrahidrofolate; OAA, oxalacetate; BCAA, branched-chain amino acids; BCKA, branched-chain keto acids; OT, oxythiamine; siTKTL1, siRNA targeting transketolase-like 1; FCCP, carbonilcyanide p-trifluoromethoxyphenylhydrazone. *These reactions can take place either in the cytosol or the mitochondria.

channeling of the glycolytic intermediate 3-phosphoglycerate into the synthesis of serine, and subsequently to glycine. The failure of PC-3M cells to accumulate serine and glycine is suggestive of a high demand for these amino acids for biosynthesis (nucleotides and proteins) and one-carbon metabolism (which yields NADPH and ATP).

Disruption of one-carbon metabolism by using folate antagonists such as methotrexate could be a logical strategy to target this subpopulation. However, although PC-3S cells do not use serine and glycine as extensively as PC-3M cells, they also rely on reversible reactions involving one-carbon metabolism in order to, hypothetically, avoid an excessive accumulation of glycine which could lead to inhibition of cell proliferation (*297*). As a consequence, methotrexate treatment would probably affect the proliferation of PC-3S cells as well.

A very novel proposal which has emerged from the metabolic analysis performed in this thesis is the targeting of the cell pH buffering system as a potential therapeutic strategy for those cells which display a marked Warburg effect with a concomitant lactate production. Recently, numerous studies have linked the alteration of pH homeostasis with tumor progression but mostly focused on proteins that exchange or pump protons to reduce intracellular acidity (*219, 334*). On the basis of recent findings (*218*) together with our own observations, we propose that, in our dual-cell model, especially in the CSC subpopulation, ammonia produced from enzymatic reactions, such as the glutaminase reaction, contribute to the neutralization of acid buildup. We have demonstrated that PC-3M cells are more vulnerable than PC-3S cells to 1) low pH conditions (compared to standard pH) and 2) glutaminase inhibition by BPTES. Among the different functions investigated for glutamine metabolism in the experiments described in **Chapter II**, its protective role from acidity was the most remarkable in PC-3M cells. In **Figure 6.1**, we show other reactions that also release ammonia, such as those driven by GLDH and the glycine cleavage system. Targeting these enzymes or multienzyme complexes could compromise even more the proliferation and viability of PC-3M cells, not only because of their particular role in the metabolic network but also because the subsequent reduction of the intrinsic pH buffering power.

PC-3S cells also rely on glycolysis but, unlike PC-3M cells, a higher proportion of pyruvate derived from glucose is directed to the TCA cycle and OXPHOS, which makes these cells more vulnerable to the inhibition of mitochondrial respiration by several mitochondrial drugs (e.g. oligomycin, FCCP, rotenone and antimycin). Another potential compound that could be considered for targeting this subpopulation is the antidiabetic drug metformin. The mechanism of action of metformin is believed to be

the inhibition of OXPHOS through inhibition of mitochondrial complex I, leading to an ATP/AMP imbalance, which results in activation of the LKB1-AMPK pathway (*335*). What makes this drug especially interesting to target PC-3S cells is that, as a consequence of activation of the AMPK signaling pathway, metformin also causes a downregulation of acetyl-CoA carboxylase, fatty acid synthase, citrate lyase and HMG-CoA reductase, which are involved in fatty acid and cholesterol synthesis (*336*). As fatty acid synthesis is favored in PC-3S cells, metformin treatment could reduce lipogenesis and compromise not only cell growth but also membrane synthesis and composition, subsequently affecting the formation of membrane protrusions important for invasion. Indeed, several studies have reported a potential role for metformin in metastasis by targeting the EMT process (*337-338*). At the same time, metformin has been widely described as a specific drug that targets CSC subpopulations (*338-340*). Based on the experiment described in **Chapter II**, in which the effect of oligomycin on ATP content was evaluated, we would expect metformin to alter ATP levels to a greater extent in PC-3S cells than in PC-3M cells, and therefore metformin would differentially target the non-CSC subpopulation. Additionally, a combinatorial therapeutic strategy can be envisioned to target PC-3S cells, based on the inhibition of OXPHOS with metformin and the subsequent compensatory glycolysis with 2-DG (*341*).

Regarding the PPP, the converse TKT and G6PDH expression and activity profiles observed in our dual-cell model revealed differential preferences in the use of the oxidative and non-oxidative branches to sustain the main metabolic needs of these cells. We have found that synthesis of ribose to build up nucleotides is the main priority for the highly proliferative PC-3M cells, whereas the production of reducing equivalents for fatty acid synthesis and protection from oxidative stress is favored in PC-3S cells. These different requirements result in a different use of both branches of the PPP, as depicted in **Figures 6.2** and **6.3**. Inhibition of total transketolase activity by oxythiamine, and thus disruption of the non-oxidative branch, did not substantially affect the proliferation of these cells, suggesting that the oxidative branch can efficiently provide the precursors required by PC-3M and PC-3S cells. The specific inhibition of G6PDH or, better yet, the combined inhibition of G6PDH and TKT would probably be more deleterious to these cell subpopulations, as targeting parallel

pathways that drive nucleic acid synthesis is a more efficient strategy to inhibit tumor cell growth (*146*). On the other hand, specific inhibition of TKTL1 by siRNA is a promising strategy, especially to target the non-CSC subpopulation, but the precise transketolase-independent mechanisms underlying this vulnerability remain to be elucidated.

Collectively, the characterization of the different cell metabolic pathways described herein support the conclusion that CSC and EMT phenotypes can be mutually uncoupled and associated with specific metabolic reprogramming in order to sustain cell proliferation, survival and maintenance, and that distinct CSC and non-CSC metabolic programs can be targeted with specific interventions. Our observations establish new grounds for tumor subpopulation-specific and combined therapeutic strategies with potential impacts on the management of metastatic disease.

7. CONCLUSIONS

7. CONCLUSIONS

1. Prostate epithelial cells displaying a CSC phenotype (PC-3M) and a high metastatic potential preferentially rely on aerobic glycolysis (Warburg effect) for bioenergetics. This trait confers them not only with metabolic precursors to sustain their high potential for replication but also contributes to the maintenance of stemness and pluripotency. The prostate CSC subpopulation shows low coupling between glycolysis and OXPHOS through pyruvate derived from glucose because of low PDH activity.

   PC-3M cells display an increased metabolic flexibility to utilize different carbon sources, such as fatty acids, glutamine and other amino acids, that offset the decreased diversion of glucose-derived carbons into the TCA cycle and OXPHOS. This characteristic also enables PC-3M cells to better adapt to nutrient-poor environments as they rapidly switch their metabolic pathways depending on the available resources. Considering their biological role, metabolic flexibility may support the survival of PC-3M cells when they initiate the metastatic route and also contribute to the adaptation to the foreign soil for formation of a new tumor bulk in the metastatic site.

2. Prostate mesenchymal cells expressing the EMT program (PC-3S) and endowed with a high invasive capacity display a strong coupling between aerobic glycolysis and OXPHOS and a strong dependence on the mitochondrial metabolism for bioenergetics. Their low proliferation rate can be efficiently sustained by this preferred metabolic route and a more active mitochondrial metabolism results in ROS production that may contribute to the redox signaling involved in the promotion of the EMT program. Consequently, these cells express increased levels of glutathione that may provide an adequate antioxidant defense system to prevent the harmful effects of excessive ROS accumulation.

3. PC-3M and PC-3S cells differentially reprogram the use of the oxidative and non-oxidative branches of the Pentose Phosphate Pathway to sustain their distinct

metabolic needs. Glycolytic intermediates are preferentially funneled to ribose synthesis in the CSC subpopulation to build up nucleotides whereas the generation of NADPH is more crucial for the non-CSC subpopulations to counteract their higher oxidative stress and sustain fatty acid synthesis.

4. Glutamine metabolism substantially contributes to TCA reactions in PC-3M as less glucose-derived pyruvate is internalized into the mitochondria. For PC-3S cells, glutamine is required for biosynthesis of glutathione and both glucose and glutamine are necessary for these cells to display a proper mitochondrial function. PC-3M cells are more dependent than PC-3S cells on the glutaminase reaction for proliferation and survival and this reliance lies mainly on the increased need for PC-3M cells to neutralize the excessive levels of protons (lactic acid) that result from their marked Warburg effect, which is achieved by the ammonia molecules released from glutamine metabolism.

5. The high metabolic flexibility displayed by prostate CSC subpopulation also includes the participation of many metabolic routes involving the metabolism of amino acids. The enhancement of serine, glycine and one-carbon metabolism, the uptake of ketogenic amino acids, proline metabolism, among others, provide PC-3M cells with an extensive metabolic dynamics and expand the range of resources that they can use not only to obtain metabolic precursors but also to balance their redox status (NAD^+/NADH and $NADP^+$/NADPH) for metabolic processes to continue (e.g. glycolysis) and protect them from excessive acidity derived from a high glycolytic rate.

8. REFERENCES

8. REFERENCES

1. Ferlay, J., Soerjomataram, I. I., Dikshit, R., Eser, S., Mathers, C., Rebelo, M., Parkin, D. M., Forman, D. D., and Bray, F. (2014) Cancer incidence and mortality worldwide: sources, methods and major patterns in GLOBOCAN 2012, *Int J Cancer*.
2. Hanahan, D., and Weinberg, R. A. (2011) Hallmarks of cancer: the next generation, *Cell 144*, 646-674.
3. Vogelstein, B., and Kinzler, K. W. (2004) Cancer genes and the pathways they control, *Nat Med 10*, 789-799.
4. Kareva, I., and Hahnfeldt, P. (2013) The emerging "hallmarks" of metabolic reprogramming and immune evasion: distinct or linked?, *Cancer Res 73*, 2737-2742.
5. Pietras, K., and Ostman, A. (2010) Hallmarks of cancer: interactions with the tumor stroma, *Exp Cell Res 316*, 1324-1331.
6. Baeriswyl, V., and Christofori, G. (2009) The angiogenic switch in carcinogenesis, *Semin Cancer Biol 19*, 329-337.
7. Alitalo, K., Tammela, T., and Petrova, T. V. (2005) Lymphangiogenesis in development and human disease, *Nature 438*, 946-953.
8. Hiratsuka, S., Watanabe, A., Aburatani, H., and Maru, Y. (2006) Tumour-mediated upregulation of chemoattractants and recruitment of myeloid cells predetermines lung metastasis, *Nat Cell Biol 8*, 1369-1375.
9. Kaplan, R. N., Riba, R. D., Zacharoulis, S., Bramley, A. H., Vincent, L., Costa, C., MacDonald, D. D., Jin, D. K., Shido, K., Kerns, S. A., Zhu, Z., Hicklin, D., Wu, Y., Port, J. L., Altorki, N., Port, E. R., Ruggero, D., Shmelkov, S. V., Jensen, K. K., Rafii, S., and Lyden, D. (2005) VEGFR1-positive haematopoietic bone marrow progenitors initiate the pre-metastatic niche, *Nature 438*, 820-827.
10. Wels, J., Kaplan, R. N., Rafii, S., and Lyden, D. (2008) Migratory neighbors and distant invaders: tumor-associated niche cells, *Genes Dev 22*, 559-574.
11. Cardenas-Navia, L. I., Mace, D., Richardson, R. A., Wilson, D. F., Shan, S., and Dewhirst, M. W. (2008) The pervasive presence of fluctuating oxygenation in tumors, *Cancer Res 68*, 5812-5819.
12. Sharma, M. K., Seidlitz, E. P., and Singh, G. (2010) Cancer cells release glutamate via the cystine/glutamate antiporter, *Biochem Biophys Res Commun 391*, 91-95.
13. Bogenrieder, T., and Herlyn, M. (2003) Axis of evil: molecular mechanisms of cancer metastasis, *Oncogene 22*, 6524-6536.
14. Rak, J. W., St Croix, B. D., and Kerbel, R. S. (1995) Consequences of angiogenesis for tumor progression, metastasis and cancer therapy, *Anticancer Drugs 6*, 3-18.
15. Folkman, J. (1996) Fighting cancer by attacking its blood supply, *Sci Am 275*, 150-154.
16. Bissell, M. J., and Hines, W. C. (2011) Why don't we get more cancer? A proposed role of the microenvironment in restraining cancer progression, *Nat Med 17*, 320-329.
17. Bendas, G., and Borsig, L. (2012) Cancer cell adhesion and metastasis: selectins, integrins, and the inhibitory potential of heparins, *Int J Cell Biol 2012*, 676731.
18. Cavallaro, U., and Christofori, G. (2004) Cell adhesion and signalling by cadherins and Ig-CAMs in cancer, *Nat Rev Cancer 4*, 118-132.
19. Egeblad, M., and Werb, Z. (2002) New functions for the matrix metalloproteinases in cancer progression, *Nat Rev Cancer 2*, 161-174.
20. Yang, J., and Weinberg, R. A. (2008) Epithelial-mesenchymal transition: at the crossroads of development and tumor metastasis, *Dev Cell 14*, 818-829.
21. Thiery, J. P. (2003) Epithelial-mesenchymal transitions in development and pathologies, *Curr Opin Cell Biol 15*, 740-746.

22. Trimboli, A. J., Fukino, K., de Bruin, A., Wei, G., Shen, L., Tanner, S. M., Creasap, N., Rosol, T. J., Robinson, M. L., Eng, C., Ostrowski, M. C., and Leone, G. (2008) Direct evidence for epithelial-mesenchymal transitions in breast cancer, *Cancer Res 68*, 937-945.
23. Huber, M. A., Kraut, N., and Beug, H. (2005) Molecular requirements for epithelial-mesenchymal transition during tumor progression, *Curr Opin Cell Biol 17*, 548-558.
24. Yoshiura, K., Kanai, Y., Ochiai, A., Shimoyama, Y., Sugimura, T., and Hirohashi, S. (1995) Silencing of the E-cadherin invasion-suppressor gene by CpG methylation in human carcinomas, *Proc Natl Acad Sci U S A 92*, 7416-7419.
25. Gravdal, K., Halvorsen, O. J., Haukaas, S. A., and Akslen, L. A. (2007) A switch from E-cadherin to N-cadherin expression indicates epithelial to mesenchymal transition and is of strong and independent importance for the progress of prostate cancer, *Clin Cancer Res 13*, 7003-7011.
26. Cano, A., Perez-Moreno, M. A., Rodrigo, I., Locascio, A., Blanco, M. J., del Barrio, M. G., Portillo, F., and Nieto, M. A. (2000) The transcription factor snail controls epithelial-mesenchymal transitions by repressing E-cadherin expression, *Nat Cell Biol 2*, 76-83.
27. Peinado, H., Olmeda, D., and Cano, A. (2007) Snail, Zeb and bHLH factors in tumour progression: an alliance against the epithelial phenotype?, *Nat Rev Cancer 7*, 415-428.
28. Medici, D., Hay, E. D., and Olsen, B. R. (2008) Snail and Slug promote epithelial-mesenchymal transition through beta-catenin-T-cell factor-4-dependent expression of transforming growth factor-beta3, *Mol Biol Cell 19*, 4875-4887.
29. Lamouille, S., Subramanyam, D., Blelloch, R., and Derynck, R. (2013) Regulation of epithelial-mesenchymal and mesenchymal-epithelial transitions by microRNAs, *Curr Opin Cell Biol 25*, 200-207.
30. Thiery, J. P., Acloque, H., Huang, R. Y., and Nieto, M. A. (2009) Epithelial-mesenchymal transitions in development and disease, *Cell 139*, 871-890.
31. Gregory, P. A., Bert, A. G., Paterson, E. L., Barry, S. C., Tsykin, A., Farshid, G., Vadas, M. A., Khew-Goodall, Y., and Goodall, G. J. (2008) The miR-200 family and miR-205 regulate epithelial to mesenchymal transition by targeting ZEB1 and SIP1, *Nat Cell Biol 10*, 593-601.
32. Ru, P., Steele, R., Newhall, P., Phillips, N. J., Toth, K., and Ray, R. B. (2012) miRNA-29b suppresses prostate cancer metastasis by regulating epithelial-mesenchymal transition signaling, *Mol Cancer Ther 11*, 1166-1173.
33. Zhang, J., Zhang, H., Liu, J., Tu, X., Zang, Y., Zhu, J., Chen, J., and Dong, L. (2012) miR-30 inhibits TGF-beta1-induced epithelial-to-mesenchymal transition in hepatocyte by targeting Snail1, *Biochem Biophys Res Commun 417*, 1100-1105.
34. Warzecha, C. C., Jiang, P., Amirikian, K., Dittmar, K. A., Lu, H., Shen, S., Guo, W., Xing, Y., and Carstens, R. P. (2010) An ESRP-regulated splicing programme is abrogated during the epithelial-mesenchymal transition, *EMBO J 29*, 3286-3300.
35. Lester, R. D., Jo, M., Montel, V., Takimoto, S., and Gonias, S. L. (2007) uPAR induces epithelial-mesenchymal transition in hypoxic breast cancer cells, *J Cell Biol 178*, 425-436.
36. Yang, M. H., Wu, M. Z., Chiou, S. H., Chen, P. M., Chang, S. Y., Liu, C. J., Teng, S. C., and Wu, K. J. (2008) Direct regulation of TWIST by HIF-1alpha promotes metastasis, *Nat Cell Biol 10*, 295-305.
37. Ng, W. K. (2002) Fine-needle aspiration cytology findings of an uncommon micropapillary variant of pure mucinous carcinoma of the breast: review of patients over an 8-year period, *Cancer 96*, 280-288.
38. Christiansen, J. J., Rajasekaran, S. A., Inge, L., Cheng, L., Anilkumar, G., Bander, N. H., and Rajasekaran, A. K. (2005) N-glycosylation and microtubule integrity are involved in apical targeting of prostate-specific membrane antigen: implications for immunotherapy, *Mol Cancer Ther 4*, 704-714.

39. Thiery, J. P. (2002) Epithelial-mesenchymal transitions in tumour progression, *Nat Rev Cancer 2*, 442-454.
40. Bukholm, I. K., Nesland, J. M., and Borresen-Dale, A. L. (2000) Re-expression of E-cadherin, alpha-catenin and beta-catenin, but not of gamma-catenin, in metastatic tissue from breast cancer patients [seecomments], *J Pathol 190*, 15-19.
41. Wong, I. Y., Javaid, S., Wong, E. A., Perk, S., Haber, D. A., Toner, M., and Irimia, D. (2014) Collective and individual migration following the epithelial-mesenchymal transition, *Nat Mater*.
42. Schwitalla, S. (2014) Tumor cell plasticity: the challenge to catch a moving target, *J Gastroenterol 49*, 618-627.
43. Wang, W., Quan, Y., Fu, Q., Liu, Y., Liang, Y., Wu, J., Yang, G., Luo, C., Ouyang, Q., and Wang, Y. (2014) Dynamics between cancer cell subpopulations reveals a model coordinating with both hierarchical and stochastic concepts, *PLoS One 9*, e84654.
44. Yu, Z., Pestell, T. G., Lisanti, M. P., and Pestell, R. G. (2012) Cancer stem cells, *Int J Biochem Cell Biol 44*, 2144-2151.
45. Mani, S. A., Guo, W., Liao, M. J., Eaton, E. N., Ayyanan, A., Zhou, A. Y., Brooks, M., Reinhard, F., Zhang, C. C., Shipitsin, M., Campbell, L. L., Polyak, K., Brisken, C., Yang, J., and Weinberg, R. A. (2008) The epithelial-mesenchymal transition generates cells with properties of stem cells, *Cell 133*, 704-715.
46. Morel, A. P., Lievre, M., Thomas, C., Hinkal, G., Ansieau, S., and Puisieux, A. (2008) Generation of breast cancer stem cells through epithelial-mesenchymal transition, *PLoS One 3*, e2888.
47. Sethi, S., Macoska, J., Chen, W., and Sarkar, F. H. (2010) Molecular signature of epithelial-mesenchymal transition (EMT) in human prostate cancer bone metastasis, *Am J Transl Res 3*, 90-99.
48. Floor, S., van Staveren, W. C., Larsimont, D., Dumont, J. E., and Maenhaut, C. (2011) Cancer cells in epithelial-to-mesenchymal transition and tumor-propagating-cancer stem cells: distinct, overlapping or same populations, *Oncogene 30*, 4609-4621.
49. Celia-Terrassa, T., Meca-Cortes, O., Mateo, F., de Paz, A. M., Rubio, N., Arnal-Estape, A., Ell, B. J., Bermudo, R., Diaz, A., Guerra-Rebollo, M., Lozano, J. J., Estaras, C., Ulloa, C., Alvarez-Simon, D., Mila, J., Vilella, R., Paciucci, R., Martinez-Balbas, M., de Herreros, A. G., Gomis, R. R., Kang, Y., Blanco, J., Fernandez, P. L., and Thomson, T. M. (2012) Epithelial-mesenchymal transition can suppress major attributes of human epithelial tumor-initiating cells, *J Clin Invest 122*, 1849-1868.
50. Tsuji, T., Ibaragi, S., and Hu, G. F. (2009) Epithelial-mesenchymal transition and cell cooperativity in metastasis, *Cancer Res 69*, 7135-7139.
51. Medema, J. P. (2013) Cancer stem cells: the challenges ahead, *Nat Cell Biol 15*, 338-344.
52. Iliopoulos, D., Hirsch, H. A., Wang, G., and Struhl, K. (2011) Inducible formation of breast cancer stem cells and their dynamic equilibrium with non-stem cancer cells via IL6 secretion, *Proc Natl Acad Sci U S A 108*, 1397-1402.
53. Biddle, A., Liang, X., Gammon, L., Fazil, B., Harper, L. J., Emich, H., Costea, D. E., and Mackenzie, I. C. (2011) Cancer stem cells in squamous cell carcinoma switch between two distinct phenotypes that are preferentially migratory or proliferative, *Cancer Res 71*, 5317-5326.
54. Tibbe, A. G., Miller, M. C., and Terstappen, L. W. (2007) Statistical considerations for enumeration of circulating tumor cells, *Cytometry A 71*, 154-162.
55. Hayes, D. F., and Smerage, J. (2008) Is there a role for circulating tumor cells in the management of breast cancer?, *Clin Cancer Res 14*, 3646-3650.
56. Muller, V., Stahmann, N., Riethdorf, S., Rau, T., Zabel, T., Goetz, A., Janicke, F., and Pantel, K. (2005) Circulating tumor cells in breast cancer: correlation to bone marrow

micrometastases, heterogeneous response to systemic therapy and low proliferative activity, *Clin Cancer Res 11*, 3678-3685.
57. Holohan, C., Van Schaeybroeck, S., Longley, D. B., and Johnston, P. G. (2013) Cancer drug resistance: an evolving paradigm, *Nat Rev Cancer 13*, 714-726.
58. Oskarsson, T., Batlle, E., and Massague, J. (2014) Metastatic stem cells: sources, niches, and vital pathways, *Cell Stem Cell 14*, 306-321.
59. Zhang, X. H., Wang, Q., Gerald, W., Hudis, C. A., Norton, L., Smid, M., Foekens, J. A., and Massague, J. (2009) Latent bone metastasis in breast cancer tied to Src-dependent survival signals, *Cancer Cell 16*, 67-78.
60. Chang, L., Graham, P. H., Hao, J., Ni, J., Bucci, J., Cozzi, P. J., Kearsley, J. H., and Li, Y. (2013) Acquisition of epithelial-mesenchymal transition and cancer stem cell phenotypes is associated with activation of the PI3K/Akt/mTOR pathway in prostate cancer radioresistance, *Cell Death Dis 4*, e875.
61. Oskarsson, T., Acharyya, S., Zhang, X. H., Vanharanta, S., Tavazoie, S. F., Morris, P. G., Downey, R. J., Manova-Todorova, K., Brogi, E., and Massague, J. (2011) Breast cancer cells produce tenascin C as a metastatic niche component to colonize the lungs, *Nat Med 17*, 867-874.
62. Paget, S. (1989) The distribution of secondary growths in cancer of the breast. 1889, *Cancer Metastasis Rev 8*, 98-101.
63. Chu, J. E., Xia, Y., Chin-Yee, B., Goodale, D., Croker, A. K., and Allan, A. L. (2014) Lung-derived factors mediate breast cancer cell migration through CD44 receptor-ligand interactions in a novel ex vivo system for analysis of organ-specific soluble proteins, *Neoplasia 16*, 180-191.
64. Bubendorf, L., Schopfer, A., Wagner, U., Sauter, G., Moch, H., Willi, N., Gasser, T. C., and Mihatsch, M. J. (2000) Metastatic patterns of prostate cancer: an autopsy study of 1,589 patients, *Hum Pathol 31*, 578-583.
65. Brabletz, T. (2012) To differentiate or not--routes towards metastasis, *Nat Rev Cancer 12*, 425-436.
66. Vega, S., Morales, A. V., Ocana, O. H., Valdes, F., Fabregat, I., and Nieto, M. A. (2004) Snail blocks the cell cycle and confers resistance to cell death, *Genes Dev 18*, 1131-1143.
67. Mejlvang, J., Kriajevska, M., Vandewalle, C., Chernova, T., Sayan, A. E., Berx, G., Mellon, J. K., and Tulchinsky, E. (2007) Direct repression of cyclin D1 by SIP1 attenuates cell cycle progression in cells undergoing an epithelial mesenchymal transition, *Mol Biol Cell 18*, 4615-4624.
68. Tsai, J. H., Donaher, J. L., Murphy, D. A., Chau, S., and Yang, J. (2012) Spatiotemporal regulation of epithelial-mesenchymal transition is essential for squamous cell carcinoma metastasis, *Cancer Cell 22*, 725-736.
69. Shimono, Y., Zabala, M., Cho, R. W., Lobo, N., Dalerba, P., Qian, D., Diehn, M., Liu, H., Panula, S. P., Chiao, E., Dirbas, F. M., Somlo, G., Pera, R. A., Lao, K., and Clarke, M. F. (2009) Downregulation of miRNA-200c links breast cancer stem cells with normal stem cells, *Cell 138*, 592-603.
70. Gao, D., Joshi, N., Choi, H., Ryu, S., Hahn, M., Catena, R., Sadik, H., Argani, P., Wagner, P., Vahdat, L. T., Port, J. L., Stiles, B., Sukumar, S., Altorki, N. K., Rafii, S., and Mittal, V. (2012) Myeloid progenitor cells in the premetastatic lung promote metastases by inducing mesenchymal to epithelial transition, *Cancer Res 72*, 1384-1394.
71. Liu, S., Cong, Y., Wang, D., Sun, Y., Deng, L., Liu, Y., Martin-Trevino, R., Shang, L., McDermott, S. P., Landis, M. D., Hong, S., Adams, A., D'Angelo, R., Ginestier, C., Charafe-Jauffret, E., Clouthier, S. G., Birnbaum, D., Wong, S. T., Zhan, M., Chang, J. C., and Wicha, M. S. (2014) Breast Cancer Stem Cells Transition between Epithelial and Mesenchymal States Reflective of their Normal Counterparts, *Stem Cell Reports 2*, 78-91.

72. Hennessy, B. T., Gonzalez-Angulo, A. M., Stemke-Hale, K., Gilcrease, M. Z., Krishnamurthy, S., Lee, J. S., Fridlyand, J., Sahin, A., Agarwal, R., Joy, C., Liu, W., Stivers, D., Baggerly, K., Carey, M., Lluch, A., Monteagudo, C., He, X., Weigman, V., Fan, C., Palazzo, J., Hortobagyi, G. N., Nolden, L. K., Wang, N. J., Valero, V., Gray, J. W., Perou, C. M., and Mills, G. B. (2009) Characterization of a naturally occurring breast cancer subset enriched in epithelial-to-mesenchymal transition and stem cell characteristics, *Cancer Res 69*, 4116-4124.
73. Lim, E., Vaillant, F., Wu, D., Forrest, N. C., Pal, B., Hart, A. H., Asselin-Labat, M. L., Gyorki, D. E., Ward, T., Partanen, A., Feleppa, F., Huschtscha, L. I., Thorne, H. J., Fox, S. B., Yan, M., French, J. D., Brown, M. A., Smyth, G. K., Visvader, J. E., and Lindeman, G. J. (2009) Aberrant luminal progenitors as the candidate target population for basal tumor development in BRCA1 mutation carriers, *Nat Med 15*, 907-913.
74. Prat, A., Parker, J. S., Karginova, O., Fan, C., Livasy, C., Herschkowitz, J. I., He, X., and Perou, C. M. (2010) Phenotypic and molecular characterization of the claudin-low intrinsic subtype of breast cancer, *Breast Cancer Res 12*, R68.
75. Creighton, C. J., Li, X., Landis, M., Dixon, J. M., Neumeister, V. M., Sjolund, A., Rimm, D. L., Wong, H., Rodriguez, A., Herschkowitz, J. I., Fan, C., Zhang, X., He, X., Pavlick, A., Gutierrez, M. C., Renshaw, L., Larionov, A. A., Faratian, D., Hilsenbeck, S. G., Perou, C. M., Lewis, M. T., Rosen, J. M., and Chang, J. C. (2009) Residual breast cancers after conventional therapy display mesenchymal as well as tumor-initiating features, *Proc Natl Acad Sci U S A 106*, 13820-13825.
76. Singh, A., and Settleman, J. (2010) EMT, cancer stem cells and drug resistance: an emerging axis of evil in the war on cancer, *Oncogene 29*, 4741-4751.
77. Li, X., Lewis, M. T., Huang, J., Gutierrez, C., Osborne, C. K., Wu, M. F., Hilsenbeck, S. G., Pavlick, A., Zhang, X., Chamness, G. C., Wong, H., Rosen, J., and Chang, J. C. (2008) Intrinsic resistance of tumorigenic breast cancer cells to chemotherapy, *J Natl Cancer Inst 100*, 672-679.
78. Cheng, G. Z., Chan, J., Wang, Q., Zhang, W., Sun, C. D., and Wang, L. H. (2007) Twist transcriptionally up-regulates AKT2 in breast cancer cells leading to increased migration, invasion, and resistance to paclitaxel, *Cancer Res 67*, 1979-1987.
79. Ansieau, S., Bastid, J., Doreau, A., Morel, A. P., Bouchet, B. P., Thomas, C., Fauvet, F., Puisieux, I., Doglioni, C., Piccinin, S., Maestro, R., Voeltzel, T., Selmi, A., Valsesia-Wittmann, S., Caron de Fromentel, C., and Puisieux, A. (2008) Induction of EMT by twist proteins as a collateral effect of tumor-promoting inactivation of premature senescence, *Cancer Cell 14*, 79-89.
80. Liu, Y., El-Naggar, S., Darling, D. S., Higashi, Y., and Dean, D. C. (2008) Zeb1 links epithelial-mesenchymal transition and cellular senescence, *Development 135*, 579-588.
81. Deonarain, M. P., Kousparou, C. A., and Epenetos, A. A. (2009) Antibodies targeting cancer stem cells: a new paradigm in immunotherapy?, *MAbs 1*, 12-25.
82. Gupta, P. B., Onder, T. T., Jiang, G., Tao, K., Kuperwasser, C., Weinberg, R. A., and Lander, E. S. (2009) Identification of selective inhibitors of cancer stem cells by high-throughput screening, *Cell 138*, 645-659.
83. Li, Y., VandenBoom, T. G., 2nd, Kong, D., Wang, Z., Ali, S., Philip, P. A., and Sarkar, F. H. (2009) Up-regulation of miR-200 and let-7 by natural agents leads to the reversal of epithelial-to-mesenchymal transition in gemcitabine-resistant pancreatic cancer cells, *Cancer Res 69*, 6704-6712.
84. Singh, A., Greninger, P., Rhodes, D., Koopman, L., Violette, S., Bardeesy, N., and Settleman, J. (2009) A gene expression signature associated with "K-Ras addiction" reveals regulators of EMT and tumor cell survival, *Cancer Cell 15*, 489-500.
85. Takahashi-Yanaga, F., and Kahn, M. (2010) Targeting Wnt signaling: can we safely eradicate cancer stem cells?, *Clin Cancer Res 16*, 3153-3162.

86. Feldmann, G., Fendrich, V., McGovern, K., Bedja, D., Bisht, S., Alvarez, H., Koorstra, J. B., Habbe, N., Karikari, C., Mullendore, M., Gabrielson, K. L., Sharma, R., Matsui, W., and Maitra, A. (2008) An orally bioavailable small-molecule inhibitor of Hedgehog signaling inhibits tumor initiation and metastasis in pancreatic cancer, *Mol Cancer Ther 7*, 2725-2735.
87. Dubrovska, A., Kim, S., Salamone, R. J., Walker, J. R., Maira, S. M., Garcia-Echeverria, C., Schultz, P. G., and Reddy, V. A. (2009) The role of PTEN/Akt/PI3K signaling in the maintenance and viability of prostate cancer stem-like cell populations, *Proc Natl Acad Sci U S A 106*, 268-273.
88. Farnie, G., and Clarke, R. B. (2007) Mammary stem cells and breast cancer--role of Notch signalling, *Stem Cell Rev 3*, 169-175.
89. Hirsch, H. A., Iliopoulos, D., Tsichlis, P. N., and Struhl, K. (2009) Metformin selectively targets cancer stem cells, and acts together with chemotherapy to block tumor growth and prolong remission, *Cancer Res 69*, 7507-7511.
90. Vazquez-Martin, A., Oliveras-Ferraros, C., Del Barco, S., Martin-Castillo, B., and Menendez, J. A. (2011) The anti-diabetic drug metformin suppresses self-renewal and proliferation of trastuzumab-resistant tumor-initiating breast cancer stem cells, *Breast Cancer Res Treat 126*, 355-364.
91. Levine, A. J., and Puzio-Kuter, A. M. (2010) The control of the metabolic switch in cancers by oncogenes and tumor suppressor genes, *Science 330*, 1340-1344.
92. Yang, M., Soga, T., and Pollard, P. J. (2013) Oncometabolites: linking altered metabolism with cancer, *J Clin Invest 123*, 3652-3658.
93. Ward, P. S., and Thompson, C. B. (2012) Metabolic reprogramming: a cancer hallmark even warburg did not anticipate, *Cancer Cell 21*, 297-308.
94. Warburg, O. (1956) On the origin of cancer cells, *Science 123*, 309-314.
95. Gogvadze, V., Zhivotovsky, B., and Orrenius, S. (2010) The Warburg effect and mitochondrial stability in cancer cells, *Mol Aspects Med 31*, 60-74.
96. Finley, L. W., Zhang, J., Ye, J., Ward, P. S., and Thompson, C. B. (2013) SnapShot: cancer metabolism pathways, *Cell Metab 17*, 466-466 e462.
97. Munoz-Pinedo, C., El Mjiyad, N., and Ricci, J. E. (2012) Cancer metabolism: current perspectives and future directions, *Cell Death Dis 3*, e248.
98. Koppenol, W. H., Bounds, P. L., and Dang, C. V. (2011) Otto Warburg's contributions to current concepts of cancer metabolism, *Nat Rev Cancer 11*, 325-337.
99. Som, P., Atkins, H. L., Bandoypadhyay, D., Fowler, J. S., MacGregor, R. R., Matsui, K., Oster, Z. H., Sacker, D. F., Shiue, C. Y., Turner, H., Wan, C. N., Wolf, A. P., and Zabinski, S. V. (1980) A fluorinated glucose analog, 2-fluoro-2-deoxy-D-glucose (F-18): nontoxic tracer for rapid tumor detection, *J Nucl Med 21*, 670-675.
100. Winnard, P. T., Jr., Pathak, A. P., Dhara, S., Cho, S. Y., Raman, V., and Pomper, M. G. (2008) Molecular imaging of metastatic potential, *J Nucl Med 49 Suppl 2*, 96S-112S.
101. de Souza, A. C., Justo, G. Z., de Araujo, D. R., and Cavagis, A. D. (2011) Defining the molecular basis of tumor metabolism: a continuing challenge since Warburg's discovery, *Cell Physiol Biochem 28*, 771-792.
102. Pfeiffer, T., Schuster, S., and Bonhoeffer, S. (2001) Cooperation and competition in the evolution of ATP-producing pathways, *Science 292*, 504-507.
103. Locasale, J. W., and Cantley, L. C. (2010) Altered metabolism in cancer, *BMC Biol 8*, 88.
104. Semenza, G. L. (2008) Tumor metabolism: cancer cells give and take lactate, *J Clin Invest 118*, 3835-3837.
105. Pavlides, S., Whitaker-Menezes, D., Castello-Cros, R., Flomenberg, N., Witkiewicz, A. K., Frank, P. G., Casimiro, M. C., Wang, C., Fortina, P., Addya, S., Pestell, R. G., Martinez-Outschoorn, U. E., Sotgia, F., and Lisanti, M. P. (2009) The reverse Warburg effect: aerobic glycolysis in cancer associated fibroblasts and the tumor stroma, *Cell Cycle 8*, 3984-4001.

106. Draoui, N., and Feron, O. (2011) Lactate shuttles at a glance: from physiological paradigms to anti-cancer treatments, *Dis Model Mech 4*, 727-732.
107. Bonuccelli, G., Tsirigos, A., Whitaker-Menezes, D., Pavlides, S., Pestell, R. G., Chiavarina, B., Frank, P. G., Flomenberg, N., Howell, A., Martinez-Outschoorn, U. E., Sotgia, F., and Lisanti, M. P. (2010) Ketones and lactate "fuel" tumor growth and metastasis: Evidence that epithelial cancer cells use oxidative mitochondrial metabolism, *Cell Cycle 9*, 3506-3514.
108. Deberardinis, R. J., Sayed, N., Ditsworth, D., and Thompson, C. B. (2008) Brick by brick: metabolism and tumor cell growth, *Curr Opin Genet Dev 18*, 54-61.
109. Foster, R., Griffin, S., Grooby, S., Feltell, R., Christopherson, C., Chang, M., Sninsky, J., Kwok, S., and Torrance, C. (2012) Multiple metabolic alterations exist in mutant PI3K cancers, but only glucose is essential as a nutrient source, *PLoS One 7*, e45061.
110. Manning, B. D., and Cantley, L. C. (2007) AKT/PKB signaling: navigating downstream, *Cell 129*, 1261-1274.
111. Soliman, G. A. (2013) The role of mechanistic target of rapamycin (mTOR) complexes signaling in the immune responses, *Nutrients 5*, 2231-2257.
112. Semenza, G. L. (2010) HIF-1: upstream and downstream of cancer metabolism, *Curr Opin Genet Dev 20*, 51-56.
113. Dang, C. V., Kim, J. W., Gao, P., and Yustein, J. (2008) The interplay between MYC and HIF in cancer, *Nat Rev Cancer 8*, 51-56.
114. Shackelford, D. B., and Shaw, R. J. (2009) The LKB1-AMPK pathway: metabolism and growth control in tumour suppression, *Nat Rev Cancer 9*, 563-575.
115. Kim, J. W., and Dang, C. V. (2005) Multifaceted roles of glycolytic enzymes, *Trends Biochem Sci 30*, 142-150.
116. Morfouace, M., Lalier, L., Oliver, L., Cheray, M., Pecqueur, C., Cartron, P. F., and Vallette, F. M. (2014) Control of glioma cell death and differentiation by PKM2-Oct4 interaction, *Cell Death Dis 5*, e1036.
117. Lunt, S. Y., and Vander Heiden, M. G. (2011) Aerobic glycolysis: meeting the metabolic requirements of cell proliferation, *Annu Rev Cell Dev Biol 27*, 441-464.
118. Pollak, N., Dolle, C., and Ziegler, M. (2007) The power to reduce: pyridine nucleotides--small molecules with a multitude of functions, *Biochem J 402*, 205-218.
119. Tibbetts, A. S., and Appling, D. R. (2010) Compartmentalization of Mammalian folate-mediated one-carbon metabolism, *Annu Rev Nutr 30*, 57-81.
120. Du, W., Jiang, P., Mancuso, A., Stonestrom, A., Brewer, M. D., Minn, A. J., Mak, T. W., Wu, M., and Yang, X. (2013) TAp73 enhances the pentose phosphate pathway and supports cell proliferation, *Nat Cell Biol 15*, 991-1000.
121. Wang, J., Yuan, W., Chen, Z., Wu, S., Chen, J., Ge, J., and Hou, F. (2012) Overexpression of G6PD is associated with poor clinical outcome in gastric cancer, *Tumour Biol 33*, 95-101.
122. Zampella, E. J., Bradley, E. L., Jr., and Pretlow, T. G., 2nd. (1982) Glucose-6-phosphate dehydrogenase: a possible clinical indicator for prostatic carcinoma, *Cancer 49*, 384-387.
123. Kaushik, A. K., Vareed, S. K., Basu, S., Putluri, V., Putluri, N., Panzitt, K., Brennan, C. A., Chinnaiyan, A. M., Vergara, I. A., Erho, N., Weigel, N. L., Mitsiades, N., Shojaie, A., Palapattu, G., Michailidis, G., and Sreekumar, A. (2014) Metabolomic profiling identifies biochemical pathways associated with castration-resistant prostate cancer, *J Proteome Res 13*, 1088-1100.
124. Tsouko, E., Khan, A. S., White, M. A., Han, J. J., Shi, Y., Merchant, F. A., Sharpe, M. A., Xin, L., and Frigo, D. E. (2014) Regulation of the pentose phosphate pathway by an androgen receptor-mTOR-mediated mechanism and its role in prostate cancer cell growth, *Oncogenesis 3*, e103.

125. Li, D., Zhu, Y., Tang, Q., Lu, H., Li, H., Yang, Y., Li, Z., and Tong, S. (2009) A new G6PD knockdown tumor-cell line with reduced proliferation and increased susceptibility to oxidative stress, *Cancer Biother Radiopharm 24*, 81-90.
126. Filosa, S., Fico, A., Paglialunga, F., Balestrieri, M., Crooke, A., Verde, P., Abrescia, P., Bautista, J. M., and Martini, G. (2003) Failure to increase glucose consumption through the pentose-phosphate pathway results in the death of glucose-6-phosphate dehydrogenase gene-deleted mouse embryonic stem cells subjected to oxidative stress, *Biochem J 370*, 935-943.
127. Zhang, C., Zhang, Z., Zhu, Y., and Qin, S. (2014) Glucose-6-phosphate dehydrogenase: a biomarker and potential therapeutic target for cancer, *Anticancer Agents Med Chem 14*, 280-289.
128. Coy, J. F., Dressler, D., Wilde, J., and Schubert, P. (2005) Mutations in the transketolase-like gene TKTL1: clinical implications for neurodegenerative diseases, diabetes and cancer, *Clin Lab 51*, 257-273.
129. Diaz-Moralli, S., Tarrado-Castellarnau, M., Alenda, C., Castells, A., and Cascante, M. (2011) Transketolase-like 1 expression is modulated during colorectal cancer progression and metastasis formation, *PLoS One 6*, e25323.
130. Foldi, M., Stickeler, E., Bau, L., Kretz, O., Watermann, D., Gitsch, G., Kayser, G., Zur Hausen, A., and Coy, J. F. (2007) Transketolase protein TKTL1 overexpression: A potential biomarker and therapeutic target in breast cancer, *Oncol Rep 17*, 841-845.
131. Krockenberger, M., Engel, J. B., Schmidt, M., Kohrenhagen, N., Hausler, S. F., Dombrowski, Y., Kapp, M., Dietl, J., and Honig, A. (2010) Expression of transketolase-like 1 protein (TKTL1) in human endometrial cancer, *Anticancer Res 30*, 1653-1659.
132. Schultz, H., Kahler, D., Branscheid, D., Vollmer, E., Zabel, P., and Goldmann, T. (2008) TKTL1 is overexpressed in a large portion of non-small cell lung cancer specimens, *Diagn Pathol 3*, 35.
133. Schmidt, M., Voelker, H. U., Kapp, M., Krockenberger, M., Dietl, J., and Kammerer, U. (2010) Glycolytic phenotype in breast cancer: activation of Akt, up-regulation of GLUT1, TKTL1 and down-regulation of M2PK, *J Cancer Res Clin Oncol 136*, 219-225.
134. Riganti, C., Gazzano, E., Polimeni, M., Aldieri, E., and Ghigo, D. (2012) The pentose phosphate pathway: an antioxidant defense and a crossroad in tumor cell fate, *Free Radic Biol Med 53*, 421-436.
135. Schwaab, J., Horisberger, K., Strobel, P., Bohn, B., Gencer, D., Kahler, G., Kienle, P., Post, S., Wenz, F., Hofmann, W. K., Hofheinz, R. D., and Erben, P. (2011) Expression of Transketolase like gene 1 (TKTL1) predicts disease-free survival in patients with locally advanced rectal cancer receiving neoadjuvant chemoradiotherapy, *BMC Cancer 11*, 363.
136. Xu, X., Zur Hausen, A., Coy, J. F., and Lochelt, M. (2009) Transketolase-like protein 1 (TKTL1) is required for rapid cell growth and full viability of human tumor cells, *Int J Cancer 124*, 1330-1337.
137. Yuan, W., Wu, S., Guo, J., Chen, Z., Ge, J., Yang, P., and Hu, B. (2010) Silencing of TKTL1 by siRNA inhibits proliferation of human gastric cancer cells in vitro and in vivo, *Cancer Biol Ther 9*, 710-716.
138. Zhang, S., Yang, J. H., Guo, C. K., and Cai, P. C. (2007) Gene silencing of TKTL1 by RNAi inhibits cell proliferation in human hepatoma cells, *Cancer Lett 253*, 108-114.
139. Cascante, M., Centelles, J. J., Veech, R. L., Lee, W. N., and Boros, L. G. (2000) Role of thiamin (vitamin B-1) and transketolase in tumor cell proliferation, *Nutr Cancer 36*, 150-154.
140. Boros, L. G., Puigjaner, J., Cascante, M., Lee, W. N., Brandes, J. L., Bassilian, S., Yusuf, F. I., Williams, R. D., Muscarella, P., Melvin, W. S., and Schirmer, W. J. (1997) Oxythiamine and dehydroepiandrosterone inhibit the nonoxidative synthesis of ribose and tumor cell proliferation, *Cancer Res 57*, 4242-4248.

141. Boros, L. G., Torday, J. S., Lim, S., Bassilian, S., Cascante, M., and Lee, W. N. (2000) Transforming growth factor beta2 promotes glucose carbon incorporation into nucleic acid ribose through the nonoxidative pentose cycle in lung epithelial carcinoma cells, *Cancer Res 60*, 1183-1185.
142. Pelicano, H., Martin, D. S., Xu, R. H., and Huang, P. (2006) Glycolysis inhibition for anticancer treatment, *Oncogene 25*, 4633-4646.
143. Patra, K. C., and Hay, N. (2014) The pentose phosphate pathway and cancer, *Trends Biochem Sci 39*, 347-354.
144. Blum, R., and Kloog, Y. (2014) Metabolism addiction in pancreatic cancer, *Cell Death Dis 5*, e1065.
145. Verdegem, D., Moens, S., Stapor, P., and Carmeliet, P. (2014) Endothelial cell metabolism: parallels and divergences with cancer cell metabolism, *Cancer Metab 2*, 19.
146. Ramos-Montoya, A., Lee, W. N., Bassilian, S., Lim, S., Trebukhina, R. V., Kazhyna, M. V., Ciudad, C. J., Noe, V., Centelles, J. J., and Cascante, M. (2006) Pentose phosphate cycle oxidative and nonoxidative balance: A new vulnerable target for overcoming drug resistance in cancer, *Int J Cancer 119*, 2733-2741.
147. Zanuy, M., Ramos-Montoya, A., Villacanas, O., Canela, N., Miranda, A., Aguilar, E., Agell, N., Bachs, O., Rubio-Martinez, J., Pujol, M. D., Lee, W. N., Marin, S., and Cascante, M. (2012) Cyclin-dependent kinases 4 and 6 control tumor progression and direct glucose oxidation in the pentose cycle, *Metabolomics 8*, 454-464.
148. de Atauri, P., Benito, A., Vizan, P., Zanuy, M., Mangues, R., Marin, S., and Cascante, M. (2011) Carbon metabolism and the sign of control coefficients in metabolic adaptations underlying K-ras transformation, *Biochim Biophys Acta 1807*, 746-754.
149. Ying, H., Kimmelman, A. C., Lyssiotis, C. A., Hua, S., Chu, G. C., Fletcher-Sananikone, E., Locasale, J. W., Son, J., Zhang, H., Coloff, J. L., Yan, H., Wang, W., Chen, S., Viale, A., Zheng, H., Paik, J. H., Lim, C., Guimaraes, A. R., Martin, E. S., Chang, J., Hezel, A. F., Perry, S. R., Hu, J., Gan, B., Xiao, Y., Asara, J. M., Weissleder, R., Wang, Y. A., Chin, L., Cantley, L. C., and DePinho, R. A. (2012) Oncogenic Kras maintains pancreatic tumors through regulation of anabolic glucose metabolism, *Cell 149*, 656-670.
150. Mitsuishi, Y., Taguchi, K., Kawatani, Y., Shibata, T., Nukiwa, T., Aburatani, H., Yamamoto, M., and Motohashi, H. (2012) Nrf2 redirects glucose and glutamine into anabolic pathways in metabolic reprogramming, *Cancer Cell 22*, 66-79.
151. Jiang, P., Du, W., Wang, X., Mancuso, A., Gao, X., Wu, M., and Yang, X. (2011) p53 regulates biosynthesis through direct inactivation of glucose-6-phosphate dehydrogenase, *Nat Cell Biol 13*, 310-316.
152. Menendez, J. A., and Lupu, R. (2007) Fatty acid synthase and the lipogenic phenotype in cancer pathogenesis, *Nat Rev Cancer 7*, 763-777.
153. Guillou, H., Zadravec, D., Martin, P. G., and Jacobsson, A. (2010) The key roles of elongases and desaturases in mammalian fatty acid metabolism: Insights from transgenic mice, *Prog Lipid Res 49*, 186-199.
154. Bauer, D. E., Hatzivassiliou, G., Zhao, F., Andreadis, C., and Thompson, C. B. (2005) ATP citrate lyase is an important component of cell growth and transformation, *Oncogene 24*, 6314-6322.
155. Hatzivassiliou, G., Zhao, F., Bauer, D. E., Andreadis, C., Shaw, A. N., Dhanak, D., Hingorani, S. R., Tuveson, D. A., and Thompson, C. B. (2005) ATP citrate lyase inhibition can suppress tumor cell growth, *Cancer Cell 8*, 311-321.
156. Liao, J., Qian, F., Tchabo, N., Mhawech-Fauceglia, P., Beck, A., Qian, Z., Wang, X., Huss, W. J., Lele, S. B., Morrison, C. D., and Odunsi, K. (2014) Ovarian cancer spheroid cells with stem cell-like properties contribute to tumor generation, metastasis and chemotherapy resistance through hypoxia-resistant metabolism, *PLoS One 9*, e84941.

157. Zaytseva, Y. Y., Rychahou, P. G., Gulhati, P., Elliott, V. A., Mustain, W. C., O'Connor, K., Morris, A. J., Sunkara, M., Weiss, H. L., Lee, E. Y., and Evers, B. M. (2012) Inhibition of fatty acid synthase attenuates CD44-associated signaling and reduces metastasis in colorectal cancer, *Cancer Res 72*, 1504-1517.
158. Hu, J., Liu, Z., and Wang, X. (2013) Does TP53 mutation promote ovarian cancer metastasis to omentum by regulating lipid metabolism?, *Med Hypotheses 81*, 515-520.
159. Cheng, T., Sudderth, J., Yang, C., Mullen, A. R., Jin, E. S., Mates, J. M., and DeBerardinis, R. J. (2011) Pyruvate carboxylase is required for glutamine-independent growth of tumor cells, *Proc Natl Acad Sci U S A 108*, 8674-8679.
160. Saqcena, M., Mukhopadhyay, S., Hosny, C., Alhamed, A., Chatterjee, A., and Foster, D. A. (2014) Blocking anaplerotic entry of glutamine into the TCA cycle sensitizes K-Ras mutant cancer cells to cytotoxic drugs, *Oncogene*.
161. Mazurek, S., Boschek, C. B., Hugo, F., and Eigenbrodt, E. (2005) Pyruvate kinase type M2 and its role in tumor growth and spreading, *Semin Cancer Biol 15*, 300-308.
162. Vander Heiden, M. G., Locasale, J. W., Swanson, K. D., Sharfi, H., Heffron, G. J., Amador-Noguez, D., Christofk, H. R., Wagner, G., Rabinowitz, J. D., Asara, J. M., and Cantley, L. C. (2010) Evidence for an alternative glycolytic pathway in rapidly proliferating cells, *Science 329*, 1492-1499.
163. Kung, C., Hixon, J., Choe, S., Marks, K., Gross, S., Murphy, E., DeLaBarre, B., Cianchetta, G., Sethumadhavan, S., Wang, X., Yan, S., Gao, Y., Fang, C., Wei, W., Jiang, F., Wang, S., Qian, K., Saunders, J., Driggers, E., Woo, H. K., Kunii, K., Murray, S., Yang, H., Yen, K., Liu, W., Cantley, L. C., Vander Heiden, M. G., Su, S. M., Jin, S., Salituro, F. G., and Dang, L. (2012) Small molecule activation of PKM2 in cancer cells induces serine auxotrophy, *Chem Biol 19*, 1187-1198.
164. Luo, W., Hu, H., Chang, R., Zhong, J., Knabel, M., O'Meally, R., Cole, R. N., Pandey, A., and Semenza, G. L. (2011) Pyruvate kinase M2 is a PHD3-stimulated coactivator for hypoxia-inducible factor 1, *Cell 145*, 732-744.
165. Locasale, J. W. (2013) Serine, glycine and one-carbon units: cancer metabolism in full circle, *Nat Rev Cancer 13*, 572-583.
166. Tedeschi, P. M., Markert, E. K., Gounder, M., Lin, H., Dvorzhinski, D., Dolfi, S. C., Chan, L. L., Qiu, J., DiPaola, R. S., Hirshfield, K. M., Boros, L. G., Bertino, J. R., Oltvai, Z. N., and Vazquez, A. (2013) Contribution of serine, folate and glycine metabolism to the ATP, NADPH and purine requirements of cancer cells, *Cell Death Dis 4*, e877.
167. Jain, M., Nilsson, R., Sharma, S., Madhusudhan, N., Kitami, T., Souza, A. L., Kafri, R., Kirschner, M. W., Clish, C. B., and Mootha, V. K. (2012) Metabolite profiling identifies a key role for glycine in rapid cancer cell proliferation, *Science 336*, 1040-1044.
168. Zhang, W. C., Shyh-Chang, N., Yang, H., Rai, A., Umashankar, S., Ma, S., Soh, B. S., Sun, L. L., Tai, B. C., Nga, M. E., Bhakoo, K. K., Jayapal, S. R., Nichane, M., Yu, Q., Ahmed, D. A., Tan, C., Sing, W. P., Tam, J., Thirugananam, A., Noghabi, M. S., Pang, Y. H., Ang, H. S., Mitchell, W., Robson, P., Kaldis, P., Soo, R. A., Swarup, S., Lim, E. H., and Lim, B. (2012) Glycine decarboxylase activity drives non-small cell lung cancer tumor-initiating cells and tumorigenesis, *Cell 148*, 259-272.
169. Schapira, A. H. (2012) Mitochondrial diseases, *Lancet 379*, 1825-1834.
170. Wallace, D. C. (2012) Mitochondria and cancer, *Nat Rev Cancer 12*, 685-698.
171. Weinberg, F., Hamanaka, R., Wheaton, W. W., Weinberg, S., Joseph, J., Lopez, M., Kalyanaraman, B., Mutlu, G. M., Budinger, G. R., and Chandel, N. S. (2010) Mitochondrial metabolism and ROS generation are essential for Kras-mediated tumorigenicity, *Proc Natl Acad Sci U S A 107*, 8788-8793.
172. Collins, Y., Chouchani, E. T., James, A. M., Menger, K. E., Cocheme, H. M., and Murphy, M. P. (2012) Mitochondrial redox signalling at a glance, *J Cell Sci 125*, 801-806.
173. Rizzuto, R., De Stefani, D., Raffaello, A., and Mammucari, C. (2012) Mitochondria as sensors and regulators of calcium signalling, *Nat Rev Mol Cell Biol 13*, 566-578.

174. Chalah, A., and Khosravi-Far, R. (2008) The mitochondrial death pathway, *Adv Exp Med Biol 615*, 25-45.
175. Guppy, M., Leedman, P., Zu, X., and Russell, V. (2002) Contribution by different fuels and metabolic pathways to the total ATP turnover of proliferating MCF-7 breast cancer cells, *Biochem J 364*, 309-315.
176. Rodriguez-Enriquez, S., Vital-Gonzalez, P. A., Flores-Rodriguez, F. L., Marin-Hernandez, A., Ruiz-Azuara, L., and Moreno-Sanchez, R. (2006) Control of cellular proliferation by modulation of oxidative phosphorylation in human and rodent fast-growing tumor cells, *Toxicol Appl Pharmacol 215*, 208-217.
177. Pasdois, P., Deveaud, C., Voisin, P., Bouchaud, V., Rigoulet, M., and Beauvoit, B. (2003) Contribution of the phosphorylable complex I in the growth phase-dependent respiration of C6 glioma cells in vitro, *J Bioenerg Biomembr 35*, 439-450.
178. Mayevsky, A. (2009) Mitochondrial function and energy metabolism in cancer cells: past overview and future perspectives, *Mitochondrion 9*, 165-179.
179. Smolkova, K., Plecita-Hlavata, L., Bellance, N., Benard, G., Rossignol, R., and Jezek, P. (2011) Waves of gene regulation suppress and then restore oxidative phosphorylation in cancer cells, *Int J Biochem Cell Biol 43*, 950-968.
180. Vega-Naredo, I., Loureiro, R., Mesquita, K. A., Barbosa, I. A., Tavares, L. C., Branco, A. F., Erickson, J. R., Holy, J., Perkins, E. L., Carvalho, R. A., and Oliveira, P. J. (2014) Mitochondrial metabolism directs stemness and differentiation in P19 embryonal carcinoma stem cells, *Cell Death Differ 21*, 1560-1574.
181. Suganuma, K., Miwa, H., Imai, N., Shikami, M., Gotou, M., Goto, M., Mizuno, S., Takahashi, M., Yamamoto, H., Hiramatsu, A., Wakabayashi, M., Watarai, M., Hanamura, I., Imamura, A., Mihara, H., and Nitta, M. (2010) Energy metabolism of leukemia cells: glycolysis versus oxidative phosphorylation, *Leuk Lymphoma 51*, 2112-2119.
182. Moreno-Sanchez, R., Rodriguez-Enriquez, S., Marin-Hernandez, A., and Saavedra, E. (2007) Energy metabolism in tumor cells, *FEBS J 274*, 1393-1418.
183. Weinberg, F., and Chandel, N. S. (2009) Mitochondrial metabolism and cancer, *Ann N Y Acad Sci 1177*, 66-73.
184. Raimundo, N., Baysal, B. E., and Shadel, G. S. (2011) Revisiting the TCA cycle: signaling to tumor formation, *Trends Mol Med 17*, 641-649.
185. Chen, J. Q., and Russo, J. (2012) Dysregulation of glucose transport, glycolysis, TCA cycle and glutaminolysis by oncogenes and tumor suppressors in cancer cells, *Biochim Biophys Acta 1826*, 370-384.
186. Cardaci, S., and Ciriolo, M. R. (2012) TCA Cycle Defects and Cancer: When Metabolism Tunes Redox State, *Int J Cell Biol 2012*, 161837.
187. Mycielska, M. E., Broke-Smith, T. P., Palmer, C. P., Beckerman, R., Nastos, T., Erguler, K., and Djamgoz, M. B. (2006) Citrate enhances in vitro metastatic behaviours of PC-3M human prostate cancer cells: status of endogenous citrate and dependence on aconitase and fatty acid synthase, *Int J Biochem Cell Biol 38*, 1766-1777.
188. Panov, A., and Orynbayeva, Z. (2013) Bioenergetic and antiapoptotic properties of mitochondria from cultured human prostate cancer cell lines PC-3, DU145 and LNCaP, *PLoS One 8*, e72078.
189. Parsons, D. W., Jones, S., Zhang, X., Lin, J. C., Leary, R. J., Angenendt, P., Mankoo, P., Carter, H., Siu, I. M., Gallia, G. L., Olivi, A., McLendon, R., Rasheed, B. A., Keir, S., Nikolskaya, T., Nikolsky, Y., Busam, D. A., Tekleab, H., Diaz, L. A., Jr., Hartigan, J., Smith, D. R., Strausberg, R. L., Marie, S. K., Shinjo, S. M., Yan, H., Riggins, G. J., Bigner, D. D., Karchin, R., Papadopoulos, N., Parmigiani, G., Vogelstein, B., Velculescu, V. E., and Kinzler, K. W. (2008) An integrated genomic analysis of human glioblastoma multiforme, *Science 321*, 1807-1812.

190. Yan, H., Parsons, D. W., Jin, G., McLendon, R., Rasheed, B. A., Yuan, W., Kos, I., Batinic-Haberle, I., Jones, S., Riggins, G. J., Friedman, H., Friedman, A., Reardon, D., Herndon, J., Kinzler, K. W., Velculescu, V. E., Vogelstein, B., and Bigner, D. D. (2009) IDH1 and IDH2 mutations in gliomas, *N Engl J Med 360*, 765-773.
191. Ward, P. S., Patel, J., Wise, D. R., Abdel-Wahab, O., Bennett, B. D., Coller, H. A., Cross, J. R., Fantin, V. R., Hedvat, C. V., Perl, A. E., Rabinowitz, J. D., Carroll, M., Su, S. M., Sharp, K. A., Levine, R. L., and Thompson, C. B. (2010) The common feature of leukemia-associated IDH1 and IDH2 mutations is a neomorphic enzyme activity converting alpha-ketoglutarate to 2-hydroxyglutarate, *Cancer Cell 17*, 225-234.
192. Grassian, A. R., Lin, F., Barrett, R., Liu, Y., Jiang, W., Korpal, M., Astley, H., Gitterman, D., Henley, T., Howes, R., Levell, J., Korn, J. M., and Pagliarini, R. (2012) Isocitrate dehydrogenase (IDH) mutations promote a reversible ZEB1/microRNA (miR)-200-dependent epithelial-mesenchymal transition (EMT), *J Biol Chem 287*, 42180-42194.
193. Baysal, B. E. (2003) On the association of succinate dehydrogenase mutations with hereditary paraganglioma, *Trends Endocrinol Metab 14*, 453-459.
194. Pollard, P. J., Wortham, N. C., and Tomlinson, I. P. (2003) The TCA cycle and tumorigenesis: the examples of fumarate hydratase and succinate dehydrogenase, *Ann Med 35*, 632-639.
195. Eng, C., Kiuru, M., Fernandez, M. J., and Aaltonen, L. A. (2003) A role for mitochondrial enzymes in inherited neoplasia and beyond, *Nat Rev Cancer 3*, 193-202.
196. Selak, M. A., Armour, S. M., MacKenzie, E. D., Boulahbel, H., Watson, D. G., Mansfield, K. D., Pan, Y., Simon, M. C., Thompson, C. B., and Gottlieb, E. (2005) Succinate links TCA cycle dysfunction to oncogenesis by inhibiting HIF-alpha prolyl hydroxylase, *Cancer Cell 7*, 77-85.
197. Launonen, V., Vierimaa, O., Kiuru, M., Isola, J., Roth, S., Pukkala, E., Sistonen, P., Herva, R., and Aaltonen, L. A. (2001) Inherited susceptibility to uterine leiomyomas and renal cell cancer, *Proc Natl Acad Sci U S A 98*, 3387-3392.
198. Tomlinson, I. P., Alam, N. A., Rowan, A. J., Barclay, E., Jaeger, E. E., Kelsell, D., Leigh, I., Gorman, P., Lamlum, H., Rahman, S., Roylance, R. R., Olpin, S., Bevan, S., Barker, K., Hearle, N., Houlston, R. S., Kiuru, M., Lehtonen, R., Karhu, A., Vilkki, S., Laiho, P., Eklund, C., Vierimaa, O., Aittomaki, K., Hietala, M., Sistonen, P., Paetau, A., Salovaara, R., Herva, R., Launonen, V., and Aaltonen, L. A. (2002) Germline mutations in FH predispose to dominantly inherited uterine fibroids, skin leiomyomata and papillary renal cell cancer, *Nat Genet 30*, 406-410.
199. Kim, J. W., Tchernyshyov, I., Semenza, G. L., and Dang, C. V. (2006) HIF-1-mediated expression of pyruvate dehydrogenase kinase: a metabolic switch required for cellular adaptation to hypoxia, *Cell Metab 3*, 177-185.
200. LeBleu, V. S., O'Connell, J. T., Gonzalez Herrera, K. N., Wikman, H., Pantel, K., Haigis, M. C., de Carvalho, F. M., Damascena, A., Domingos Chinen, L. T., Rocha, R. M., Asara, J. M., and Kalluri, R. (2014) PGC-1alpha mediates mitochondrial biogenesis and oxidative phosphorylation in cancer cells to promote metastasis, *Nat Cell Biol 16*, 992-1003.
201. Porporato, P. E., Payen, V. L., Perez-Escuredo, J., De Saedeleer, C. J., Danhier, P., Copetti, T., Dhup, S., Tardy, M., Vazeille, T., Bouzin, C., Feron, O., Michiels, C., Gallez, B., and Sonveaux, P. (2014) A mitochondrial switch promotes tumor metastasis, *Cell Rep 8*, 754-766.
202. Palorini, R., Votta, G., Balestrieri, C., Monestiroli, A., Olivieri, S., Vento, R., and Chiaradonna, F. (2014) Energy metabolism characterization of a novel cancer stem cell-like line 3AB-OS, *J Cell Biochem 115*, 368-379.
203. Vlashi, E., Lagadec, C., Vergnes, L., Reue, K., Frohnen, P., Chan, M., Alhiyari, Y., Dratver, M. B., and Pajonk, F. (2014) Metabolic differences in breast cancer stem cells and differentiated progeny, *Breast Cancer Res Treat 146*, 525-534.

204. Thangavelu, K., Chong, Q. Y., Low, B. C., and Sivaraman, J. (2014) Structural basis for the active site inhibition mechanism of human kidney-type glutaminase (KGA), *Sci Rep 4*, 3827.
205. Cassago, A., Ferreira, A. P., Ferreira, I. M., Fornezari, C., Gomes, E. R., Greene, K. S., Pereira, H. M., Garratt, R. C., Dias, S. M., and Ambrosio, A. L. (2012) Mitochondrial localization and structure-based phosphate activation mechanism of Glutaminase C with implications for cancer metabolism, *Proc Natl Acad Sci U S A 109*, 1092-1097.
206. DeBerardinis, R. J., Mancuso, A., Daikhin, E., Nissim, I., Yudkoff, M., Wehrli, S., and Thompson, C. B. (2007) Beyond aerobic glycolysis: transformed cells can engage in glutamine metabolism that exceeds the requirement for protein and nucleotide synthesis, *Proc Natl Acad Sci U S A 104*, 19345-19350.
207. Xiao, M., Yang, H., Xu, W., Ma, S., Lin, H., Zhu, H., Liu, L., Liu, Y., Yang, C., Xu, Y., Zhao, S., Ye, D., Xiong, Y., and Guan, K. L. (2012) Inhibition of alpha-KG-dependent histone and DNA demethylases by fumarate and succinate that are accumulated in mutations of FH and SDH tumor suppressors, *Genes Dev 26*, 1326-1338.
208. Yang, C., Sudderth, J., Dang, T., Bachoo, R. M., McDonald, J. G., and DeBerardinis, R. J. (2009) Glioblastoma cells require glutamate dehydrogenase to survive impairments of glucose metabolism or Akt signaling, *Cancer Res 69*, 7986-7993.
209. Son, J., Lyssiotis, C. A., Ying, H., Wang, X., Hua, S., Ligorio, M., Perera, R. M., Ferrone, C. R., Mullarky, E., Shyh-Chang, N., Kang, Y., Fleming, J. B., Bardeesy, N., Asara, J. M., Haigis, M. C., DePinho, R. A., Cantley, L. C., and Kimmelman, A. C. (2013) Glutamine supports pancreatic cancer growth through a KRAS-regulated metabolic pathway, *Nature 496*, 101-105.
210. Gao, P., Tchernyshyov, I., Chang, T. C., Lee, Y. S., Kita, K., Ochi, T., Zeller, K. I., De Marzo, A. M., Van Eyk, J. E., Mendell, J. T., and Dang, C. V. (2009) c-Myc suppression of miR-23a/b enhances mitochondrial glutaminase expression and glutamine metabolism, *Nature 458*, 762-765.
211. Wise, D. R., DeBerardinis, R. J., Mancuso, A., Sayed, N., Zhang, X. Y., Pfeiffer, H. K., Nissim, I., Daikhin, E., Yudkoff, M., McMahon, S. B., and Thompson, C. B. (2008) Myc regulates a transcriptional program that stimulates mitochondrial glutaminolysis and leads to glutamine addiction, *Proc Natl Acad Sci U S A 105*, 18782-18787.
212. Yuneva, M., Zamboni, N., Oefner, P., Sachidanandam, R., and Lazebnik, Y. (2007) Deficiency in glutamine but not glucose induces MYC-dependent apoptosis in human cells, *J Cell Biol 178*, 93-105.
213. Yuneva, M. O., Fan, T. W., Allen, T. D., Higashi, R. M., Ferraris, D. V., Tsukamoto, T., Mates, J. M., Alonso, F. J., Wang, C., Seo, Y., Chen, X., and Bishop, J. M. (2012) The metabolic profile of tumors depends on both the responsible genetic lesion and tissue type, *Cell Metab 15*, 157-170.
214. Mullen, A. R., Wheaton, W. W., Jin, E. S., Chen, P. H., Sullivan, L. B., Cheng, T., Yang, Y., Linehan, W. M., Chandel, N. S., and DeBerardinis, R. J. (2012) Reductive carboxylation supports growth in tumour cells with defective mitochondria, *Nature 481*, 385-388.
215. Metallo, C. M., Gameiro, P. A., Bell, E. L., Mattaini, K. R., Yang, J., Hiller, K., Jewell, C. M., Johnson, Z. R., Irvine, D. J., Guarente, L., Kelleher, J. K., Vander Heiden, M. G., Iliopoulos, O., and Stephanopoulos, G. (2012) Reductive glutamine metabolism by IDH1 mediates lipogenesis under hypoxia, *Nature 481*, 380-384.
216. Reitman, Z. J., Duncan, C. G., Poteet, E., Winters, A., Yan, L. J., Gooden, D. M., Spasojevic, I., Boros, L. G., Yang, S. H., and Yan, H. (2014) Cancer-associated isocitrate dehydrogenase 1 (IDH1) R132H mutation and d-2-hydroxyglutarate stimulate glutamine metabolism under hypoxia, *J Biol Chem 289*, 23318-23328.
217. Baenke, F., Peck, B., Miess, H., and Schulze, A. (2013) Hooked on fat: the role of lipid synthesis in cancer metabolism and tumour development, *Dis Model Mech 6*, 1353-1363.

218. Huang, W., Choi, W., Chen, Y., Zhang, Q., Deng, H., He, W., and Shi, Y. (2013) A proposed role for glutamine in cancer cell growth through acid resistance, *Cell Res 23*, 724-727.
219. Parks, S. K., Chiche, J., and Pouyssegur, J. (2013) Disrupting proton dynamics and energy metabolism for cancer therapy, *Nat Rev Cancer 13*, 611-623.
220. Nissim, I., Sahai, A., Sandler, R. S., and Tannen, R. L. (1994) The intensity of acidosis differentially alters the pathways of ammoniagenesis in LLC-PK1 cells, *Kidney Int 45*, 1014-1019.
221. Webb, B. A., Chimenti, M., Jacobson, M. P., and Barber, D. L. (2011) Dysregulated pH: a perfect storm for cancer progression, *Nat Rev Cancer 11*, 671-677.
222. Stock, C., and Schwab, A. (2009) Protons make tumor cells move like clockwork, *Pflugers Arch 458*, 981-992.
223. Pavlou, M. P., Dimitromanolakis, A., and Diamandis, E. P. (2013) Coupling proteomics and transcriptomics in the quest of subtype-specific proteins in breast cancer, *Proteomics 13*, 1083-1095.
224. Habermann, J. K., Bundgen, N. K., Gemoll, T., Hautaniemi, S., Lundgren, C., Wangsa, D., Doering, J., Bruch, H. P., Nordstroem, B., Roblick, U. J., Jornvall, H., Auer, G., and Ried, T. (2011) Genomic instability influences the transcriptome and proteome in endometrial cancer subtypes, *Mol Cancer 10*, 132.
225. Turan, N., Kalko, S., Stincone, A., Clarke, K., Sabah, A., Howlett, K., Curnow, S. J., Rodriguez, D. A., Cascante, M., O'Neill, L., Egginton, S., Roca, J., and Falciani, F. (2011) A systems biology approach identifies molecular networks defining skeletal muscle abnormalities in chronic obstructive pulmonary disease, *PLoS Comput Biol 7*, e1002129.
226. Urbanczyk-Wochniak, E., Luedemann, A., Kopka, J., Selbig, J., Roessner-Tunali, U., Willmitzer, L., and Fernie, A. R. (2003) Parallel analysis of transcript and metabolic profiles: a new approach in systems biology, *EMBO Rep 4*, 989-993.
227. Kell, D. B., Brown, M., Davey, H. M., Dunn, W. B., Spasic, I., and Oliver, S. G. (2005) Metabolic footprinting and systems biology: the medium is the message, *Nat Rev Microbiol 3*, 557-565.
228. Nagrath, D., Caneba, C., Karedath, T., and Bellance, N. (2011) Metabolomics for mitochondrial and cancer studies, *Biochim Biophys Acta 1807*, 650-663.
229. Beckonert, O., Keun, H. C., Ebbels, T. M., Bundy, J., Holmes, E., Lindon, J. C., and Nicholson, J. K. (2007) Metabolic profiling, metabolomic and metabonomic procedures for NMR spectroscopy of urine, plasma, serum and tissue extracts, *Nat Protoc 2*, 2692-2703.
230. Cascante, M., and Marin, S. (2008) Metabolomics and fluxomics approaches, *Essays Biochem 45*, 67-81.
231. Winter, G., and Kromer, J. O. (2013) Fluxomics - connecting 'omics analysis and phenotypes, *Environ Microbiol 15*, 1901-1916.
232. Orth, J. D., Thiele, I., and Palsson, B. O. (2010) What is flux balance analysis?, *Nat Biotechnol 28*, 245-248.
233. Hyduke, D. R., Lewis, N. E., and Palsson, B. O. (2013) Analysis of omics data with genome-scale models of metabolism, *Mol Biosyst 9*, 167-174.
234. Feist, A. M., and Palsson, B. O. (2010) The biomass objective function, *Curr Opin Microbiol 13*, 344-349.
235. Duarte, N. C., Becker, S. A., Jamshidi, N., Thiele, I., Mo, M. L., Vo, T. D., Srivas, R., and Palsson, B. O. (2007) Global reconstruction of the human metabolic network based on genomic and bibliomic data, *Proc Natl Acad Sci U S A 104*, 1777-1782.
236. Hao, T., Ma, H. W., Zhao, X. M., and Goryanin, I. (2012) The reconstruction and analysis of tissue specific human metabolic networks, *Mol Biosyst 8*, 663-670.

237. Thiele, I., Swainston, N., Fleming, R. M., Hoppe, A., Sahoo, S., Aurich, M. K., Haraldsdottir, H., Mo, M. L., Rolfsson, O., Stobbe, M. D., Thorleifsson, S. G., Agren, R., Bolling, C., Bordel, S., Chavali, A. K., Dobson, P., Dunn, W. B., Endler, L., Hala, D., Hucka, M., Hull, D., Jameson, D., Jamshidi, N., Jonsson, J. J., Juty, N., Keating, S., Nookaew, I., Le Novere, N., Malys, N., Mazein, A., Papin, J. A., Price, N. D., Selkov, E., Sr., Sigurdsson, M. I., Simeonidis, E., Sonnenschein, N., Smallbone, K., Sorokin, A., van Beek, J. H., Weichart, D., Goryanin, I., Nielsen, J., Westerhoff, H. V., Kell, D. B., Mendes, P., and Palsson, B. O. (2013) A community-driven global reconstruction of human metabolism, *Nat Biotechnol 31*, 419-425.
238. Lazar, M. A., and Birnbaum, M. J. (2012) Physiology. De-meaning of metabolism, *Science 336*, 1651-1652.
239. Pal, C., Papp, B., and Posfai, G. (2014) The dawn of evolutionary genome engineering, *Nat Rev Genet 15*, 504-512.
240. Park, J. M., Kim, T. Y., and Lee, S. Y. (2009) Constraints-based genome-scale metabolic simulation for systems metabolic engineering, *Biotechnol Adv 27*, 979-988.
241. Kumar, V. S., and Maranas, C. D. (2009) GrowMatch: an automated method for reconciling in silico/in vivo growth predictions, *PLoS Comput Biol 5*, e1000308.
242. Kim, H. U., Kim, S. Y., Jeong, H., Kim, T. Y., Kim, J. J., Choy, H. E., Yi, K. Y., Rhee, J. H., and Lee, S. Y. (2011) Integrative genome-scale metabolic analysis of Vibrio vulnificus for drug targeting and discovery, *Mol Syst Biol 7*, 460.
243. Park, J. M., Song, H., Lee, H. J., and Seung, D. (2013) Genome-scale reconstruction and in silico analysis of Klebsiella oxytoca for 2,3-butanediol production, *Microb Cell Fact 12*, 20.
244. Antoniewicz, M. R. (2013) 13C metabolic flux analysis: optimal design of isotopic labeling experiments, *Curr Opin Biotechnol 24*, 1116-1121.
245. Crown, S. B., and Antoniewicz, M. R. (2013) Parallel labeling experiments and metabolic flux analysis: Past, present and future methodologies, *Metab Eng 16*, 21-32.
246. Paul Lee, W. N., Wahjudi, P. N., Xu, J., and Go, V. L. (2010) Tracer-based metabolomics: concepts and practices, *Clin Biochem 43*, 1269-1277.
247. Lane, A. N., Fan, T. W., and Higashi, R. M. (2008) Isotopomer-based metabolomic analysis by NMR and mass spectrometry, *Methods Cell Biol 84*, 541-588.
248. Metallo, C. M., Walther, J. L., and Stephanopoulos, G. (2009) Evaluation of 13C isotopic tracers for metabolic flux analysis in mammalian cells, *J Biotechnol 144*, 167-174.
249. Crown, S. B., Ahn, W. S., and Antoniewicz, M. R. (2012) Rational design of (1)(3)C-labeling experiments for metabolic flux analysis in mammalian cells, *BMC Syst Biol 6*, 43.
250. Boros, L. G., Lerner, M. R., Morgan, D. L., Taylor, S. L., Smith, B. J., Postier, R. G., and Brackett, D. J. (2005) [1,2-13C2]-D-glucose profiles of the serum, liver, pancreas, and DMBA-induced pancreatic tumors of rats, *Pancreas 31*, 337-343.
251. Munger, J., Bennett, B. D., Parikh, A., Feng, X. J., McArdle, J., Rabitz, H. A., Shenk, T., and Rabinowitz, J. D. (2008) Systems-level metabolic flux profiling identifies fatty acid synthesis as a target for antiviral therapy, *Nat Biotechnol 26*, 1179-1186.
252. Yoo, H., Antoniewicz, M. R., Stephanopoulos, G., and Kelleher, J. K. (2008) Quantifying reductive carboxylation flux of glutamine to lipid in a brown adipocyte cell line, *J Biol Chem 283*, 20621-20627.
253. Nargund, S., and Sriram, G. (2013) Designer labels for plant metabolism: statistical design of isotope labeling experiments for improved quantification of flux in complex plant metabolic networks, *Mol Biosyst 9*, 99-112.
254. Ahn, W. S., and Antoniewicz, M. R. (2013) Parallel labeling experiments with [1,2-(13)C]glucose and [U-(13)C]glutamine provide new insights into CHO cell metabolism, *Metab Eng 15*, 34-47.

255. Antoniewicz, M. R., Kelleher, J. K., and Stephanopoulos, G. (2006) Determination of confidence intervals of metabolic fluxes estimated from stable isotope measurements, *Metab Eng 8*, 324-337.
256. Alcarraz-Vizan, G., Boren, J., Lee, W. N., and Cascante, M. (2010) Histone deacetylase inhibition results in a common metabolic profile associated with HT29 differentiation, *Metabolomics 6*, 229-237.
257. Marin, S., Chiang, K., Bassilian, S., Lee, W. N., Boros, L. G., Fernandez-Novell, J. M., Centelles, J. J., Medrano, A., Rodriguez-Gil, J. E., and Cascante, M. (2003) Metabolic strategy of boar spermatozoa revealed by a metabolomic characterization, *FEBS Lett 554*, 342-346.
258. Marin, S., Lee, W. N., Bassilian, S., Lim, S., Boros, L. G., Centelles, J. J., FernAndez-Novell, J. M., Guinovart, J. J., and Cascante, M. (2004) Dynamic profiling of the glucose metabolic network in fasted rat hepatocytes using [1,2-13C2]glucose, *Biochem J 381*, 287-294.
259. Selivanov, V. A., Puigjaner, J., Sillero, A., Centelles, J. J., Ramos-Montoya, A., Lee, P. W., and Cascante, M. (2004) An optimized algorithm for flux estimation from isotopomer distribution in glucose metabolites, *Bioinformatics 20*, 3387-3397.
260. Selivanov, V. A., Meshalkina, L. E., Solovjeva, O. N., Kuchel, P. W., Ramos-Montoya, A., Kochetov, G. A., Lee, P. W., and Cascante, M. (2005) Rapid simulation and analysis of isotopomer distributions using constraints based on enzyme mechanisms: an example from HT29 cancer cells, *Bioinformatics 21*, 3558-3564.
261. Selivanov, V. A., Marin, S., Lee, P. W., and Cascante, M. (2006) Software for dynamic analysis of tracer-based metabolomic data: estimation of metabolic fluxes and their statistical analysis, *Bioinformatics 22*, 2806-2812.
262. de Mas, I. M., Selivanov, V. A., Marin, S., Roca, J., Oresic, M., Agius, L., and Cascante, M. (2011) Compartmentation of glycogen metabolism revealed from 13C isotopologue distributions, *BMC Syst Biol 5*, 175.
263. Zhou, W., Choi, M., Margineantu, D., Margaretha, L., Hesson, J., Cavanaugh, C., Blau, C. A., Horwitz, M. S., Hockenbery, D., Ware, C., and Ruohola-Baker, H. (2012) HIF1alpha induced switch from bivalent to exclusively glycolytic metabolism during ESC-to-EpiSC/hESC transition, *EMBO J 31*, 2103-2116.
264. Suchorolski, M. T., Paulson, T. G., Sanchez, C. A., Hockenbery, D., and Reid, B. J. (2013) Warburg and Crabtree effects in premalignant Barrett's esophagus cell lines with active mitochondria, *PLoS One 8*, e56884.
265. Cheng, G., Zielonka, J., McAllister, D., Tsai, S., Dwinell, M. B., and Kalyanaraman, B. (2014) Profiling and targeting of cellular bioenergetics: inhibition of pancreatic cancer cell proliferation, *Br J Cancer 111*, 85-93.
266. Rogers, G. W., Brand, M. D., Petrosyan, S., Ashok, D., Elorza, A. A., Ferrick, D. A., and Murphy, A. N. (2011) High throughput microplate respiratory measurements using minimal quantities of isolated mitochondria, *PLoS One 6*, e21746.
267. Harney, A. S., Meade, T. J., and LaBonne, C. (2012) Targeted inactivation of Snail family EMT regulatory factors by a Co(III)-Ebox conjugate, *PLoS One 7*, e32318.
268. Puisieux, A., Brabletz, T., and Caramel, J. (2014) Oncogenic roles of EMT-inducing transcription factors, *Nat Cell Biol 16*, 488-494.
269. Ni, J., Cozzi, P., Hao, J., Duan, W., Graham, P., Kearsley, J., and Li, Y. (2014) Cancer stem cells in prostate cancer chemoresistance, *Curr Cancer Drug Targets 14*, 225-240.
270. Feng, W., Gentles, A., Nair, R. V., Huang, M., Lin, Y., Lee, C. Y., Cai, S., Scheeren, F. A., Kuo, A. H., and Diehn, M. (2014) Targeting unique metabolic properties of breast tumor initiating cells, *Stem Cells 32*, 1734-1745.
271. Dong, C., Yuan, T., Wu, Y., Wang, Y., Fan, T. W., Miriyala, S., Lin, Y., Yao, J., Shi, J., Kang, T., Lorkiewicz, P., St Clair, D., Hung, M. C., Evers, B. M., and Zhou, B. P. (2013) Loss of

FBP1 by Snail-mediated repression provides metabolic advantages in basal-like breast cancer, *Cancer Cell 23*, 316-331.
272. Kaighn, M. E., Narayan, K. S., Ohnuki, Y., Lechner, J. F., and Jones, L. W. (1979) Establishment and characterization of a human prostatic carcinoma cell line (PC-3), *Invest Urol 17*, 16-23.
273. Kozlowski, J. M., Fidler, I. J., Campbell, D., Xu, Z. L., Kaighn, M. E., and Hart, I. R. (1984) Metastatic behavior of human tumor cell lines grown in the nude mouse, *Cancer Res 44*, 3522-3529.
274. Lee, W. N., Boros, L. G., Puigjaner, J., Bassilian, S., Lim, S., and Cascante, M. (1998) Mass isotopomer study of the nonoxidative pathways of the pentose cycle with [1,2-13C2]glucose, *Am J Physiol 274*, E843-851.
275. Vander Heiden, M. G., Cantley, L. C., and Thompson, C. B. (2009) Understanding the Warburg effect: the metabolic requirements of cell proliferation, *Science 324*, 1029-1033.
276. Barbi de Moura, M., Vincent, G., Fayewicz, S. L., Bateman, N. W., Hood, B. L., Sun, M., Suhan, J., Duensing, S., Yin, Y., Sander, C., Kirkwood, J. M., Becker, D., Conrads, T. P., Van Houten, B., and Moschos, S. J. (2012) Mitochondrial respiration--an important therapeutic target in melanoma, *PLoS One 7*, e40690.
277. Rodriguez-Enriquez, S., Gallardo-Perez, J. C., Marin-Hernandez, A., and Moreno-Sanchez, R. (2012) The Warburg Hypothesis and the ATP Supply In Cancer Cells Is Oxidative Phosphorylation impaired in malignant neoplasias?, *Curr Pharm Biotechnol*.
278. Elia, U., and Flescher, E. (2013) Combined chemotherapy or biotherapy with jasmonates: targeting energy metabolism for cancer treatment, *Curr Pharm Biotechnol 14*, 331-341.
279. Hamanaka, R. B., and Chandel, N. S. (2012) Targeting glucose metabolism for cancer therapy, *J Exp Med 209*, 211-215.
280. Pacini, N., and Borziani, F. (2014) Cancer stem cell theory and the warburg effect, two sides of the same coin?, *Int J Mol Sci 15*, 8893-8930.
281. Rehman, J. (2010) Empowering self-renewal and differentiation: the role of mitochondria in stem cells, *J Mol Med (Berl) 88*, 981-986.
282. Takubo, K., Nagamatsu, G., Kobayashi, C. I., Nakamura-Ishizu, A., Kobayashi, H., Ikeda, E., Goda, N., Rahimi, Y., Johnson, R. S., Soga, T., Hirao, A., Suematsu, M., and Suda, T. (2013) Regulation of glycolysis by Pdk functions as a metabolic checkpoint for cell cycle quiescence in hematopoietic stem cells, *Cell Stem Cell 12*, 49-61.
283. Mao, P., Joshi, K., Li, J., Kim, S. H., Li, P., Santana-Santos, L., Luthra, S., Chandran, U. R., Benos, P. V., Smith, L., Wang, M., Hu, B., Cheng, S. Y., Sobol, R. W., and Nakano, I. (2013) Mesenchymal glioma stem cells are maintained by activated glycolytic metabolism involving aldehyde dehydrogenase 1A3, *Proc Natl Acad Sci U S A 110*, 8644-8649.
284. Gao, M. Q., Choi, Y. P., Kang, S., Youn, J. H., and Cho, N. H. (2010) CD24+ cells from hierarchically organized ovarian cancer are enriched in cancer stem cells, *Oncogene 29*, 2672-2680.
285. Hansson, J., Rafiee, M. R., Reiland, S., Polo, J. M., Gehring, J., Okawa, S., Huber, W., Hochedlinger, K., and Krijgsveld, J. (2012) Highly coordinated proteome dynamics during reprogramming of somatic cells to pluripotency, *Cell Rep 2*, 1579-1592.
286. Zhang, J., Nuebel, E., Daley, G. Q., Koehler, C. M., and Teitell, M. A. (2012) Metabolic regulation in pluripotent stem cells during reprogramming and self-renewal, *Cell Stem Cell 11*, 589-595.
287. Folmes, C. D., Nelson, T. J., Martinez-Fernandez, A., Arrell, D. K., Lindor, J. Z., Dzeja, P. P., Ikeda, Y., Perez-Terzic, C., and Terzic, A. (2011) Somatic oxidative bioenergetics transitions into pluripotency-dependent glycolysis to facilitate nuclear reprogramming, *Cell Metab 14*, 264-271.

288. Langbein, S., Zerilli, M., Zur Hausen, A., Staiger, W., Rensch-Boschert, K., Lukan, N., Popa, J., Ternullo, M. P., Steidler, A., Weiss, C., Grobholz, R., Willeke, F., Alken, P., Stassi, G., Schubert, P., and Coy, J. F. (2006) Expression of transketolase TKTL1 predicts colon and urothelial cancer patient survival: Warburg effect reinterpreted, *Br J Cancer 94*, 578-585.
289. Hu, L. H., Yang, J. H., Zhang, D. T., Zhang, S., Wang, L., Cai, P. C., Zheng, J. F., and Huang, J. S. (2007) The TKTL1 gene influences total transketolase activity and cell proliferation in human colon cancer LoVo cells, *Anticancer Drugs 18*, 427-433.
290. Carracedo, A., Cantley, L. C., and Pandolfi, P. P. (2013) Cancer metabolism: fatty acid oxidation in the limelight, *Nat Rev Cancer 13*, 227-232.
291. Ito, K., and Suda, T. (2014) Metabolic requirements for the maintenance of self-renewing stem cells, *Nat Rev Mol Cell Biol 15*, 243-256.
292. Anderson, A. S., Roberts, P. C., Frisard, M. I., Hulver, M. W., and Schmelz, E. M. (2014) Ovarian tumor-initiating cells display a flexible metabolism, *Exp Cell Res*.
293. Folmes, C. D., Dzeja, P. P., Nelson, T. J., and Terzic, A. (2012) Metabolic plasticity in stem cell homeostasis and differentiation, *Cell Stem Cell 11*, 596-606.
294. Cuyas, E., Corominas-Faja, B., and Menendez, J. A. (2014) The nutritional phenome of EMT-induced cancer stem-like cells, *Oncotarget 5*, 3970-3982.
295. Fan, J., Ye, J., Kamphorst, J. J., Shlomi, T., Thompson, C. B., and Rabinowitz, J. D. (2014) Quantitative flux analysis reveals folate-dependent NADPH production, *Nature 510*, 298-302.
296. Vazquez, A., Markert, E. K., and Oltvai, Z. N. (2011) Serine biosynthesis with one carbon catabolism and the glycine cleavage system represents a novel pathway for ATP generation, *PLoS One 6*, e25881.
297. Labuschagne, C. F., van den Broek, N. J., Mackay, G. M., Vousden, K. H., and Maddocks, O. D. (2014) Serine, but not glycine, supports one-carbon metabolism and proliferation of cancer cells, *Cell Rep 7*, 1248-1258.
298. Lewis, C. A., Parker, S. J., Fiske, B. P., McCloskey, D., Gui, D. Y., Green, C. R., Vokes, N. I., Feist, A. M., Vander Heiden, M. G., and Metallo, C. M. (2014) Tracing compartmentalized NADPH metabolism in the cytosol and mitochondria of mammalian cells, *Mol Cell 55*, 253-263.
299. Traverso, N., Ricciarelli, R., Nitti, M., Marengo, B., Furfaro, A. L., Pronzato, M. A., Marinari, U. M., and Domenicotti, C. (2013) Role of glutathione in cancer progression and chemoresistance, *Oxid Med Cell Longev 2013*, 972913.
300. Lu, J., Tan, M., and Cai, Q. (2014) The Warburg effect in tumor progression: Mitochondrial oxidative metabolism as an anti-metastasis mechanism, *Cancer Lett*.
301. Brand, M. D. (2000) Uncoupling to survive? The role of mitochondrial inefficiency in ageing, *Exp Gerontol 35*, 811-820.
302. Sauvanet, C., Duvezin-Caubet, S., di Rago, J. P., and Rojo, M. (2010) Energetic requirements and bioenergetic modulation of mitochondrial morphology and dynamics, *Semin Cell Dev Biol 21*, 558-565.
303. Westrate, L. M., Drocco, J. A., Martin, K. R., Hlavacek, W. S., and MacKeigan, J. P. (2014) Mitochondrial morphological features are associated with fission and fusion events, *PLoS One 9*, e95265.
304. Mishra, P., Carelli, V., Manfredi, G., and Chan, D. C. (2014) Proteolytic cleavage of Opa1 stimulates mitochondrial inner membrane fusion and couples fusion to oxidative phosphorylation, *Cell Metab 19*, 630-641.
305. Mullen, A. R., Hu, Z., Shi, X., Jiang, L., Boroughs, L. K., Kovacs, Z., Boriack, R., Rakheja, D., Sullivan, L. B., Linehan, W. M., Chandel, N. S., and DeBerardinis, R. J. (2014) Oxidation of alpha-ketoglutarate is required for reductive carboxylation in cancer cells with mitochondrial defects, *Cell Rep 7*, 1679-1690.

306. Liu, W., and Phang, J. M. (2012) Proline dehydrogenase (oxidase) in cancer, *Biofactors 38*, 398-406.
307. Liu, W., Le, A., Hancock, C., Lane, A. N., Dang, C. V., Fan, T. W., and Phang, J. M. (2012) Reprogramming of proline and glutamine metabolism contributes to the proliferative and metabolic responses regulated by oncogenic transcription factor c-MYC, *Proc Natl Acad Sci U S A 109*, 8983-8988.
308. Morfouace, M., Lalier, L., Bahut, M., Bonnamain, V., Naveilhan, P., Guette, C., Oliver, L., Gueguen, N., Reynier, P., and Vallette, F. M. (2012) Comparison of spheroids formed by rat glioma stem cells and neural stem cells reveals differences in glucose metabolism and promising therapeutic applications, *J Biol Chem 287*, 33664-33674.
309. Tomiyama, A., Serizawa, S., Tachibana, K., Sakurada, K., Samejima, H., Kuchino, Y., and Kitanaka, C. (2006) Critical role for mitochondrial oxidative phosphorylation in the activation of tumor suppressors Bax and Bak, *J Natl Cancer Inst 98*, 1462-1473.
310. Kaplon, J., Zheng, L., Meissl, K., Chaneton, B., Selivanov, V. A., Mackay, G., van der Burg, S. H., Verdegaal, E. M., Cascante, M., Shlomi, T., Gottlieb, E., and Peeper, D. S. (2013) A key role for mitochondrial gatekeeper pyruvate dehydrogenase in oncogene-induced senescence, *Nature 498*, 109-112.
311. Sutendra, G., and Michelakis, E. D. (2013) Pyruvate dehydrogenase kinase as a novel therapeutic target in oncology, *Front Oncol 3*, 38.
312. Le, A., Lane, A. N., Hamaker, M., Bose, S., Gouw, A., Barbi, J., Tsukamoto, T., Rojas, C. J., Slusher, B. S., Zhang, H., Zimmerman, L. J., Liebler, D. C., Slebos, R. J., Lorkiewicz, P. K., Higashi, R. M., Fan, T. W., and Dang, C. V. (2012) Glucose-independent glutamine metabolism via TCA cycling for proliferation and survival in B cells, *Cell Metab 15*, 110-121.
313. Anso, E., Mullen, A. R., Felsher, D. W., Mates, J. M., Deberardinis, R. J., and Chandel, N. S. (2013) Metabolic changes in cancer cells upon suppression of MYC, *Cancer Metab 1*, 7.
314. Seltzer, M. J., Bennett, B. D., Joshi, A. D., Gao, P., Thomas, A. G., Ferraris, D. V., Tsukamoto, T., Rojas, C. J., Slusher, B. S., Rabinowitz, J. D., Dang, C. V., and Riggins, G. J. (2010) Inhibition of glutaminase preferentially slows growth of glioma cells with mutant IDH1, *Cancer Res 70*, 8981-8987.
315. Wise, D. R., Ward, P. S., Shay, J. E., Cross, J. R., Gruber, J. J., Sachdeva, U. M., Platt, J. M., DeMatteo, R. G., Simon, M. C., and Thompson, C. B. (2011) Hypoxia promotes isocitrate dehydrogenase-dependent carboxylation of alpha-ketoglutarate to citrate to support cell growth and viability, *Proc Natl Acad Sci U S A 108*, 19611-19616.
316. van den Heuvel, A. P., Jing, J., Wooster, R. F., and Bachman, K. E. (2012) Analysis of glutamine dependency in non-small cell lung cancer: GLS1 splice variant GAC is essential for cancer cell growth, *Cancer Biol Ther 13*, 1185-1194.
317. Loureiro, R., Mesquita, K. A., Oliveira, P. J., and Vega-Naredo, I. (2013) Mitochondria in cancer stem cells: a target for therapy, *Recent Pat Endocr Metab Immune Drug Discov 7*, 102-114.
318. Gammon, L., Biddle, A., Heywood, H. K., Johannessen, A. C., and Mackenzie, I. C. (2013) Sub-sets of cancer stem cells differ intrinsically in their patterns of oxygen metabolism, *PLoS One 8*, e62493.
319. Giannoni, E., Parri, M., and Chiarugi, P. (2012) EMT and oxidative stress: a bidirectional interplay affecting tumor malignancy, *Antioxid Redox Signal 16*, 1248-1263.
320. Sabharwal, S. S., and Schumacker, P. T. (2014) Mitochondrial ROS in cancer: initiators, amplifiers or an Achilles' heel?, *Nat Rev Cancer 14*, 709-721.
321. Fukawa, T., Kajiya, H., Ozeki, S., Ikebe, T., and Okabe, K. (2012) Reactive oxygen species stimulates epithelial mesenchymal transition in normal human epidermal keratinocytes via TGF-beta secretion, *Exp Cell Res 318*, 1926-1932.

322. Berridge, M. V., Herst, P. M., and Tan, A. S. (2010) Metabolic flexibility and cell hierarchy in metastatic cancer, *Mitochondrion 10*, 584-588.
323. Haraguchi, M., Indo, H. P., Iwasaki, Y., Iwashita, Y., Fukushige, T., Majima, H. J., Izumo, K., Horiuchi, M., Kanekura, T., Furukawa, T., and Ozawa, M. (2013) Snail modulates cell metabolism in MDCK cells, *Biochem Biophys Res Commun 432*, 618-625.
324. Omeir, R. L., Teferedegne, B., Foseh, G. S., Beren, J. J., Snoy, P. J., Brinster, L. R., Cook, J. L., Peden, K., and Lewis, A. M., Jr. (2011) Heterogeneity of the tumorigenic phenotype expressed by Madin-Darby canine kidney cells, *Comp Med 61*, 243-250.
325. Cory, J. G., and Cory, A. H. (2006) Critical roles of glutamine as nitrogen donors in purine and pyrimidine nucleotide synthesis: asparaginase treatment in childhood acute lymphoblastic leukemia, *In Vivo 20*, 587-589.
326. Estrella, V., Chen, T., Lloyd, M., Wojtkowiak, J., Cornnell, H. H., Ibrahim-Hashim, A., Bailey, K., Balagurunathan, Y., Rothberg, J. M., Sloane, B. F., Johnson, J., Gatenby, R. A., and Gillies, R. J. (2013) Acidity generated by the tumor microenvironment drives local invasion, *Cancer Res 73*, 1524-1535.
327. Porter, L. D., Ibrahim, H., Taylor, L., and Curthoys, N. P. (2002) Complexity and species variation of the kidney-type glutaminase gene, *Physiol Genomics 9*, 157-166.
328. Duran, R. V., Oppliger, W., Robitaille, A. M., Heiserich, L., Skendaj, R., Gottlieb, E., and Hall, M. N. (2012) Glutaminolysis activates Rag-mTORC1 signaling, *Mol Cell 47*, 349-358.
329. Cairns, R. A., Harris, I. S., and Mak, T. W. (2011) Regulation of cancer cell metabolism, *Nat Rev Cancer 11*, 85-95.
330. Phang, J. M., Liu, W., Hancock, C., and Christian, K. J. (2012) The proline regulatory axis and cancer, *Front Oncol 2*, 60.
331. Li, J., Dong, L., Wei, D., Wang, X., Zhang, S., and Li, H. (2014) Fatty acid synthase mediates the epithelial-mesenchymal transition of breast cancer cells, *Int J Biol Sci 10*, 171-180.
332. Scott, K. E., Wheeler, F. B., Davis, A. L., Thomas, M. J., Ntambi, J. M., Seals, D. F., and Kridel, S. J. (2012) Metabolic regulation of invadopodia and invasion by acetyl-CoA carboxylase 1 and de novo lipogenesis, *PLoS One 7*, e29761.
333. Kee, H. J., and Cheong, J. H. (2014) Tumor bioenergetics: an emerging avenue for cancer metabolism targeted therapy, *BMB Rep 47*, 158-166.
334. Gorbatenko, A., Olesen, C. W., Boedtkjer, E., and Pedersen, S. F. (2014) Regulation and roles of bicarbonate transporters in cancer, *Front Physiol 5*, 130.
335. Shaw, R. J., Lamia, K. A., Vasquez, D., Koo, S. H., Bardeesy, N., Depinho, R. A., Montminy, M., and Cantley, L. C. (2005) The kinase LKB1 mediates glucose homeostasis in liver and therapeutic effects of metformin, *Science 310*, 1642-1646.
336. Cantoria, M. J., Boros, L. G., and Meuillet, E. J. (2014) Contextual inhibition of fatty acid synthesis by metformin involves glucose-derived acetyl-CoA and cholesterol in pancreatic tumor cells, *Metabolomics 10*, 91-104.
337. Cufi, S., Vazquez-Martin, A., Oliveras-Ferraros, C., Martin-Castillo, B., Joven, J., and Menendez, J. A. (2010) Metformin against TGFbeta-induced epithelial-to-mesenchymal transition (EMT): from cancer stem cells to aging-associated fibrosis, *Cell Cycle 9*, 4461-4468.
338. Rattan, R., Ali Fehmi, R., and Munkarah, A. (2012) Metformin: an emerging new therapeutic option for targeting cancer stem cells and metastasis, *J Oncol 2012*, 928127.
339. Lonardo, E., Cioffi, M., Sancho, P., Sanchez-Ripoll, Y., Trabulo, S. M., Dorado, J., Balic, A., Hidalgo, M., and Heeschen, C. (2013) Metformin targets the metabolic achilles heel of human pancreatic cancer stem cells, *PLoS One 8*, e76518.

340. Kim, T. H., Suh, D. H., Kim, M. K., and Song, Y. S. (2014) Metformin against cancer stem cells through the modulation of energy metabolism: special considerations on ovarian cancer, *Biomed Res Int 2014*, 132702.
341. Ben Sahra, I., Laurent, K., Giuliano, S., Larbret, F., Ponzio, G., Gounon, P., Le Marchand-Brustel, Y., Giorgetti-Peraldi, S., Cormont, M., Bertolotto, C., Deckert, M., Auberger, P., Tanti, J. F., and Bost, F. (2010) Targeting cancer cell metabolism: the combination of metformin and 2-deoxyglucose induces p53-dependent apoptosis in prostate cancer cells, *Cancer Res 70*, 2465-2475.

APPENDIX 1

(PAGES 191-195)

APPENDIX 1: SUPPLEMENTARY DATA FOR MASS ISOTOPOMER DISTRIBUTION OF METABOLITES FROM RESULTS PRESENTED IN CHAPTER I AND II

Metabolite	Cells	Tracer	Incubation time (h)	m0 (%)		m1 (%)		m2 (%)		m3 (%)		m4 (%)		m5 (%)		m6 (%)		Σm (%)	
				mean	SD	mean	SD	mean	SD	mean	SD	mean	SD	mean	SD	mean	SD	mean	SD
Glucose$_{extra.}$	PC-3M	50% [1,2-$^{13}C_2$]-glucose	0	53.37	0.28	0.23	0.06	45.99	0.12	0.35	0.09	0.06	0.09	0.00	0.14	0.00	0.05	46.63	0.28
	PC-3S		0	53.03	0.73	0.28	0.20	46.17	1.12	0.38	0.20	0.10	0.05	0.04	0.03	0.00	0.01	46.97	0.73
Lactate$_{extra.}$	PC-3M	50% [1,2-$^{13}C_2$]-glucose	48	78.94	0.20	1.46	0.05	19.36	0.10	0.24	0.06							21.06	1.83
	PC-3S		48	79.92	0.85	0.69	0.34	19.30	0.43	0.08	0.08							20.08	1.97
Palmitate$_{intra.}$	PC-3M	50% [1,2-$^{13}C_2$]-glucose	48	94.49	1.12	0.06	0.10	3.43	0.64	0.19	0.02	1.23	0.24	0.11	0.02	0.50	0.13	5.65	0.99
	PC-3S		48	92.18	0.22	0.00	0.00	5.02	0.08	0.18	0.05	1.96	0.05	0.08	0.02	0.59	0.06	7.91	0.13
Esterate$_{intra.}$	PC-3M	50% [1,2-$^{13}C_2$]-glucose	24	98.11	0.47	0.00	0.00	1.86	0.30	0.05	0.05	0.52	0.13	0.39	0.07	0.28	0.08	3.25	0.54
	PC-3S		24	96.92	0.38	0.00	0.00	2.97	0.21	0.03	0.03	0.88	0.10	0.25	0.04	0.33	0.03	4.51	0.32

Appendix 1.1 Mass isotopomer distribution data of analyzed metabolites in PC-3M and PC-3S cells, after incubation with 50% [1,2-$^{13}C_2$]-glucose at the indicated time periods (24 or 48 h). Initial mass isotopomer distribution of glucose (0h) is also indicated. Values are expressed as percentage of each mass isotopomer and denote mean ± SD of n=3.

Metabolite	Cells	Tracer	Incubation time (h)	m0 (%)		m1 (%)		m2 (%)		m3 (%)		m4 (%)		m5 (%)		m6 (%)		Σm (%)	
				mean	SD	mean	SD	mean	SD	mean	SD	mean	SD	mean	SD	mean	SD	mean	SD
Glutamate$_{extra.}$	PC-3M	100% [U-$^{13}C_6$]-glucose	48	95.99	0.13	0.56	0.02	3.04	0.10	0.42	0.02							4.01	0.13
(C2-C5 fragment)	PC-3S		48	87.72	0.25	1.68	0.02	8.06	0.20	2.54	0.04							12.28	0.25
Serine$_{extra.}$	PC-3M	100% [U-$^{13}C_6$]-glucose	48	90.78	0.15	1.37	0.09	0.72	0.01	7.13	0.07							9.22	0.15
	PC-3S		48	86.91	0.46	5.78	0.34	3.17	0.13	4.13	0.05							13.09	0.46
Glycine$_{extra.}$	PC-3M	100% [U-$^{13}C_6$]-glucose	48	98.56	0.16	0.26	0.05	1.18	0.11									1.44	0.16
	PC-3S		48	96.11	0.07	0.26	0.08	3.64	0.15									3.89	0.07

Appendix 1.2 Mass isotopomer distribution data of analyzed metabolites in PC-3M and PC-3S cells, after incubation with 100% [U-$^{13}C_6$]-glucose at the indicated time period (48 h). Values are expressed as percentage of each mass isotopomer and denote mean ± SD of n=3.

Metabolite	Cells	Tracer	Incubation time (h)	m0 (%)		m1 (%)		m2 (%)		m3 (%)		m4 (%)		m5 (%)		m6 (%)		Σm (%)	
				mean	SD	mean	SD	mean	SD	mean	SD	mean	SD	mean	SD	mean	SD	mean	SD
Lactate$_{extra.}$	PC-3M	100% [1,2-$^{13}C_2$]-glucose	24	66.66	0.18	1.61	0.01	31.18	0.17	0.54	0.00							33.34	0.18
	PC-3S		24	67.62	0.18	1.51	0.01	30.52	0.16	0.35	0.00							32.38	0.18
Ribose$_{intra.}$	PC-3M	100% [1,2-$^{13}C_2$]-glucose	24	52.61	1.24	20.73	0.41	10.08	0.16	8.32	0.36	7.80	0.13	0.45	0.24			47.39	1.24
	PC-3S		24	74.67	0.20	11.94	0.06	4.80	0.02	4.65	0.17	3.74	0.06	0.20	0.05			25.33	0.20
Alanine$_{extra.}$	PC-3M	100% [1,2-$^{13}C_2$]-glucose	24	73.55	0.30	1.03	0.18	23.28	0.21	2.14	0.22							26.45	0.30
	PC-3S		24	78.42	0.71	1.68	0.08	17.94	0.54	1.96	0.10							21.58	0.71
Citrate$_{intra.}$	PC-3M	100% [1,2-$^{13}C_2$]-glucose	24	65.84	0.63	2.33	0.16	19.74	0.07	5.24	0.25	4.90	0.30	1.36	0.24	0.58	0.21	34.16	0.63
	PC-3S		24	59.83	0.51	3.73	0.06	20.81	0.12	6.94	0.11	6.12	0.17	1.78	0.04	0.79	0.02	40.17	0.51
Glutamate$_{intra.}$	PC-3M	100% [1,2-$^{13}C_2$]-glucose	24	91.35	0.35	0.92	0.04	5.38	0.19	1.25	0.07	0.93	0.04	0.17	0.01			8.65	0.35
	PC-3S		24	81.36	0.34	3.00	0.05	9.88	0.15	3.08	0.07	2.18	0.06	0.50	0.01			18.64	0.34
Fumarate$_{intra.}$	PC-3M	100% [1,2-$^{13}C_2$]-glucose	24	92.54	1.54	1.44	0.64	4.54	0.54	0.74	0.26	0.74	0.32					7.46	1.54
	PC-3S		24	84.51	2.19	3.62	0.59	8.73	0.92	2.15	0.80	0.98	0.16					15.49	2.19
Malate$_{intra.}$	PC-3M	100% [1,2-$^{13}C_2$]-glucose	24	90.79	0.24	1.47	0.08	5.61	0.09	1.38	0.04	0.74	0.04					9.21	0.24
	PC-3S		24	81.90	0.29	3.98	0.04	9.55	0.18	3.05	0.05	1.52	0.04					18.10	0.29
Asparte$_{intra.}$	PC-3M	100% [1,2-$^{13}C_2$]-glucose	24	89.22	2.61	2.41	1.48	5.78	0.50	1.74	0.53	0.85	0.12					10.78	2.61
	PC-3S		24	81.57	0.25	4.14	0.00	9.59	0.17	3.17	0.05	1.53	0.03					18.43	0.25
Pyruvate$_{intra.}$	PC-3M	100% [1,2-$^{13}C_2$]-glucose	24	63.49	2.44	1.40	0.28	33.08	2.09	2.04	0.23							36.51	2.44
	PC-3S		24	69.27	2.18	3.81	0.80	25.14	2.95	1.78	0.21							30.73	2.18

Appendix 1.3 Mass isotopomer distribution data of analyzed metabolites in PC-3M and PC-3S cells, after incubation with 100% [1,2-$^{13}C_2$]-glucose at the indicated time period (24 or 48 h). Values are expressed as percentage of each mass isotopomer and denote mean ± SD of n=3.

Metabolite	Cells	Tracer	Incubation time (h)	m0 (%)		m1 (%)		m2 (%)		m3 (%)		m4 (%)		m5 (%)		m6 (%)		Σm (%)	
				mean	SD	mean	SD	mean	SD	mean	SD	mean	SD	mean	SD	mean	SD	mean	SD
Citrate$_{intra.}$	PC-3M	100% [U-$^{13}C_5$]-glutamine	24	32.36	0.31	3.84	0.21	10.03	0.08	7.72	0.35	30.15	0.71	9.92	0.10	5.98	0.17	67.64	0.31
	PC-3S		24	40.94	0.28	6.83	0.00	11.60	0.07	5.95	0.17	23.52	0.51	6.79	0.05	4.37	0.05	59.06	0.28
Glutamate$_{intra.}$	PC-3M	100% [U-$^{13}C_5$]-glutamine	24	22.97	0.06	2.69	0.15	3.04	0.15	12.36	0.37	3.91	0.07	55.05	0.70			77.03	0.06
	PC-3S		24	31.52	0.59	6.59	0.01	5.27	0.00	15.67	0.05	4.09	0.00	36.86	0.63			68.48	0.59
Fumarate$_{intra.}$	PC-3M	100% [U-$^{13}C_5$]-glutamine	24	36.24	1.09	1.46	0.20	10.73	0.27	0.45	0.60	51.11	0.86					63.76	1.09
	PC-3S		24	40.65	1.22	5.83	1.04	15.31	0.46	0.19	0.28	38.02	2.08					59.35	1.22
Malate$_{intra.}$	PC-3M	100% [U-$^{13}C_5$]-glutamine	24	31.49	0.54	3.94	0.16	11.58	0.25	9.36	0.10	43.64	1.00					68.51	0.54
	PC-3S		24	38.29	1.12	8.06	0.24	14.63	0.28	6.41	0.25	32.61	0.85					61.71	1.12
Asparte$_{intra.}$	PC-3M	100% [U-$^{13}C_5$]-glutamine	24	34.89	0.45	3.93	0.12	11.60	0.22	8.71	0.16	40.88	0.86					65.11	0.45
	PC-3S		24	40.31	1.21	8.35	0.14	14.84	0.30	5.84	0.18	30.65	0.97					59.69	1.21
Proline$_{extra.}$	PC-3M	100% [U-$^{13}C_5$]-glutamine	48	79.87	1.20	0.81	0.38	0.39	0.15	4.04	0.36	0.00	0.00	14.89	0.31			20.13	1.20
	PC-3S		48	85.09	0.84	1.49	0.05	1.51	0.04	3.75	0.06	1.88	0.23	5.54	0.49			14.18	0.66

Appendix 1.4 Mass isotopomer distribution data of analyzed metabolites in PC-3M and PC-3S cells, after incubation with 100% [U-$^{13}C_5$]-glutamine at the indicated time periods (24h). Values are expressed as percentage of each mass isotopomer and denote mean ± SD of n=3.

APPENDIX 2

(PAGES 197-217)

Published in final edited form as:
Metabolomics. 2012 June 1; 8(3): 454–464. doi:10.1007/s11306-011-0328-x.

Cyclin-dependent kinases 4 and 6 control tumor progression and direct glucose oxidation in the pentose cycle

Miriam Zanuy,
Department of Biochemistry and Molecular Biology, Faculty of Biology (Edifici Nou), University of Barcelona, Av. Diagonal 645, 08028 Barcelona, Spain. Institute of Biomedicine of the Universitat de Barcelona (IBUB) and CSIC Associated Unit, Barcelona, Spain

Antonio Ramos-Montoya,
Department of Biochemistry and Molecular Biology, Faculty of Biology (Edifici Nou), University of Barcelona, Av. Diagonal 645, 08028 Barcelona, Spain. Institute of Biomedicine of the Universitat de Barcelona (IBUB) and CSIC Associated Unit, Barcelona, Spain

Oscar Villacañas,
Department of Physical Chemistry, Institut de Recerca en Química Teòrica i Computacional (IQTCUB), Universitat de Barcelona, Martí i Franqués 1, 08028 Barcelona, Spain

Nuria Canela,
Department of Cell Biology, Immunology and Neurosciencies, Institut d'Investigacions Biomèdiques August Pi i Sunyer (IDIBAPS), Faculty of Medicine, Universitat de Barcelona, Casanova 143, 08036 Barcelona, Spain

Anibal Miranda,
Department of Biochemistry and Molecular Biology, Faculty of Biology (Edifici Nou), University of Barcelona, Av. Diagonal 645, 08028 Barcelona, Spain. Institute of Biomedicine of the Universitat de Barcelona (IBUB) and CSIC Associated Unit, Barcelona, Spain

Esther Aguilar,
Department of Biochemistry and Molecular Biology, Faculty of Biology (Edifici Nou), University of Barcelona, Av. Diagonal 645, 08028 Barcelona, Spain. Institute of Biomedicine of the Universitat de Barcelona (IBUB) and CSIC Associated Unit, Barcelona, Spain

Neus Agell,
Department of Cell Biology, Immunology and Neurosciencies, Institut d'Investigacions Biomèdiques August Pi i Sunyer (IDIBAPS), Faculty of Medicine, Universitat de Barcelona, Casanova 143, 08036 Barcelona, Spain

Oriol Bachs,
Department of Cell Biology, Immunology and Neurosciencies, Institut d'Investigacions Biomèdiques August Pi i Sunyer (IDIBAPS), Faculty of Medicine, Universitat de Barcelona, Casanova 143, 08036 Barcelona, Spain

Jaime Rubio-Martinez,

Correspondence to: Marta Cascante, martacascante@ub.edu.

Present Address: A. Ramos-Montoya, Uro-Oncology Research Group, Cancer Research UK, Cambridge Research Institute, Li Ka Shing Centre, Robinson Way, Cambridge CB2 0RE, UK
Present Address: O. Villacañas, Intelligent Pharma S.L, C/Baldiri Reixac 4, 08028 Barcelona, Spain
Miriam Zanuy and Antonio Ramos-Montoya contributed equally to this work.

Electronic supplementary material The online version of this article (doi:10.1007/s11306-011-0328-x) contains supplementary material, which is available to authorized users.

Department of Physical Chemistry, Institut de Recerca en Química Teòrica i Computacional (IQTCUB), Universitat de Barcelona, Martí i Franqués 1, 08028 Barcelona, Spain

Maria Dolors Pujol,
Department of Pharmacology and Therapeutic Chemistry, CSIC Associated Unit, Faculty of Pharmacy, Universitat de Barcelona, Joan XXIII, s/n, 08028 Barcelona, Spain

Wai-Nang P. Lee,
Department of Pediatrics, Los Angeles Biomedical Research Institute at the Harbor-UCLA Medical Center, RB1, 1124 West Carson Street, Torrance, CA 90502, USA

Silvia Marin, and
Department of Biochemistry and Molecular Biology, Faculty of Biology (Edifici Nou), University of Barcelona, Av. Diagonal 645, 08028 Barcelona, Spain. Institute of Biomedicine of the Universitat de Barcelona (IBUB) and CSIC Associated Unit, Barcelona, Spain

Marta Cascante
Department of Biochemistry and Molecular Biology, Faculty of Biology (Edifici Nou), University of Barcelona, Av. Diagonal 645, 08028 Barcelona, Spain. Institute of Biomedicine of the Universitat de Barcelona (IBUB) and CSIC Associated Unit, Barcelona, Spain

Marta Cascante: martacascante@ub.edu

Abstract

Cyclin-dependent kinases CDK4 and CDK6 are essential for the control of the cell cycle through the G_1 phase. Aberrant expression of CDK4 and CDK6 is a hallmark of cancer, which would suggest that CDK4 and CDK6 are attractive targets for cancer therapy. Herein, we report that calcein AM (the calcein acetoxymethyl-ester) is a potent specific inhibitor of CDK4 and CDK6 in HCT116 human colon adenocarcinoma cells, inhibiting retinoblastoma protein (pRb) phosphorylation and inducing cell cycle arrest in the G_1 phase. The metabolic effects of calcein AM on HCT116 cells were also evaluated and the flux between the oxidative and non-oxidative branches of the pentose phosphate pathway was significantly altered. To elucidate whether these metabolic changes were due to the inhibition of CDK4 and CDK6, we also characterized the metabolic profile of a CDK4, CDK6 and CDK2 triple knockout of mouse embryonic fibroblasts. The results show that the metabolic profile associated with the depletion of CDK4, CDK6 and CDK2 coincides with the metabolic changes induced by calcein AM on HCT116 cells, thus confirming that the inhibition of CDK4 and CDK6 disrupts the balance between the oxidative and non-oxidative branches of the pentose phosphate pathway. Taken together, these results indicate that low doses of calcein can halt cell division and kill tumor cells. Thus, selective inhibition of CDK4 and CDK6 may be of greater pharmacological interest, since inhibitors of these kinases affect both cell cycle progression and the robust metabolic profile of tumors.

Keywords

Cyclin-dependent kinases; CDK-inhibitor; Tracer-based metabolomics; Pentose phosphate pathway; Phase-plane analysis

1 Introduction

Typical proliferation of eukaryotic cells involves an orderly progression through four distinct phases of the cell cycle: G_1, S, G_2, and M (Malumbres and Barbacid 2001; Sherr 1996). The first step of the G_1/S transition of the cell cycle is regulated by cyclin-dependent kinases (CDKs: EC 2.7.11.22), CDK4 and CDK6 and their inhibitors, $p16^{INK4a}$ and $p15^{INK4b}$. According to the long-prevailing model of cell cycle control in mammalian cells,

cyclin D-CDK4, cyclin D-CDK6 and cyclin E-CDK2 complexes are sequentially required to promote cell cycle entrance from quiescence, progression through the G_1 phase and transition from the G_1 to the S-phase in response to mitogenic stimulation. Cell culture and biochemical studies have indicated that cyclin D-CDK4, cyclin D-CDK6 and cyclin E-CDK2 complexes are essential and rate-limiting for the phosphorylation and inactivation of the tumor suppressor retinoblastoma protein (pRb) and the subsequent induction of the E2F-dependent transcriptional program required to enter the S-phase (Lundberg and Weinberg 1998; Malumbres et al. 2004; Sherr and Roberts 2004). This step of the cell cycle is critical. If the cell passes through the restriction point (R), it becomes insensitive to extracellular stimuli and is committed to entering the S-phase. Since almost all the regulators of this cell cycle phase are mutated in cancer (Graf et al. 2009), this phase has been considered as a valid therapeutic target. Since most mutations in human cancers affect CDK4 and CDK6 or their regulators (Hall and Peters 1996), and preclinical data indicate that the inhibition of cyclin D-dependent kinase activity may have therapeutic benefits (Graf et al. 2009; Malumbres and Barbacid 2006; Shapiro 2006; Yu et al. 2006), interest in CDK4 and CDK6 as promising targets for inhibiting cell cycle progression has been generated.

Another important and critical feature of tumor cells is their metabolic adaptation, which provides them with metabolites and energy to progress through the cell cycle. This adaptation includes the phenomenon known as the “Warburg effect” (high glycolysis in the presence of oxygen) (Warburg 1956), a high glutamine uptake, the activation of biosynthetic pathways and the over-expression of some glycolytic isoenzymes (Vizán et al. 2008). In recent years, it has become accepted that the metabolic adaptation of tumor cells also involves an enhancement of pentose phosphate pathway (PPP) fluxes and a specific imbalance between its two branches in favor of the oxidative branch versus the non-oxidative branch to maintain the high proliferative rates (Kuo et al. 2000; Poulsen and Frederiksen 1981; Ramos-Montoya et al. 2006). In previous studies, we have demonstrated that this balance between the oxidative and non-oxidative branches of the PPP is necessary to maintain the metabolic efficiency of the cancer cell for growth and proliferation, and that it can be a weakness in the robust tumor metabolic adaptation (Ramos-Montoya et al. 2006). PPP is also specifically regulated during cell cycle progression in tumor cells (Vizan et al. 2009).

In the present study, we identified calcein (4′5′-bis(*N*, *N*-bis(carboxymethyl) aminomethyl) fluorescein) as a putative inhibitor of CDK4 and CDK6 that mimics the natural inhibitor $p16^{INK4a}$ in HCT116 cells, through the use of new bioinformatic tools (Villacanas et al. 2002; Villacanas and Rubio-Martinez 2006), docking procedures (Rubio-Martinez et al. 2005) and molecular assays. Moreover, we provide experimental evidence that this CDK4 and CDK6 inhibitor counteracts metabolic adaptations which are characteristic of tumor cells, and that this metabolic fingerprint coincides with that obtained from a mouse embryonic fibroblast knockout for CDK4, CDK6 and CDK2 cell line. We demonstrate not only that calcein is a promising agent that could be a key factor in the development of a new family of selective cyclin D-dependent kinase inhibitors, but also that inhibition of CDK4 and CDK6 impairs metabolic adaptations that support tumor cell cycle progression.

2 Materials and methods

2.1 Materials

Dulbecco’s modified Eagle Medium (DMEM), F-12 HAM Nutrient mixture with L-glutamine, MEM-EAGLE non-essential aminoacid solution ×100, antibiotic (100 U/ml penicillin, 100 mg/ml streptomycin), Dulbecco’s Phosphate buffer saline (PBS), Trypsin EDTA solution C (0.05% trypsin–0.02% EDTA), L-glutamine solution 200 mM and sodium pyruvate solution 100 mM were obtained from Biological Industries; Fetal calf serum (FCS)

and Trizol were from Invitrogen; SDS was from Fluka; Coomassie blue was from Biorad; HEPES and $MgCl_2$ were from Applichem; A-Sepharose was from Pierce; the [γ-32P]ATP, 3000 Ci/mmol, 10 mCi/ml and ECL were from Amersham; histone H1 was from Boehringer Mannheim; Bradford reagent (500-0006), Acrylamide (161-0158) and peroxidase-coupled secondary antibody were from Bio-Rad Laboratories; anti-CDK6 (sc-177), anti-CDK4 (sc-260-R), anti-cyclin D3 (sc-182) and anti-$p16^{INK4a}$ (sc-468) were from Santa Cruz Biotechnology; anti-cyclin D1 (06-137), anti-CDK2 (06-505) and anti-cyclin B1 (05-158) were from Upstate Biotechnology; anti-actin (691001) was from MP Biomedicals; anti-phospho-Rb (Ser780) was from Cell Signaling Technology; pGST-Rb (379–928) (gift of Dr Wang, San Diego, CA, USA) fusion protein was expressed and purified following Smith and Johnson (1988) and Frangioni and Neel (1993). All other reagents were from Sigma Chemical Co.

2.2 Molecular modeling

Construction and molecular dynamics simulations of the CDK6-$p16^{INK4a}$ complex and the determination of their interactions were carried out as described (Villacanas et al. 2002). All hot spots of the CDK6-$p16^{INK4a}$ interaction surface were monitored throughout the production time to obtain its pharmacophores. Catalyst (Accelrys, Inc., San Diego, CA, USA) software was then used to obtain compounds that matched the different interaction pharmacophores. Selected compounds were docked into CDK6 with an in-house program (Rubio-Martinez 2005) and, finally, a visual structure analysis was carried out to reduce the number of final modeled complexes. More details can be found in supplementary material.

2.3 Cell culture

Human colon carcinoma HCT116 cells (donated by Dr. Capellà, the Institut Català d'Oncologia, Barcelona, Spain) were grown in DMEM:HAM's F12 (1:1), supplemented with 10% heat-inactivated FCS, 2 mM glutamine, 1 mM sodium pyruvate, 1% non-essential amino acids, 50 mU/ml penicillin and 50 μg/ml streptomycin. All cell cultures were carried out at 37°C in a humidified atmosphere with 5% CO_2.

Mouse embryonic fibroblast (Ct MEF) and mouse embryonic fibroblast knockout for CDK4, CDK6 and CDK2 (TKO MEF) cell lines, obtained from Dr. Barbacid (Centro Nacional de Investigaciones Oncológicas, Madrid, Spain) (Santamaria and Ortega 2006), were grown as a monolayer culture in minimum essential medium (DMEM with L-glutamine, without glucose or sodium pyruvate) in the presence of 10% heat-inactivated FCS, 10 mM D-glucose and 0.1% streptomycin/penicillin in standard culture conditions. They were incubated at 37°C, 80% humidity, 5% CO_2, and 3% O_2. Two different clones of each were used in order to discard the effect of immortalization: Ct MEF: LD179.10.1 and LD207.3.1 and TKO MEF: LD1043.7.1 and LD1043.6.1.

2.4 Immunoprecipitation and kinase assays

For the kinase assays, immunoprecipitations were performed as described by Harlow and Lane (Harlow and Lane 1988). HCT116 cells were lysed for 30 min at 4°C in IP buffer (50 mM HEPES pH 7.5, 150 mM NaCl, 2.5 mM EGTA, 1 mM EDTA, 0.1% Tween 20, 10% glycerol, 1 mM DTT, 1 mM phenyl methyl sulfonyl fluoride, 1 μg/ml aprotinin, 10 μg/ml leupeptin, 10 mM β-glycerophosphate, 0.1 mM Na_3VO_4 and 1 mM NaF). Lysates were sonicated twice for 10 s at 4°C and clarified by centrifugation at 10,000×*g* for 10 min. The supernatant fraction protein content was measured using the Bradford method (Bradford 1976), and 400 μg of protein from the lysates were incubated with 4 μg of antibody (CDK6, CDK4, cyclin-D1, cyclin-D3, cyclin-B1 or CDK2) or with 1 μl of normal rabbit serum or normal mouse serum (controls) O/N shaking at 4°C. Protein immunocomplexes were then incubated with 20 μl protein A-Sepharose for 1 h at 4°C, collected by centrifugation and

washed four times in IP buffer and twice in kinase buffer (50 mM HEPES pH 7.4, 10 mM $MgCl_2$, 2.5 mM EGTA, 0.1 mM Na_3VO_4, 10 mM β-glycerophosphate and 1 mM DTT). They were then incubated in kinase buffer containing 2 Ci [γ-32P]ATP and 1 μg pGST-Rb (379–928) fusion protein for CDK6 and CDK4 kinase assays, or 3 μg histone H1 for CDK1 and CDK2 kinase assays, for 30 min at 30°C in a final volume of 30 μl. The samples were pooled and redistributed to assure equal amounts of all the reagents and immunoprecipitated CDK. Finally, the samples were boiled for 5 min and electrophoresed on SDS-polyacrylamide gels, essentially as described by Laemmli (1970), and the gels were stained with coomassie brilliant blue, dried, and exposed to X-ray films at −80°C. The intensity of radioactivity was measured with Typhoon Trio and Trio 9200 (GE Healthcare). $p21^{Kip/Cip}$ and purified $p16^{INK4a}$ were used as a positive control of inhibition.

2.5 Gel electrophoresis and immunoblotting

Cells were lysed in a buffer containing 2% SDS, 67 mM Tris–HCl pH 6.8 and 10 mM EDTA and sonicated twice for 10 s (4°C). Protein content was measured according to the Lowry procedure, using bovine serum albumin (BSA) as standard. The extracts were electrophoresed in SDS-poly-acrylamide gels, essentially as described by Comin-Anduix et al. 2002 and Laemmli 1970. After electrophoresis, the proteins were transferred to Immobilon-P strips for 1.5 h at 70 V. The sheets were preincubated in TBS (20 mM Tris–HCl pH 7.5, 150 mM NaCl), 0.05% Tween 20 and 3% BSA for 1 h at room temperature and then incubated for 1 h at room temperature in TBS, 0.05% Tween 20, 3% BSA containing anti-phospho-Rb (Ser780), anti-CDK4 (sc-260), anti-CDK2 (06-505) or anti-actin (60100) antibodies. After washing in TBS, 0.05% Tween 20 (three times, 10 min each), the sheets were incubated with a peroxidase-coupled secondary antibody (1:3000 dilution) for 1 h at room temperature. After incubation, the sheets were washed twice in TBS, 0.05% Tween 20 and once in TBS. The reaction was visualized using ECL. The Image LAS-3000 Photo Version 2.0 (Fujifilm) was used to analyze the chemiluminescence.

2.6 Viability assay

The assay was performed using a variation of the method described by Mosmann (Matito et al. 2003; Mosmann 1983; Ramos-Montoya et al. 2006). Growing concentrations of the product were plated in 96-well flat-bottomed microtiter plates to a final volume of 200 μl where 1700 cells/well had been seeded 24 h before. After incubation for 72 h, MTT at a final concentration of 0.5 mg/ml was added. After 1 h of incubation, the generated *formazan* was dissolved with 100 μl of DMSO per well. The absorbance was measured on an ELISA plate reader (Merck ELISA System MIOS version 3.2., Tecan Sunrise, Tecan Group Ltd.) at 550 nm. The concentrations that caused 50% inhibition of cell viability (IC_{50}) were calculated.

2.7 Cell culture synchronization and cell cycle analysis

HCT116 cells were brought to 95% cell confluence and kept confluent for 24 h with medium containing 0.5% FCS. Cells were then seeded to 50–60% cell confluence in a medium with 10% heat-inactivated FCS. Calcein AM 2 μM was added.

In order to determine the proportion of cells in each cell cycle phase (G_1, S or G_2), cell cycle analysis was assessed with flow cytometry using a fluorescence-activated cell sorter (FACS). Approximately 500,000 cells were resuspended in 0.5 ml PBS followed by the addition of 4.5 ml 70% (v/v) ethanol (Matito et al. 2003). Cells were briefly stained in PBS containing 50 μg/ml propidium iodide, 10 μg/ml DNAse free RNAse and 0.1% Triton® X-100. FACS analysis was carried out at 488 nm in an Epics XL flow cytometer (Beckman Coulter). Data from 12,000 cells were collected and analyzed using the MultiCycle program (Phoenix Flow Systems).

2.8 Isotopologue distribution analysis

Tracer studies were carried out by incubating the cells in the presence of the corresponding incubation medium containing 10 mM glucose enriched by 50% in the tracer [1,2-$^{13}C_2$]-D-glucose. After incubation for 72 h, the cell medium was removed, thereby separating the incubation medium from the cells adhered to the dishes, and all fractions were frozen in liquid nitrogen and stored at −80°C until processing.

Mass spectral data were obtained on an HP5973 mass selective detector connected to an HP6890 gas chromatograph (HCT116 with calcein AM assays) and on a GCMS-QP2010 selective detector connected to a GC-2010 gas chromatograph from Shimadzu (Ct MEF and TKO MEF assays). The settings were as follows: GC inlet 230°C (200°C for lactate measurement), transfer line 280°C, MS source 230°C and MS Quad 150°C. An HP-5 or a DB-5MS capillary column (both: length (m), 30; internal diameter (μm), 250; film thickness (μm), 0.25) was used. Spectral data were corrected using regression analysis to extract natural ^{13}C enrichment from results (Lee et al. 1991). Measurement of ^{13}C label distribution determined the different relative distribution percentages of the isotopologues, m0 (without any ^{13}C labels), m1 (with one ^{13}C), m2 (with two ^{13}C), etc., which were reported as molar fractions. Σm is the sum of the labeled species (Σm = m1 + m2 + m3…) and is representative of the synthesized molecules of each metabolite. The total label enrichment Σmn is the weighted sum of the labeled species (Σmn = m1 × 1+m2 × 2+m3 × 3…) and is representative of the contribution of the tracer used in the synthesis of each metabolite.

Lactate from the cell culture medium was extracted with ethyl acetate after acidification with HCl. Lactate was transformed to its propylamide-heptafluorobutyric form and the ion cluster around m/z 328 (carbons 1–3 of lactate, chemical ionization) was monitored for the detection of m1 (recycled lactate through the pentose cycle) and m2 (lactate produced by glycolysis). The relative amount of glucose that is converted indirectly to lactate through the pentose cycle, known here as pentose cycle activity, is calculated by the (m1/m2)/(3 + (m1/m2)) ratio using lactate isotopologues (Lee et al. 1998).

RNA ribose was isolated by acid hydrolysis of cellular RNA after Trizol-purification of cell extracts. Ribose isolated from RNA was transformed to its aldonitrile-acetate form using hydroxylamine in pyridine and acetic anhydride. We monitored the ion cluster around the m/z 256 (carbons 1–5 of ribose, chemical ionization) to find the molar enrichment and positional distribution of ^{13}C labels in ribose (Boros et al. 1997; Lee et al. 1998). The m2 ribose originated from [1,2-$^{13}C_2$]-glucose that is converted to ribose through transketolase enzyme reactions, whereas m1 ribose originated from glucose metabolized by direct oxidation via the oxidative steps of the PPP. The isotopologues m3 and m4 come from the recycling of the previously labeled riboses. The oxidative versus non-oxidative ratio was measured as ox/non-ox = (m1 + m3)/(m2 + m3 + 2×m4).

2.9 Sugars-phosphate determination

Hexose, triose, pentose and fructose-1,6-bis-phosphates were determined in cell monolayers frozen in liquid nitrogen as described (Vizan et al. 2007). Frozen cells were briefly scraped off the plates and 100 mM acetic acid solution at 4°C was added. The obtained homogenates were centrifuged at 0.4×*g* for 10 min at 4°C, and the supernatants containing sugar phosphate molecules were separated and kept frozen at −80°C for the following liquid chromatography/mass spectrometry (LC–MS) analysis. Chromatography was performed using an Agilent 1100 Quaternary Pump (Agilent Technologies) equipped with a refrigerated autosampler. A Nucleodex *β*-OH high-performance liquid chromatography (HPLC) column, 200 × 4 mm i.d. (Panreac Química S.A.U.) with a binary gradient at a flow-rate of 0.75 ml/min was used. Solvent A consisted of 10 mM ammonium acetate pH

4.0. Solvent B consisted of acetonitrile. Before reaching the mass spectrometer, the flow-rate was split (1:3). To reduce the residual matrix effect reaching the mass spectrometer, a divert valve (VICI Valco Instruments) drained off the LC eluent during the time in which interference was detected in order to avoid contamination of the mass spectrometer. Identification of sugar phosphates was carried out in an API-3000 tandem mass spectrometer (Applied Biosystems). The multiple reaction monitoring (MRM) transitions were 259/97 for glucose-6-phosphate and fructose-6-phosphate (hexose phosphates), 199/97 for glyceraldehyde-3-phosphate and dihydroxyacetone phosphate (triose phosphates), 339/97 for fructose-1,6-*bis*phosphate and 229/97 for ribose-5-phosphate and xylulose-5-phosphate (pentose phosphates).

2.10 Data analysis and statistical methods

In vitro experiments were carried out using three cultures each time for each treatment regimen and then repeated twice. Mass spectral analyses were carried out by three independent automatic injections of 1 μl of each sample by means of the automatic sampler and accepted only if the sample standard deviation was less than 1% of the normalized peak intensity. Statistical analyses were performed using the parametric unpaired, two-tailed independent sample *t* test with 95, 99, and 99.9% confidence intervals, and $P < 0.05$, $P < 0.01$, and $P < 0.001$ were considered, respectively, to indicate significant differences in glucose carbon metabolism.

3 Results

3.1 Selection of a better CDK4 and CDK6 inhibitor

Results from CDK6-$p16^{INK4a}$ complex dynamics were used to model the interaction pattern of the putative inhibitors. The ACD 3D database (available chemical database 3D) was screened for commercial compounds that matched our query. After docking procedures, eight compounds were selected for further experimental kinase assays, with calcein being the most active (Fig. SM1, supplementary material).

3.2 Calcein selectively inhibits CDK4 and CDK6 activities, disrupting cell growth, pRb and cell cycle

To investigate whether calcein selectively inhibits CDK4 and CDK6 activities, immunoprecipitations were performed, followed by kinase assays in the presence or absence of calcein. A dose–response curve with increasing doses of calcein from 10 μM to 500 μM was carried out with immunoprecipitated CDK6 (Fig. 1a), with an IC_{50} of 75 μM. Calcein at this concentration produced similar effects when CDK4, cyclin D1 or cyclin D3 were immunoprecipitated (Fig. 1b), but did not inhibit CDK1 or CDK2 kinase activities at any of the concentrations tested (Fig. SM2.a, supplementary material). As expected from *in silico* complex dynamics, the interaction of calcein with CDK6 seemed to be through the $p16^{INK4a}$ binding site, as calcein was able to displace $p16^{INK4a}$ from the immunoprecipitated enzyme (Fig. SM2.b, supplementary material). These results demonstrate that calcein interacts selectively with CDK4 and CDK6 at the $p16^{INK4a}$ binding site, inhibiting their kinase activity without affecting CDK2 and CDK1 activities.

To examine whether calcein penetrates the cell membrane and inhibits intracellular CDK4 and CDK6 activities, we used human colon adenocarcinoma HCT116 cells, as they have a silenced wild-type $p16^{INK4A}$ gene and only express a mutant allele (Myohanen et al. 1998). Increasing doses of calcein in the media induced a progressive inhibition of HCT116 cell viability, presenting a rather high IC_{50} of 400 μM after 72 h of treatment. The calcein acetoxymethyl-ester (calcein AM) and *tert*-butoxy methyl ester (calcein tBM), which are more lipophilic and diffusible through the cytoplasmic membrane than the non-esterified

calcein, induced a stronger inhibition of HCT116 cell viability, with IC_{50} values of 0.6 and 80 μM, respectively. Treatment of HCT116 cells with the non-esterified calcein or with calcein AM decreased the phosphorylation of the serine 780 of pRb, which is a specific target for CDK4 and CDK6 (Fig. 2a). In addition, calcein AM arrested the cell cycle in G_1 of synchronous HCT116 cells (Fig. 2b).

All these data suggest a molecular mechanism of action of calcein and its esters through the inhibition of CDK4 and CDK6, which in turn affects cell cycle regulation.

3.3 Metabolic effects caused by the inhibition of the CDKs responsible for G_1/S transition

HCT116 human colon adenocarcinoma cells exposed to increasing concentrations of calcein AM were incubated for 72 h with 10 mM glucose 50% enriched in [1,2-$^{13}C_2$]-D-glucose. The calcein AM concentrations were the IC_{25} (0.36 μM), IC_{50} (0.61 μM) and IC_{75} (1.0 μM) after 72 h of treatment. In parallel, we also performed incubations with immortalized mouse embryonic fibroblasts (Ct MEF) control and knockout for CDK4, CDK6 and CDK2 (TKO MEF) in the presence of the same tracer, to check whether the metabolic changes induced by calcein AM on HCT116 cells were characteristic of the inhibition of the CDKs responsible for the G_1/S transition. These MEF cell lines (Ct and TKO) constitute an additional new tool that could elucidate the effects of the permanent absence of these CDKs in vivo and their contributions to cell cycle progression and the robust tumor metabolic adaptation.

Lactate and ribose from RNA synthesized from the tracer [1,2-$^{13}C_2$]-D-glucose were measured using gas chromatography coupled to mass spectrometry (GC–MS). Table 1 shows the pondered values of the ^{13}C-enriched isotopologues, m1/Σm and m2/Σm, of lactate and ribose from RNA. The molar enrichment Σmn of ribose from RNA is also shown.

Lactate m2 isotopologues (lactate molecules that contain two ^{13}C atoms) originated from [1,2-$^{13}C_2$]-D-glucose converted to lactate through glycolysis, whereas lactate m1 isotopologues originated from the metabolization of the tracer through the oxidative step of the PPP and then recycled to glycolysis via the non-oxidative PPP. Calcein AM induced a dose–response decrease of m1/Σm and an increase of m2/Σm in HCT116 cells. This drop of m1/Σm suggests that calcein AM reduces the contribution of the oxidative PPP flux in lactate synthesis. Similarly, when MEF cell lines were incubated with [1,2-$^{13}C_2$]-D-glucose, the deletion of CDK4, CDK6 and CDK2 reduced m1/Σm lactate, indicating that TKO MEF cells had a reduced contribution of the oxidative pathway of PPP in lactate synthesis. Moreover, the pentose cycle activity decreased progressively in HCT116 cells treated with growing doses of calcein AM, and was 13.75% lower in the condition where the cells were treated with the calcein AM IC_{75} concentration (0.026 ± 0.001 in Ct vs. 0.023 ± 0.001 in IC_{75}). Similarly, pentose cycle activity in TKO MEF cells was 32.35% lower than in Ct MEF (0.040 ± 0.002 in Ct vs. 0.027 ± 0.008 in TKO). This decreased pentose cycle activity reinforced the hypothesis of a diminution of the oxidative PPP flux and a decrease in its contribution to glucose metabolism when the G_1/S-phase of the cell cycle is perturbed.

Calcein AM treatment in HCT116 cells also resulted in a slight decrease in the incorporation of ^{13}C atoms from glucose into nucleic acid ribose (Table 1). The average number of ^{13}C atoms per ribose molecule (Σmn) was reduced by 20% at the dose of IC_{75} of calcein AM in HCT116 cells. As suggested by the above-described decrease in lactate m1/Σm data, the reduction of ribose synthesis in HCT116 cells could be caused by reduced substrate flux through the oxidative steps of the PPP. Furthermore, calcein AM treatment in HCT116 cells caused a dose-dependent m1/Σm decrease as well as a linear increase of m2/Σm ribose (Table 1). This was in accordance with the results obtained in lactate measurements and denoted a clear attenuation of the flux through the oxidative PPP.

Furthermore, TKO MEFs had a lower proliferation rate than Ct MEFs (Ct MEF: 0.26 h^{-1} vs. TKO MEF: 0.12 h^{-1}), the total label incorporation in ribose (Σmn) being lower than that of Ct MEFs (Table 1). Moreover, deletion of CDK4, CDK6 and CDK2 resulted in a decrease in the percentage of ribose m1/Σm and an increase in ribose m2/Σm, which suggests a decrease in the use of the oxidative branch of the PPP. This was in accordance with the results obtained in lactate measurements and denoted a clear attenuation of the flux through the oxidative PPP. Similarly, the oxidative/non-oxidative ratio of PPP was 14% lower for TKO MEFs than for Ct MEFs (0.78 ± 0.00 and 0.91 ± 0.01, respectively). Equally, all calcein AM treatments showed a lower oxidative/non-oxidative ratio of PPP compared to the control treatments (8.42, 18, and 31.90% lower for the IC_{25}, IC_{50}, and IC_{75} treated HCT116, respectively, 1.27 ± 0.00 being for control HCT116 cells). It has been reported that this ratio is higher in tumor cells compared to normal cells (Ramos-Montoya et al. 2006).

To provide information on the relative importance of the two pathways of pentose phosphate production for the viability of the cell, we used phenotype phase-plane analysis. Phenotype phase-plane analysis is the analysis of substrate production and utilization of cells and is an important aspect of reaction network analysis (Edwards et al. 2002; Lee 2006). Figure 3 contains the phase-plane analysis of the normalized ribose isotopologues m1 and m2, where values for oxidative ribose synthesis are plotted against non-oxidative ribose synthesis. The line of optimality is arbitrarily defined as the line drawn through the point for the basal state (Ct Control treatment or Ct MEF) corresponding to conditions satisfying the optimal conditions for growth (objective function). The slope of the line represents the optimal ratio of ribose formed through the oxidative pentose phosphate pathway to a given level of non-oxidative ribose synthesis for the tumor cells. When a line is drawn from a phenotype (a point on the phase-plane), parallel to the major axis, the intersection between the line of optimality and the parallel line indicates the degree of optimality relative to the basal state. Using metabolic phenotype phase-plane analysis, we saw that increasing doses of calcein AM or the deletion of the main CDKs of the G_1/S-phase transition resulted in a more dramatic imbalance between oxidative/non-oxidative PPP.

According to these data, the representation of m1/Σm *vs* m2/Σm in a phenotype phase-plane analysis confirmed the same tendency as in calcein AM-treated cells: the deletion of the CDKs, which phosphorylate pRb, caused an imbalance of the PPP towards the non-oxidative branch (Fig. 3).

3.4 Sugar phosphate pool decreases when cell cycle does not progress

Changes in the absolute concentrations of the intermediary sugar phosphates reflect variations in the metabolic flux profile distribution. Pentose phosphate, triose phosphate and hexose phosphate pools were quantified in HCT116 cells treated with IC_{50} of calcein AM (0.6 μM) and control and TKO MEFs (data not shown). Inhibition of CDK4 and CDK6 function using a calcein AM inhibitor or the knockout cell model resulted in decrease in the concentration of fructose-1,6-*bis*phosphate, pentose and triose phosphate intermediaries. Although, these changes were not significant, they showed a tendency in which the arrest in the G_1 phase of the cell cycle alters the profile of sugar phosphate concentrations.

4 Discussion

Evidence indicates that CDK4 and CDK6 are excellent targets for the design of new anti-tumor drugs (Landis et al. 2006; Yu et al. 2006; Malumbres and Barbacid 2006; Marzec et al. 2006). However, the design of good specific inhibitors against the activity of these kinases has not been successful until now. Different strategies have been employed in the search for good inhibitors but almost none of them have been successful due to their unspecificity and the subsequent side effects (Fry et al. 2004; McInnes 2008; Menu et al.

2008). Thus, there is emerging interest in developing new strategies to search for selective inhibitors of CDK4 and CDK6 for cancer chemotherapy (Mahale et al. 2006). To this end, in this study we used a new set of bioinformatic tools to design CDK4 and CDK6 inhibitors that mimic their natural inhibitor $p16^{INK4a}$. One of these inhibitors was calcein.

Calcein AM is a fluorescent dye that localizes intracellularly after esterase-dependent cellular trapping and has shown cytotoxic activity against various established human tumor cell lines at relatively low concentrations (Jonsson et al. 1996; Liminga et al. 2000). Furthermore, Liminga and collaborators found that calcein AM caused a strong apoptotic response within hours of exposure and tested it on a panel of ten different cell lines, but they failed to find its precise mechanism of action to inhibit cell proliferation (Liminga et al. 1999; Liminga et al. 2000; Liminga et al. 1995). According to our results, calcein carboxylic esters easily penetrate HCT116 cells, inhibiting cell viability at relatively low doses compared with the non-esterified calcein. We have also shown that calcein (the active form inside the cell of the calcein AM ester) specifically inhibited CDK4 and CDK6 (cyclin D-related activities), inducing inhibition of pRb phosphorylation, which is required for entering the S-phase of the cell cycle (Lundberg and Weinberg 1998; Malumbres et al. 2004). The potential of calcein to avoid the entrance of treated cells into the S-phase was further validated here, as calcein AM treatment on HCT116 cells provoked a strong G_1-phase cell cycle arrest.

Having elucidated the effects of calcein on the cell cycle, we proceeded to characterize in depth the effects of inhibiting CDK4 and CDK6 activities on the metabolic profile of the HCT116 cells. We have previously demonstrated that the balance between oxidative and non-oxidative branches of the PPP is essential to maintain proliferation in cancer cells and is a vulnerable target within the cancer metabolic network for potential new therapies for overcoming drug resistance (Ramos-Montoya et al. 2006). Our results here show that increasingly high calcein AM concentrations result in a stronger imbalance of PPP in favor of the non-oxidative branch (Fig. 4). Using metabolic phenotype phase-plane analysis, we deduced that the most efficient doses of calcein AM in the inhibition of tumor cell growth result in a more dramatic imbalance between oxidative and non-oxidative branches of PPP. The perturbation of this imbalance results in a state of metabolic inefficiency and consequently could lead to a pause in cell proliferation or even cell apoptosis. To ensure that the metabolic alterations induced by calcein AM in HCT116 cells were due to the specific inhibition of CDK4 and CDK6 activities induced by this compound, we also characterized the metabolic profile of control (Ct) and triple knockout (TKO) MEFs. These results showed that the lack of functionality of CDK4, CDK6 and CDK2 induced changes in the metabolic profile of fibroblasts that correlate with the alterations induced by calcein AM in the metabolic profile of HCT116 tumor cells. These results support our hypothesis that inhibition of CDK4 and CDK6 was responsible for the oxidative/non-oxidative imbalance in PPP induced by calcein AM.

We recently reported a specific increase in the activities of two key enzymes of PPP, glucose-6-phosphate dehydrogenase for the oxidative branch and transketolase for the non-oxidative branch, during the S/G_2 phases of the cell cycle, in particular during the S-phase, when the synthesis of nucleotides is required. Such an increase in the PPP enzyme activities correlates with a relative increase in the pentose phosphate pool and a progressive increase in the balance between oxidative and non-oxidative branches of PPP in the S and G_2 phases (Vizan et al. 2009). This means that the contribution of the oxidative branch to ribose-5-phosphate synthesis is relatively increased when the cycle progresses through the S-phase (Vizan et al. 2009). In this article, the results support this assertion, showing a decrease in this balance when HCT116 cells were treated with calcein AM or when fibroblasts did not express functional CDK4, CDK6, and CDK2 and their progress through the cell cycle was

compromised. Moreover, ^{13}C incorporation from glucose into RNA ribose was lower both in HCT116 treated with calcein AM and in TKO MEFs, indicating that ribose-5-phosphate synthesis decreases when the entrance of the cell into the S-phase is inhibited. Additionally, in this work we have shown that the imbalance in PPP induced by the inhibition of CDK4 and CDK6 is able to slightly compromise the balance in the overall central carbon metabolic network of the cell, which is reflected in a non-significant change in the levels of intermediary sugar phosphates (Fig. 4). The results presented in this paper regarding the metabolic consequences of the inhibition of CDK4 and CDK6 highlights the metabolic requirements of the cell cycle and points to CDK4 and CDK6 as interesting drug targets to be explored in a wider range of cancer types.

5 Concluding remarks

The forced imbalance of the PPP towards the oxidative branch is a possible Achilles' heel in the robust tumor metabolic adaptation. It has been shown that effective anti-tumor strategies against this target can be designed not only with drugs that force this imbalance even further (Ramos-Montoya et al. 2006), but also using drugs that recover the oxidative/non-oxidative balance in the non-tumor cells. The data presented here demonstrate that the inhibition of CDK4 and CDK6 using calcein AM not only inhibits the progression of the cell cycle, but also disrupts this oxidative/non-oxidative imbalance of PPP, which has been described as essential for tumor proliferation, reinforcing the interest of CDK4 and CDK6 as targets in cancer therapy.

Furthermore, we suggest that calcein could be a key factor in the development of a new family of selective cyclin D-dependent kinases inhibitors based on its structure. The improved understanding of the specific effects of the inhibition of CDK4 and CDK6 on tumor cell central metabolic networks shown in this paper opens up new avenues for the design of combination therapies with drugs that directly inhibit those pathways and also to the use of specific CDK4 and CDK6 inhibitors to impair metabolic adaptations that support tumor cell cycle progression.

Supplementary Material

Refer to Web version on PubMed Central for supplementary material.

Acknowledgments

The authors thank Mrs Ursula Valls for her technical support in the experiments and Dr David Santamaria for his help in MEF procedures. MEF cells were a generous gift from Dr Mariano Barbacid, CNIO-Madrid (Spain). This study was supported by the projects SAF2008-00164 (to MC) and SAF2007-60491 (to NA) and by RD06/0020/0046 (to MC), RD06/0020/0010 (to OB) from Red Temática de Investigación Cooperativa en Cáncer (RTICC), Instituto de Salud Carlos III, all of them funded by the Ministerio de Ciencia e Innovación-Spanish government and European Regional Development Funds (ERDF) "Una manera de hacer Europa". It has also received financial support from the European Union-funded project ETHERPATHS (FP7-KBBE-222639) (http://www.etherpaths.org/) and from the Agència de Gestió d'Ajuts Universitaris i de Recerca (AGAUR)-Generalitat de Catalunya (2009SGR01308 and predoctoral fellowship of M.Z.). Mass spectrometry facility was supported by NIH grants to WNP Lee from UCLA Center of Excellence (PO1 AT003960-01) and from Harbor-UCLA GCRC (MO1 RR00425-33). MC acknowledges the support received through the prize "ICREA Academia" for excellence in research, funded by ICREA foundation-Generalitat de Catalunya.

Abbreviations

Calcein AM	Calcein acetoxymethyl-ester
CDK	Cyclin-dependent kinase

DMEM	Dulbecco's modified eagle medium
FCS	Fetal calf serum
Ct MEF	Mouse embryonic fibroblast
PBS	Phosphate buffer saline
PPP	Pentose phosphate pathway
pRb	Retinoblastoma protein
TKO MEF	Mouse embryonic fibroblast knockout for CDK4, CDK6 and CDK2

References

Boros LG, Puigjaner J, Cascante M, Lee WN, Brandes JL, Bassilian S, et al. Oxythiamine and dehydroepiandrosterone inhibit the nonoxidative synthesis of ribose and tumor cell proliferation. Cancer Research. 1997; 57:4242–4248. [PubMed: 9331084]

Bradford MM. A rapid and sensitive method for the quantitation of microgram quantities of protein utilizing the principle of protein-dye binding. Analytical Biochemistry. 1976; 72:248–254. [PubMed: 942051]

Comin-Anduix B, Boros LG, Marin S, Boren J, Callol-Massot C, Centelles JJ, et al. Fermented wheat germ extract inhibits glycolysis/pentose cycle enzymes and induces apoptosis through poly(ADP-ribose) polymerase activation in Jurkat T-cell leukemia tumor cells. Journal of Biological Chemistry. 2002; 277:46408–46414. [PubMed: 12351627]

Edwards JS, Ramakrishna R, Palsson BO. Characterizing the metabolic phenotype: a phenotype phase plane analysis. Biotechnology and Bioengineering. 2002; 77:27–36. [PubMed: 11745171]

Frangioni JV, Neel BG. Solubilization and purification of enzymatically active glutathione S-transferase (pGEX) fusion proteins. Analytical Biochemistry. 1993; 210:179–187. [PubMed: 8489015]

Fry DW, Harvey PJ, Keller PR, Elliott WL, Meade M, Trachet E, et al. Specific inhibition of cyclin-dependent kinase 4/6 by PD 0332991 and associated antitumor activity in human tumor xenografts. Molecular Cancer Therapeutics. 2004; 3:1427–1438. [PubMed: 15542782]

Graf F, Koehler L, Kniess T, Wuest F, Mosch B, Pietzsch J. Cell cycle regulating kinase Cdk4 as a potential target for tumor cell treatment and tumor imaging. Journal of Oncology. 2009; 2009:106378. [PubMed: 19551155]

Hall M, Peters G. Genetic alterations of cyclins, cyclin-dependent kinases, and Cdk inhibitors in human cancer. Advances in Cancer Research. 1996; 68:67–108. [PubMed: 8712071]

Harlow, E.; Lane, D., editors. Antibodies: a laboratory manual. New York: Cold Spring Harbor Laboratory Press; 1988. p. 469

Jonsson B, Liminga G, Csoka K, Fridborg H, Dhar S, Nygren P, et al. Cytotoxic activity of calcein acetoxymethyl ester (calcein/AM) on primary cultures of human haematological and solid tumours. European Journal of Cancer. 1996; 32A:883–887. [PubMed: 9081371]

Kuo W, Lin J, Tang TK. Human glucose-6-phosphate dehydrogenase (G6PD) gene transforms NIH 3T3 cells and induces tumors in nude mice. International Journal of Cancer. 2000; 85:857–864.

Laemmli UK. Cleavage of structural proteins during the assembly of the head of bacteriophage T4. Nature. 1970; 227:680–685. [PubMed: 5432063]

Landis MW, Pawlyk BS, Li T, Sicinski P, Hinds PW. Cyclin D1-dependent kinase activity in murine development and mammary tumorigenesis. Cancer Cell. 2006; 9:13–22. [PubMed: 16413468]

Lee WNP. Characterizing phenotype with tracer based metabolomics. Metabolomics. 2006; 2:31–39.

Lee WN, Boros LG, Puigjaner J, Bassilian S, Lim S, Cascante M. Mass isotopomer study of the nonoxidative pathways of the pentose cycle with [1,2–13C2]glucose. American Journal of Physiology. 1998; 274:E843–E851. [PubMed: 9612242]

Lee WN, Byerley LO, Bergner EA, Edmond J. Mass isotopomer analysis: theoretical and practical considerations. Biological Mass Spectrometry. 1991; 20:451–458. [PubMed: 1768701]

Liminga G, Jonsson B, Nygren P, Larsson R. On the mechanism underlying calcein-induced cytotoxicity. European Journal of Pharmacology. 1999; 383:321–329. [PubMed: 10594326]

Liminga G, Martinsson P, Jonsson B, Nygren P, Larsson R. Apoptosis induced by calcein acetoxymethyl ester in the human histiocytic lymphoma cell line U-937 GTB. Biochemical Pharmacology. 2000; 60:1751–1759. [PubMed: 11108790]

Liminga G, Nygren P, Dhar S, Nilsson K, Larsson R. Cytotoxic effect of calcein acetoxymethyl ester on human tumor cell lines: drug delivery by intracellular trapping. Anticancer Drugs. 1995; 6:578–585. [PubMed: 7579562]

Lundberg AS, Weinberg RA. Functional inactivation of the retinoblastoma protein requires sequential modification by at least two distinct cyclin-cdk complexes. Molecular and Cellular Biology. 1998; 18:753–761. [PubMed: 9447971]

Mahale S, Aubry C, Jenkins PR, Marechal JD, Sutcliffe MJ, Chaudhuri B. Inhibition of cancer cell growth by cyclin dependent kinase 4 inhibitors synthesized based on the structure of fascaplysin. Bioorganic Chemistry. 2006; 34(5):287–297. [PubMed: 16904725]

Malumbres M, Barbacid M. To cycle or not to cycle: a critical decision in cancer. Nature Reviews Cancer. 2001; 1:222–231.

Malumbres M, Barbacid M. Is cyclin D1-CDK4 kinase a bona fide cancer target? Cancer Cell. 2006; 9:2–4. [PubMed: 16413464]

Malumbres M, Sotillo R, Santamaria D, Galan J, Cerezo A, Ortega S, et al. Mammalian cells cycle without the D-type cyclin-dependent kinases Cdk4 and Cdk6. Cell. 2004; 118:493–504. [PubMed: 15315761]

Marzec M, Kasprzycka M, Lai R, Gladden AB, Wlodarski P, Tomczak E, et al. Mantle cell lymphoma cells express predominantly cyclin D1a isoform and are highly sensitive to selective inhibition of CDK4 kinase activity. Blood. 2006; 108:1744–1750. [PubMed: 16690963]

Matito C, Mastorakou F, Centelles JJ, Torres JL, Cascante M. Antiproliferative effect of antioxidant polyphenols from grape in murine Hepa-1c1c7. European Journal of Nutrition. 2003; 42:43–49. [PubMed: 12594540]

McInnes C. Progress in the evaluation of CDK inhibitors as anti-tumor agents. Drug Discovery Today. 2008; 13:875–881. [PubMed: 18639646]

Menu E, Garcia J, Huang X, Di Liberto M, Toogood PL, Chen I, et al. A novel therapeutic combination using PD 0332991 and bortezomib: study in the 5T33MM myeloma model. Cancer Research. 2008; 68:5519–5523. [PubMed: 18632601]

Mosmann T. Rapid colorimetric assay for cellular growth and survival: application to proliferation and cytotoxicity assays. Journal of Immunological Methods. 1983; 65:55–63. [PubMed: 6606682]

Myohanen SK, Baylin SB, Herman JG. Hypermethylation can selectively silence individual p16ink4A alleles in neoplasia. Cancer Research. 1998; 58:591–593. [PubMed: 9485004]

Poulsen HS, Frederiksen P. Glucose-6-phosphate dehydrogenase activity in human breast cancer. Lack of association with oestrogen receptor content. Acta Pathol Microbiol Scand [A]. 1981; 89:263–270.

Ramos-Montoya A, Lee WNP, Bassilian S, Lim S, Trebukhina RV, Kazhyna MV, et al. Pentose phosphate cycle oxidative and non-oxidative balance: a new vulnerable target for overcoming drug resistance in cancer. International Journal of Cancer. 2006; 119:2733–2741.

Rubio-Martinez, J.; Pinto, M.; Tomas, MS.; Perez, JJ. Dock_Dyn: a program for fast molecular docking using molecular dynamics information. University of Barcelona and Technical University of Catalonia; 2005.

Santamaria D, Ortega S. Cyclins and CDKS in development and cancer: lessons from genetically modified mice. Frontiers in Bioscience. 2006; 11:1164–1188. [PubMed: 16146805]

Shapiro GI. Cyclin-dependent kinase pathways as targets for cancer treatment. Journal of Clinical Oncology. 2006; 24:1770–1783. [PubMed: 16603719]

Sherr CJ. Cancer cell cycles. Science. 1996; 274:1672–1677. [PubMed: 8939849]

Sherr CJ, Roberts JM. Living with or without cyclins and cyclin-dependent kinases. Genes and Development. 2004; 18:2699–2711. [PubMed: 15545627]

Smith DB, Johnson KS. Single-step purification of polypeptides expressed in *Escherichia coli* as fusions with glutathione S-transferase. Gene. 1988; 67:31–40. [PubMed: 3047011]

Villacanas O, Perez JJ, Rubio-Martinez J. Structural analysis of the inhibition of Cdk4 and Cdk6 by p16(INK4a) through molecular dynamics simulations. Journal of Biomolecular Structure and Dynamics. 2002; 20:347–358. [PubMed: 12437373]

Villacanas O, Rubio-Martinez J. Reducing CDK4/6–p16(INK4a) interface. Computational alanine scanning of a peptide bound to CDK6 protein. Proteins. 2006; 63:797–810. [PubMed: 16508961]

Vizan P, Alcarraz-Vizán G, Diaz-Moralli S, Rodriguez-Prados JC, Zanuy M, Centelles JJ, et al. Quantification of intracellular phosphorylated carbohydrates in HT29 human colon adenocarcinoma cell line using liquid chromatography-electrospray ionization tandem mass spectrometry. Analytical Chemistry. 2007; 79(13):5000–5005. [PubMed: 17523595]

Vizan P, Alcarraz-Vizan G, Diaz-Moralli S, Solovjeva ON, Frederiks WM, Cascante M. Modulation of pentose phosphate pathway during cell cycle progression in human colon adenocarcinoma cell line HT29. International Journal of Cancer. 2009; 124:2789–2796.

Vizán P, Mazurek S, Cascante M. Robust metabolic adaptation underlying tumor progression. Metabolomics. 2008; 4:1–12.

Warburg O. Origin of cancer cells. Oncologia. 1956; 9:75–83. [PubMed: 13335077]

Yu Q, Sicinska E, Geng Y, Ahnstrom M, Zagozdzon A, Kong Y, et al. Requirement for CDK4 kinase function in breast cancer. Cancer Cell. 2006; 9:23–32. [PubMed: 16413469]

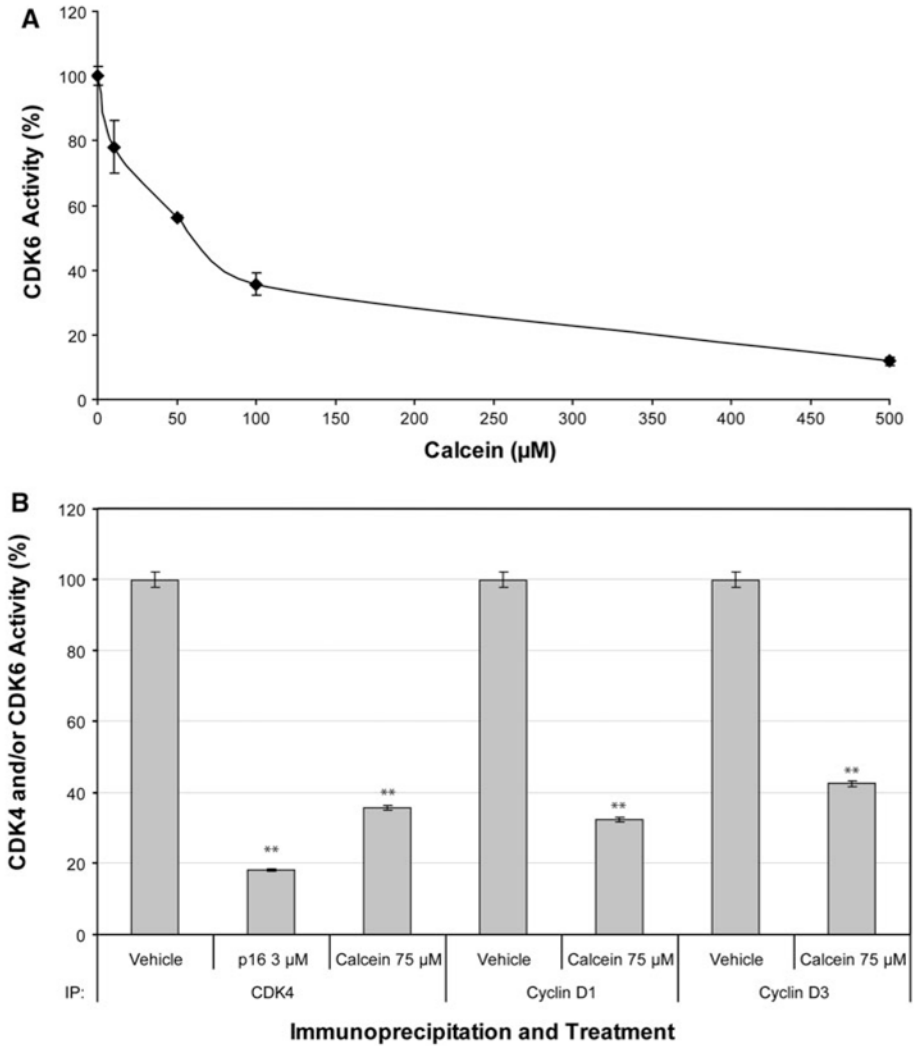

Fig. 1.

Effect of calcein on kinase assays in inmunoprecipitated CDK6, CDK4, cyclin D1, and cyclin D3. **a** Dose–effect curve of non-esterified calcein on CDK6 activity (10–500 μM). **b** CDK4, cyclin D1 and cyclin D3 immunoprecipitations and kinase assays tested in the presence of 75 μM of non-esterified calcein and $p16^{INK4a}$ (3 μM). pGST-Rb (379–928) fusion protein was used as a substrate. Mean + SD; $n = 3$. (*) indicates $P < 0.05$ and (**) indicates $P < 0.01$ compared to vehicle

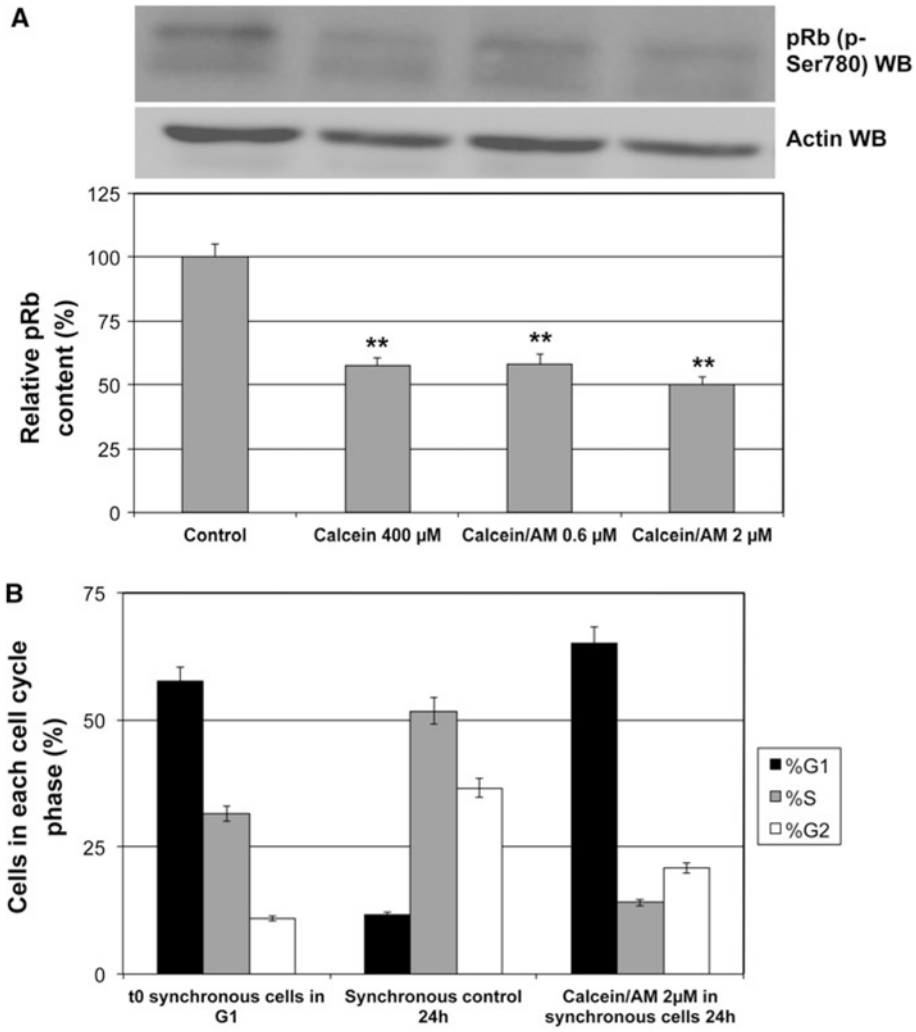

Fig. 2.

Phosphorylation of serine780 of pRb and cell cycle analysis. **a** HCT116 cells were treated with 400 μM or with 0.6 and 2 μM of calcein AM for 24 h and the extracts were blotted specifically against phosphoserine 780 of pRb. **b** Synchronous HCT116 cells in the G_1 phase at time 0 h (t0 synchronous control) and after 24 h with or without treatment with calcein AM 2 μM. (*) indicates $P < 0.05$ and (**) indicates $P < 0.01$. Both experiments were performed three times (Mean + SD; $n = 3$). One representative example is shown in each case

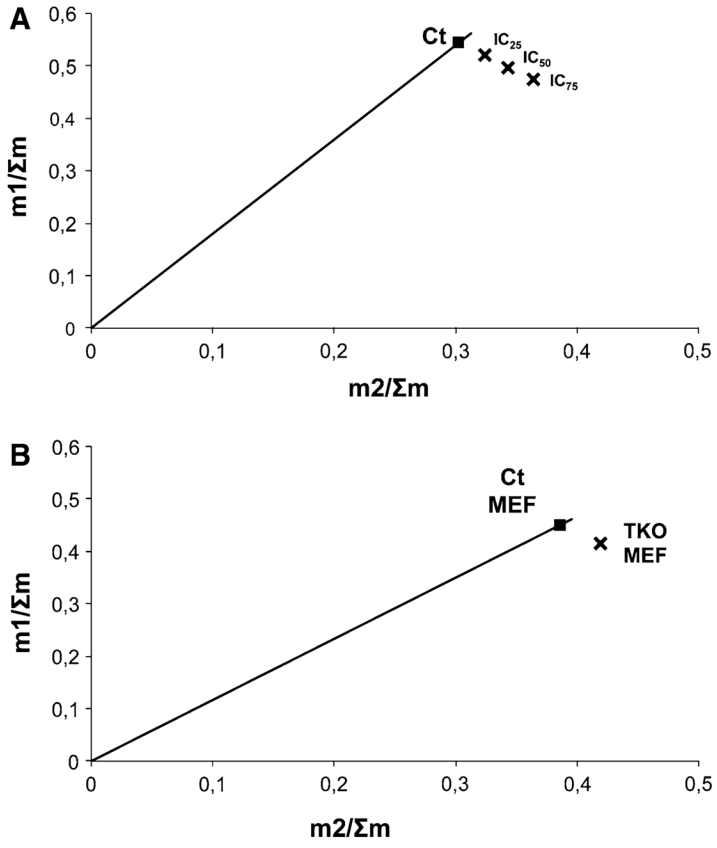

Fig. 3.

^{13}C ribose label distribution. Phase-plane analysis of the normalized ribose isotopologues m1 and m2. **a** HCT116 cells treated without (Ct) or with IC_{25}, IC_{50}, and IC_{75} doses of calcein AM; and **b** the control mouse embryonic fibroblasts (Ct MEF) and the MEF knockout for CDK4, CDK6, and CDK2 (TKO MEF)

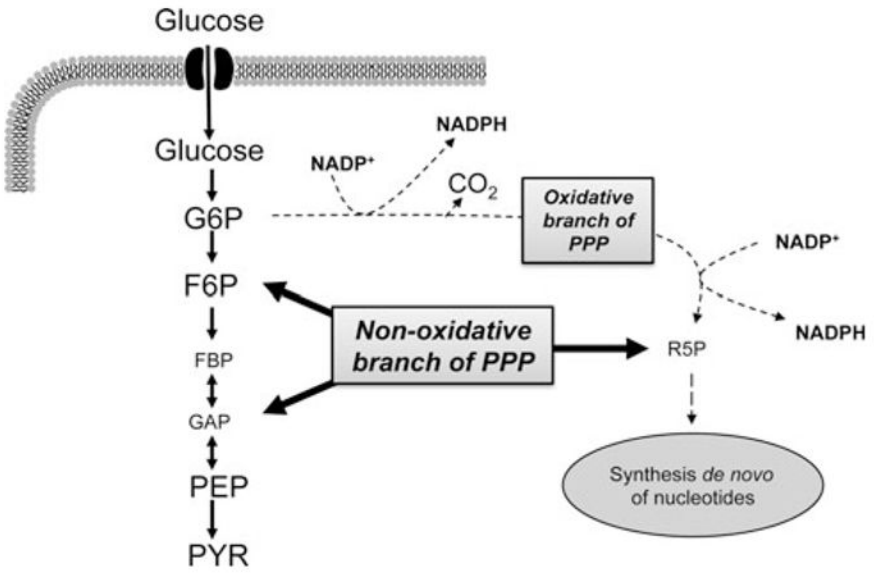

Fig. 4.

Metabolic changes associated to CDK4/6 inhibition. CDK4 and CDK6 inhibition leads to an imbalance between the oxidative and non-oxidative branches of the pentose phosphate pathway towards the non-oxidative branch. *Thick lines* indicate enhanced metabolic routes. *Dotted lines* indicate less active metabolic routes and *smaller font sizes* indicate lower intermediate concentrations

Table 1

Isotopologue distribution in lactate and ribose. M1/Σm and m2/Σm were determined in lactate isolated from incubation medium and in ribose isolated from RNA. Σmn in ribose isolated from RNA was also measured

Isotopologue distribution analysis						
	HCT116				**MEF**	
Lactate	Ct	IC_{25}	IC_{50}	IC_{75}	Ct	TKO
m1/Σm	0.075 ± 0.003	0.075 ± 0.001	0.064 ± 0.003 **	0.065 ± 0.002 **	0.104 ± 0.000	0.070 ± 0.020 *
m2Σm	0.919 ± 0.003	0.918 ± 0.002	0.928 ± 0.002 **	0.926 ± 0.002 *	0.835 ± 0.049	0.843 ± 0.043
Ribose	Ct	IC_{25}	IC_{50}	IC_{75}	Ct	TKO
m1Σm	0.544 ± 0.003	0.522 ± 0.002 ***	0.496 ± 0.003 ***	0.474 ± 0.003 ***	0.450 ± 0.002	0.414 ± 0.002 ***
m2Σm	0.303 ± 0.000	0.324 ± 0.001 ***	0.343 ± 0.004 ***	0.364 ± 0.002 ***	0.385 ± 0.002	0.420 ± 0.002 ***
Σmn	0.839 ± 0.016	0.858 ± 0.030	0.811 ± 0.098 **	0.668 ± 0.055 *	0.754 ± 0.008	0.718 ± 0.008 **

* $P < 0.05$;

** $P < 0.01$;

*** $P < 0.001$. Experiments were performed twice. Results from one of them are shown (Mean + SD; $n = 3$)

APPENDIX 3

(PAGES 219-240)